REPUBLIQUE DU CAMEROUN
Paix – Travail – Patrie
****
UNIVERSITE DE YAOUNDE I
FACULTE DES SCIENCES
DEPARTEMENT DE PHYSIQUE
****
CENTRE DE RECHERCHE ET DE FORMATION DOCTORALE EN SCIENCES, TECHNOLOGIES ET GEOSCIENCES

REPUBLIC OF CAMEROUN
Peace – Work – Fatherland
****
UNIVERSITY OF YAOUNDE I
FACULTY OF SCIENCE
DEPARTMENT OF PHYSICS
****
POSTGRADUATE SCHOOL OF SCIENCE, TECHNOLOGY AND GEOSCIENCES

LITHOSPHERIC STRUCTURE OF THE VOLCANIC PROVINCE OF CAMEROON FROM GEOPHYSICAL DATA

Thesis submitted and defended publicly in fulfillment of the requirements for the Award of the Degree of Doctorat/PhD in Physics.

Par : **POKAM KENGNI Serge Hugues**
Master in Physics

Sous la direction de
TABOD Charles TABOD
Professeur., Université de Yaoundé I

Année Académique : 2020

UNIVERSITE DE YAOUNDE I
THE UNIVERSITY OF YAOUNDE I

FACULTE DES SCIENCES
FACULTY OF SCIENCE

DEPARTEMENT DE PHYSIQUE
DEPARTMENT OF PHYSICS

ATTESTATION DE CORRECTION DE LA THESE DE DOCTORAT/Ph.D

Nous, **NJANDJOCK NOUCK Philippe** (Professeur) et **MANGUELLE-DICOUM Eliézer** (Professeur Emérite), respectivement Examinateur et Président du jury de la soutenance de Thèse de Doctorat/Ph.D de Monsieur **POKAM KENGNI Serge Hugues**, Matricule **05X191**, placée sous la direction de **TABOD Charles TABOD** (Professeur) et dont l'intitulée est: « **Lithospheric structure of the Volcanic Province of Cameroon from geophysical data** » soutenue le Mercredi, **3 Juin 2020**, en vue de l'obtention du grade de Docteur/Ph.D en Physique, Spécialité **Géophysique et Géoexploration**, attestons que toutes les corrections demandées par le jury de soutenance ont été effectuées.

En foi de quoi, la présente attestation lui est délivrée pour servir et valoir ce que de droit.

Fait à Yaoundé le 11 JUIN 2020

Examinateur	Chef de Département	Le Président du jury
NJANDJOCK NOUCK Philippe : *Professeur*	**NDJAKA Jean-Marie Bienvenu** : *Professeur*	**MANGUELLE-DICOUM Eliézer** : *Professeur Emérite*

DEDICATIONS

This thesis is dedicated to my entire family and especially to my wife MOPE KUATE Elisabeth and the children.

ACKNOWLEDGEMENTS

First of all, I give grace to the Lord Almighty who supports, accompanies and guides me everyday.

I wish to thank the following:

My research Supervisor, Professor TABOD Charles TABOD, to whom I express, my profound gratitude for having accepted to supervise this work; for his constant support, encouragement during this research, for the warm welcome into the geophysics laboratory and, for all the invaluable knowledge and wisdom dispensed which led to the outcome of this research work.

Professor NDJAKA Jean Marie Bienvenu, Head of the Physic Department, Faculty of Science, University of Yaoundé I, for his research vision, knowledge and advices.

The members of jury that have accepted to examine this work.

Professor Njandjock Nouck Philippe for all the guidance and advices.

All of Lecturers of the Physics Department for their teaching and guidance.

Doctor TOKAM KAMGA Alain-Pierre who not only considered me as a younger brother, but also guided into this research avenue.

Pr WOTCHOKO Pierre, Dr NDIKOUM Eric, and Mr AMAH MBAH Evans for theirs criticals, contributions in the methodology and linguistic approach to this work.

My parents Mr POKAM Basile, Mrs DOMENI Hélène Chantal, Mr FOKOU Bertrand and Mrs KANA Anastasie for their incessant daily efforts to bring me up.

My brothers and sister NZONGANG POKAM Hervé Martial, KAYO POKAM Éloge Félix, KAMDEM POKAM William Fredy, GOUNOU POKAM Blaise Pascal, TCHENDEM KEMMEGNE POKAM Laure, FOTCHEPING POKAM Eric Christel and GANGMO POKAM Wilfred for the moral, financial, material and spiritual support to the realization of this work.

My in-laws, the KUATES, for their continuous moral and spiritual support.

These acknowledgments would not be complete without thanking my classmates and friends AWOULOU Audrey, AZANMENE Eric, Dr YAP Loudi, SOH Vades, ENEME Ostwald, ABINA Gaetan, ASSEMBE Stéphane, EVINA Alban, KEMTEBOUET Celestin, ATANGANA Serge, KAMDOUM Hugues, KENMOGNE Hermann, MABOUKAM Aurélie, TSAGUE TONFACK Lydie, NGASSA Laure, NOUMBISSI Vanessa, NZUDJOM Emmanuel, SOH TANKAM Arno Blaise, TASSIADA Patrick, TATMEN Pulchérie, TSIGUIE Henry, DJOMGANG Mathurin.

And to all who contributed in one way or another to the realization of this work.

TABLE OF CONTENT

LIST OF TABLES

LIST OF FIGURES

LIST OF ABREVIATIONS AND SYMBOLS

ASCII: American Standard Code for Information Interchange
BAZ: Back Azimuth

CAR: Central Africa Republic

CASZ: Central Africa Shear Zone

CC: Congo Craton

CM: Cameroon

CMB: Core Mantle Boundary

CPS: Computer Program of Seismology

CSA: Cameroon Seismic Array

CVL: Cameroon Volcanic Line

DAS: Digital Acquisition System

EGM2008: Earth Gravity Model of 2008

E-W: East-West

FFT: Fast Fourier Transform

FSZ: Foumban Shear Zone

GMT: Generic Mapping Tool

GPS: Global Position System

GSAC: Generic Seismic Application Coding

IGMR: Institute of Geologic and Mining Research

IRIS: Incorporated Research Institute for Seismology

KC: Kulachi Craton

LVZ: Low Velocity Zone

M: Magnitude

Ma: Million d'années

MSRI : Ministry of Scientific Research and Innovation

NE-SW: North East-South West

NS: North South

PpPs: P- wave transmitted in P, reflected in P and transmitted in S

PpSs: P- wave transmitted in P, reflected in S and transmitted in S

PREM: Preliminary Reference Earth Model

Ps: P-wave converted to S phase

RF: Receiver function

SAC: Seismic Analysis Code

SFT: Source Function Time

Sp: S wave converted to P phase

TTG: Totalite-Trondhjemite Granodioriye

USA: United States of America

WAC: West Africa Craton

1-D: One dimension

a: Width of the Gassian filter

a_i: amplitude of the Dirac delta function

c: Water level parameter

D_R: Radial component seismic waveform

D_T: Tangential component seismic waveform

D_Z: Vertical component seismic waveform

E_R: Radial impulse response of the local Earth structure

E_T: Tangential impulse response of the local Earth structure

E_Z: Vertical impulse response of the local Earth structure

G: Gaussian filter

G: Second Lame parameter

H(t): possible effect of site function

H_R: Radial receiver function

H_T: Tangential receiver function

I(t): Instrument response function

K: Bulk modulus

L^2: set of the measurable functions in integrable scare

P(t): Path effects function

Q: Quality factor

S(t): Seismic source signal function

STF: Source-Time-Function

w: Angular frequency

ΔE: Dissipate energy per cycle

λ: First Lame parameter

μ: Shear modulus

ξ: Stands of the normalization parameter

ρ: Density

φ: Signal phase

ABSTRACT

The Volcanic Province of Cameroon is made of diverse reliefs such as Mountains, plateaus, and a rift. This diversity has attracted geoscientists as seen in the multitude of works already done in this area. As continuation of these works, we will study the structure of the lithosphere from recorded earthquakes data and particularly the teleseismic events which occurred around the world between the years 2005 and 2007. This data bank of three components having served in this work, has been recorded by each of the 32 seismometers installed in Cameroon during the seismic campaign carried out by, a team of geoscientists from the University of Yaounde I and the Institute of Geological and Mining Research of Cameroon in partnership with, researchers from Penn State University in the United State of America. The iterative deconvolution applied on the teleseismic P-waves obtained after selection, permitted us to get P-receiver functions. The latter were subsequently inverted in order to obtain the S-waves velocity models with respect to depth, and then associated to the synthetic receiver functions which permitted us, to explain the behavior of the wave and the structure of the medium through which they traveled.

The study area, with variation in its relief, presents three main results which differ according to the geologic structures encountered. **(1)** In the southern part regrouping the portion with mountains, the lithosphere in its crustal part, presents a thin and heterogeneous behavior, with a mean depth of 26.4 km beneath the Mount Cameroon region and mean depth of 35.8 km in other localities of this part. The average S-wave velocity is about 3.8 km/s. The lithospheric depth varying between 57.6 km and 78 km with a tendency to be thick in its mantle part for, an average S-waves velocity of 4.1 km/s. The boundary of the lithosphere has been determined thanks to the existence of the low velocity zone with a thickness which, also varies between 57.6 km and 116.8 km. The non-uniformity of the depth observed in this mountainous part is due on one hand, to the presence of the transition zone between the continental and the oceanic parts of the Cameroon Volcanic Line which is nothing other than the Mount Cameroon region and the other hand, to the variation of the geology settings. **(2)** In the northern part, the lithosphere in its crustal section, would presents equally the heterogeneous structure but thick behavior with a mean depth of 35.1 km for an average S-waves velocity of 3.7 km/s beneath the Adamawa plateau Region whereas, it is thin and heterogeneous with a mean depth of 28 km beneath the Garoua rift Region for a S-waves velocity of 3.8 km/s. The lithosphere in its mantle portion appears on contrary thin in nature beneath the Adamawa plateau Region whereas, it is thick beneath the Garoua rift region with an average S-waves velocity of 3.9 km/s. The depth of this lithosphere would varies between 73.8 km and 85 km on one hand and between 42 km and 67.2 km on other hand respectively in the

Adamawa plateau Region and in the Garoua rift Region. These results of the lithospheric depth beneath the Volcanic Province of Cameroon confirm the fact that, the lithosphere is shallower beneath the rift than plateau and mountains. The low velocity zone that permitted to delimitate the depth of the lithosphere has also the thickness which varies between 73.8 km and 116.7 km beneath the Adamawa plateau Region on one hand and between 42 km and 118.8 km beneath Garoua rift Region on other hand. **(3)** The synthetic receiver functions associated to the S-waves velocity models gave rise to Ps converted phase and PpPs, PpSs multiple converted phases which indicate that, the wave went through conversions at the level of the Moho. The identical times of these phases and multiple phases however differ according to the locality. This expresses the heterogeneous structure of the crust beneath the Volcanic Province of Cameroon. But some exceptions have been obtained at the CM09, CM15, CM21 and CM31 stations located respectively in Ekona, Nkongsamba, Tibati and Yagoua localities where, the results were not easy to interpret. This could due by development of the volcanic activity in Ekona and Nkongsamba localities on one hand and the development of the fault activity in Tibati and Yagoua on the other hand.

These said results obtained were compared to those existing in the literature. Some similarities were obtained (the depth and structural behavior of the crust followed by the S-waves velocity, the existence of the Low Velocity Zone, the converted phases and multiple converted phases of the wave at the Moho level). But equally slight differences are observed (the times of the converted phase and multiples converted phases of the S-waves and the lithospheric depth). This could be due to the types of data used on one hand (gravity data, seismic explosions data and surface waves data) in the others studies but, equally due to the method employed on other hand (potential method, stack of the receiver functions) in the others studies.

Key words: Volcanic Province of Cameroon; Teleseismic; Receiver Functions; Inversion; Lithosphere; Low Velocity Zone

RÉSUMÉ

La Province Volcanique du Cameroun est repartie en divers reliefs que sont les montagnes, les plateaux et les rifts. Cette diversité a alimenté la culture des geoscientistes de par la multitude des travaux déjà effectués le long de cette zone. Dans la continuité de ces travaux, nous étudierons la structure de la lithosphère à partir des données de tremblements de terre et plus particulièrement des téléseismismes ayant eu lieu dans le monde entre les années 2005 et 2007. La banque des dites données à trois composantes ayant servi à cette étude, a été enregistré par chacun des 32 sismomètres installés au Cameroun pendant cette période lors de la campagne sismique effectuée par une équipe de goscientistes de l'Université de Yaoundé I, de l'institut de recherche géologique et minière du Cameroun en partenariat avec les chercheurs de l'Université Penn State au États Unis. La déconvolution itérative appliquée sur les ondes P- téléseismiques obtenues après sélection a permis d'obtenir des << fonctions récepteurs-P>>. Ces dernières sont par la suite inversées afin d'obtenir des modèles de vitesse des ondes S, fonction de la profondeur, associées à des fonctions récepteurs synthétiques permettant d'expliquer le comportement de l'onde et de la structure du milieu traversé.

La zone d'étude, avec sa variation de relief, présente trois principaux résultats qui diffèrent selon les structures géologiques rencontrées. **(1)** Dans la partie Sud regroupant les Monts, la lithosphère dans sa partie crustale, présente un comportement mince et hétérogène avec une profondeur moyenne de 26,4 km dans la région du mont Cameroun et 35,8 km dans les autres localités de cette partie. La vitesse moyenne des ondes S est de 3,8 km/s. Dans sa partie mantellique, la lithosphère présente un comportement épais avec une limite variante entre 57,6 km et 78 km pour une vitesse moyenne des ondes S de 4,1 km/s. Cette limite de la lithosphère a été déterminée grâce à l'existence d'une zone de faible vitesse dont, la profondeur varie également entre 57,6 km et 118,8 km. La non-uniformité observée sur la profondeur en dessous de cette partie de la Province Volcanique du Cameroun serait dûe d'une part, à la présence de la zone de transition entre la partie continentale et océanique de la ligne volcanique du Cameroun qui, n'est rien d'autre que la Région du mont Cameroun et d'autre part à la variation des paramètres géologiques. **(2)** Dans la partie Nord, la lithosphère dans sa section crustale présenterait une structure également hétérogène mais épaisse avec une profondeur moyenne de 35,1 km dans la Région du plateau de l'Adamaoua, mince et hétérogène dans la région du rift de Garoua avec une profondeur moyenne de 28 km pour des vitesses des ondes S de 3,7 km/s et 3,8 km/s respectivement. La lithosphère dans sa partie mantellique, a un comportement contrairement mince en dessous de la Région du plateau de l'Adamaoua et épais en-dessous de la Région du Rift

de Garoua moyennant une vitesse des ondes S de 3,9 km/s. La profondeur de la lithosphère varierait respectivement entre 73,8 km et 85 km d'une part dans la Région du plateau de l'Adamaoua et entre 42 km et 67,2 km d'autre part dans a Région du Rift de Garoua. Ces valeurs de la profondeur de la lithosphère traduit bel et bien le faite que, la lithosphère est moins profonde sous les rifts que sous les plateaux et les monts. La zone de faible vitesse ayant permis de délimiter ces profondeurs de la lithosphère a également des épaisseurs variantes entre 73,8 km et 116,7 km d'une part dans la Région du plateau de l'Adamaoua et entre 42 km et 118,8 km dans la Région du rift de Garoua d'autre part. **(3)** Les fonctions récepteurs synthétiques associées aux modèles de vitesse des ondes S ont permis de ressortir des phases converties Ps, des phases converties multiples PpPs et PpSs traduisant le fait que, l'onde a réellement subit des conversions au niveau du Moho. Le temps de ces phases et phases multiples diffèrent néanmoins par rapport au type et la localité traversée. Ceci traduisant ainsi le caractère hétérogène de la croûte sous la Province Volcanique du Cameroun. Mais, certaines exceptions ont été obtenu aux stations CM09, CM15, CM21 et CM31 respectivement situées dans les localités de Ekona, Nkongsamba, Tibati et Yagoua où, les résultats n'ont pas été facile à interpréter. Ceci serait due au développement d'une activité volcanique dans les localités de Ekona et Nkongsamba d'une part et au développement d'une activité de faille dans les localités de Tibati et Yagoua d'autre part.

Les dits résultats ainsi obtenus sont par la suite comparés à ceux existants déjà dans la littérature. Des similitudes ont été obtenues (la profondeur et le comportement structural de la croûte suivie de la vitesse des ondes S, l'existence de la zone de faible vitesse, les phases et phases multiples converties de l'onde au niveau du Moho). Mais, également des légères différences (le temps de phase et phases multiples converties de l'onde S et la profondeur de la croûte et de la lithosphère) qui, seraient dûes aux types de données utilisées dans d'autres études d'une part (données gravimétriques, sismiques explosives et des ondes de surface) mais, également de la méthode employée d'autre part (méthodes potentielles, stack des fonctions récepteurs) dans d'autres études.

Mots clés : Province Volcanique du Cameroun ; Téléseismes ; Fonctions récepteurs ; Inversion; Lithosphère, Zone de faible Vitesse

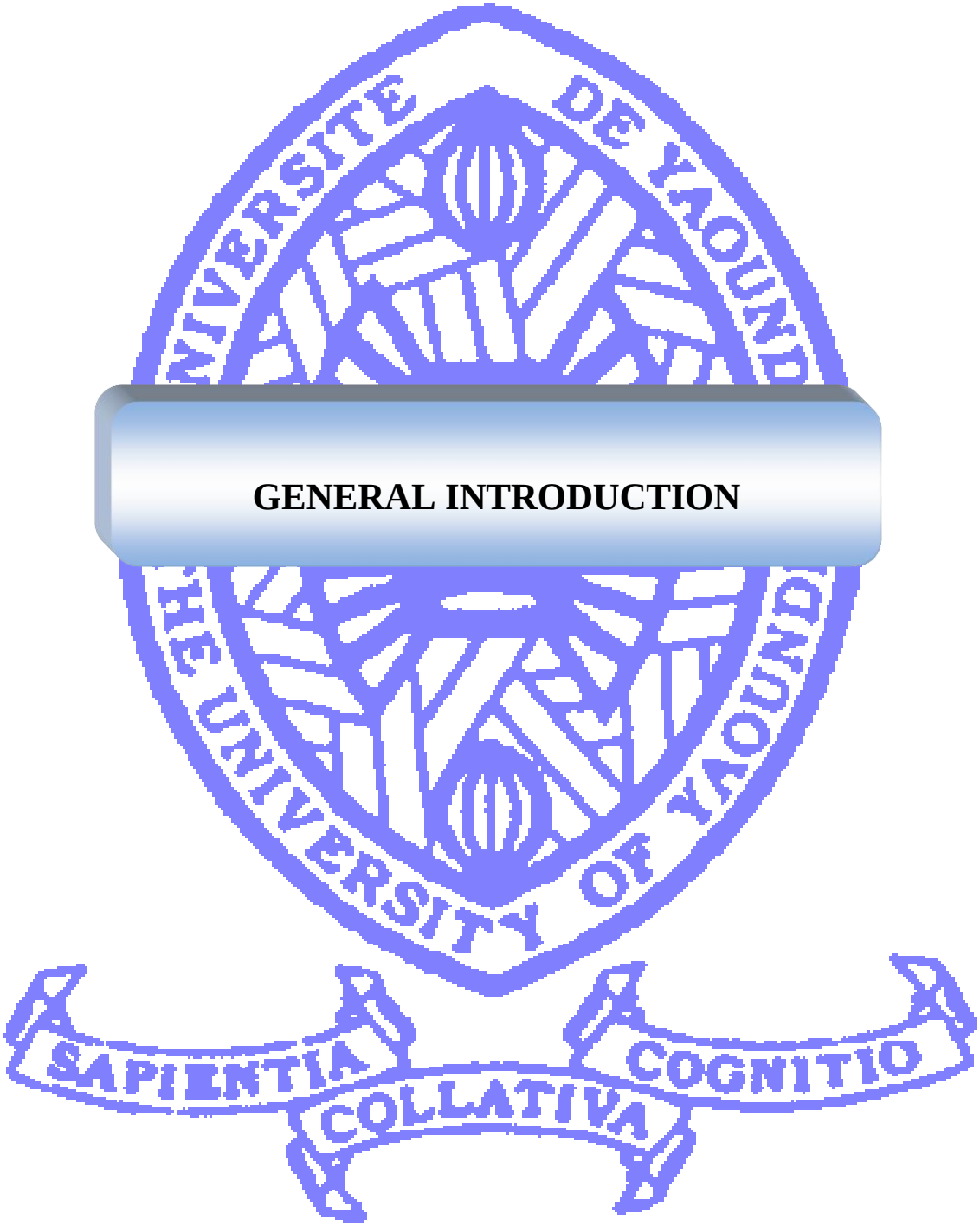

GENERAL INTRODUCTION

Knowledge of the structure of the earth and more importantly that of the lithosphere is a major subject of scientific curiosity to geologists and geophysicists due to its composition. Though, geophysical exploration is most often under minded, it is part and parcel of geological prospection. Evidently, its advantage lies in its accuracy in both shallow depth prospections using active methods like seismic explosion, electromagnetism and geoelectricity on one hand and in deep explorations using passive methods like, gravimetry, magnetism and earthquake seismology on other hand.

Major problems regularly encountered are the sourcing of data and the controversial correlations between geophysics data and geologic reality. Once the relative problem of data is solved, it is important to apply the right methodology to bring out information such as the depth or the thickness of the various layers, the density of the rocks and the velocity of the propagation of the waves in order to map the study area.

Within the scope of this thesis, we shall bring forth the 1-D cartography of the lithospheric structure along the Volcanic Province of Cameroon from earthquake data and more precisely teleseismic data derived from a seismic campaign carried out between January 2005 and February 2007 by a team of geoscientists of the departments of physics and geology of the University of Yaoundé I and that of PEEN State University of USA in collaboration with the Institute of Geologic and Mining Research of Cameroon under the supervision of the Ministry of Scientific Research and Innovation (MSRI) of Cameroon. The P-S receiver function method will be applied using teleseismic data in order to bring out a S waves velocity model as a function of depth, which will then permit us suggest the structure of the lithosphere of our area of study.

In order to attain our objectives, our work is presented in three chapters. The Chapter 1 which is based on literature review and problem statement will focus on the presentation of our study area, followed by the geologic description of the said zone and next by a summary of previous geophysics works. An emphasis will also be laid on general principles of earthquakes and receiver functions technique and we will then end with a problem statement. In chapter II, a description and presentation of data used in this study is done and this is followed by the methodology of processing the data. Equally, in this chapter a general review of the inverse theory and the description of the inversion of the receiver functions are done. In chapter III we present the different results obtained followed by their interpretations and lastly a discussion shall be done in order to make a clear comparison. To complete our work a general conclusion is given and finally, some suggestions for the further studies in this region are provided.

CHAPTER I: LITERATURE REVIEW AND PROBLEM STATEMENT

This chapter treats the presentation of the study area that take in account to the geographic, geology and tectonic setting followed by, the previous geophysical works that have been carried out. After this, we then review the tools, materials and technics that intervene in this work. We shall end with the limitations of the previous works in order to bring out the problematic and fix the objective of this work.

I- Presentation of the study area

I.1 Geographic settings and the origin of the Cameroon Volcanic Line (CVL)

The volcanic province of Cameroon is the part of Cameroon regrouping the main volcanic centers (**Figure I.1**) of the Cameroon Volcanic Line. This last line is a Y-shaped tectonomagmatic megastructure **(Figure I.1)** in western Central Africa which is divided in continental and oceanic sectors. It comprises more than 60 anorogenic ring complexes (70–30 Ma) (Ngako et al., 2006) and 12 volcanic massifs (51.8 Ma to recent) in the continental segment (Wandji et al., 2009). Its oceanic sector is composed of six major volcanoes in the Atlantic Ocean (Déruelle et al., 2007), three (Biao, Santa Isabel and San Carlos) on Bioko Island (Fernando Poo) and one on each of Pagalu (Annobon), Sao Tomé and Principe volcanic islands. The continental domain consists of many small and four central volcanoes (Mount Cameroon, Mount Manengouba, Mount Bambouto and Mount Oku) in Cameroon and (Biu Plateau) to the North-East of Nigeria. These result in a major active N30°E tectonomagmatic structure in both oceanic and continental lithosphere (Fitton, 1987), that stretches for more than 1600 km, with a width of up to 100 km. It runs from Pagalu Island in the Gulf of Guinea to Lake Chad in the interior of Africa (Fitton, 1980; Fitton and Dunlop, 1985; Lee et al., 1994). Only Mount Cameroon volcano located at the boundary of the continental and oceanic sectors of the Cameroon volcanic line is still magmatically active (Fitton, 1983; Déruelle et al., 2007; Suh et al., 2003).

The origin of the CVL is still controversial (Déruelle et al., 1991). Some authors such as (Morgan, 1983) think that, it is the surface expression of a hotspot chain. Meanwhile, Lee et al. (1994) have suggested the involvement of an active plume to explain the NE–SW time-related spread of initiation of volcanism in the oceanic sector and proposed that the Cameroon volcanic Line originated from an enriched sub-lithospheric “hot zone” periodically fed and melted by a deep plume. But, the hotspot model is not explicable because there is no systematic migration in the inception of volcanism with time, as deduced from published isotopic ages. Numerous hypotheses have been proposed to explain the characteristics of the magmatism along the Cameroon Volcanic Line and to locate its source. Halliday et al. (1990) suggested that the magmatism of the Cameroon volcanic line results from melting of a fossil plume that was emplaced in the Mesozoic at the continental–oceanic boundary.

According to the relief met, one distinguishes varied geological and tectonic settings.

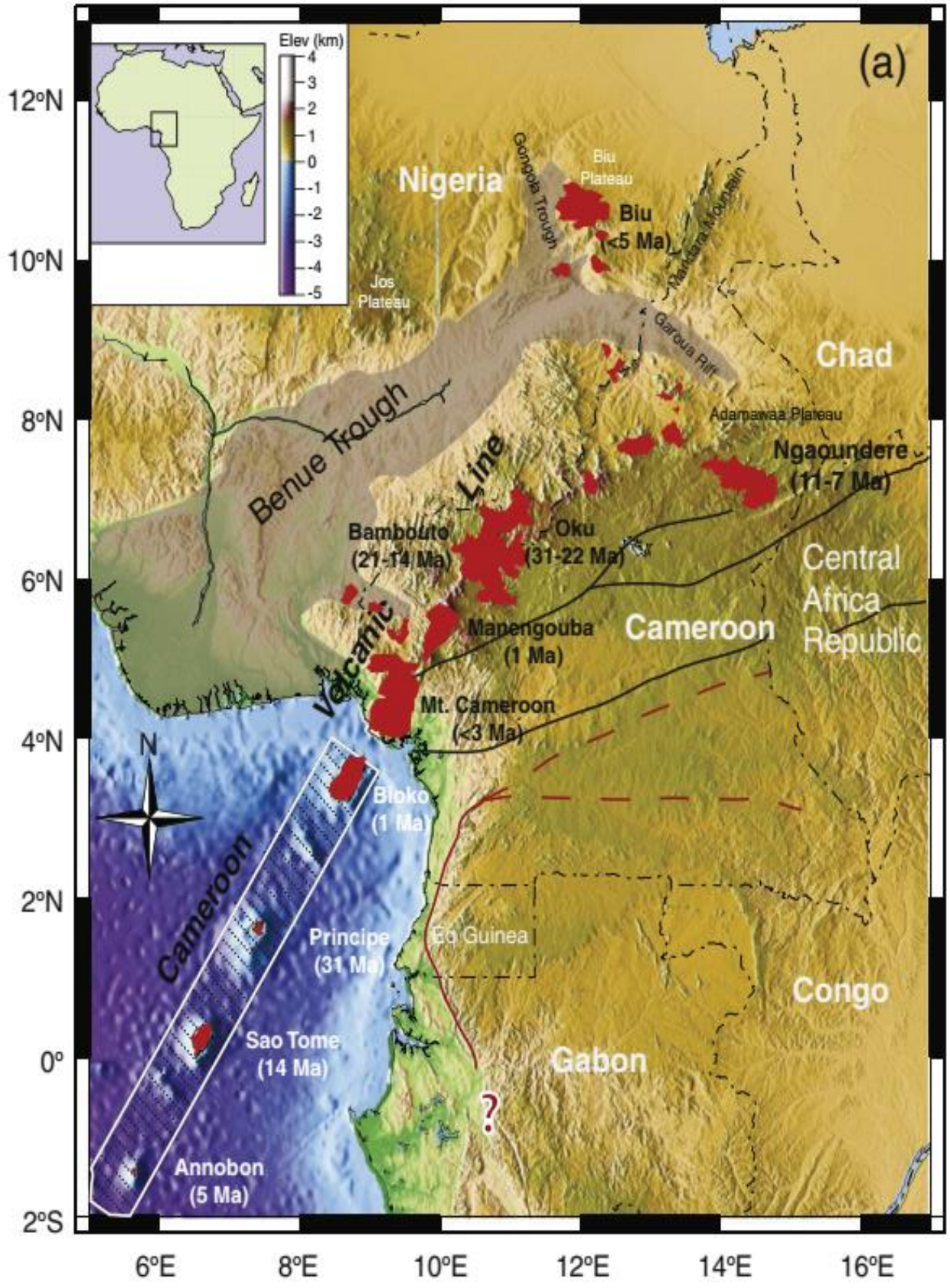

Figure.I.1: Location of the Cameroon Volcanic Line with the major volcanic centers.

I.2 Geologic and tectonic settings

I.2.1 Geologic settings

The Volcanic Province of Cameroon is characterized by three main reliefs which are: the mounts in the South; the plateau and the rift in the North. Therefore, it can be divided on two main zones: the southern part regrouping the different mounts and the northern part taking in account of plateau and rift. Situated between the latitudes 3°30´ and 6°33´N and the longitudes 8°50' and 11°27'E, the southern part is the major part of the Volcanic province of Cameroon constituted by the Mounts (mount Cameroon, mount Manengouba, mount Bambouto and mount Oku). This part has the particularity that, it contents the transition zone between oceanic and continental parts of the CVL because, both positive Bouguer anomalies (which are generally found on oceanic area) and negative Bouguer anomalies common on continent area are observed in the study area (Marcel et al., 2010). The geologic settings of the Southern part (**Figure I.2 (A)**) vary according to the mounts met. Thus, the mount Manengouba is made up of basalt, trachyte and rhyolite lavas; the mount Cameroon, which is the largest of the continental volcanoes, is made of lavas that are mainly of alkaline basic type (Hedberg, 1968, Deruelle et al., 2007), the mount Bamboutos lavas are mainly alkali basalts and trachytes and mount Oku is composed of transitional basalt, quartz trachyte and rhyolite (Fitton and Dunlop, 1985). The whole area is subject to many geological events, such as: the deadly magmatic gas releases in Monoun and Nyos lakes in 1984 and 1986, respectively in the West and North-West region of Cameroon and the volcanic eruptions of mount Cameroon (which the last eruption happens in the year 2000) with many seismic events regularly recorded in the area (Marcel et al., 2010).

The Northern part of volcanic province of Cameroon extends between latitudes 6°N and 11°N and between longitudes 11°E to 16°E. This area is sandwiched between the Adamawa plateau in the South and the Mokolo Plateau in the North. It is bounded to the West by the Federal Republic of Nigeria and to the East by the Republic of Chad (**Figure I.2 (B)**). It is characterized by two main reliefs being a Plateau (Adamawa and Mokolo plateaus) and the rift (Garoua rift). The basement of the Adamawa plateau region consists of a Precambrian magmatic gneiss complex that recorded Pan-African granitization (Dumont, 1987). That basement is overlain by a sequence of basaltic to andesitic lavas that are largely of tertiary age (Le Maréchal and Vincent, 1971). These lavas are essentially alkaline indicating an affinity to continental rifts (Kampunzu et al., 1986). The sedimentary formations here are mainly composed of conglomerates and marl of the Cretaceous Mbere and Djerem troughs, (Lasserre, 1961; Le Maréchal and Vincent, 1971). These formations have undergone intense tectonic activities resulting in the displacement of basin structures which were frequently filled by volcanic material upwelling through deep fractures in

the Adamawa plateau region. In the Garoua rift region, the structural and geological (**Figure I.2 (B)**) studies make by Elf-Serepca (1981) and Regnoult (1986) show that, the Garoua basin is an E–W to N120 trending trough infilled by Middle to Upper Cretaceous marine sandstones. These sediments have also been described by Roch et al. (1953) and Schwoerer (1965). The Garoua sandstone series overlap an approximately E–W trending trough called the Tcheboa trough, similar to the Figuil, Hama-koussou and Mayo-Oulo basins (Ndjeng, 1994, Ndjeng and Brunet, 1998**).** The whole region of the Garoua basin presents outcrops of sandstone and intrusive granites, which form the basement complex below the sediments, and intrusive diorites along the Poli-Lere axis (Poudjom Djomani et al., 1992). Some hypovolcanic dykes are also found within the Garoua sandstones.

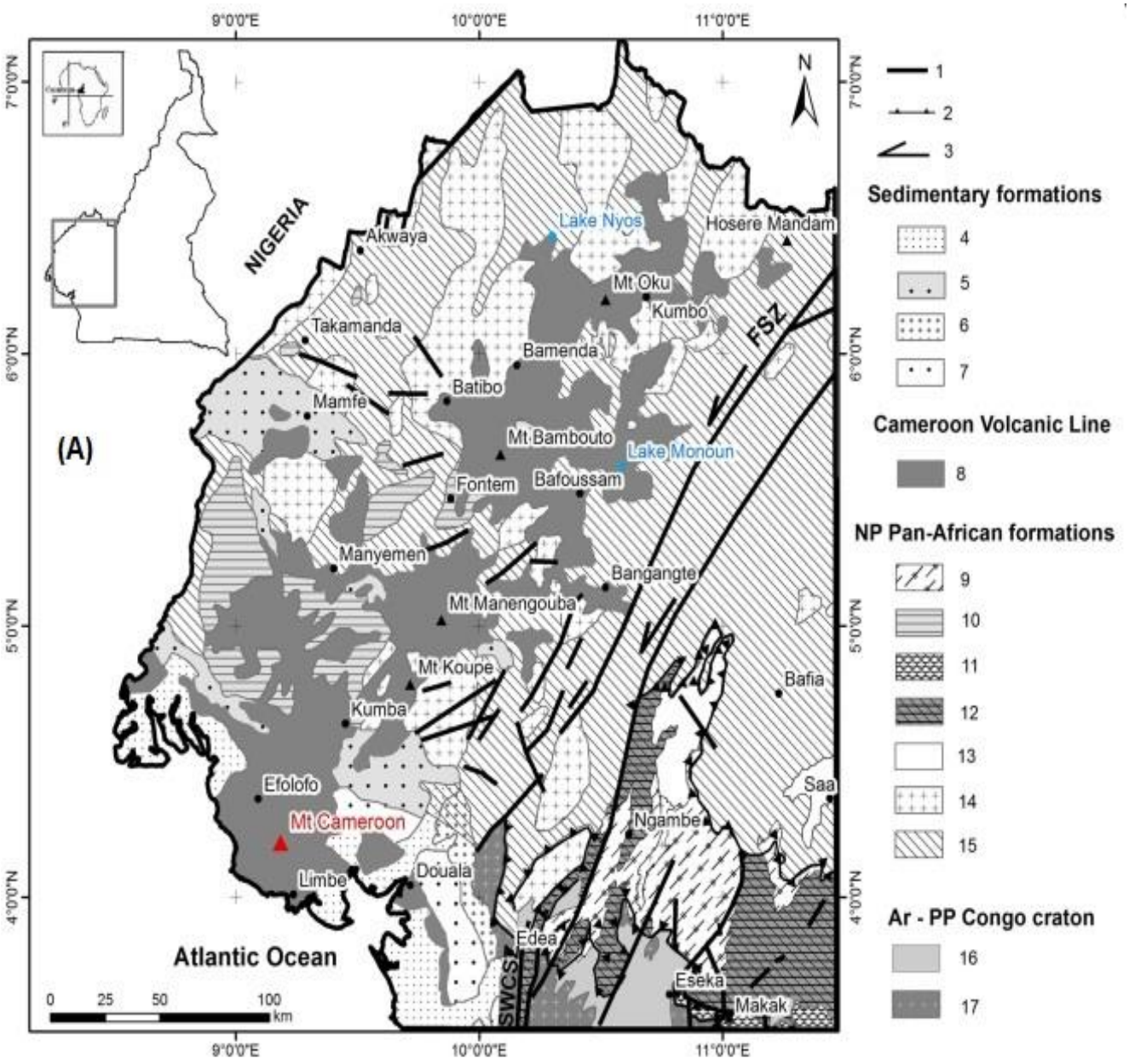

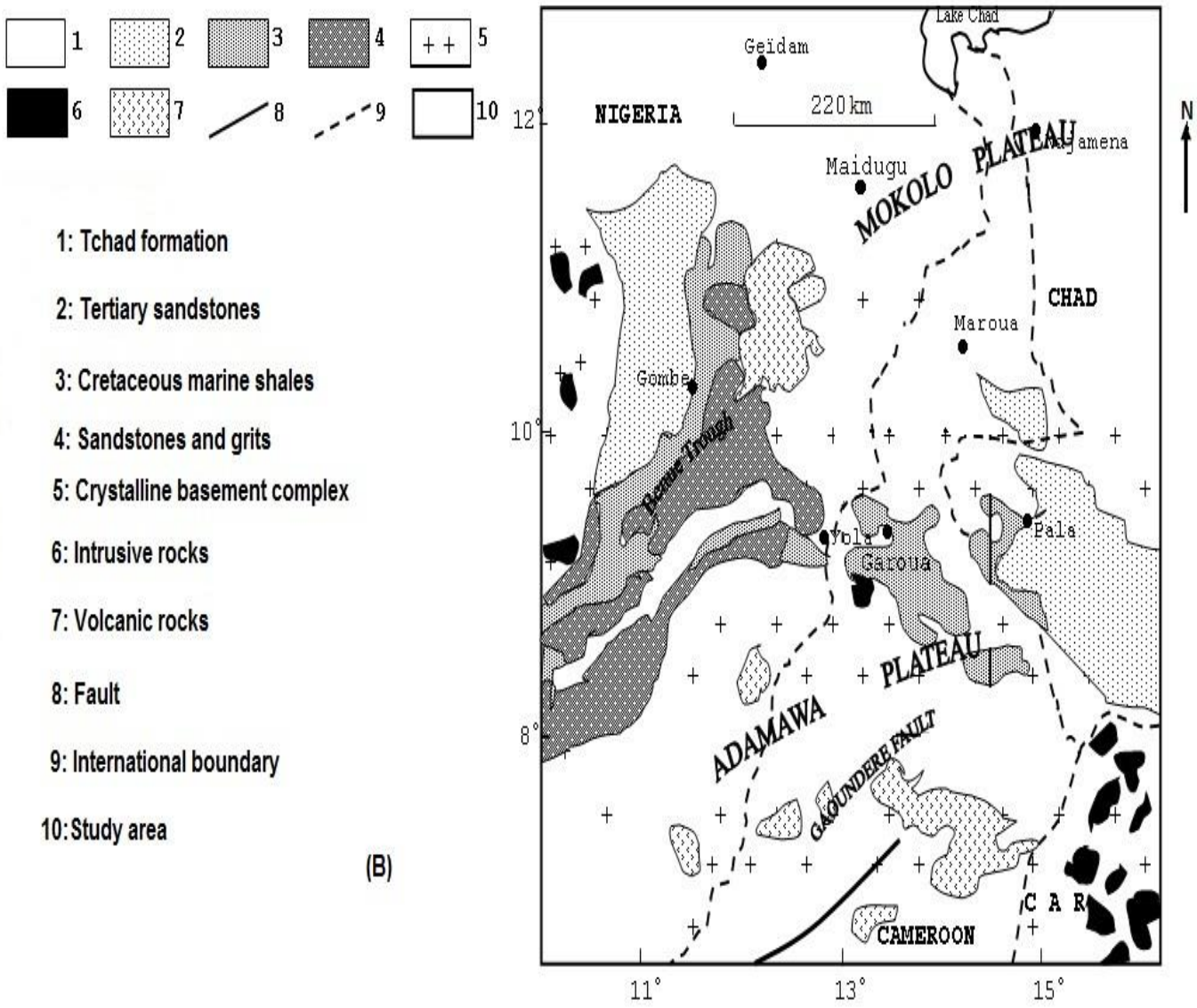

Figure I.2: Geological map of volcanic province of Cameroon. (A) Southern part (modified after Marcel et al., 2018); (B) Northern part (modified Kamguia et al., 2005)

I.2.2 Tectonic settings

The Cameroon Volcanic Line (CVL), which overlaps the continental margin, interacts with three other major tectonic features crossing Cameroon **(Figure I.3):** The Benue Trough located to the West to the Line, the Central African Shear Zone (CASZ) in the East trending N70°E across the line and a small part of Congo craton located in southern Cameroon.

a) The Benue Trough

The Benue Trough (**Figure I.3**) is a NE-SW trending basin that extends from the Niger delta basin (Gulf of Guinea) to Lake Chad. Its origin is thought to be linked to the opening of the South Atlantic Ocean in the cretaceous times (Guiraud and Maurin, 1992). The Yola Garoua

or Garoua Rift and the Mamfe basin are known as its eastward extensions in Cameroon. The Y-shape of the CVL is similar to the shape of the adjacent Benue trough (Fitton, 1987) and suggests an interaction during the formation of both structures. In fact, the alkali basalts of the Benue Trough are geochemically and isotopically similar to those of the CVL (Coulon et al., 1996). The orientation of the trough seems to be controlled by a northeast trending dextral shear zones of late Pan-African age (Guiraud and Maurin, 1992). Volcanic activities reported in the trough were particularly important during cretaceous and early tertiary times (Wilson and Guiraud, 1992).

b) The Central African Shear Zone

The Central African Shear Zone (CASZ) is a major tectonic feature of Africa extending from the Darfur in Sudan across Central Africa to the Adamawa Plateau region (Dorbath et al., 1986). In this region, the CASZ (**Figure I.3**) runs south-westwards, constituting the Foumban Shear Zone (FSZ) which is considered to be a continuation of the Pernambuco lineaments in Brazil (Burke et al., 1971; Browne and Fairhead, 1983). This shear zone is masked in south western Cameroon by the widespread tertiary to recent volcanic cover.

c) The Congo craton

The Congo craton is an ancient Precambrian structure that occupies a large part of Central Africa. Its northern portion (in Cameroon) is referred to as the Ntem Complex (Vicat et al., 1996). The Congo Craton in Cameroon consists predominantly of Archean rocks with some reworked and resedimented material formed in the Paleoproterozoic (Tchameni et al., 2001). The Archean period began before 3.14 Ga during which Paleoarchaean protocrusts were formed. Evidence of the existence of these protocrusts has been pointed out in the Ntem complex and they represent the protholiths of the Archean greenstone belts of the Congo Craton (Nsifa, 2006; Tchameni et al., 2001). Large segments of the preserved Archaean continental crust are made up of an association of mafic to ultramafic extrusive rocks and, metasediments that form the classic greenstone belts surrounded by magmatic rocks of the tonalite-trondhjemite-granodiorite (TTG) suite (Tchameni, 1997). The Paleo Proterozoic evolution of the Ntem Complex is equivalent to the Eburnean orogenic cycle, characterized by intrusion of mafic doleritic dykes. This cycle ended with a thermal or hydrothermal event at around 1800 Ma (Nsifa, 2006; Tchameni et al., 2001). The boundary between the Panafrican belt and the Congo Craton occupies part of southern Cameroon and progresses towards the North of Central African Republic (Boukeke, 1994). In this region the Congo Craton, underthrusts the Panafrican block, along an intracrustal discontinuity.

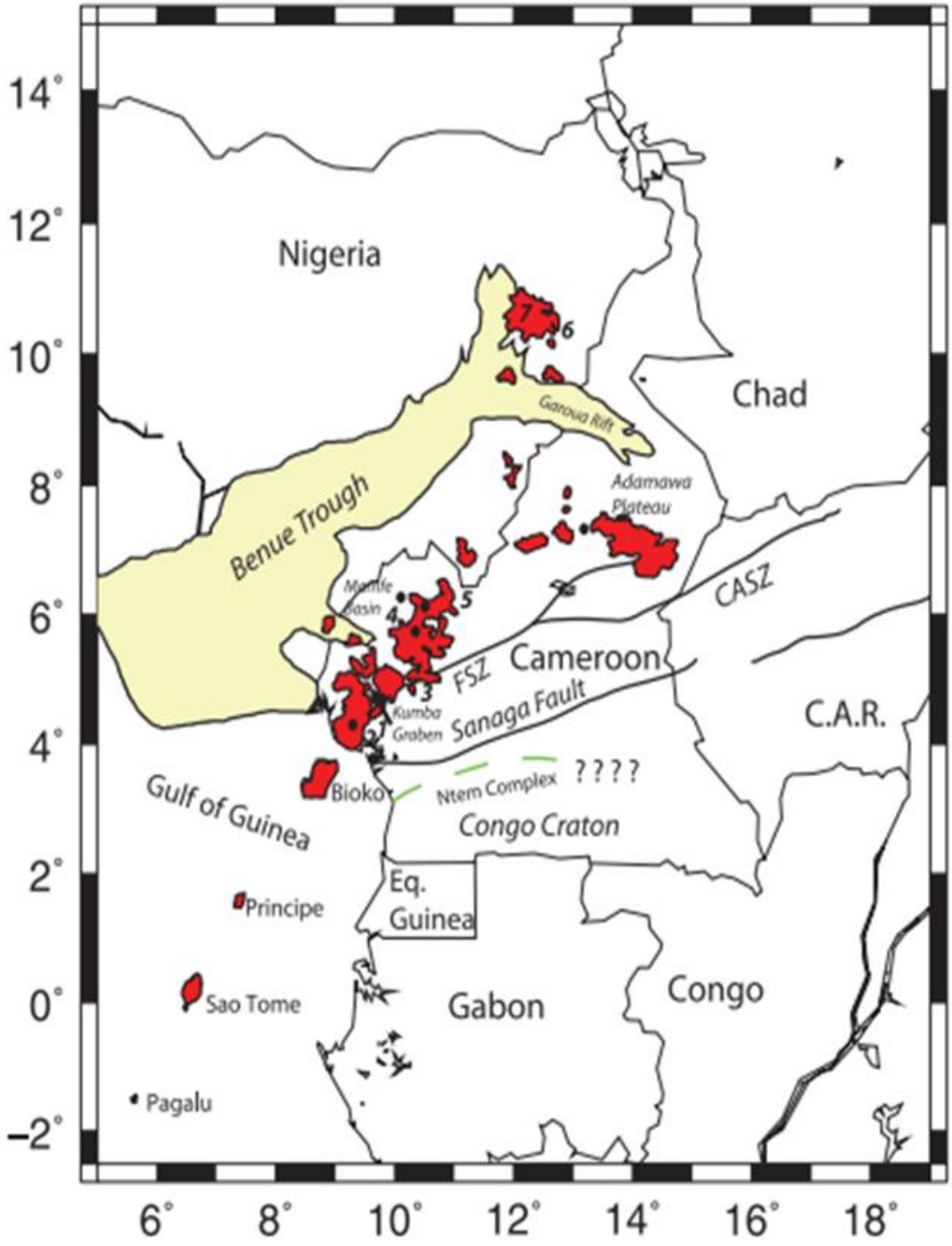

Figure I.3. Tectonic map of the study area. Volcanic areas that are part of the CVL are shown in red. The approximate northern boundary of the Congo Craton is shown with a green dashed line. FSZ: Foumban shear zone; CASZ: Central African shear zone (modified after Tokam et al., 2010).

I.3 Previous geophysical works

Several geophysical studies have been conducted in some parts or the entire Volcanic Province of Cameroon. Geophysical data for this area have been treated using active method on one hand in the domain of the geoelectric, electromagnetism and seismic explosion as well as the passive method on other hand in the domain of the gravity and earthquake seismology.

I.3.1 Geophysical works using active method

The main works using this type of method concern those of:

- Stuart et al. (1985) used records of quarry blasts (active source seismic data) on a North-South profile across the Adamawa plateau performed a study of the crustal structure associated with the Adamawa plateau and the Garoua Rift. This study revealed a considerable thinning of the Crust when moving south of the Adamawa Plateau towards the Garoua Rift region. The Crust thins from 33 km south of the Adamawa Plateau to about 23 km at the Garoua rift region.

- Nouayou (2005) led a geophysical survey in the Mamfe basin by prospecting Audio and Helio magnetotelluriques. This survey led to the setting in evidence of the structures propitious to an exploitation of hydrocarbons as the faults and the domes.

- Aretouyap et al. (2014) applying ordinary Kriging analysis on the geoelectrical data to investigate the spatial distribution of the non- standard parameters in the Adamawa Plateau. The global water quality index for the region was calculated and its value is equal to 82.11.

- Aretouyap et al. (2018) analyze the transmissivity values to reveal the existence of two aquifer trends in the Adamawa plateau region: Trend-1 with transmissivity values ranging from 34.22 to 39.27 m^2/day with an average value of 35.44, and Trend-2, with transmissivity values of 7.87–34.44 m^2/day with an average value of 16.56.

I.3.2 Geophysical works using passive methods

Concerning the seismic and gravity data of the passive method,

- Fairhead and Reeves (1977) presented a tentative lithospheric thickness map of the African continent based on the interpretation of teleseismic delay times and regional Bouguer anomalies. As a result they found undulations of the lithosphere-asthenosphere transition which seemed to be more pronounced in the south-eastern part of Africa, whereas the lithosphere in the central and north-western parts is estimated as being thicker on average and flatter at its base.

- Nnange et al. (1985) reported that the installation of the Yaoundé seismograph station in February 1982 provided the first permanent observatory for monitoring earthquake activity in Cameroon. The station recorded two earthquakes in 1983 out of the region of Mount

Cameroon, the only area known as seismically active. The first occurred close to the Northern margin of Congo Craton and the second close to Foumban shear zone.

- Dorbath et al. (1986) performed a tomographic inversion of residual teleseismic P-wave. Results presented the Adamawa plateau as the interaction of a regional anomalous upper mantle zone associated with the West African rift system and the CASZ. Such a region would provide a conduit for heat flow to the surface.
- Ambeh et al. (1989) did the first detailed instrumental seismicity survey ever in any area of Cameroon using a permanent network of 6 stations installed in late 1984 following the eruption of Mount Cameroon in 1982. The permanent array was augmented in the period December 1985 - March 1986 by 8 temporary stations. The survey confirmed the fact that the seismicity in Cameroon is confined mostly to the Mount Cameroon region.
- Tabod (1991) in his thesis, investigated the regional seismicity of the volcanic province of western Cameroon including the Foumban shear zone and also studied the crust and upper mantle velocity structure in the region using regional and teleseismic earthquake data. He established that the regional seismicity of the volcanic province of western Cameroon is concentrated around Mount Cameroon volcano and sorted out the evidence of some seismicity associated with the Foumban shear zone and Congo craton margin. The velocity structure inferred from P wave tomography shows that, the region around Mount Cameroon and Lake Nyos are dominated by a slower crust and a less heterogeneous mantle. The crustal thickness there is probably greater than 33 km.
- Tabod et al. (1992) also suggest the existence of the Low velocity Zone beneath the volcanoes of the continental sector of the Cameroon Volcanic Line (CVL)
- Plomerova et al. (1993) used gravity data and active teleseismic P and PKP arrivals times recorded by a network of 40 seismic stations deployed along a 300 km profile across the Adamawa plateau at the northern end of the CVL to deduce a thinned lithosphere beneath the CASZ and that, the lithosphere-asthenosphere transition is about 70 km. From the difference in orientation of P-wave velocities in the sub-crustal lithosphere beneath the northern and the southern part of the region, they suggested that both blocks probably originated from different tectonic settings before coming together and thus postulated that Africa must be broken into at least two fragments along the Benue Trough and its northern continuation.
- The gravity data used by Poudjom et al. (1995) permit to establish the correspondence between the crustal thickness and Bouguer anomaly maps which revealed a particular feature of a thin Crust beneath the Garoua Rift associated with relatively positive

Bouguer gravity anomalies, while low Bouguer gravity anomalies beneath Adamawa Plateau is also related to a thin Crust.

- Poudjom et al. (1997) used the gravity data to state that, the broad negative Bouguer anomaly over the Adamawa Plateau is modeling as a 40 km thinning of the lithosphere where a hot, low-density asthenospheric body replaces the high-density upper mantle at about 80 km deep. The gravity model agrees with the seismic data which suggests the existence of the Low Velocity Zone (LVZ) within the upper mantle beneath the uplift. The Central positive anomaly, although very localized, is due to a thinning of the crust by about 10 km relatively to the South of the plateau.

- The off-shore part of the CVL has been investigated using reflection seismology and gravity data (Meyers et al., 1998). The study showed that this portion of the CVL could not represent a hotspots trace. The authors proposed that all the West African linear volcanic chains form parallel hotlines that are products of mantle upwelling between Rayleigh-Bernard-type cylindrical convective rolls formed in the upper mantle. The driving force for these convective rolls might be a combination of heat transfer across and unidirectional shear along the 670 km discontinuity from convective currents in the lower mantle.

- Nnange et al. (2000) used a spectral analysis applied to the same kind of dataset revealed rather a normal crust of about 33 km thick beneath the Adamawa Plateau.

- Ndougssa (2004) studied the superficial and deep structures in the sedimentary basin of Mamfe from the gravity data of several profiles parallel oriented North-South. He evaluated the width of the basin to about 40 km and the thickness of the sediments to 6 km.

- Pasyanos (2005) developed at continental scale, the first surface wave Group velocity model including the whole Africa continent. The map gives useful information on investigating large structures. It appears from the model that within Cameroon, the signature of the Congo craton in the south constrasts with the Panafrican mobile belt in the north. However, due to the lack of dense seismic networks, the West African region does not provide good ray path coverage across Cameroon and consequently large uncertainties on estimates of earth parameter.

- Kamguia et al. (2005) in the cretaceous basin of Garoua; used the analytical technic based on the polynomial fitting. The data obtained have been interpreted along four profiles to determine the geometry of the basin, the thickness of its sediments as well as the structure of the basement below these sediments. They found that, the regional Bouguer anomaly map obtained from the third-order polynomial fitting presents a relative positive anomaly trending eastwards. The corresponding residual anomaly map shows negative anomalies of short wavelength. The models proposed from this interpretation are characterized by the accumulation of sandstone in the

basin. The thickness of these sediments has been estimated to be up to 4 km. The continental crust below the basin is thinner (about 24 km) than the normal crust, but may be a little thicker to the east. This thinning is probably due to the extensional process of basin formation in the Cretaceous. The Moho is found to be uplifted in the basin, and would be the result of this extension and the associated thermal and isostatic compensation.

- Pasyanos and Nyblade (2007) studied the lithospheric structure of Africa, Arabia and adjacent oceanic regions with fundamental mode surface waves over a broad period range. In the process, they developed a crustal thickness map of Africa. Main features observed include crustal thickness increases under the West African, Congo, and Kalahari cratons.

- Ateba et al. (2009) performed a study on eruptive and earthquake activities related to the 2000 eruption of Mt Cameroon. They tested a velocity model with a thin Crust of 20 km that gave better results on earthquake location around the volcano than a previous model of 33 km thick Crust (Stuart et al., 1985).

- Reusch (2009) using P and S arrivals from teleseismic events recorded during the Cameroon seismic experiment (2005 – 2007), performed a tomographic study of the Upper Mantle across Cameroon. This study revealed that models for the origin of the CVL invoking plumes or reactivated shear zones are not consistent with the shape of the thermal anomaly observed, but are consistent with a model of CVL originating from Upper Mantle convection initiated by edge flow along the northern margin of the Congo Craton lithosphere.

- Tokam et al. (2010**)** used joint inversion of Rayleigh wave group velocities and receiver functions to show that crustal thickness (35–39 km) and velocity structure is similar beneath the CVL and the Pan African Oubanguides Belt to the south of the CVL, the crust is thicker (43–48 km) under the northern margin of the Congo Craton where it is characterized by shear wave velocities ≥4.0 km s^{-1} in its lower part and finally the crust is thinner (26–31 km) under the Garoua rift and the coastal plain. In addition, a fast velocity layer (*V*s of 3.6–3.8 km s^{-1}) in the upper crust is found beneath many of the seismic stations.

- Fishwick (2010) used the surface waves tomography to indicate that the mantle beneath the CVL is characterized by slow seismic wave velocity and the lithosphere-asthenosphere boundary is shallower than 100 km (~60 km).

- Marcel et al. (2010) investigated the Moho discontinuity depth along southern part of CVL with EGM2008 data and found values ranging from 19 to 34 km. These authors suggested that gravity data derived from EGM2008 can efficiently be used to overcome the absence and the rarity of terrestrial gravity data. EGM2008 gravity data are therefore suitable for mountainous and

volcanic areas where terrestrial gravity surveys cannot easily be covered such as the present study area.

- Reusch et al. (2010) used body wave tomography to image the mantle seismic structure beneath Cameroon using data from the 2005–2007 CBSE network. They found that a continuous low velocity zone (δV_S = -2 to -3%) underlies the entire CVL to a depth of at least 300 km and attributed this to a thermal anomaly of at least 280 K.

- Reusch et al. (2011) stacked the receiver functions using a 3-D velocity model, revealing *Ps* conversions from the mantle transition zone discontinuities at depths of ∼410 and 660 km. Results yield a nearly uniform transition zone thickness (251 ± 10 km) that is similar to the global average, implying that any thermal anomalies in the upper mantle beneath the CVL do not extend as deep as the transition zone.

- Gallacher and Bastow (2012) stacked receiver functions to study crustal structure using earthquakes recorded by the Cameroon Broadband Seismic Experiment. In regions of the CVL unaffected by the Cretaceous extension associated with the breakup of Gondwana (e.g., the Garoua rift), Vp/Vs ratios are markedly low (network average 1.74) compared to hot spots elsewhere, providing no evidence for either melt or cooled mafic crustal intrusions due to CVL magmatism. The character of P-to-S conversions from beneath the CVL also indicates that, lower-crustal intrusions (often termed underplate) are not present beneath the region.

- Milelli *et* al. (2012) invoked a linear asthenospheric upwelling caused by instability within the subcontinental lithosphere mantle at the edge of a continent.

- Recently, Guidarelli and Aoudia (2016) investigated the lithospheric structure of Cameroon by inverting Rayleigh waves obtained from the cross-correlation of ambient seismic noise. They measured group velocity dispersion curves from the reconstructed Rayleigh waves in the period range 10–35 s and then inverted the group velocities for tomographic images. After the tomography, the group velocities were then inverted together with longer period group velocity measurements from existing literature, to compute a 3-D *S*-wave velocity model of the Cameroon lithosphere down to 100 km of depth. They found that, the Cameroon Volcanic Line (CVL) appears as a segmented feature exhibiting different physical properties along strike. The active Mt Cameroon volcano is underlain by very low velocities, unlike the other segments of the CVL. The along-strike variations in crustal structure suggest that lateral heterogeneities in lithospheric thickness and physical properties have influenced the location and distribution of magmatism. The crust beneath the Central African Shear Zone exhibits a sizeable low velocity anomaly. The

lithosphere beneath Cameroon is characterized by a heterogeneous crust with a relatively constant thickness and a low velocity uppermost mantle at the edge of the Congo Craton.

- Marcel et al. (2018), also used the same gravity data derived from the geopotential field model EGM2008, to investigate the subsurface of the CVL. The methodology involves upward continuation, horizontal gradient, maxima of horizontal gradient–upward continuation combination and Euler deconvolution techniques. The lineament maps inferred from this geopotential field model confirms several known lineaments and reveals new ones covered by lava flows. The known lineaments are interpreted as faults or geological contacts such as the Foumban fault and the Pan-African Belt Congo Craton contact.
- More recently, Pokam et al. (2018) applied the receiver functions technic on the teleseismic data recorded between years 2005 and 2007 to study thickness of the lithospheric mantle and the Low Velocity Zone (LVZ) in the Adamawa plateau region. The authors shown that, the region is characterize by the existence of a thick crust having an average thickness of about 35.2 km and a corresponding S wave velocity of 3.7 km/s. For an average S wave velocity of 4.4 km/s the lithospheric mantle appears to be thin in nature and has a thickness that varies from 39 km and 49.6 km. Beyond the lower lithospheric mantle, there exists a low velocity zone, whose thickness varies between 20 km and 43.9 km. The variation of the low velocity zone leads to variation of the lower boundary of the lithospheric mantle boundary at the depths ranging from 73.8 km and 85 km. in the same year. The same authors investigate the lithospheric structure of the Garoua rift that is the Northern part of CVL using the same teleseismic data. The main results obtained by the inversion of the receiver functions shown that, the lithosphere present a thin comportment in its crustal part with the mean Moho depth of 28 km and S wave velocity of 3.7 km/s. In its mantle part, the lithosphere present a thick comportment with the thickness that varying between 42 km and 67.2 km, with the deepest lithosphere situated at the center that is Garoua and least deep situated at Yagoua in the North. The Low velocity zone that permit to determine the lithospheric depth has also the thickness that varying between 42 km and 118.8 km. the synthetic receiver functions associated to shear velocity model show that the wave has really undergoes on one hand the conversion and multiple conversion with the existing phase Ps and subsequence reverberations PpPs and PpSs with the mean time of 3.7s, 11s and 17.6s respectively and the attenuation shown by the decreasing of the amplitude of those phases on other hand according to a South-North direction of Garoua rift.

I.4 Generalities of the receiver functions method

The receiver functions method is a powerful technique for imaging the crustal and upper mantle characteristics of the Earth especially at a local level. The basic idea of the receiver function method is that, the teleseismic waveforms contain information that can be used to predict and make the investigation of the crustal and mantle structures underneath seismic stations. In order to understand the receiver function method, some basic knowledge about the Earth's structure and seismology has to be introduced.

I.4.1. Structure of the Earth

In reality, the Earth has a shape that approximates to an oblate spheroid, and a complex structural interior. Looking into the Earth from the surface, the basic layers are the upper solid crust, rigid mantle, liquid outer core and solid inner core. Most earthquakes occur in the crust, and the crust-mantle boundary is called the Mohorovicic discontinuity, usually just named Moho. This Moho is identified by the increase and sudden decrease of body waves velocity. The thickness of the crust varies globally from 8 km under the Mid-oceanic ridges to 70 km under high mountains. A typical crustal thickness under continents is 30 km. The continental crust is often complicated and needs to be approximated by several layers. A crustal model may include soft and hard sediments, followed by upper, middle and lower crust. In some areas, the model may be simpler consisting only of upper and lower crust, separated by the Conrad discontinuity. The mantle extends to the core-mantle boundary (CMB). It is divided into the upper mantle and lower mantle by an area around 660 km of depth (the transition zone) where there are sharp velocity gradients. There is a world-wide low velocity layer in the upper mantle in the depth range of 100-250 km which is however not well developed or even absent under large precambrian cratonic areas. The relatively rigid mantle and crust above the low velocity zone is called the lithosphere while the area below is called the asthenosphere (extending down to about 400 km). The core is divided into the outer liquid core and the inner solid core with a sharp boundary at 5100 km.

One of the ways to describe the structure of the earth is a representation by a velocity model. The first modern earth model was made by Jeffreys and Bullen (1940) (JB-model). This was in the days before computers and represented a monumental amount of manual calculations. It is seen that the most pronounced discontinuity is at the core-mantle boundary where the P-velocity decreases drastically and no S-waves can pass due to the outer core being liquid. The JB-model was later revised, when much more data and computer power became available and in 1991, the IASP91 model was launched (Kennett and Engdahl, 1991). The latest generally recognized model is the AK135 (Kennett et al., 1995), which is an improvement over the IASP91, especially for

velocities in the earth's core and it is now considered as the best model for global earthquake location.

The parts of the Earth which are particularly important at the time of the application of the receiver function method are firstly the boundary between the crust and mantle, secondly, the lithosphere because it is shared between crust and mantle and contain the focus of earthquakes and lastly the transition zone.

I.4.2 Earthquakes

An earthquake (also known as a quake, tremor or temblor) is the shaking of the surface of the earth, resulting from the sudden release of energy in the Earth's lithosphere that creates seismic waves. Earthquakes are caused by faulting which is a sudden lateral or vertical movement of rock along a rupture (break) of the surface. It is recorded by a seismometer and the signal (seismogram) obtained is described as the convolution product of four functions given by the **equation (I.1)**.

$$S(t) = STF(t) * P(t) * I(t) * H(t) \qquad (I.1)$$

STF is earthquake source-time function, P is along-path effects function, I is instrument response function, H is possible effect of site function, t is the time and * is the convolution product.

The power of an earthquake can be quantified by its magnitude. The point of origin of an earthquake is called hypocenter or focus and it is located in the lithosphere. The point of the surface directly above the hypocenter is called the epicenter of the earthquake (**Figure I.4**).

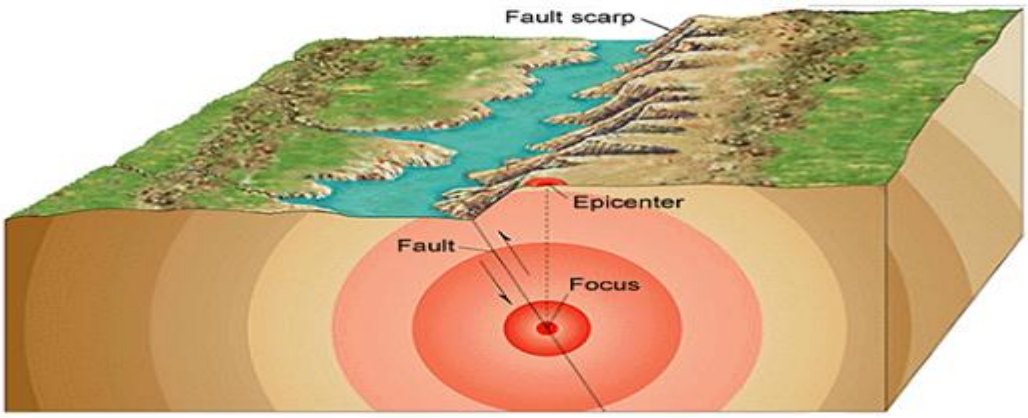

Figure I.4: Hypocenter and epicenter localization of earthquake (Victor, 1999)

Earthquakes can be classified using the origin, the magnitude and the epicentral distance.

a) Classification of earthquakes using the origin

There are four different types of earthquakes: Tectonic, volcanic, collapse and explosion.

- A tectonic earthquake is one that occurs when the earth's crust breaks due to geological forces on rocks and adjoining plates that cause physical and chemical changes.
- A volcanic earthquake is any earthquake that results from tectonic forces which occur in conjunction with volcanic activity.
- Collapse earthquake are small earthquakes in underground caverns and mines that are caused by seismic waves produced from the explosion of rock on the surface.
- An explosion earthquake is an earthquake that is the result of the detonation of a nuclear and (or) chemical device.

b) Classification of earthquakes using the magnitude

Seismologists once used words like small, medium or large to describe an earthquake size. After the introduction of the Richter magnitude-scale, depending on magnitude, one can distinguish six types of earthquakes **(Table I.1):**

Table I.1: Classification of earthquakes using magnitude

$M < 1$	Ultra-microearthquake
$1 < M < 3$	Microearthquake
$3 < M < 5$	Small earthquake
$5 < M < 7$	Moderate earthquake
$7 < M < 8$	Major or Large earthquake
$M \geq 8$	Great earthquake

c) Classification of earthquakes using epicentral distance

Following the epicentral distance (which is the distance from epicenter to any point of interest), one distinguishes three types of earthquakes:

- Local earthquakes: these are those whose the epicentral distance is lower or equal to 10°
- Regional earthquakes which are those whose epicentral distance is between 10° and 20°
- Teleseismic earthquakes which are those whose epicentral distance is between 20° and 103°.

I.4.3 Seismic waves

Seismic waves are waves of energy caused by the sudden breaking of rock within the earth or an explosion. These are the energy that travels through the earth and is recorded on seismographs. There are several different kinds of seismic waves (**Figure I.5**), and they all move in different ways. The two main types of waves are body waves and surface waves. Body waves

can travel through the earth's inner layers, but surface waves can only move along the surface of the planet like ripples on water. Earthquakes radiate seismic energy as both body and surface waves.

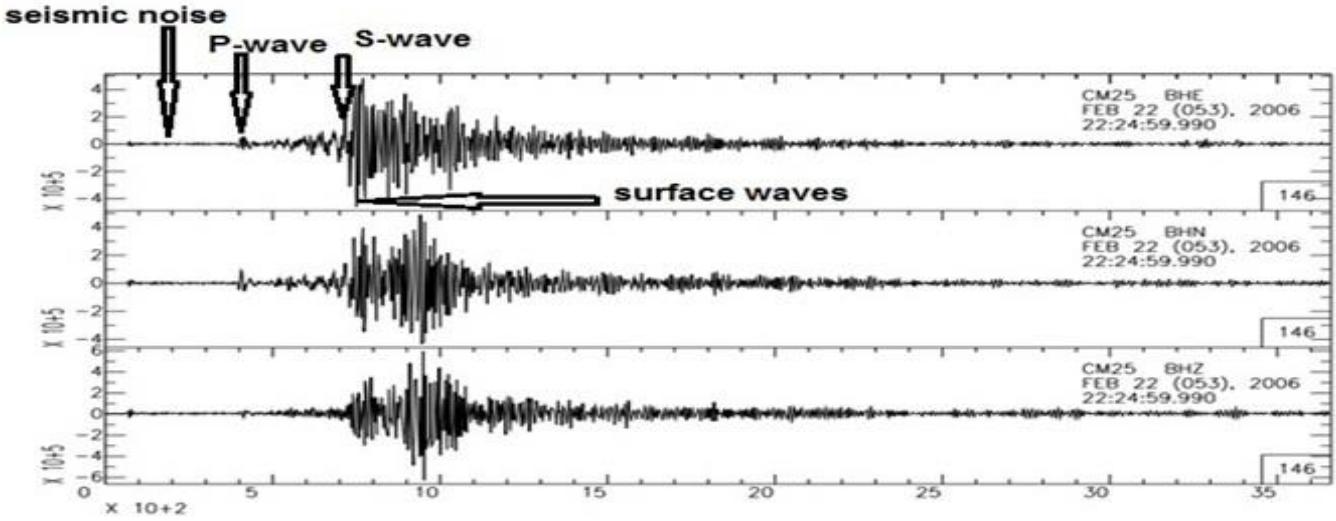

Figure I.5: Different types of seismic waves

a) Body waves

Body waves travel through the interior of the Earth along paths controlled by the material properties in terms of density and modulus (stiffness). The density and modulus, in turn, vary according to temperature, composition, and material phase. This effect resembles the refraction of light waves. Two types of particle motion result in two types of body waves: Primary and Secondary waves.

Primary waves or P-waves **(Figure I.6)** are compressional waves that are longitudinal in nature. They are pressure waves that travel faster than other waves through the earth to arrive at seismograph stations first, hence the name "Primary". These waves can travel through any type of material, including fluids, and can travel nearly 1.7 times faster than the S waves. In air, they take the form of sound wave, hence they travel at the speed of sound. Typical speeds are 330 m/s in air, 1450 m/s in the water and, about 5000 m/s in the granite. This is the fastest kind of seismic wave and its velocity is given by **equation (I.2)**.

$$V_P = \sqrt{\frac{K+\frac{4}{3}\mu}{\rho}} \quad \text{or} \quad V_P = \sqrt{\frac{\lambda + 2\mu}{\rho}} \qquad \textbf{(I.2)}$$

where ***K*** is the bulk modulus (the modulus of incompressibility), is the shear modulus (modulus of rigidity, sometimes denoted as ***G*** and also called the second Lame parameter), is the density of the material through which the wave propagates, and is the first Lam parameter.

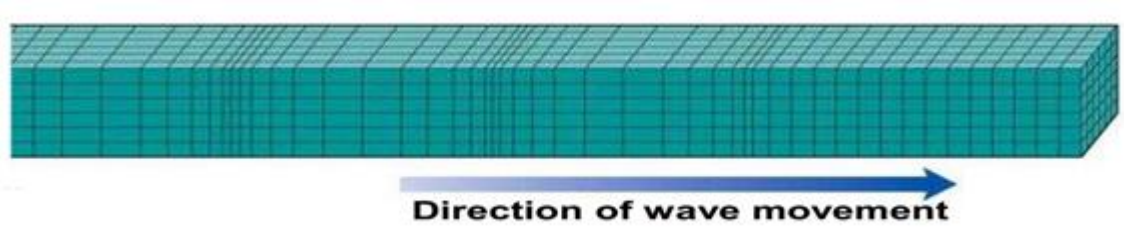

Figure I.6: Illustration of primary wave (Chapellier and Marie,1998)

S-waves or secondary waves **(Figure I.7)** are shear waves that are transverse in nature. Following an earthquake event, S-waves arrive at seismograph stations after the faster-moving P-waves and displace the ground perpendicular to the direction of propagation. Depending on the propagation direction, the wave can take on different surface characteristics; for example, in the case of horizontally polarized S waves, the ground moves alternately to one side and then the other. S-waves can travel only through solids, as fluids (liquids and gases) do not support shear stresses. S-waves are slower than P-waves, and speeds are typically around 60% of that of P-waves in any given material. The S-wave speed V_S given by **equation (I.3)** depends on the shear modulus and the density.

$$V_S = \sqrt{\frac{\mu}{\rho}} \qquad \textbf{(I.3)}$$

is the shear modulus (modulus of rigidity, sometimes denoted as ***G*** and also called the second Lamé parameter), is the density of the material through which the wave propagates,

An important distinguishing characteristic of an S-wave is its inability to propagate through fluids or gases because a fluid cannot transmit a shear stress and S-waves are waves that shear the material. In general, earthquakes generate larger shear waves than compressional waves and much of the damage close to an earthquake is the result of strong shaking caused by shear waves.

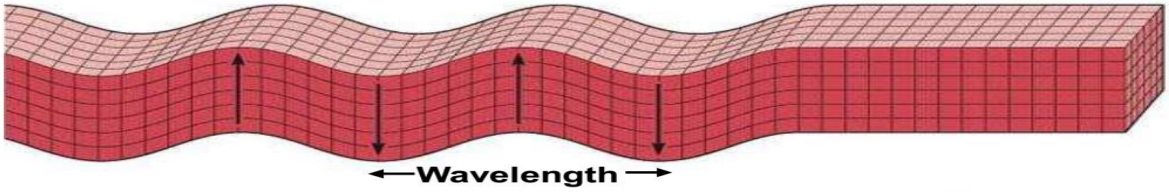

Figure I.7: Illustration of secondary wave (Chapellier and Marie, 1998)

b) Surface waves

Travelling only through the crust, surface waves are of a lower frequency than body waves, and are easily distinguished on a seismogram as a result of this. Though they arrive after body waves, it is surface waves that are almost entirely responsible for the damage and destruction associated with earthquakes. This damage and the strength of the surface waves are reduced in deeper earthquakes. They are subdivided into two types: Love waves and Rayleigh waves.

Love waves **(Figure I.8)** are the first kind of surface waves which, are transverse waves that vibrate the ground in the horizontal direction perpendicular to the direction that the waves are traveling. They are formed by the interaction of S waves with Earth's surface and shallow structure and are dispersive waves. The speed at which a dispersive wave travels depends on the wave's period. In general, earthquakes generate Love waves over a range of periods from 1000 to a fraction of a second, and each period travels at a different velocity but the typical range of velocities is between 2 and 6 km/s. Another important characteristic of Love waves is that the amplitude of ground vibration caused by a Love waves decreases with depth. Like the velocity, the rate of amplitude decrease with depth also depends on the period.

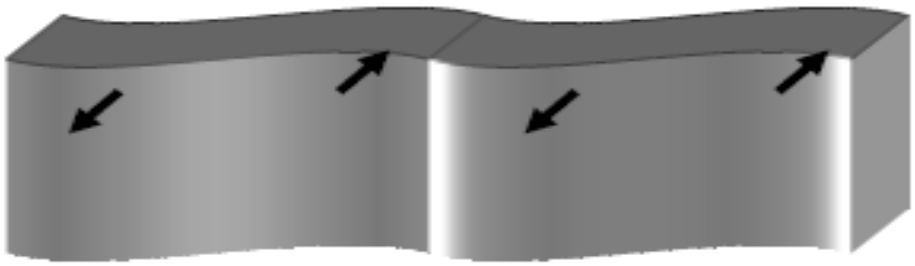

Figure I.8: Illustration of Love wave (Chapellier and Marie, 1998)

Rayleigh waves **(Figure I.9)** are the slowest of all the seismic wave types and in some ways the most complicated. Like Love waves they are dispersive so the particular speed at which they travel depends on the wave period and the near-surface geologic structure, and they also decrease in amplitude with depth. Typical speeds for Rayleigh waves are on the order of 1 to 5 km/s.

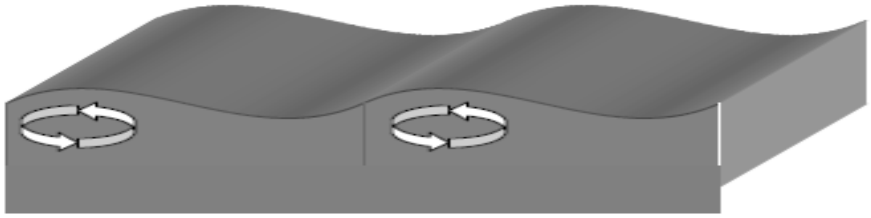

Figure I.9: Illustration of Rayleigh wave (Chapellier and Marie, 1998)

I.4.4 Seismic waves propagation

The difference in wave speed has a profound influence on the nature of seismograms. Since the travel time of a wave is equal to the distance the wave has traveled, divided by the average speed the wave moved during transmission, it is expected that the fastest waves arrive at a seismometer first. Thus, if a looked is taken at a seismogram (**Figure I.5**), it is expected to see the first wave to arrive to be a P-wave (the fastest), then the S-wave, and finally, the Love and Rayleigh (the slowest) waves. Although we have neglected differences in the travel path (which correspond to differences in travel distance) and the abundant waves that reverberate within Earth, the overall character is as have been described. The fact that the waves travel at speeds which depend on the material properties (elastic moduli and density) allows seismic wave observations to be used to investigate the interior structure of the planet. The travel times, or the travel times and the amplitudes of waves are used to infer the existence of features within the planet, and this is an active area of seismological research. To understand how to "see" into the earth using vibrations, a study of how waves interact with the rocks that make up earth must be undertaken. Several types of interactions between waves and the subsurface geology (i.e. the rocks) are commonly observable on seismograms namely: refraction; reflection; dispersion; diffraction and attenuation

a) Refraction and reflexion

When a wave encounters a change in material properties (seismic velocities and / or density) its energy is split into reflected and refracted waves. If a P wave hits a boundary between different seismic velocities, four different waves may be generated: a transmitted P wave; a converted transmitted S wave purely polarized in the vertical plane of propagation (SV-wave); a reflected P wave; and a reflected converted SV wave **(Figure I.10).** The geometry of these waves is also governed by Snell's Law given by **equation (I.4)**.

$$\frac{\sin i}{V_{p1}} = \frac{\sin j}{V_{s1}} = \frac{\sin i'}{V_{P2}} = \frac{\sin j'}{V_{S2}} \qquad \textbf{(I.4)}$$

In the case of an S_H wave hit the boundary, which is purely polarized in the horizontal plane, there is only a transmitted and a reflected SH wave, but no conversion into P or SV possible. If a single incident wave is split into multiple scattered waves, energy must be partitioned between these waves.

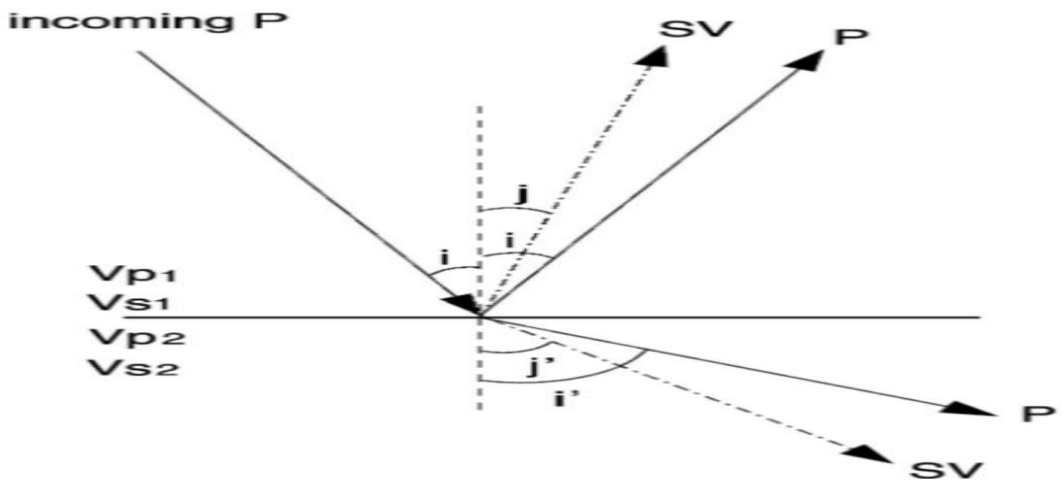

Figure. I.10: An incident P wave at a solid-solid boundary (shown is the case where $v_1 < v_2$) generates a reflected and a transmitted P waves and a reflected and transmitted SV wave. Snell's Law governs the angular relationship between the rays of the resultant waves (modified by Bormann Peter, 2000)

b) Dispersion

The penetration depth below the surface increases with wavelength **λ** of the wave. This is comparable to the frequency-dependent skin effect of electromagnetic waves propagating in a conducting medium with a free surface. Since the types of rocks, their rigidity and bulk modulus change with depth, the velocities of surface waves change accordingly since the longer waves reach deeper parts of the Earth. This results in a frequency dependence of their horizontal propagation velocity, called dispersion. Accordingly, while body-wave arrivals with no or negligibly small dispersion only (due to intrinsic attenuation) appear in seismic records as rather impulsive onsets or short transient wavelets (with the shape and duration depending on the bandwidth of the seismograph), the dispersion of surface waves form long oscillating wave trains. Their duration increases with distance.

c) Diffraction

Diffraction is the phenomenon of transmission of energy by non-geometric ray paths. In seismology, diffraction occurs whenever the radius of curvature of a reflecting interface is less than a few wavelengths of the propagating wave. Seismic diffraction is important for example in steep-angle reflection data in the presence of sharp boundaries. But there are also long-period diffracted waves such as P_{dif} and S_{dif} which are "bended" around the core-mantle boundary into the core shadow zone beyond about 100° epicentral distance. Only little short-period P- and S-wave energy is observed in this shadow zone. In fact, the edge of a discontinuity/impedance

contrast acts like a secondary source according to Huygen's principle and radiates energy forward in all directions.

d) Attenuation

Amplitudes of seismic waves are not only controlled by geometrical spreading or focusing and by the reflection and transmission coefficients that occur at discontinuities. Besides this, wave amplitudes may be reduced because of energy loss due to inelastic material behavior or internal friction during wave propagation. These effects are called attenuation. Also, scattering of energy at small-scale heterogeneities along the travel paths may reduce amplitudes of seismic waves. In the case of such scattering attenuation, however, the integrated energy in the total wavefield remains constant, while attenuation results in loss of mechanical wave energy, e.g., by transformation into heat. The wave attenuation is usually expressed in terms of the dimensionless quality factor Q given by **equation (I.5)**.

$$Q = 2\pi E/\Delta E \qquad \textbf{(I.5)}$$

where ΔE is the dissipated energy per cycle. Large energy loss means low Q and vice versa, i.e., Q is inversely proportional to the attenuation.

I.4.5 The receiver functions

A receiver function is defined as the response of the velocity structure beneath a seismic receiver (seismic station) to an impulsive plane wave generated by an earthquake at teleseismic distance. These responses originate from the different paths traveled by waveforms from teleseismic waves. When a propagating body wave hits an interface, the waveform energy is transmitted, reflected, and possibly converted, depending on the properties of the interfacing materials and the incident angle of the wave. The Moho is an example of such an interface, specifically a solid - solid interface as it is the boundary between solid crust and mantle. As a P-wave travels up through the mantle and hits the Moho, most of the waveform will continue transmitted as a P - wave, while some part of the waveform will be converted and transmitted as an S - wave. These waves arrive at the seismic station as responses identified as the Direct P wave and Ps. The reflection of the transmitted P-waves at the interface can cause multiple conversions (PpPs, PsPs) which are wave signals reflected back up from the Moho interface (**Figure I.11**). In addition, some of the initial waveform is "lost", as it is reflected back down into the mantle as P and S - waves; these waves are for the receiver function method not considered. Reflections that are to be considered however, are the reflections occurring at the free surface (crust - air interface).

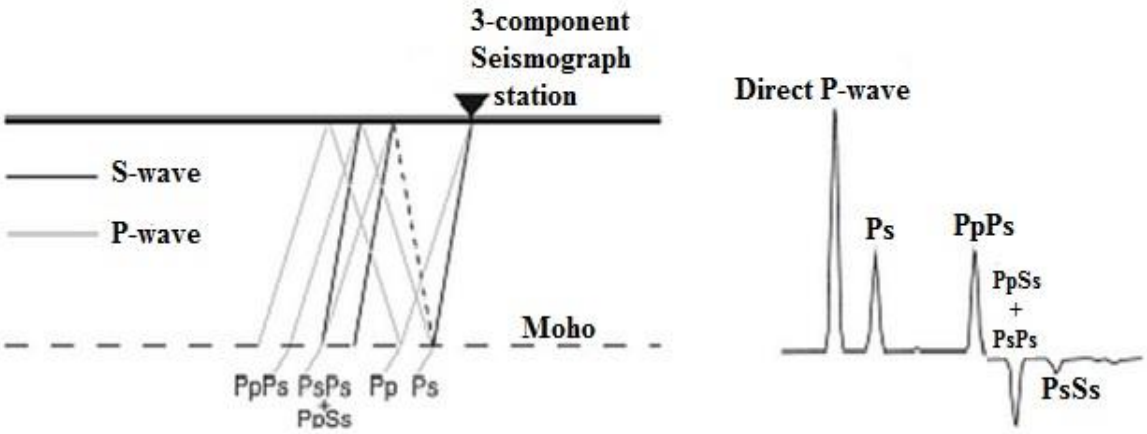

Figure I.11: Receiver function analysis of Earth structure beneath a seismograph station (left). The arrivals, and subsequent reverberations, can be isolated by receiver function analysis (right) (modified by Ammon, 1991)

The receiver functions are estimated by deconvolving the vertical component of a teleseismic P-wave record from its radial component. The concept is simple, but reliable implementation is difficult. The implementation difficulties stem from the instability of deconvolution. This has led to the use of a variety of stabilization methods in order to estimate the receiver function. They include frequency domain déconvolution; water level deconvolution (Langston, 1979); Owens et al., 1984; Ammon, 1991) and iterative time domain deconvolution performed by Ligorría and Ammon (1999).

Mathematically, three components seismic waveform recording **D** in time domain due to a teleseismic *P* wave can be written as **equation (I.6**) (Langston, 1979):

$$D_Z(t) = S(t)*I(t)*E_Z(t)$$

$$D_R(t) = S(t)*I(t)*E_R(t) \qquad \textbf{(I.6)}$$

$$D_T(t) = S(t)*I(t)*E_T(t)$$

where, I(t) is the impulse response of the instrument, S(t) is the seismic source function, E(t) is the impulse response of the local earth structure and * is the convolution operator, subscripts V, R and T represent the vertical, radial and tangential components, respectively.

a) Frequency domain deconvolution

In the frequency domain one can express the seismic waveform recording D as **equation (I.7)** by using the Fourier transform.

$$\mathbf{D_V(w) = S(w) \times I(w) \times E_V(w)}$$
$$\mathbf{D_R(w) = S(w) \times I(w) \times E_R(w)} \qquad \textbf{(I.7)}$$
$$\mathbf{D_T(w) = S(w) \times I(w) \times E_T(w)}$$

where $Dv(\omega)$ is a Fourier Transform of $Dv(t)$. From the above equation, source and instrument terms can be eliminated by simple division to produce radial receiver function, $H_R(\omega)$ given by **equation (I.8):**

$$H_R(w) = \frac{D_R(w)}{D_V(w)} = \frac{E_R(w)}{E_V(w)} \qquad \textbf{(I.8)}$$

Langston (1979) noted that, the vertical component of ground motion for a steeply incident *P* wave consists of a large direct arrival followed by only minor arrivals due to crustal reverberations and phase conversions. Therefore, he proposed $E_V(t) \approx \delta(t)$, where, $\delta(t)$ is the Dirac delta function. This is referred as source equalization scheme. And thus, $H_R(\omega) \approx E_R(\omega)$. The radial receiver function is therefore approximately equal to the radial impulse response of the earth structure, similarly the tangential receiver function, $H_T(\omega) \approx E_T(\omega)$. In the presence of noise as in real data, the approach is unstable. Therefore **equation I.8** was modified following *Clayton and Wiggins* (1976). The modification involves introduction of a minimum allowable amplitude level, the water level, for the amplitude spectrum of the vertical component.

b) Water-level Deconvolution

Langston (1979) developed a procedure that use the water-level stabilization method (Clayton and Wiggins, 1976) and a low-pass Gaussian filter to remove high-frequency noise not filtered by the water-level. The water-level deconvolution is the way to avoid division by small numbers by replacing small values in the denominator with a fraction of the maximum value (for all frequencies) value of the denominator. This fraction is called the water-level parameter (the water-level is the fraction multiplied by the maximum denominator amplitude), and is chosen by trial and error techniques. The consequence of replacing small values with larger values in the denominator is an attenuation of frequencies for which the vertical component has small amplitude. At times the water-level can act as a high-pass, low-pass, and notch filter. An illustration of the water-level deconvolution is shown on **Figure I.12**.

Using the conjugated complex Z^* of Z, **equation (I.8)** can be rewritten as follow

$$H(\omega) = \frac{R(\omega)Z^*(\omega)}{Z(\omega)Z^*(\omega)} \qquad \textbf{(I.9)}$$

Thus, the water level method substitutes **equation (I.9)** with

$$H(\omega) = \frac{R(\omega)Z^*(\omega)}{\phi(\omega)} G(\omega) \qquad \textbf{(I.10)}$$

Where $\phi(\omega) = \max\left[Z(\omega)Z^*(\omega), c\max\left\{Z(\omega)Z^*\right\}\right]$,

and $G(\omega) = \xi \exp\left(\frac{-\omega^2}{4a^2}\right)$,

c is the water level parameter, ξ stands for the normalization parameter, and $G(\omega)$ is a Gaussian filter.

The width ***a*** of the Gaussian filter is chosen such that, the width of the Gaussian match the width of the direct P-wave (Langston, 1979).

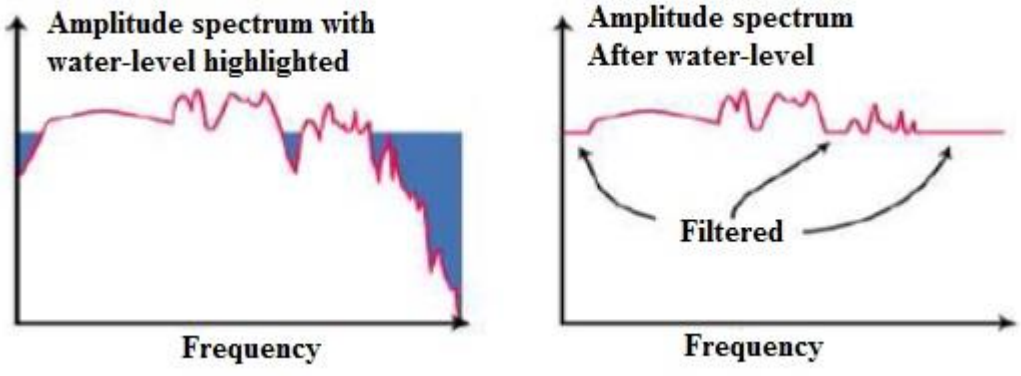

Figure I.12: The water level deconvolution method. (Ammon, 1997).

Careful parameterization is important to construct reliable receiver functions from waveform data because it is critically dependent on two parameters *a* and *c*. The Gaussian width factor *a* is approximately chosen to exclude the high frequency noise introduced during deconvolution or limit the effect of high frequency scattered energy (Langston, 1979). The choice of *c* for a particular deconvolution is not always clear cut. This can be interpreted as a factor, which trades off amplitude resolution with arrival time resolution. If *c* = 0, the deconvolution is the best estimate of the true impulse response and therefore provides the best arrival time resolution.

If *c* = 1, the deconvolution represents the least-square estimate of the true arrival amplitude. As the relative amplitudes of phases within the seismogram are of prime interest, the value of *c* is selected as small as possible for a better resolution of arrival times. Therefore, the trade-off is between the arrival time resolution and noise level. In practice, the deconvolution is

performed for every event over a range of *c* values (0.0001to 1) and the judgment is made based on the result.

The true or the absolute amplitudes of the receiver function is estimated by deconvolving the vertical component from itself (using the same water level parameter as in the horizontal component deconvolution), called the averaging function, and then normalize the horizontal receiver function by the maximum amplitude of this "vertical component" deconvolution. These account for the amplitude modification to the receiver function, which results from the water fill stabilization. True amplitude receiver function retains the relative amplitude of the converted phases to the direct P-wave arrival. Ammon (1991) and Cassidy (1992) showed the use of true amplitude to get information on the shallow structure and dipping interfaces, respectively and found this as more robust than the techniques of modeling normalized amplitudes.

c) Iterative time domain deconvolution

Iterative deconvolution is a time domain technique, originally developed to estimate large earthquake source time functions (Kikuchi and Kanamori, 1982) and later adopted to the receiver function computation (Ligorria and Ammon, 1999). To proceed with this technique, the vertical and horizontal components of the seismogram are cross correlated. A receiver function peak is placed at a time lag corresponding to the point of maximum cross correlation. Then this estimate of the receiver function is convolved with the source wavelet to create a prediction of the observed trace, and the result is subtracted from the original observed trace. This process is iterated until a certain value of misfit is reached (Ligorria and Ammon, 1999). Here, receiver functions are interpreted as linear combinations of Dirac delta function *δ(t)*, shifted in time, each of them related to a different ray reverberating through the layers beneath the recording station. Mathematically, receiver function signal can be written as **equation (I.11):**

$$\mathbf{RF\ (t)} = \sum_{i=1}^{n} a_i\ \delta(t - t_i) \qquad \mathbf{(I.11)}$$

where a_i is the amplitude of the Dirac delta function at time t_i, obtained at the $\mathbf{i^{th}}$ iteration. Iterative deconvolution method follows a least square minimization of the difference between observed horizontal seismogram (radial component in receiver function) and predicted signal generated by the convolution of an iteratively updated spike train with the corresponding vertical component seismogram. This method is based on the use of cross-correlation function to estimate the lag and amplitude of the 26 spikes that compose the final receiver function. The following steps are involved at each iteration *i* for computing iterative deconvolution:

(i) Cross-correlation between the radial component $\left(R^{(i-1)}\right)$ and the vertical component (V) (where $R^{(0)}$ is the original radial seismogram).

(ii) Location of time t_i of cross-correlallogram's maximimum amplitude a_i'

(iii) Determination of scalar coefficient a_i that best fits the time shifted V component with $R^{(i-1)}$. It consists of minimizing the quantity:

$$\mathbf{C} = \left|\boldsymbol{R^{(i)} - a_i V * \delta(t - t_i}\right|^2 \quad \textbf{(I.12)}$$

where * is convolution operator and $\boldsymbol{a_i}$ is given by: $a_i = a_i'$ / V.V, where dot is the zero time cross-correlation.

(iv) Addition of Dirac delta function of amplitude a_i at time t_i to the current receiver function.

(v) Calculation of residual $R^{(i)}$ from $R^{(i-1)}$ using the relation:

$$\boldsymbol{R^{(i)} = R^{(i-1)} - a_i V * \delta(t - t_i)} \quad \textbf{(I.13)}$$

(vi) Return to the next iteration. The process is stopped when misfit between the receiver function convolved with the vertical component and the radial component with additional spikes becomes insignificant or when most of the R component energy is reduced. **Fguire I 13** show the receiver function compute by iterative time domain deconvolution

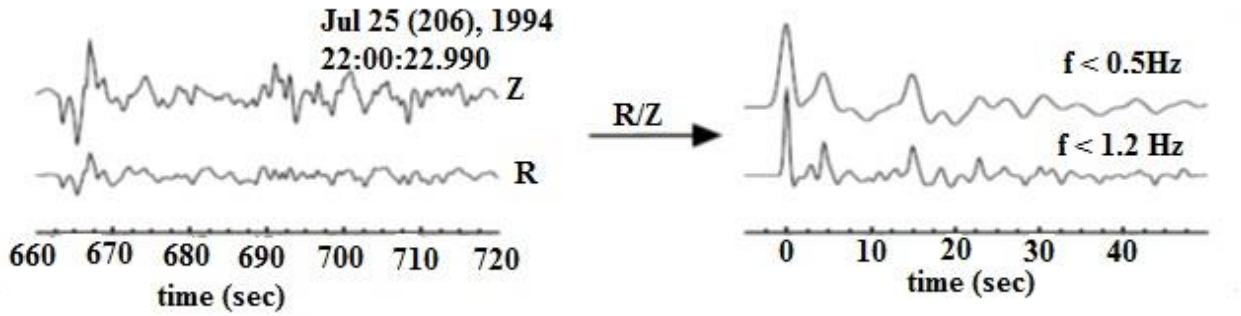

Figure I.13: Example showing radial receiver functions computed using the iterative time domain deconvolution by Ligorria and Ammon (1999) with a real data**.** There are computed for two overlapping frequency bands corresponding to Gaussian width factors a = 1.0 and a = 2.5 (from Julia et al., 2005).

Comparing the different types of deconvolution technique, it came out that: The frequency domain techniques suffer more from side lobe residue at the base of receiver function peaks because of numerical artifacts from the Fast Fourier Transform (FFT) and the time domain methods require a longer run-time but offer more flexibility and reduce the existence of side lobes.

They are also desirable because they are fully-automated and provide an objective mechanism for stopping the iterations and the percent change of the misfit. Because the user can self-select the shape of the receiver function peaks, the results of the time domain method presented by Liggoria and Ammon (1999) verge on looking almost too good and give a sense of false security. However, the forward method is preferable when the data set is small or smaller events are being used because it spikes the major features of the receiver function first before looking at the smaller details (Liggoria and Ammon, 1999**).**

1.4.6 The receiver functions method

Receiver function method is a passive seismic method commonly used by geophysicists to image discontinuities and estimate layer thicknesses within the crust and upper mantle structures beneath a seismic station. The method is based on the energy converted either from P- to S- or from S- to P-wave energy at the velocity discontinuities below a recording seismic station. So there exists two types of receiver function methods

a) P receiver functions method

Seismic phases converted from P to S underneath the receiver are particularly useful in studies of the crust and mantle (Ammon, 1991). Due to the lower velocity of S waves in comparison to P waves, the converted S waves arrive after the onset of the direct P wave within the P wave coda path. By extracting the small P-to-S (Ps) converted energy from the large P wave and measuring the time delay between the two phases, it is possible to "map" seismic discontinuities beneath stations. The frequency band of teleseismic body waves covers the range of one to several seconds and thus lies between controlled source methods (several Hertz) and surface-wave methods (many seconds). The theoretical background of the technique was described by Vinnik (1977), Burdick and Langston (1977), Langston (1979), Owens et al. (1984), Kind and Vinnik (1988), Kosarev et al. (1999), and Zandt et al. (1986).

The essential points in processing the observed data are:

- If data from different types of seismic sensors and/or short-period seismic stations with different frequency responses are used, it is necessary to restitute the broad-band ground displacement in order to make the signals better to compare. However, restoring longer periods from short period instruments is only possible for large magnitudes and depends on the transfer function of the sensor and the sampling rate. Furthermore, long period noise is also increased by restitution. The main frequencies of teleseismic body waves lie between 1 Hz and 0.1 Hz. High-pass filtering may be necessary after restitution to suppress long period noise.
- Rotation of the original EW, NS and Z components of the P-wave group into the ray coordinate system R, T and Z. R contains mainly P-energy, T mainly SV-energy, and Z mainly

SH-energy. The theoretical back azimuth is used to determine the radial component, and the angle of incidence is determined from the radial-vertical covariance matrix of the P-signal of the original data. This energy depends mainly on the S-velocity distribution underneath the station (Kind and Anderson, 1995).

- Deconvolution of the R and T-components with the P-signal on the Z-component in the time domain. Deconvolution is used as a source-equalization procedure because it excludes effects of the rupture process and of the ray-path below the converting interfaces. Differences in the source durations and magnitudes are equalized, permitting the summation of many different events. Amplitude ratios are preserved by this procedure. The P waveform on the Z-component is used to generate the time-domain wave shaping deconvolution filter. After deconvolution, all components are normalized to the maximum of Z (Kind et al., 1995).
- Summation of many events from a large distance and azimuth range. Before summation, the data are corrected for distance move-out for direct P-to-S conversions using the IASP91 reference model (Kennett, 1991; Kennett and Engdahl, 1991) and a standard slowness of 6.4 s per degree, corresponding to a reference epicentral distance of 67° (Yuan et al., 1997). Thus, summation of records from different distances is possible in order to improve the signal-to-noise ratio and therefore the stability and reliability of the observations.

The processed receiver functions are usually filtered in order to enhance signals and to suppress noise. The choice of an inappropriate filter can heavily influence the information contained in the recorded data. Since the recorded signals have to be assumed to be mixed phase, the processing of the data avoids pre-filtering of the data.

b) S receiver function method

While the receiver function method analysing P-to-S conversions (P receiver function method) has been used successfully for quite a long time to investigate the crust and mantle structures, the study of S-to-P (Sp) conversions (**Figure I.14**) is not a routine method yet. Although there are early works using S-to-P conversions (e.g. Bath and Stefánnson, 1966; Burdick and Langston, 1977; Sacks and Snoke, 1977; Bock and Kind, 1991), the use of these phases has only recently become more popular after receiver function analysis, meaning coordinate rotation and deconvolution, was also applied to the S waves in order to isolate the S-to-P converted phases from the incident S phases (Farra and Vinnik, 2000; Vinnik and Farra, 2002; Vinnik et al., 2003; Vinnik et al., 2004). Hence, this method is called S receiver function method. It was applied by Li et al. (2004), for mapping particularly the lithosphere-asthenosphere transition. A comprehensive overview about the S receiver function method applied to synthetic seismograms is given by Yuan et al. (2006). As the converted P leg of the ray travels with a higher wave velocity than the direct S

leg, S-to-P converted phases arrive at the receiver prior to the S wave onset, while the multiple reverberations appear after the S onset. Boundaries such as the lithosphere asthenosphere transition, which are often obscured in the P receiver functions by crustal multiple reverberations arriving in the same time interval, can thus be better observed in the S receiver functions.

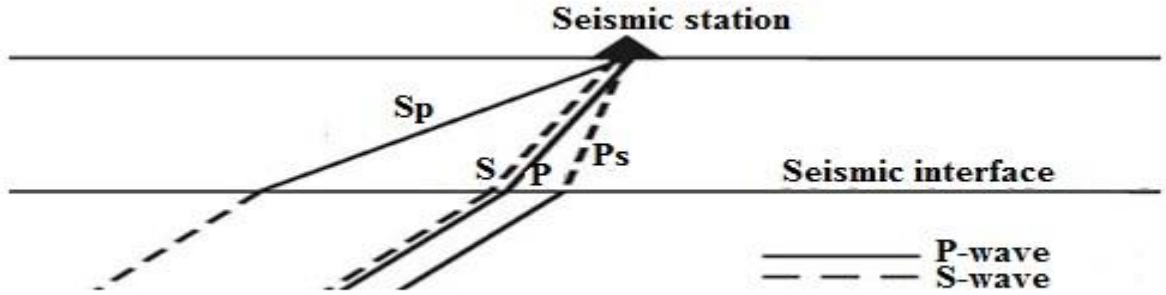

Figure I.14: Ray paths of Sp and Ps converted phases (modified after Vinnik et al., 2003).

c) Comparisons between the two methods

However, due to the ray geometry, the use of the S receiver functions has some limitations. Converted Sp phases from the lithosphere-asthenosphere boundary are best observed at epicentral distances between 60 - 85° (Faber and Müller, 1980; Yuan et al., 2006). S receiver functions are much noisier than P receiver functions, primarily because they arrive after the P wave. S waves have a lower frequency content, hence a lower spatial resolution than P waves. The conversion coefficients of the Moho for Sp conversions are negative and of the lithosphere-asthenosphere transition positive, i.e. the sign of amplitudes is opposite to those of Ps conversions. The sign of amplitudes depends on the definition of Z components (downward positive), the sign of the velocity contrast at the discontinuities (downward positive at Moho, downward negative at lithosphere-asthenosphere transition) and the polarity of the triggering phase. The absolute conversion coefficients of Sp phases decrease with increasing epicentral distance (Yuan et al., 2006). For epicentral distances of 60 - 85°, the conversion coefficient of the Moho varies between -0.165 and -0.12, and that of the lithosphere-asthenosphere transition between 0.043 and 0.024 (Yuan et al., 2006).

An important limitation to receiver functions in the vertical-radial (*Z-R*) coordinate system is that the *P* wave has non-zero incidence and is therefore not completely isolated onto the vertical component, which results in a large pulse at near zero lag-time in the deconvolved radial component. This near zero-lag pulse implies that thin layers near the surface may be poorly resolved due to the dominant energy near zero lag-time and the large negative side lobe arising from Gibbs effects. That important limitation is added at the fact that the Receiver functions are

sensitive to shear velocity contrasts and vertical travel times and they are non-unique velocity-depth trade off. The advantages is situated at a way to invert for S wave velocity (Vs) structure under a single station , a sensitive to gradients (discontinuities) in Vs velocity and needed complement to crustal tomography.

I.5 Problem statement and objective of the thesis

I.5.1 Problem statment

The Volcanic Province of Cameroon has become a large laboratory for geoscientists of the world because of its geologic diversity as, mountains (mount Cameroon; mounts Bamboutos; Oku mount and Mandaras mount), Plateaus (Adamawa plateau and Bamoun plateau) and a rift (Garoua rift). These volcanic centers have already been the subject of several geological and geophysical works. From the geophysical point of view, several works have been done using various types of data and methods. Among these works, one can cite those of Aretouyap et al. (2014) and Aretouyap et al. (2018) which uses the Krigage technique on geoelectrtic data in the Adamawa plateau Region. Earlier, Stuart et al. (1985) used artificial or active seismic sources to delimit the crust respectively to 23 km and 33 km of depth to the North and to the South of the Garoua rift plateau. Later, the same data base was used by Tabod et al. (1992) to show the existence of a Low Velocity Zone and further indicate the thickness of the crust to about 33 km in the continental part of the Cameroon Volcanic Line. Poudjom et al, (1997) used gravity data to limit the lithosphere to around 80 km in the Adamaoua plateau region after having confirmed the existence of the Low Velocity Zone already evoked by Tabod et al. (1992). Marcel et al. (2010) used airborne gravity data to suggest an asthenopheric upwelling and the limit of Moho to between 19 km and 34 km along the Cameroon Volcanic Line. Tokam et al. (2010) applied a new technique (receiver functions method) on the passive seismic data coming from the earthquakes recorded between 2005 and 2007. In this last work, surface waves are extracted and inverted to delimit the crust along the Cameroon Volcanic Line to between 35 km and 39 km of depth.

From what precedes, everything becomes clear. Investigations of the lithosphere have been done with artificial seismic sources which led to interpretations leaning on inappropriate velocity models (Stuart et *al.*, 1985; Tabod et al. 1992 and Plomerova et al., 1993) or superficial structure in addition to being localized (Aretouyap et al., 2014 Aretouyap et al., 2018) and for layers limited to within 100 m of depth, in addition to the use of surface waves travelling only through the crust (Tokam et al., 2010) and tomographic models (Fishwick, 2010) that has limited vertical resolution. The other seismic investigations using the same surface waves travelling only through the crust provided important measurements and high-resolution image of the lithospheric structure in

Cameroon using the stack method of the receiver functions resulting from the surface waves (Gallacher and Bastow, 2012 and Guidarelli and Aoudia, 2016) or focused mainly on the mantle (Reusch, 2009), Reusch et al., 2010 and Reusch et al., 2011)**.** Equally investigations were also done with potential methods (Poudjom et al., 1995; Kamguia et al., 2005; Marcel et al., 2010; and Marcel et al., 2018) that present a low resolution power. Motivated by these partial studies of the lithosphere using the artificial sources, the potential method, the surfaces waves and equally by the fact that, the lithosphere-asthenosphere boundary remain a controversial subject in Earth science, and particularly beneath Cameroon Volcanic Line, another vision has been added to the analyses of data based on body waves, particularly the P-waves. This type has the advantage to arrive on first on the seismogram and contains in the first seconds of coda the information on the structure under the seismic station and having the properties to propagate beyond the crust for the study of the entire lithosphere.

I.5.2 Objective of the work

The main objective of this work is to establish the first 1-D S-velocity model of the lithosphere beneath the volcanic center of Cameroon in order to show the first model of the structure of the lithosphere. The last model will help us to delimit the Moho depth and the lithosphere-asthenosphere boundary (LAB) beneath the different volcanic centers of Cameroon follow by the comportment of the medium. To reach at this goal, we will select among the recorded earthquakes in the word between February 2005 and January 2007, the teseismic events having a magnitude $m_b \geq 5.5$ (because a certain signal strength is required) and epicentral distance ranges between 30° and 95°. Once this first step is finished, the second consists in extracting the temporal interval of the signal containing the primary P- waves. These waves will be treated thereafter by the receiver functions inversion method in order to obtain the 1-D S –waves velocity profile of the earth substructure at the mean depth of 200 km associated to the synthetic receiver functions.

The knowledge of the study area has permitted to highlight the context of our work and, to bring out the problematic. In addition, once the necessary tools to go ahead with the work will be mastered, it would be important to present the methods and the data in addition to the materials used on the land.

CHAPTER II:
DATA, METHODOLOGY AND PROCESSING

This chapter presents the data used, according to the equipment that permitted us to collect them. The methodology applied on the data is described and some results coming from the different steps of processing are presented. The inverse theory of the receiver functions is also presented to conclude this chapter.

II.1 Data

The data used in this study come from the Cameroon Seismic Array (CSA) that operated for two years from January 2005 to January 2007 through the ongoing project of seismic study of Cameroon, done in cooperation between Institute of Geologic and Mining Research (IRGM)-Cameroon) placed under the tutelage of the Ministry of the Scientific Research and Innovation (MSRI), The Pennsylvania State University (USA), The Washington University in St Louis (USA) and The University of Yaoundé 1 (Cameroon).

II.1.1 Equipments and network

Since the experiment was primarily devoted to geophysical study of the Cameroon Volcanic Line, the equipment (**Figure II.1**) used was consisted of:

- Four types of three components seismometers protected by sensors generally buried under the ground (Guralp CMG 3T; Guralp CMG 40T, Guralp ESP, Streckeisen STS-2) to record earthquakes,
- reftek Digital Acquisition System (DAS) to save data recorded by the sismometer,
- two batteries with solar panels to generate and maintain autonomy of energy to the batteries respectively
- GPS to collect the geographic information and the time

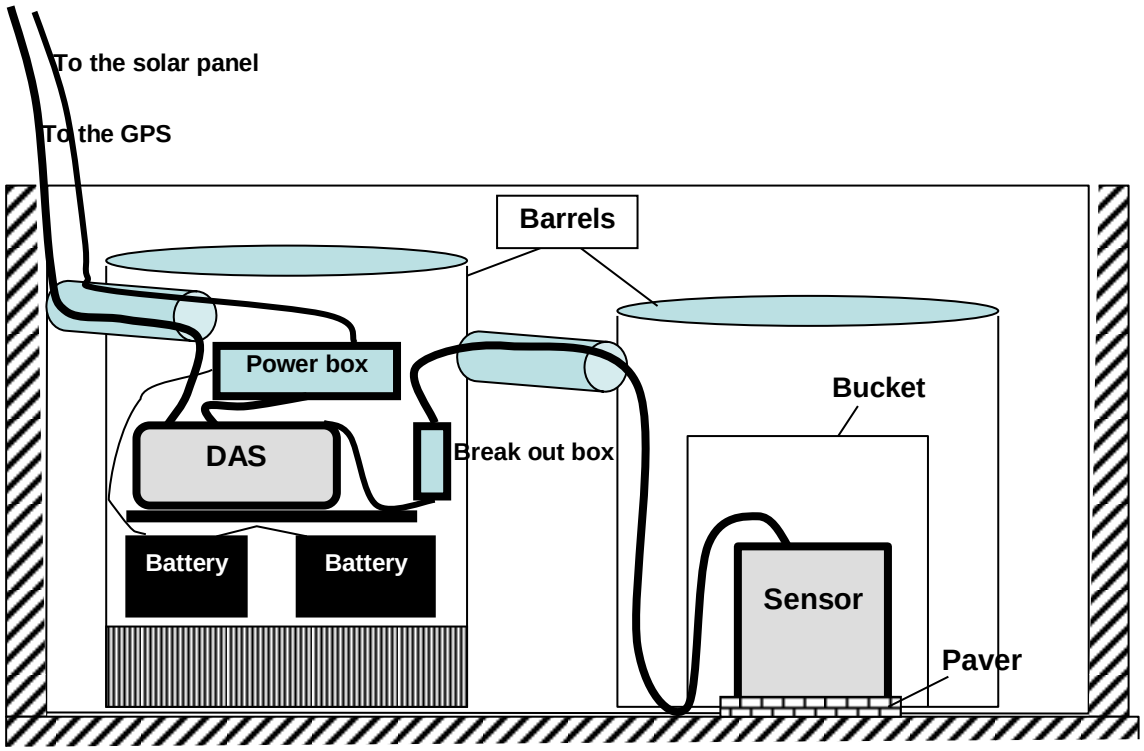

Figure II.1: Vertical section of one buried seismic station (modified after Tokam, 2010)

The sensor (seismometer), the GPS (clock) and the two 12 volts batteries are connected to the DAS through a breakout box. Data are recorded onto two disks (1 or 2 Gb capacity each) able to store up to 6 months of data. These equipments have been installed in 32 localities of Cameroon. The **Figure II.2** presents an example of the installation dispositive **(a)** at one area and

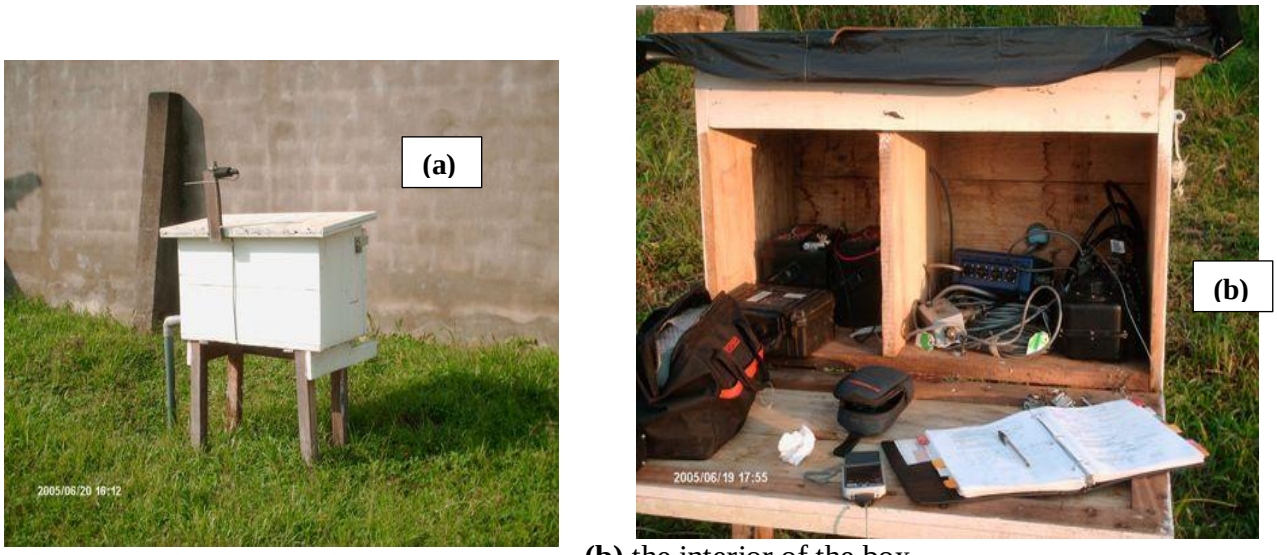

(b) the interior of the box.

Figure II.2: Installation of equipments (modified after Tokam, 2010)

II.1.2. Cameroon seismic station array

The location of seismic stations is usually constrained by both seismological and geological requirements. It is important that a seismic station be installed on hard rock to reduce the signal-to-noise level and to ensure good coupling of the instrument with the earth. The stations have to be situated across the structure of interest. Usually, the ideal sites for seismic stations are hardly convenient ones in the field. The location of the seismic stations thus depended upon:

- The accessibility of the area,
- The site noise level
- The safety and security of the site.

According to preliminary seismological and geological studies of the area, 32 stations were installed in Cameroon during the 2005-2007 periods.

a) Initial array (January 2005 – January 2006)

The Cameroon experiment started with the installation of an array of 8 seismic stations in January 2005 (**Figure II.3 red colour**). It was primarily intended to aid in resolving crustal and mantle features associated to presence of the Cameroon Volcanic Line (CVL). The array recorded 46 earthquakes throughout the world with the magnitude range between 4.5 – 6.4 on the Richter graduation. Particularly on March 19th, 2005, a local earthquake of magnitude 4.3 occurred in Monatele (Cameroon) and felt in Yaoundé and its neighborhoods, a few hundred kilometers from the epicenter. Many local earthquakes of lower magnitude were also recorded by the array, most of them having their epicenter close to Mount Cameroon

b) Extended array (January 2006 – January 2007)

The second stage of the Cameroon experiment started with the effective extension of the array with 24 (**Figure II.3 yellow colour**) additional broadband seismometers early January 2006 increasing the number of stations to 32. Thus the array could provide a large amount of data with a better resolution of station coverage (distance between two neighbor stations mostly in the range 50 ~ 150 Km) leading to high resolution regional or local studies. For that period, the array recorded 55 earthquakes throughout the world with the magnitude range between 4.5 – 6.5. **Table II.1** gives characteristics on the different stations used.

Table II.1: Characteristics of the different Cameroon seismic station array

STATION	TOWN	ONDATE	ONTIME	LATITUDE (°)	LONGITUDE (°)	ELEVATION (km)
CM01	Campo	2006017	12:07	2.3873	9.8321	0.028
CM02	Mintom	2006011	15:41	2.6984	13.2888	0.625
CM03	Yokadouma	2006017	15:45	3.5190	15.0344	0.557
CM04	Sangmelima	2006010	15:08	2.9792	11.9596	0.698
CM05	Kribi	2006016	11:51	2.9404	9.9121	0.027
CM06	Ambam	2005017	18:06	2.3850	11.2680	0.614
CM07	Yaounde	2005009	13:13	3.8700	11.4560	0.741
CM08	Douala	2006013	17:51	3.9074	9.8612	0.035
CM09	Ekona	2005013	15:02	4.2340	9.3280	0.355
CM10	Ngambe	2006027	14:35	4.2234	10.6189	0.607
CM11	Abong Mbang	2006020	10:56	3.9803	13.1878	0.694
CM12	Ntui	2006024	16:32	4.4810	11.6337	0.466
CM13	Kumba	2006011	15:14	4.5870	9.4610	0.194
CM14	Batouri	2006016	14:53	4.4215	14.3583	0.628
CM15	Nkongsamba	2006012	16:52	5.0325	9.9314	1.068
CM16	Foumbot	2006028	12:30	5.4788	10.5709	1.079
CM17	Yoko	2006023	10:59	5.5461	12.3121	1.030
CM18	Mamfe	2005011	17:24	5.7230	9.3550	0.196
CM19	Magba	2006026	13:41	5.9736	11.2305	0.739
CM20	Wum (Obang)	2006020	16:04	6.2242	10.0523	0.605
CM21	Tibati	2006015	11:17	6.4657	12.6234	0.876
CM22	Ngaoundal	2006014	9:57	6.4758	13.2667	0.975
CM23	Ndu	2006027	13:26	6.3690	10.7914	2.017
CM24	Meiganga	2005015	9:52	6.5230	14.2880	1.052
CM25	Banyo	2006017	9:20	6.7588	11.8100	1.127
CM26	Ngaoundere	2005014	16:24	7.2650	13.5480	1.229
CM27	Tignere	2006018	12:46	7.3582	12.6659	1.118
CM28	Poli	2006020	9:07	8.4680	13.2356	0.481
CM29	Garoua	2005018	10:42	9.3470	13.3850	0.265
CM29	Garoua	2006026	10:42	9.3470	13.3850	0.265
CM30	Figuil	2006023	9:24	9.7558	13.9575	0.297
CM31	Yagoua	2006024	10:05	10.3266	15.2610	0.332
CM32	Maroua	2005020	13:35	10.6186	14.3718	0.422
CM32	Maroua	2005294	18:52	10.6186	14.3718	0.422

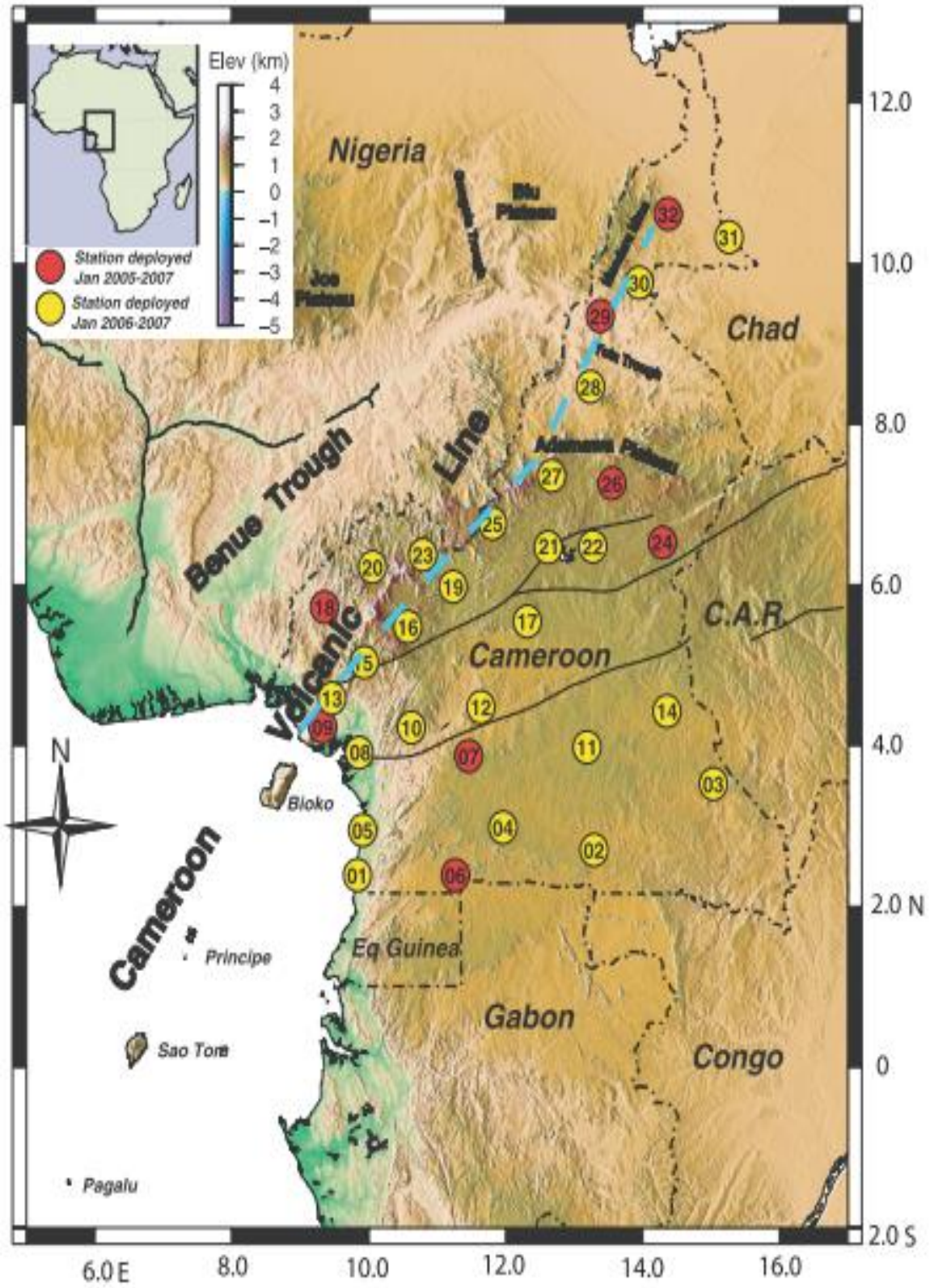

Figure II.3: Colour elevation map showing seismic station locations**.** The dashed light blue line shows the location of the Cameroon Volcanic Line profile. Circled numbers refer to station codes, for example, 01 refers to station CM01.

II.I.3 Dataset

During the two years of operation, (January 2005-January 2007) seismic data were recorded as a time series of the movement of the earth. Such a time series is called a seismogram and usually the movement in three directions (vertical Z, east-west EW, and north south NS) is recorded. Thus, around 146 earthquakes have been recorded by the 32 Cameroon seismic stations array. On these earthquakes, worldwide seismic catalogs were used to select teleseismic events recorded by the CSA (Cameroon Seismic Array) during its running time period to construct a list of events which was used to request data from IRIS, in SAC digital format. These data were later used to compute the receiver functions to achieve the objective of this work. After, the teleseismic events that occurred at epicentral distances between 30° and 95° (because for measurements closer than 30°, the P-wave of the waveform is complicated by upper mantle travel path effects. On the other hand, if it is farther than 95°, the station is located within the shadow zone of the direct P-wave) with magnitudes $M_b \geq 5.5$ (Table II.2) were selected (because a certain signal strength is required and earthquakes with smaller magnitudes do not generate clear peaks and troughs in the waveforms)**.**

Table II.2: Events with magnitude $M_b \geq 5.5$ used for the study

Event date mm/dd/yy	Event time h:min:s	Latitude(°)	Longitude (°)	Depth (km)	Magnitude	Epicentral distance(°)
10/20/05	21:40:04:01	38.152	26.751	10	5.5	33.1
12/05/05	12:19:56:06	-6.224	29.83	22	6.4	21
12/09/05	23:30:23:09	-6.176	29.709	10	5.5	20.9
01/08/06	11:34:55:06	36.311	23.212	66	6.5	30.2
02/22/06	22:19:07:01	-21.324	33.583	11	6.5	34.5
03/15/06	14:19:48:07	-21.136	33.719	10	6.5	33.9
09/17/06	07:30:11:00	-17.694	41.827	10	5.5	37
09/24/06	22:56:21:07	-17.737	41.814	10	5.6	37.5

II.2 Methodology and processing

II.2.1 Methodology

The receiver function methodology has been used to investigate the lithospheric structure across the volcanic province of Cameroon. The technique was first introduced by Langston (1979, 1981) to examine crustal structure beneath three components recording stations while Vinnik (1977) had taken a similar approach to detect upper-mantle discontinuities by introducing delay and some techniques. Since then the method has been developed steadily. A significant

improvement of the resolution of the technique occurred by utilizing unique advantages of the digital broad-band data (e.g. Owens et al., 1984) and as the technique was applied to data from arrays and networks of seismometers and hence producing receiver function images along profiles. The description of this technique has been done well previously in the chapter I. This study uses receiver function analysis as the main method of investigation to construct a model for the S-wave velocity structure using teleseismic P-waves arriving at a receiver. When the waves arrive, they contain valuable information about the structure near the source, mantle path effects and the structure of the crust directly beneath the receiver. The receiver function is calculated by deconvolution of the radial component from the vertical component of the P-waveforms. There is some pre-processing (preparation of seismogram) concerning the seismogram to do before computing the receiver function.

II.2.2 Processing

This treatment has been done from the computer software in the seismology package written by Herrmann and Ammon (2002) that is: Application Coding (**GSAC**) which is a software server that does the rotation of the seismic events components; the Seismic Analysis Code (**SAC**) which is a software of computation of the receiver functions passing through of signal filtering, windowing of the seismograms and deconvolution of the signal; Computer Programs of Seismology (**CPS**) that is a software used in the inversion of the receiver functions to get the velocity models structure; the Generic Mapping Tool (**GMT**) which is a software used for the representation of the seismic stations. The processing follows two procedures:

- computation of the receiver functions
- Inversion of the receiver functions

II.2.2.1 Computation of the receiver functions

Receiver Functions were successfully computed using data from 146 teleseismic earthquakes **(Annex 1)** that occurred between 30° and 95° epicentral distance with magnitude greater or equal to 5.5. **Figure II.4** illustrates the geographic location of the different events used to compute the receiver functions.

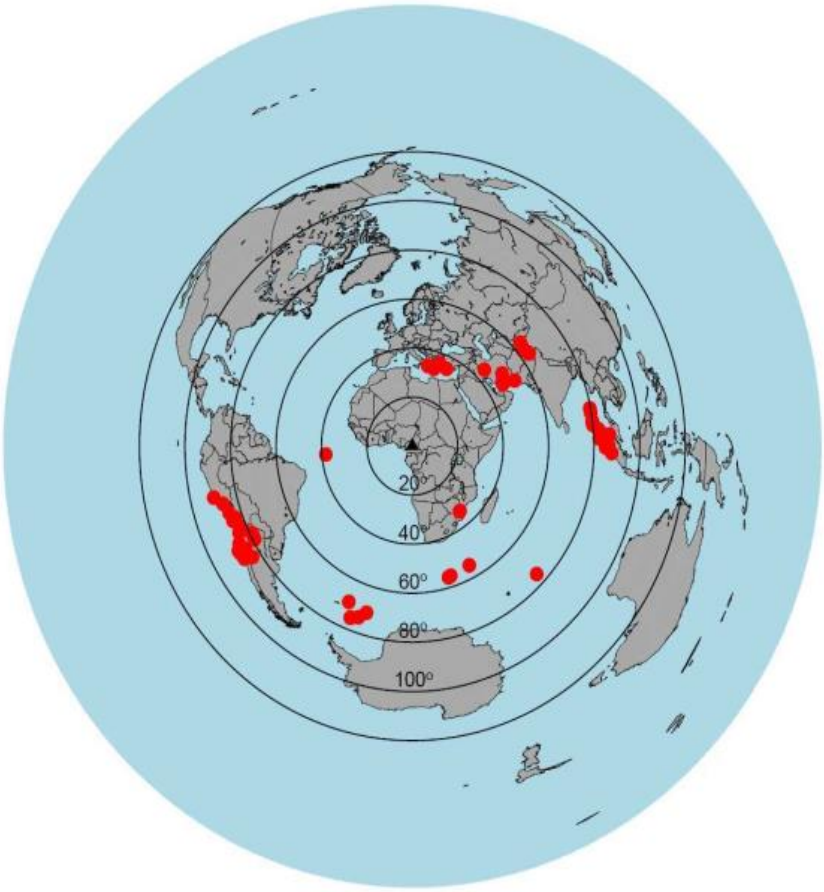

Figure II.4. Geographic location of teleseismic events used to estimate thereceiver functions (small solid red circles). The solid black triangle is the centre of the Cameroon seismic network. Large circles show distance in 20° increments from the centre of Network.

The computation of the receiver functions obeys two main steps which are:

- Preparation of the seismogram which concerns the pre-processing
- Deconvolution of signal in order to obtain the receiver functions

a) Preparation of seismogram

This step respects the following procedures:

Data format: The program used in this study takes use of the Seismic Analysis Code (SAC) format. Thus, in order to continue the processing, a file conversion had to be performed. Because the recorded data are on the ASCII format, it is imperative to convert to the SAC format before all utilization. This is made by the command **asctosac**. This program converts a ASCII trace file to a SAC binary trace file. The advantage of Seismic Analysis Code (SAC) is that, in general, its purpose an interactive program designed for the study of time sequential signals. Emphasis has been placed on analysis tools used by research seismologists. A SAC data file contains a single

data component recorded at a single seismic station. Each data file also contains a header record that describes the contents of that file. Certain header entries must be present (e.g., the number of data points, the file type, etc.). Others are always present for certain file types (e.g., sampling interval, start time, etc. for evenly spaced time series). Other header variables are simply informational and are not used directly by the program. Although the SAC analysis software only runs on Unix platforms and the general format is binary, there is also an ASCII version that can be used on any platform.

- **Event selection:** Several million earthquakes occur in the world each year. There are however a few criteria that needs to be met in order for the earthquakes to be beneficial for imaging purposes. First, certain signal strength is required; this is dependent on the magnitude of the earthquake. Secondly, the event epicenter must be within a certain distance interval from the seismic station in order to get propagation paths resulting in signal arrivals usable for the receiver function method (wave propagation through the mantle and crust, resulting in P-S conversions). These waves are called teleseismic waves, and are for P-waves defined as waves originating from earthquakes at a radial distance farther than 30°. For the purposes of this thesis, only events with body wave magnitude greater than 5.5, occurring at epicentral distances between 30° and 95° from a seismic station, were considered suitable events.
- **Instrument responses and gains:** If the instrument response of the components is matched, you do not have to remove the instrument effects before proceeding, but you must ensure that the gains are equalized before proceeding to the receiver function deconvolution. If the instruments are not matched, you should remove or replace them with a set of uniform instrument responses.
- **Inspection and selection of seismograms:** This step is to examine the quality of the signal **(Figure II.5)**. This is done by a visual inspection of seismograms in order to confirm the presence of the signal and if the different types of waves which appear on the three components of the seismogram can be identified. For receiver function studies, records in general must exhibit clear seismic phases (different types of waves) on seismograms.

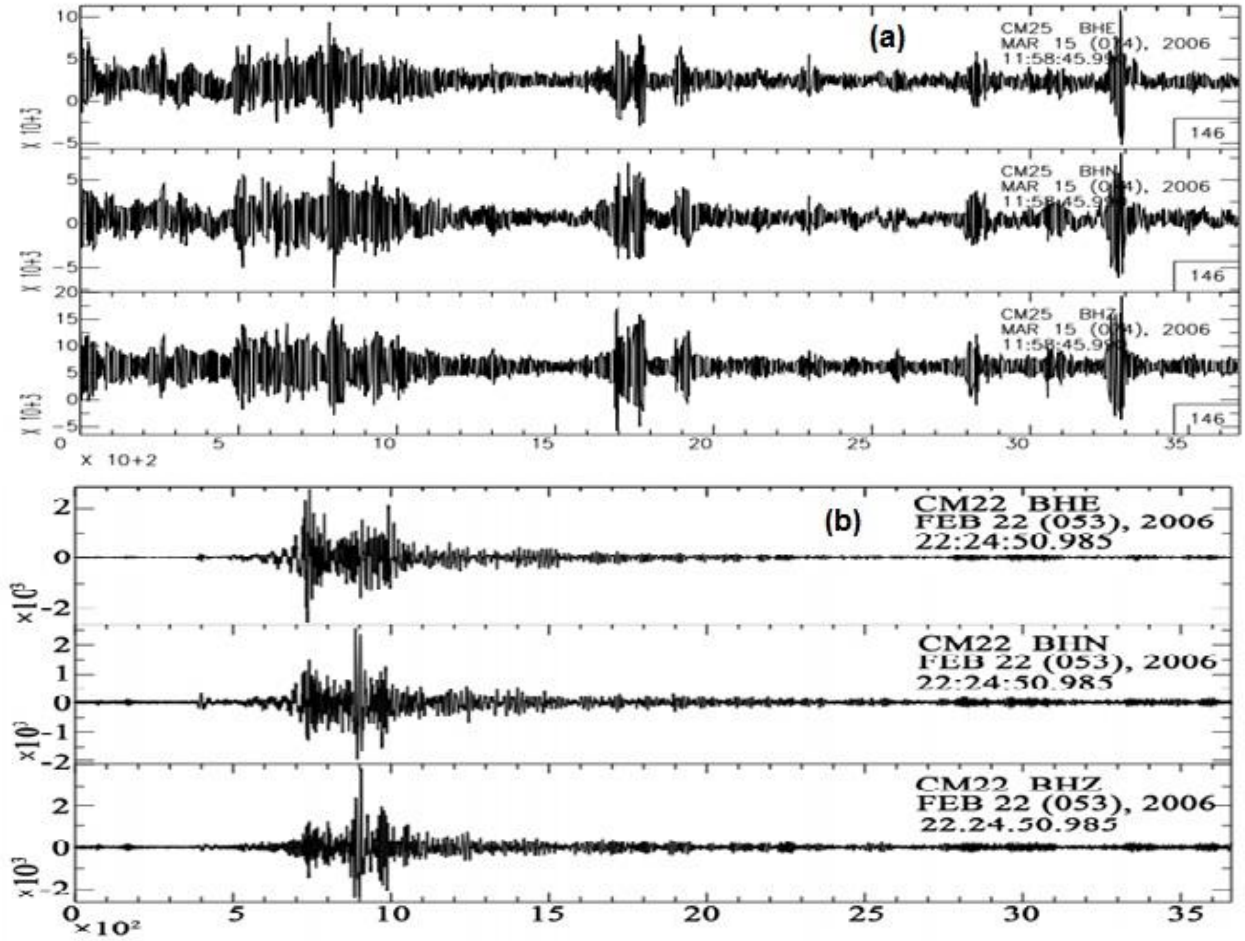

Figure II.5: Three components of seismogram recorded at stations CM22 and CM25 (a) bad signal; (b) good signal. Horizontal axis corresponds to the time in second(s) while the vertical axis corresponds to the amplitude in micrometer (μm).

This figure shows us how we can differentiate the bad signal from the good one by the visual inspection. Here, it is possible to detect the different types of waves (body and surface waves) in the case of the **Figure II.5 (b)** with respect to **Figure II.5 (a)**. The different seismograms used in this study are presented in **Annex 2.**

- **Windowing the P-waves then filter:** This step consists of windowing the P waveform from the pre-signal noise and the rest of the seismic signal. The amount of record that we use depends somewhat on the seismogram. We want to isolate the P-waveform from the remaining signal. For the usual teleseismic distances (30° to 95°) we are usually safe by using about 60 seconds of signal "leader" and 60 seconds of signal following the onset of the P wave. The precise duration can vary if needed, but these are typical values. At times, details in the estimated receiver function may be sensitive to substantial (10 s) variations in length, and you can get a feel for the variations by comparing several lengths of signal during the source equalization

procedure. From the oneset, since the P-wave occurs at 80 s in the seismogram, it would be necessary to window it between 20 s and 140 s into the seismogram (**Figure II.6**). We also should remove the mean and taper the ends of the signal to avoid signal processing artifacts later in the processing.

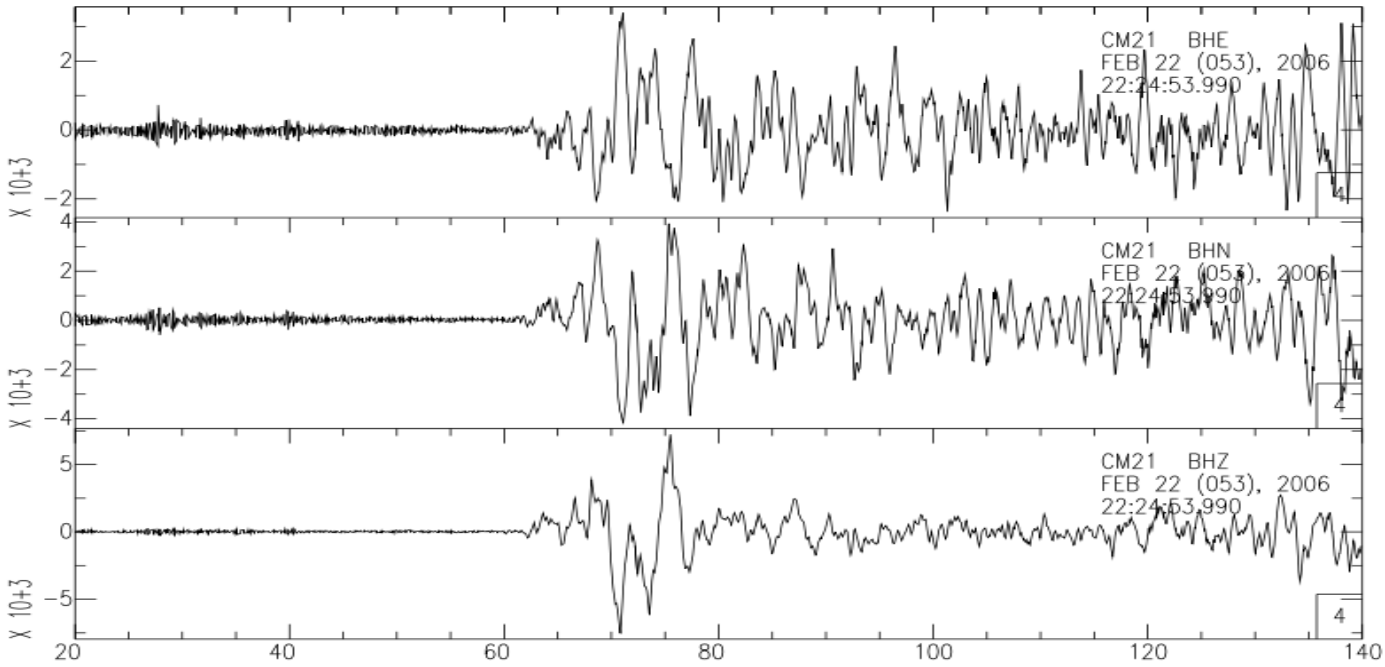

Figure II.6: Three components of seismogram recorded at station CM22, windowed and filtered

In this figure, we observe clearly that, the time axis has been reduced between 20 s to 140 s from the original signal.

- Rotation of seismograms: Rotating seismograms is a conceptual aspect in receiver function estimates. Seismograms are rotated in great circle paths to obtain radial and transverse seismograms necessary to compute radial and transverse receiver functions respectively. Seismograms are recorded along the vertical (Z), North-south (N) and East-West (E) directions. Rotation consists of transforming the ZNE components into the ZRT **(Figure II.7 and Figure II.8)**. The two horizontal components N and E are rotated into the radial R and tangential T components as follows:

$$\begin{bmatrix} R \\ T \\ Z \end{bmatrix} = \begin{bmatrix} \cos\theta & \sin\theta & 0 \\ -\sin\theta & \cos\theta & 0 \\ 0 & 0 & 1 \end{bmatrix} \begin{bmatrix} E \\ N \\ Z \end{bmatrix} \qquad \textbf{(II.1)}$$

where $\theta = 3\pi/2 - \chi$ and χ is the back azimuth. The back azimuth (BAZ) describes the angle between the vector pointing from the seismic station to the earthquake and the vector pointing from the seismic station to the north. The ZRT is a 2D rotation where the Z direction is conserved as in the original ZNE seismograms.

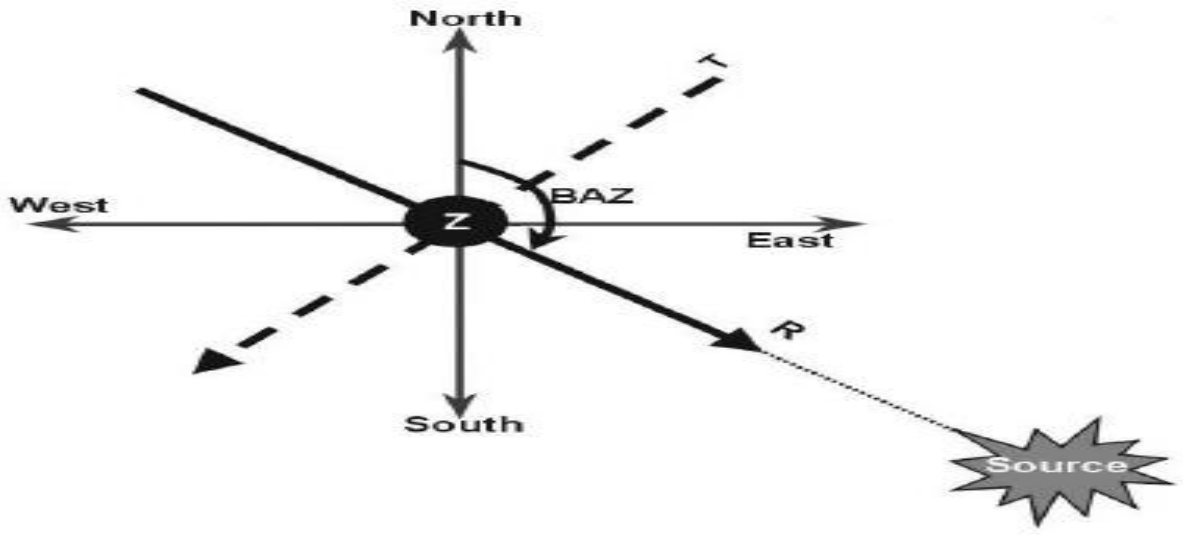

Figure II.7. The rotation from ZNE to ZRT. (Jansson, 2008**).**

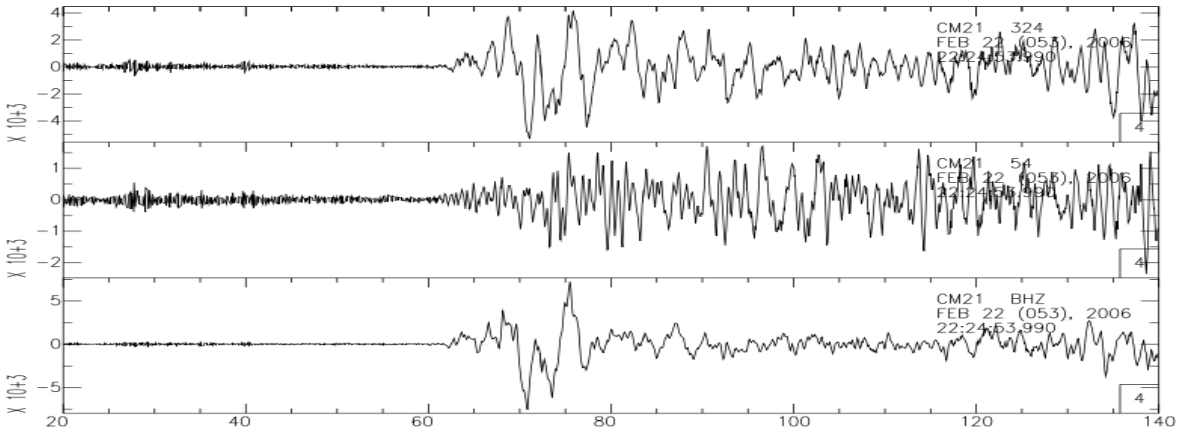

Figure II.8: Three components of seismogram recorded at station CM22 and modified to ZRT

b) Deconvolution of the signal and extraction of the receiver function

The earliest receiver function studies such as Phinney (1964) worked in the frequency domain using the ratio of amplitude spectra to estimate the gross characteristics of structure. The

works of Clayton and Wiggins (1976) extended the method to include water-level-stabilization and phase information by using a complex frequency-domain ratio and inverse transforming back into the time domain. Langston (1979) continued the advancements further and moreover developed a source equalization procedure to remove the effects of near-source structure and source time functions. For this study, an iterative time-domain deconvolution approach is used because it does not require selecting water level in frequency domain to calculate the receiver functions at each station; following the method of Ligorría and Ammon (1999). This technique is an adaptation of the work by Kikuchi and Kanamori (1982) who proposed a method to estimate far-field source time functions. Advantages of using this technique over other deconvolution techniques in the frequency domains is first of all that the time-domain iterative approach requires no choice of optimal stabilization parameters such as water-level, damping or time-domain smoothing. Secondly, the iterative approach is causal, such that, it is easy to identify receiver functions that cannot satisfy the defining convolution.

There is a convolutional relation between the vertical and radial components of motion. The receiver function $E_{Ri}(t)$, is related to the radial R(t), and vertical Z(t) components through **equation (II.2):**

$$\mathbf{R(t) = Z(t) * E_{Ri}(t)} \qquad \mathbf{(II.2)}$$

The foundation of the iterative deconvolution approach is a least-squares minimization of the difference between the observed horizontal seismogram and a predicted signal generated by the convolution of an iteratively updated spike train with the vertical-component seismogram (Ligorría and Ammon, 1999). The vertical component *Z(t)* is first cross-correlated with the radial component *R(t)* to estimate the lag of the first and largest spike in the receiver function. Then the convolution of the current estimate of the receiver function E_{Ri} (t) and the vertical component seismogram is subtracted from the radial-component seismogram **(equation II.3)**.

$$\mathbf{R(t) - Z(t) * E_{Ri}(t) = 0} \qquad \mathbf{(II.3)}$$

Throughout the iteration, the misfit between the vertical and receiver-function convolution and the radial component seismogram is reduced, and the iteration halts when the reduction in misfit with additional spikes becomes insignificant. **Saciterd** performs a time domain deconvolution. This program was written by Hermann Ammon (2002) and its important aspect is that the deconvolution is expressed as a sequence of Gaussian filtered impulses. The Gaussian of 2.5 is a value commonly used in receiver-function analysis (Ligorria and Ammon, 1999) corresponding to a low frequency band with $f \leq 0.5$ Hz after 100 iterations. To be able to evaluate the result of the deconvolution, the misfit between the radial seismogram and the final receiver function estimate convolved with the observed vertical component was computed. This misfit

value was used to identify poor events not suited for further investigation. Only deconvolution resulting in a receiver function reproducing more than 85% of the signal were accepted (**Figure II.9 (a)**) because the P-direct phase (first peak) having the biggest amplitude than the Ps conversion (second high peak) is noticed all together translating the good receiver function whereas the solutions that did not meet the 85% criteria was rejected (**Figure II.9 (b))** because the first two phases have the same amplitudes that translate the bad quality of the receiver function. In addition, for each event, the section of the receiver function sorted according to epicentral distance is visually inspected to check that, a coherent signal corresponding to Pmp phase (the P-to-S conversion and the multiple conversion on the Moho) is present a few seconds after the P wave arrival. Output files are constituted respectively by: decon.out that is named **Rftn** receiver function for Gaussian; observed that is original numerator convolved with Gaussian; numerator that is original numerator convolved with Gaussian; denominator that is original numerator convolved with Gaussian and predicted which is the Receiver function for Gaussian

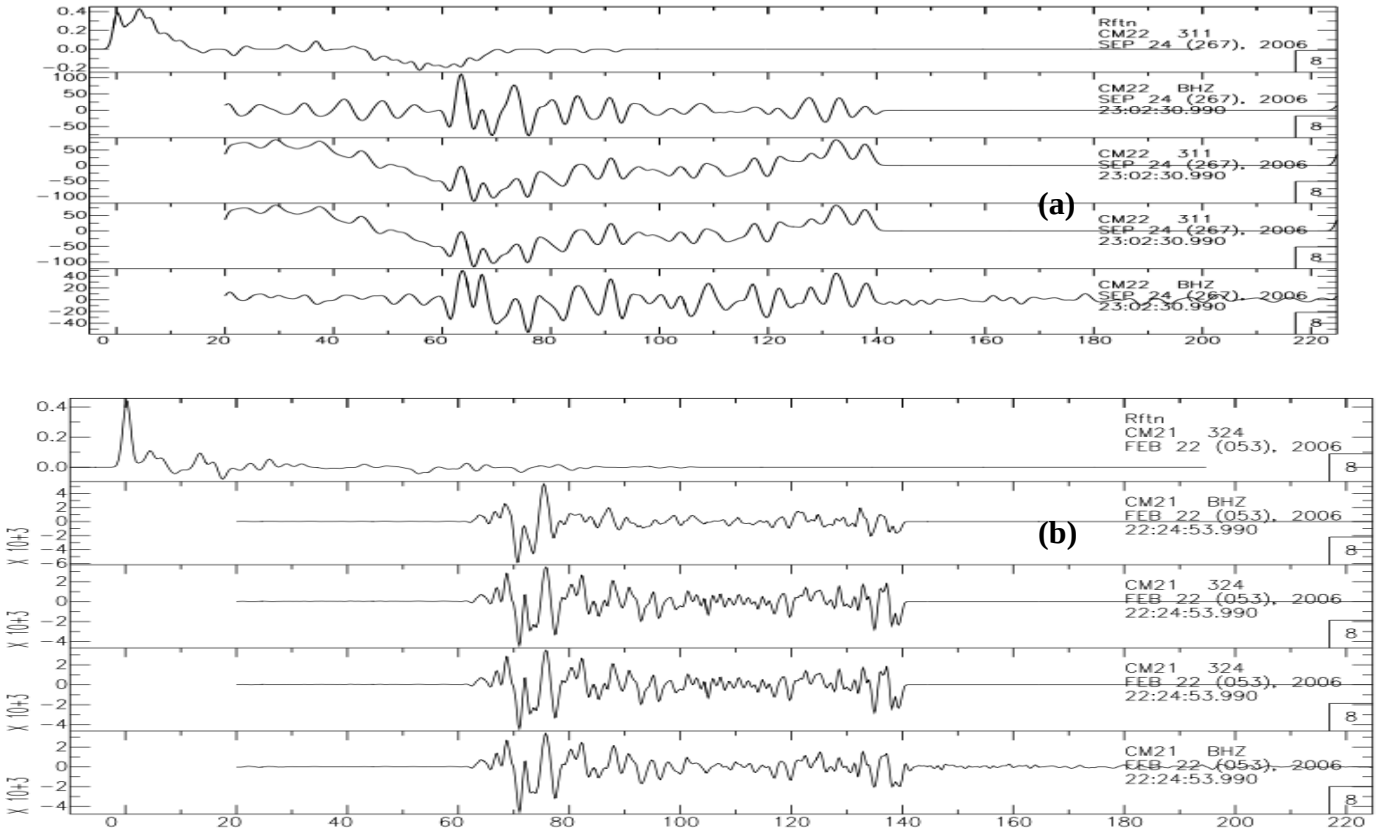

Figure II.9: Iterative deconvolution result obtain at the CM22 station **(a)** deconvolution of the signal with the misfit less that 85% and **(b)** greater that 85%

Focusing our objective on the 1-D cartography of the earth structure, we need to extract the radial path of the receiver function **(Figure II.10)** to apply the inversion method.

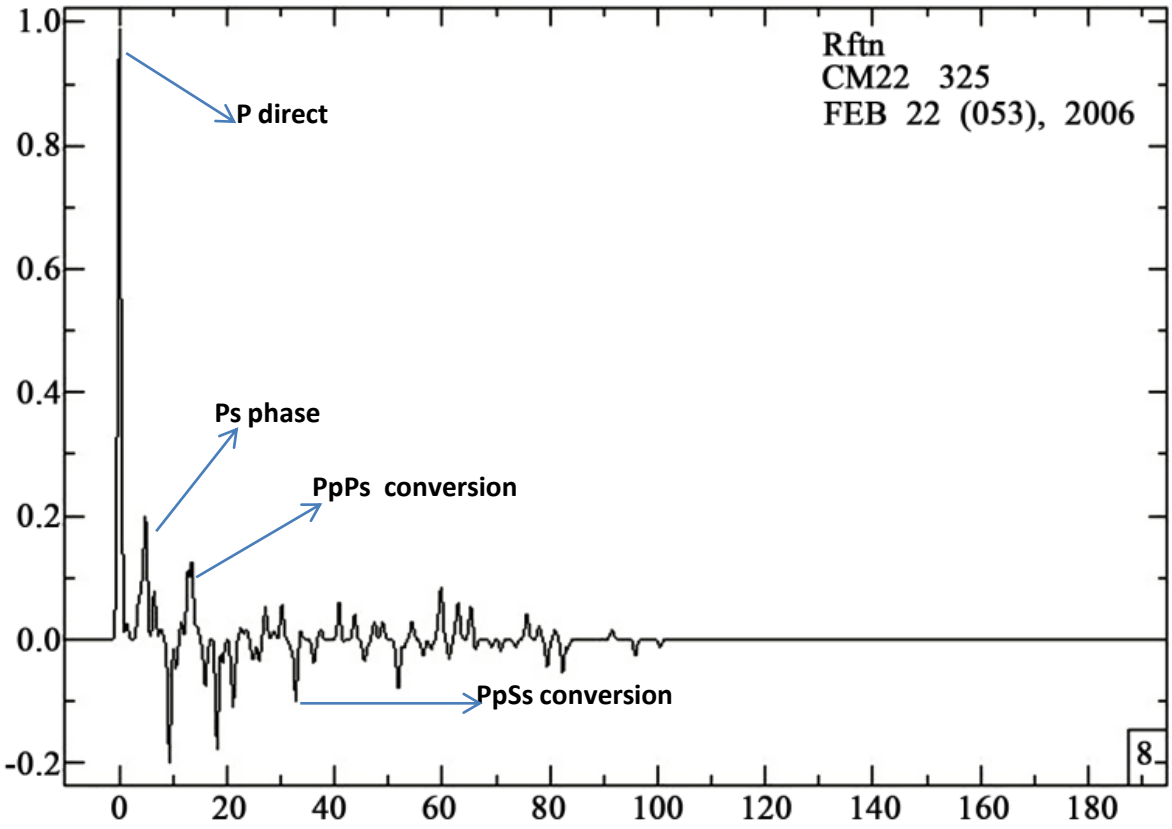

Figure II.10. Example of the radial receiver function computed from station CM22 using the teleseismic events.

In this radial receiver function, we observe clearly the different types of wave phases: the P-direct phase, the Ps conversion phase and the multiple conversions (PpPs and PpSs). The different receiver functions computed in order to inverse in this study are presented in **Annex (3)**

II.2.2.2 Inversion of the receiver functions

a) Inversion theory

Inverse problems are commonly solved in applied sciences. In such problems, a researcher uses a set of methods to extract useful inferences about the world from physical measurements. These methods are also referred to as Inverse theory. The laws of physics allow us to simulate the actions and interactions of physical parameters within a given system called the model. This model is a representation of a natural system (the earth, the subsurface, the atom...) and is described by a set of model parameters (velocity, density, conductivity....). This model, once excited, yields a set of measurable quantities: the data. The system of equations relating the data **d** to the model m is called the forward problem and is denoted

$$\mathbf{d = G\,(m)} \qquad \textbf{(II.4)}$$

where **G (m)**is a set of mathematical equations dependent on **m**.

The reverse action consists in finding the model **m** that explains a set of observed data $\mathbf{d_{obs}}$ and is called the inverse problem. The complexity of the inverse problem is closely related to the complexity of the forward problem. The latter must be known in order to determine the inverse solution. Often, this answer is an estimate and differs from the true model because the forward modeling provides incomplete information on the model. Furthermore, the forward problem is an approximation and the model is a simplified representation of the true system. In addition, the observed data are recorded by instruments and thus contain noise. In waveform inversion, we aim to recover a quantitative representation of a model of the subsurface. The model is most often characterized by the P-wave velocity varying with depth although other quantities may be accounted for (S-wave, quality factor....). The information used as data are the seismic traces recorded at the earth's surface by receivers. These receivers record in time the signal propagated through the sub-surface from a source. A straight forward solution to the inverse problem is to define the inverse operator $\mathbf{G^{-1}}$ such that the estimated solution is given by **equation (II.5)**:

$$\mathbf{m = G^{-1}(d)} \qquad \textbf{(II.5)}$$

These methods will be referred to as direct methods. In order to avoid the estimation of the inverse operator, local methods may be used which aim to estimate the model update $\Delta\mathbf{m}$ of an priori model $\mathbf{m_0}$ such as **equation (II.6):**

$$\mathbf{m = m_0 + \Delta m} \qquad \textbf{(II.6)}$$

The model update is found by minimizing the misfit function, measuring the mismatch between the observed and forward modeled data. These methods are local in the sense that the path leading to the inverse solution depends on the initial guess of the model $\mathbf{m_0}$.

Direct and local methods are widely used in seismic exploration and we will focus in this theory on the resolution of the inverse problem in the case where the forward problem is linear and non-linear.

The objective of an inverse problem is to find the best model parameters **m** such that

$$\mathbf{d = G\,(m)} \qquad \textbf{(II.7)}$$

Where, in an operator describes the explicit relationship between the observed data and the model parameters **m**. In various contexts, the operator is called forward operator, observation operator, or observation function. In the most general context, **G** represents the governing equations that relate the model parameters to the observed data **d** (i.e., the governing physics). Looking at the objective of the inverse problem, there exists two types of inverse problem: linear inverse problem and non-linear inverse problem.

- **Linear inverse problem**

In the case of a discrete linear inverse problem describing a linear system, and (the best model) are vectors, and the problem can be written as

$$\mathbf{d = Gm} \qquad \textbf{(II.8)}$$

Where is a matrix (an operator), often called the observation matrix.

Because we cannot directly invert the observation matrix, we use methods from optimization to solve the inverse problem. To do so, we define a goal, also known as an objective function, for the inverse problem. The goal is a functional that measures how close the predicted data from the recovered model fits the observed data. In the case where we have perfect data (i.e. no noise) and perfect physical understanding (i.e. we know the physics) then the recovered model should fit the observed data perfectly. The standard objective function, , is usually of the form:

$$\boldsymbol{\Phi = \|d - Gm\|_2^2} \qquad \textbf{(II.9)}$$

Which || || represents the $\mathbf{L^2}$ norm of the misfit between the observed data and the predicted data from the model. We use the L^{-2} norm here as a generic measurement of the distance between the predicted data and the observed data, but other norms are possible for use. The view of the objective function is to minimize the difference between the predicted and observed data. To minimize the objective function (i.e. solve the inverse problem) we compute the gradient of the objective function using the same rationale as we would to minimize a function of only one variable. The gradient of the objective function is given by **(equation II.10)**:

$$\boldsymbol{\nabla m} \; . \; \Phi = 2\,(G^T.G.m - G^T.d) \qquad \textbf{(II.10)}$$

Where $\boldsymbol{G^T}$ denotes the matrix transpose of $\boldsymbol{G}$.

Simplifying the expression above, we obtain **equation (II.11)**:

$$\boldsymbol{G^T.G.m = G^T\,d} \qquad \textbf{(II.11)}$$

After rearrangement, the equation above becomes **equation (II.12)**

$$\boldsymbol{m = (G^T.G)^{-1}\,G^T\,d} \qquad \textbf{(II.12)}$$

- **Non-linear inverse problem**

Non-linear inverse problems have a more complex relationship between data and model, represented by the **equation (II.13).**

$$\mathbf{d = G\,(m)} \qquad \textbf{(II.13)}$$

where is a non-linear operator and cannot be separated to represent a linear mapping of the model parameters that form into the data.

b) Inversion of the receiver functions

Some important level of the inverse theory is the tomography. In seismology, solving inverse problems implies to deal with earthquake sources and earth structure. Data are recorded as seismograms and are used backwards to characterize the earthquakes that generated the seismic waves and the medium through which the waves traveled.

Receiver functions are traditionally inverted to obtain an S-wave velocity model that produces an estimation of shear velocity structure under a given seismic station. There is no guarantee that a unique inversion result will be obtained, as the method seeks to minimize the differences between observed and synthetic (or predicted) receiver functions. The inversion was performed using the Rftn96 program developed by Julià et al. (2000) and Julià et al. (2003). The method is based on a linearized inversion procedure that minimizes a weighted combination of least squares norms for each data set, a model roughness norm and a vector-difference norm between inverted and pre-set model parameters. The velocity models obtained are consequently a compromise between fitting the observations, model simplicity and a priori constraints. The velocity models are associated to the synthetic receiver functions. Synthetic seismograms are generated using a fast three dimension ray tracing scheme based on (Langston, 1977). The earth model is parameterized in terms of constant velocity, planar, dipping layers over half-space. The P and S wave velocities, density, strike and dip angles, and thickness are specified for each layer in the model. Synthetic vertical radial and transverse seismograms are generated by specifying a back azimuth and ray parameter for the plan of P-wave incident at the base of the model. The starting model used in this inversion consisted of an isotropic medium of constant velocity layers that increase in thickness with depth. The thicknesses of the first, second and third layers are, respectively, 45 km, 90 km and 80 km, while the thickness increases at each instant to 5 km between 0 and 45 km depth, to 10 km between 45 and 135 km and 20 km below a depth of 135 km and a linear shear wave velocity increase in the crust from 3.2 to 4.0 km/s and 4.0 to 4.7 km/s in the lithospheric mantle overlying a flattened PREM (Preliminary Reference Earth Model) model (Dziewonski and Anderson, 1981) for the mantle. Having determined path lengths of each layer, the arrival time for each phase can be calculated. Amplitudes are calculated using wave potentials in the local coordinate system and applying the appropriate reflection or transmission coefficient at each interface. In addition, to the P-arrival and Ps conversions, the synthetic seismogram may include the free-surface multiples associated with each interface.

Thirty two temporary broadband seismic stations that operated during the years 2005-2007 have been installed in Cameroon where the study area contained . Those seismic stations have permitted to record the earthquakes. The teleseismic events are therefore selected on those earthquakes and, treated by the temporal iterative déconvolution in order to obtain the P-receiver functions. Then, these receiver functions will be inverted to obtain the S-wave velocity profiles beneath the different seismic stations that are situated along the Volcanic Province of Cameroon.

The results obtained by inversion of the receiver functions are presented in the following chapter.

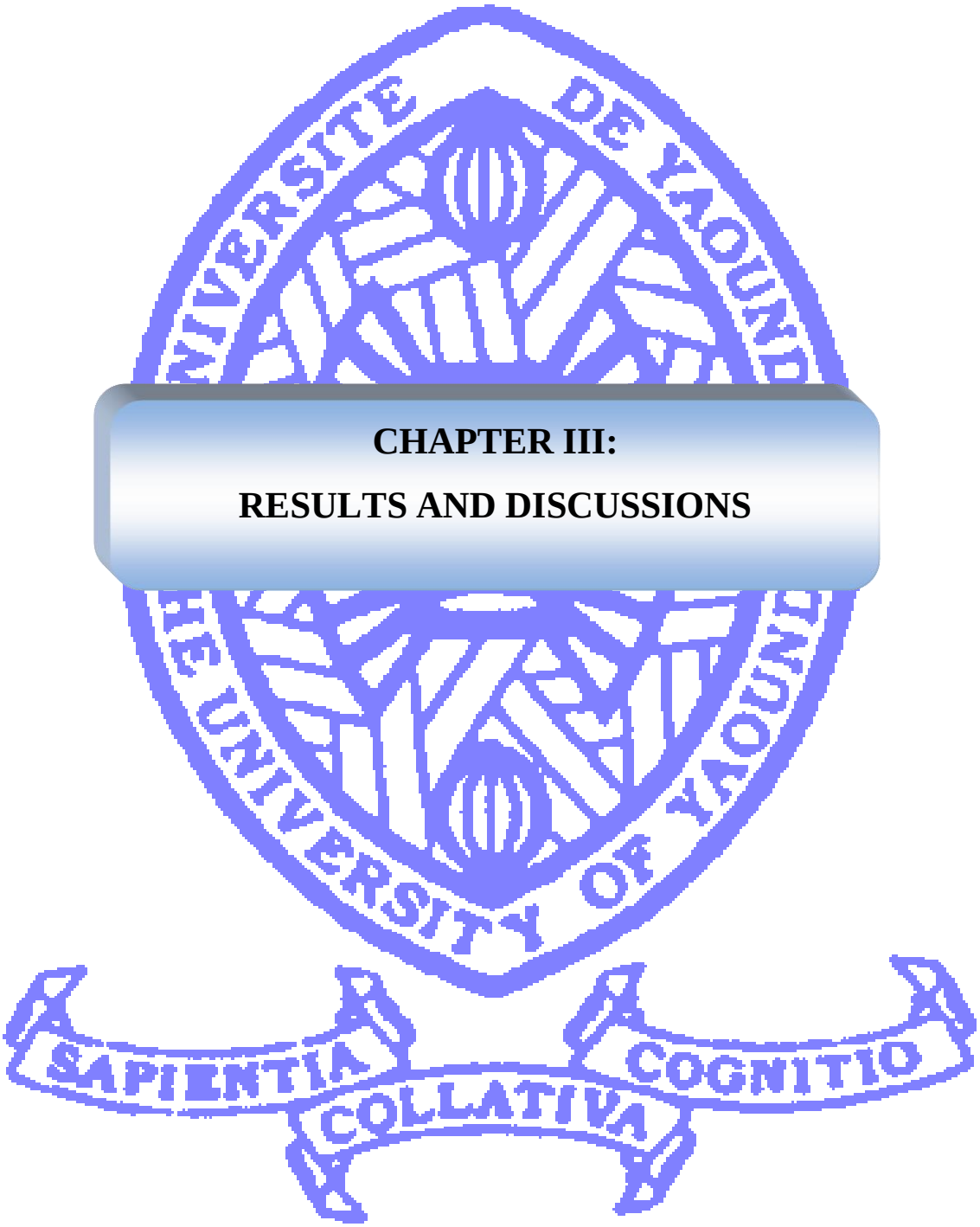

CHAPTER III:

RESULTS AND DISCUSSIONS

This chapter shall show the different results obtained after the inversion of the receiver functions followed by the interpretations. In order to compare those results between them on one hand, and those existing in the literature on other hand, a discussion will be done.

III.1 Presentation of the results and interpretations

The Volcanic Province of Cameroon is divided into two principal parts: the southern and northern parts. The Northern part is subdivided into two main regions which are the Adamawa Plateau and the Garoua Rift (**Figure III.1**).

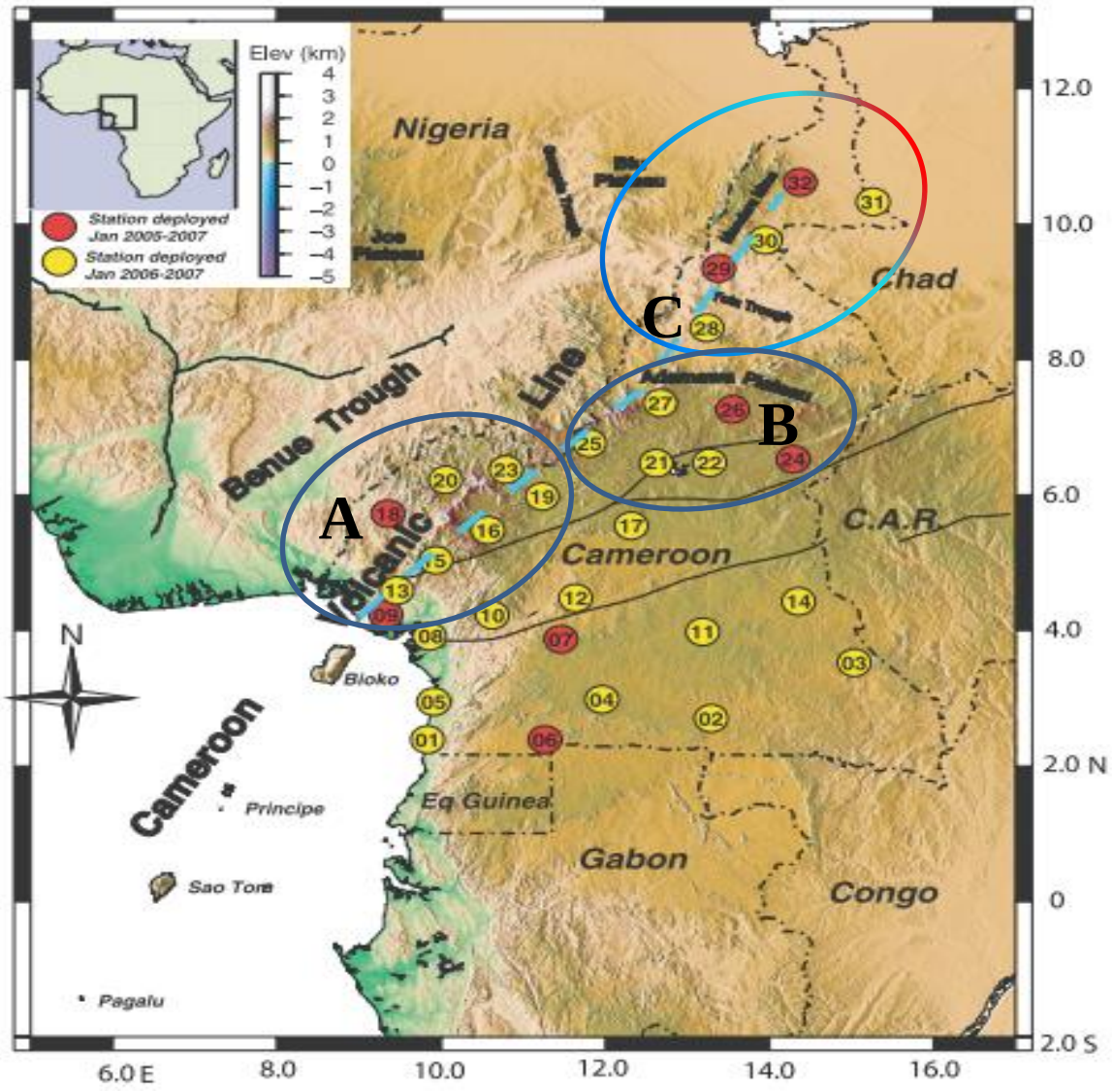

Figure III.1: Colour elevation map showing seismic station locations**.** The dashed light blue line shows the location of the Cameroon Volcanic Line profile. The different volcanic centers are represented by the ellipses. (**A**): Southern Cameroon region; (**B**) Adamawa plateau region; (**C**): Garoua rift region

Some criteria have been applied to identify the conversion and multiple conversions phases of the wave per locality. The first, second and third peaks having high positive amplitudes are identified as the P-direct phase, Ps conversion and PpP_S multiple conversion respectively and the high negative amplitude is PpSs multiple conversion. The time of the P- direct wave coincides with the origin of time (Ammon, 1991)**.** The criteria used to determine the crustal thickness or Moho depth is based on the following two assumptions. Firstly, from their difference in composition, there should be a rapid velocity increase between the crust and the Mantle. Secondly, shear wave velocity above 4.3 km/s indicates the presence of lithology with mantle compositions (Christensen, 1996; Christensen and Money, 1995). Thirdly, concerning the lithosphere thickness, the existence of the Low Velocity Zone permits to differentiate the lithosphere from asthenosphere (LAB).

III.I.I Results and interpretations of the southern part of the Volcanic Province of Cameroon

This part has 8 seismic stations (**Figure III.1. (A)**). The inversion curves followed by synthetic receiver functions are presented in **Figure III.2 (a-h)**

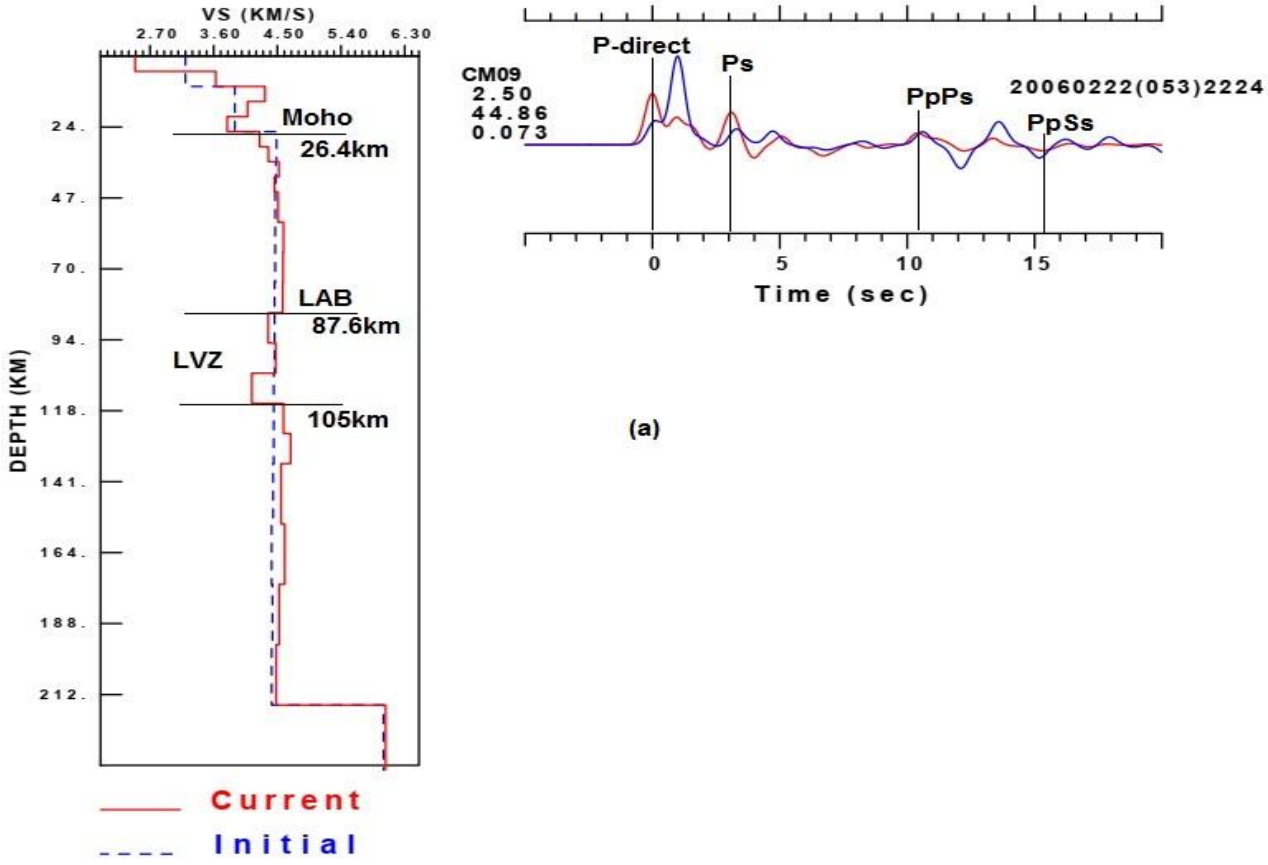

Figure III.2 (a) S-waves velocity model for CM09 station (Ekona)

This station is situated in the Ekona locality, at the foot of the Mount Cameroon. At the time of treatment of the teleseismic events recorded, only the one on February the 22th year 2006 at 10 AM 24 min have answered the initially fixed criteria. After applying the inverse method with a Gaussian of 2.5 with the ray parameter of 0.073, the synthetic receiver functions (right curves) present a low misfit of 44.86%. This low value translates the non-correlation observed on the experimental (red) and theoretical (blue) synthetic receiver functions. This non-correlation entails a difficult interpretation of the S-wave velocity model and would be due to a major volcanic activity (mount Cameroon) in this locality.

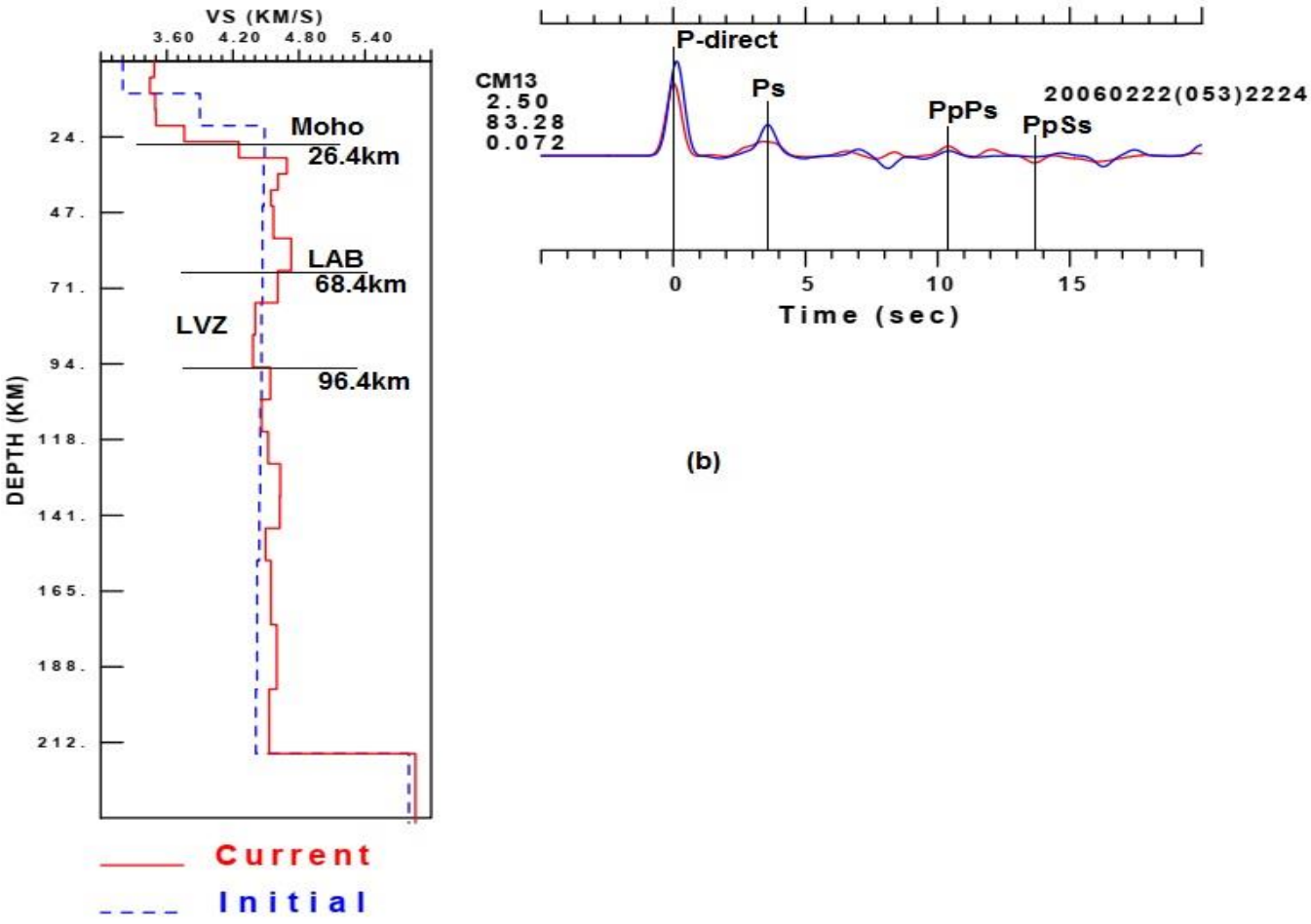

Figure III.2 (b) S-waves velocity model for CM13 station (Kumba)

This station was situated in the Kumba locality. Like obtained at the station CM09, only the corresponding teleseismic event corresponding to the 53th day of the year 2006 at 10 AM 24 min has answered the initially fixed criteria at the time of the treatment. For a ray parameter of 0.072 and the Gaussian of 2.5, a satisfactory misfit of 83.28% has been obtained at the time of the treatment. This translates a good correlation of the synthetic receiver. The P-Direct phase

corresponding at the origin of times is followed by the Ps converted phase at 3.5 s and multiple converted phases PpPs and PpSs at 10.5 s and 13.8 s, respectively. This proves that, the seismic waves have truly undergone a conversion at the level of the Moho in this locality.

Concerning the S-wave velocity model associated to the synthetic receiver functions, it appears a negative low velocity anomaly at 5 km of depth followed by a sequence of positive velocity anomaly until 28 km of depth. Based on Christensens, 1996 and Christensens Money and, 1995, the transition zone (Moho) between the crust and the upper mantle and more precisely the lithospheric mantle would be located around 26.4 km of depth. The sequence of positive velocity anomalies observed before the transition zone would translate the thick behavior of the crust. Beyond the transition zone, an alternation of positive and negative velocity anomalies is observed between 28 km and 68.4 km depth. Beyond this interval, a sequence of negative velocity anomalies is observed until 96.4 km. This last part would translate a low velocity zone (LVZ) of the upper mantle that, allows us to limit the lithosphere (LAB) to 57.6 km of depth in the Kumba locality. The alternation of the velocity anomalies observed between a transition zone and the limit of the lithosphere would translate the thin behavior of the lithospheric mantle.

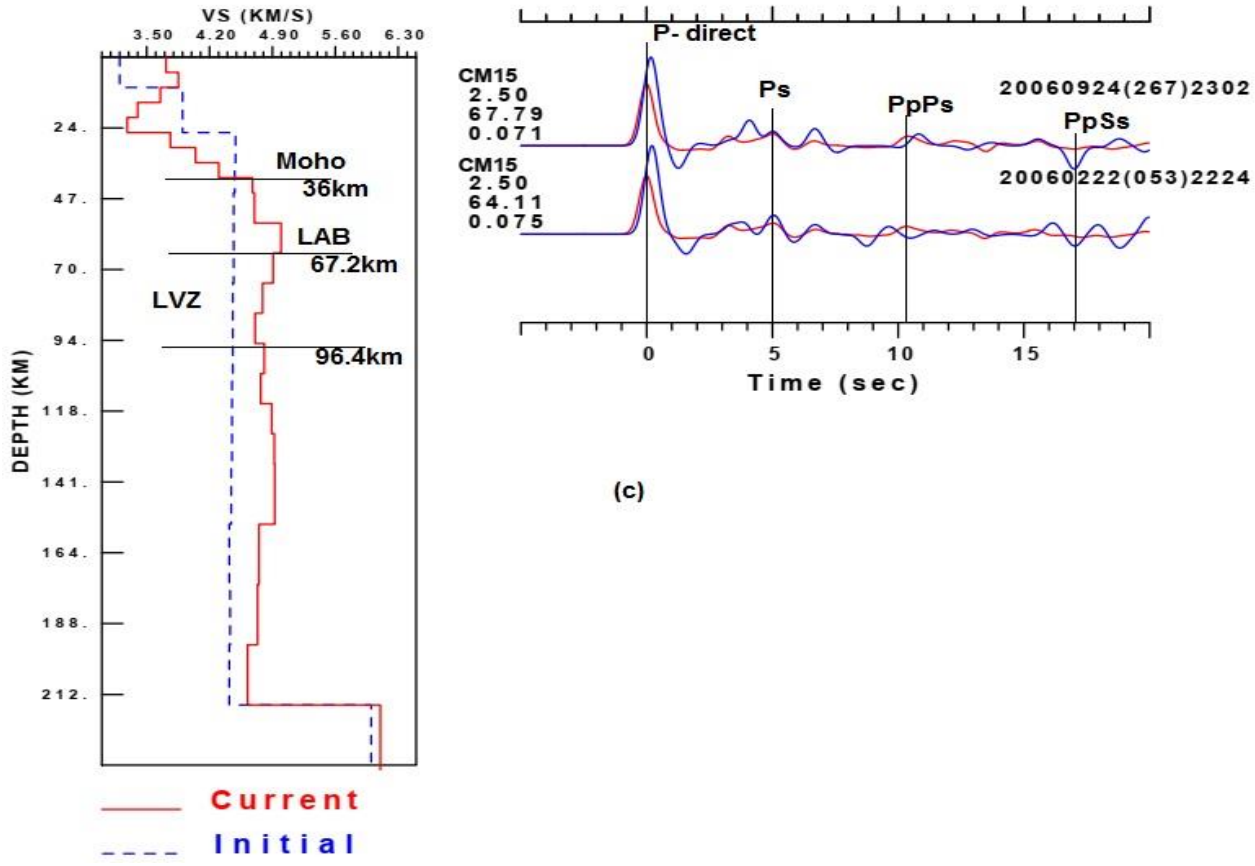

Figure III.2 (c) S-waves velocity model for CM15 station (Nkongsamba)

This station was situated at Nkongsamba locality. Two teleseismic events in occurrence, the ones on February the 22th February 2006 and September the 24th September 2006 have answered the initially fixed criteria. For the respective ray parameters 0.075 and 0.071 and a Gaussian of 2.5, the respective values of misfits of 64.11% and 67.79% have been gotten at the time of the treatment of those events. These values just above average translates translate the fact that, the signal has undergone a disruption at the time of recording. It is equally shown by the non-superposition of the peaks of P-Direct phase which is seen by the time difference. This would be due by the development of the seismic activity in this locality of Nkongsamba. Nevertheless, the converted phase Ps appears at 5 s followed respectively by the multiple converted phases PpPs and PpSs at10.5 s and 17 s. It is a proof that the wave has really undergone a conversion and of multiple conversions at the level of the Moho after all.

The S-wave velocity model obtained shows a low positive velocity anomaly at 5 km of depth followed as from 10 km, by a sequence of negative velocity anomalies until 26.4 km. Beyond this depth, a sequence of positive velocity anomalies appears until 67.2km. Hence on the basis of the assumptions of Christensen, 1996 and Christensens Money and, 1995, the transition zone between the crust and upper mantle would be located at 36 km of depth. The alternation of the velocity anomaly above the transition zone would translate the thin behavior of the crust in this locality. The positive velocity anomalies observed between the transition zone and 67.2 km of depth would translate the thick character of the lithospheric mantle. Beyond 67.2 km, a sequence of negative velocity anomalies is observed until 96.4 km of depth. This thickness would translate a low velocity zone (LVZ), which enables to limit the lithosphere at 67.2 km of depth in the locality of Nkongsamba.

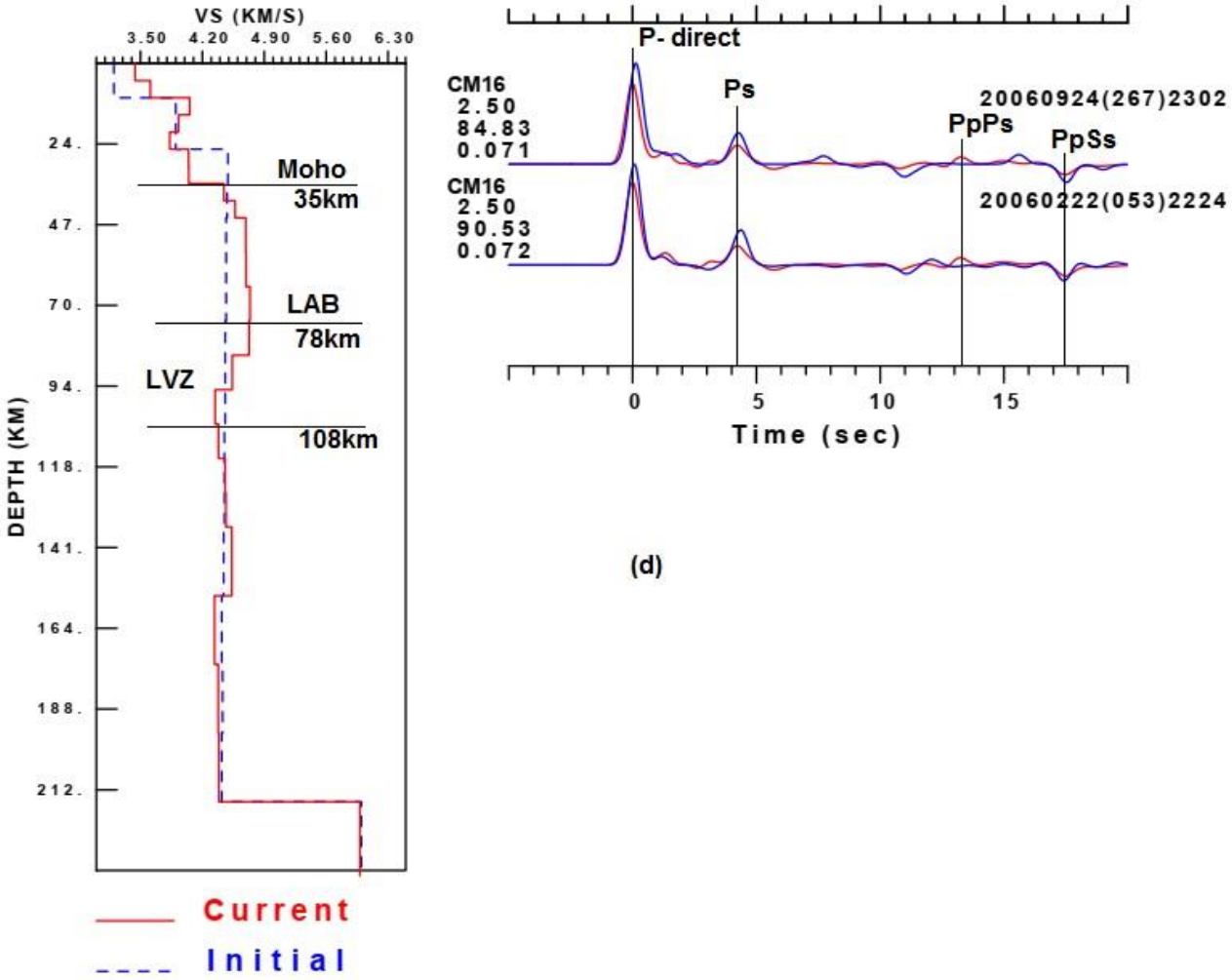

Figure III.2 (d) S-waves velocity model for CM16 station (Foumbot)

This station was situated in the locality of Foumbot in the west Cameroon. As observed for the previous station, two teleseismic events in occurrence, the ones on February the 22th and September the 24th of the year 2006 have answered the initially fixed criteria. These last events have respectively permitted to get misfits of 90.53% and 84.53% for the respective ray parameters of 0.072 and 0.071 with the Gaussian of 2.5. These values show understandably that the signal doesn't have sudden disruption at the time of recording. It is justified by the superposition of the P-Direct phase at the origin of times on the synthetic receiver functions. This phase is followed by Ps conversion at 4.2 s and multiple phases converted PpPs and PpSs at13.1 s and17.5 s, respectively. This proves that the P-seismic wave has truly undergone a conversion at the level of the Moho in this locality.

The velocity model obtained presents two positive velocity anomalies of which the strongest is located at 10 km of depth. These are followed by a sequence of low negative velocity anomalies until 20 km. Beyond this depth, a sequence of positive velocity anomalies is observed

where the strongest is located at 35 km of depth. This last depth would indicate the transition zone between the crust and upper mantle. The alternation of the positive and negative velocity anomalies observed in the crust would translate its thin character. Beyond 35 km of depth, a sequence of low positive velocity anomalies is observed until 78 km. This is followed by another sequence of but negative velocity anomalies at times until 108 km of depth. This last interval would denote a low velocity zone of the upper mantle that permits to delimit the lithosphere to 78 km of depth. The sequence of velocity anomalies observed in the lithospheric mantle would translate its thick character.

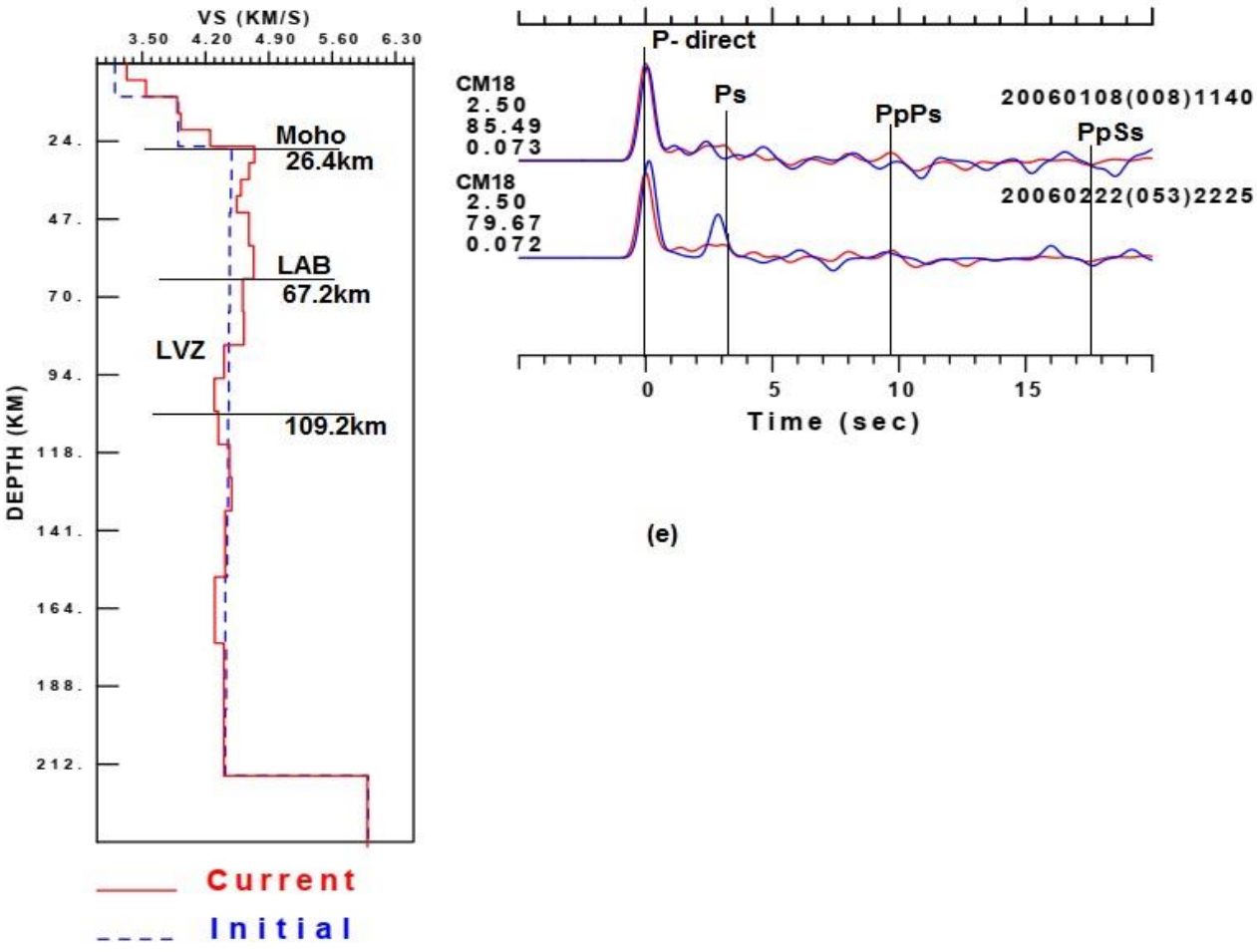

Figure III.2 (e) S-waves velocity model for CM18 station (Mamfe)

This station was situated in the locality of Mamfe in the south-west Cameroon. Two teleseismic events, in occurrence the ones on the 8th and 53rd days of the year 2006, respectively at 11 Pm 40 min and 10 Am 25 min have answered the basic criteria. For a gaussian of 2.5 and the ray parameters of 0.073 and 0.072, respectively these last events permitted to get the respective misfits of 85.49% and 79.67%. These values show that the recorded signal was very little disrupted and especially concerning the second event. This latter justified by the time difference

observed at the level of the P-Direct phase at the origin of times. This disruption would come from the proximity of the locality to the mount Cameroon. Nevertheless, there is appearance of the Ps phase converted at 3 s and multiple phases converted PpPs and PpSs at 9.8 s and 17.2 s, respectively. This proves the conversion of the wave in this locality.

The velocity model obtained shows a sequence of positive velocity anomalies until 26.4 km, of which the strongest are located at 10 km and 26.4 km. This last depth would translate the transition zone between the crust and upper mantle. The sequence of velocity anomalies observed would translate the thick character of the crust. Beyond 26.4 km, a sequence of low negative velocity anomalies followed by two positive velocity anomalies is observed until 67.2 km. Below this depth, another sequence of negative velocity anomalies appears until 109.2 km. This last interval of depth would translate the low velocity zone of the upper mantle which, permits to limit the lithosphere at 67.2 km of depth. The alternation of negative and positive velocity anomalies observed in the lithospheric mantle would translate its thin character.

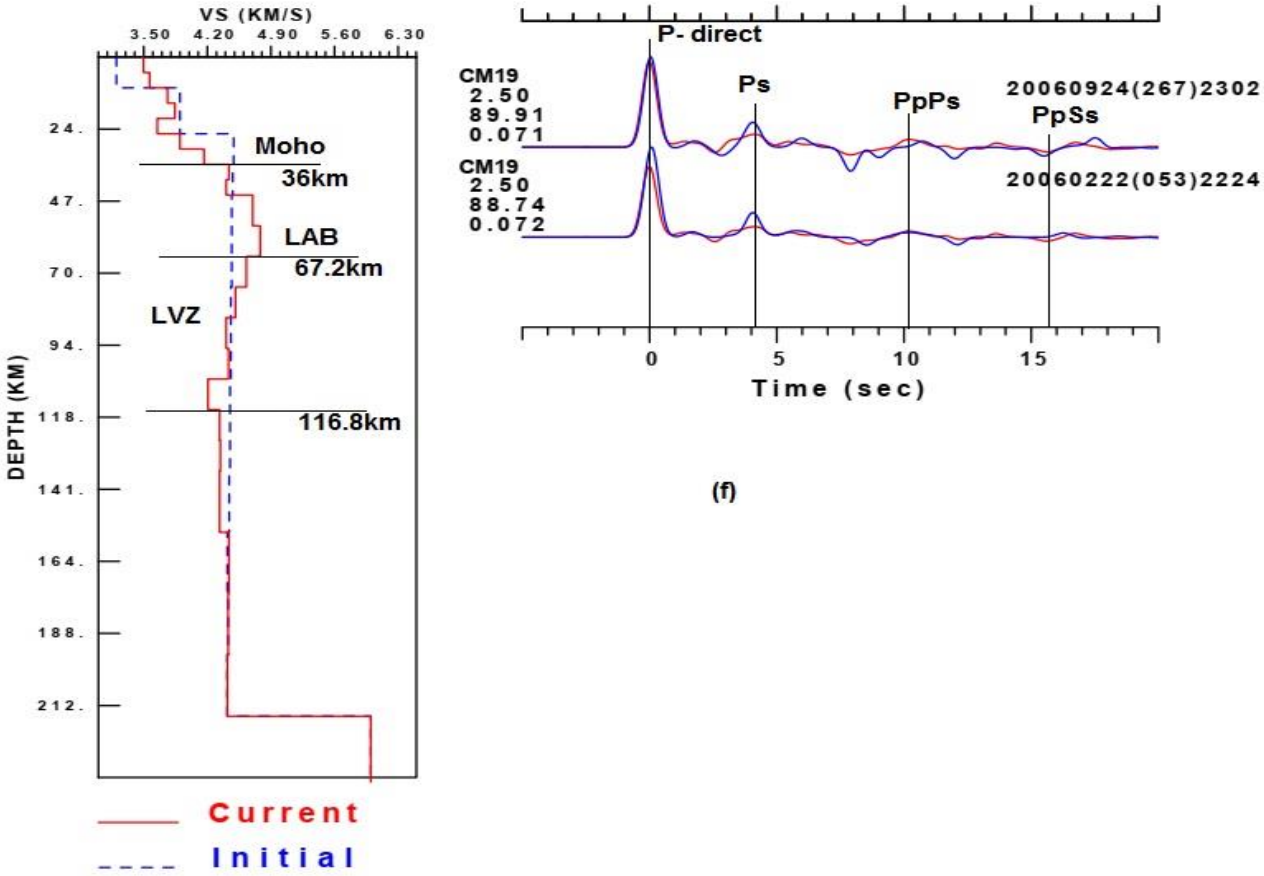

Figure III.2 (f) S-waves velocity model for CM19 station (Magba)

This station was situated in the locality of Magba in West Cameroon. As the previous station, two teleseismic events have answered the fixed criteria. It concerns those on the 53rd and 267th days of the year 2006 respectively at 10 Am 24min and 11 Am 02 min. For a Gaussian filter

of 2.5 and the ray parameters of 0.072 and 0.071 respectively, those events have respectively, permitted to get the misfits of 89.91% and 88.74%. These values show that the signal has undergone a minor disruption at the time of recording. This is justified by the superposition of the P-Direct phase at the origin of times on the synthetic receiver functions. This minor disruption would be due to the existence of a non-active volcano in the area. The P-direct phase is followed by the Ps conversion at 4 s and multiple phase conversions PpPs and PpSs at 10.1 s and 15.2 s respectively. This proves the conversion of the wave.

Observing the associated velocity model, a succession of positive velocity anomalies is observed until 20 km, of which the strongest would be located at 12 km of depth. This latter is followed by one negative velocity anomaly and three others but positive at times until 36km. According to the assumption of Christensen, 1996 and Christensens Money and, 1995, the transition zone between the crust and upper mantle would be located at 36km of depth. The alternation of positive and negative velocity anomalies observed would be synonymous of a thin crust. Beyond 36 km of depth, two positive velocity anomalies are observed until 67.2 km. Then, start a succession of negative velocity anomalies until 116.8 km of depth. This last interval of depth would indicate a low velocity zone (LVZ) permitting to limit the lithosphere at 78 km of depth in the locality of Magba. The sequence of the positive velocity anomalies observed between 36 km and 67.2 km would translate the thick character of the lithospheric mantle.

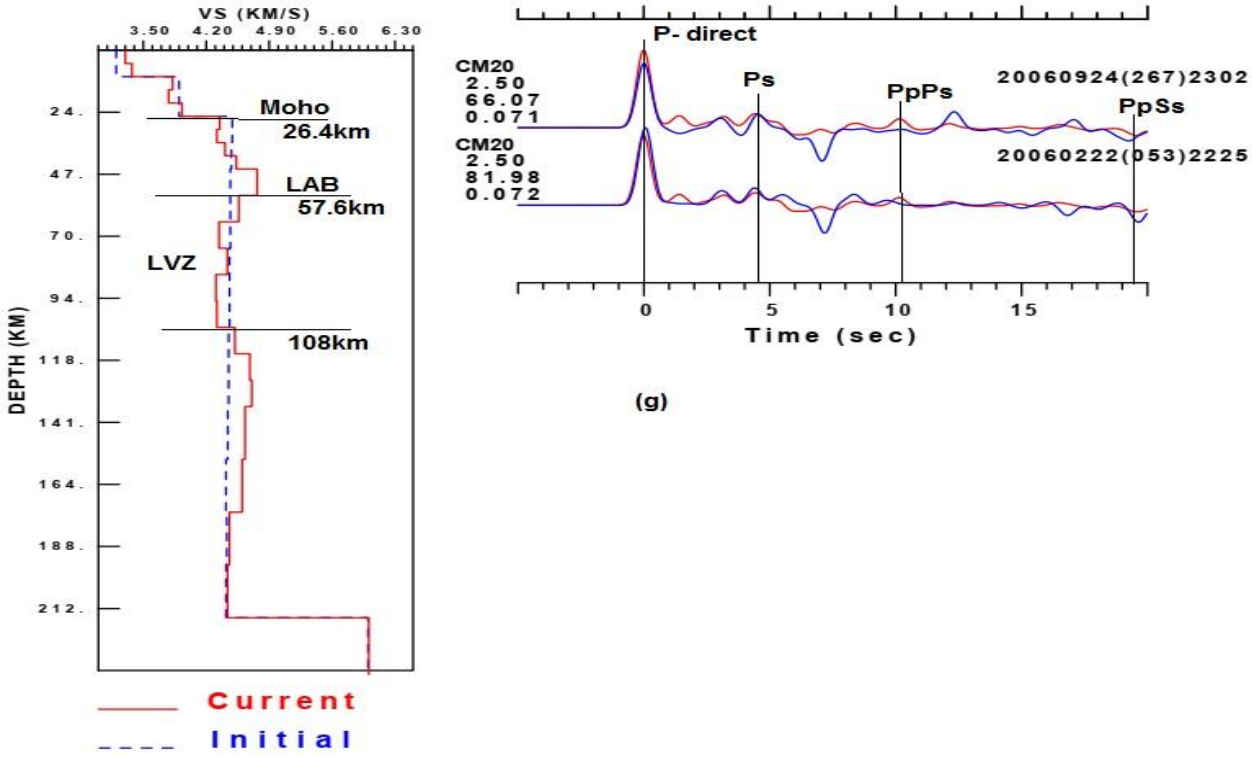

Figure III.2 (g) S-waves velocity model for CM20 station (Wum)

This station was situated at the locality of Wum in North-West Cameroon. Two teleseismic events, namely the one on the 53rd and 267th days of the year 2006 respectively at 10Am 25min and 11Am 02min have answered the basis criteria. For a Gaussian filter of 2.5 and the respective ray parameters of 0.072 and 0.071, these events have permitted to get the misfits of 66.07% and 88.98%. These values show that the signal has undergone a minor disruption at the time of recording. It is justified by the superposition of the P-Direct phase at the origin of times on the synthetic receiver function. This minor disruption would be due to the existence of a non-active volcano in the locality. The P-direct phase is followed by the converted phase Ps at 4.5 s and multiple converted phases PpPs and PpSs at 10 s and 19.5 s respectively. This proves that the wave has undergone the conversion.

The velocity profile associated with the synthetic receiver functions shows two positive velocity anomalies where the strongest is located at 10 km. This one is followed by another velocity anomaly but, earlier negative and very low and, two others velocity anomalies on contrary positive, of which the deepest and strong is located at 26.4 km of depth. Based on the criteria of determination of the transition zone between the crust and the upper mantle, it appears that it would be localized at 26.4 km of depth. The alternation of the velocity anomalies observed would translate its thin character. Beyond the transition zone, a very low velocity anomaly appears and is followed by a sequence of three positive velocity anomalies until 57.6 km. At this last depth, a sequence the negative velocity anomalies are observed until 108 km of depth. This last thickness would be a low velocity zone of the upper mantle that, allowing to fix the limit of the lithosphere at 57.6 km of depth. The lithospheric mantle would present a thick behavior due to the sequence of positive velocity anomalies observed.

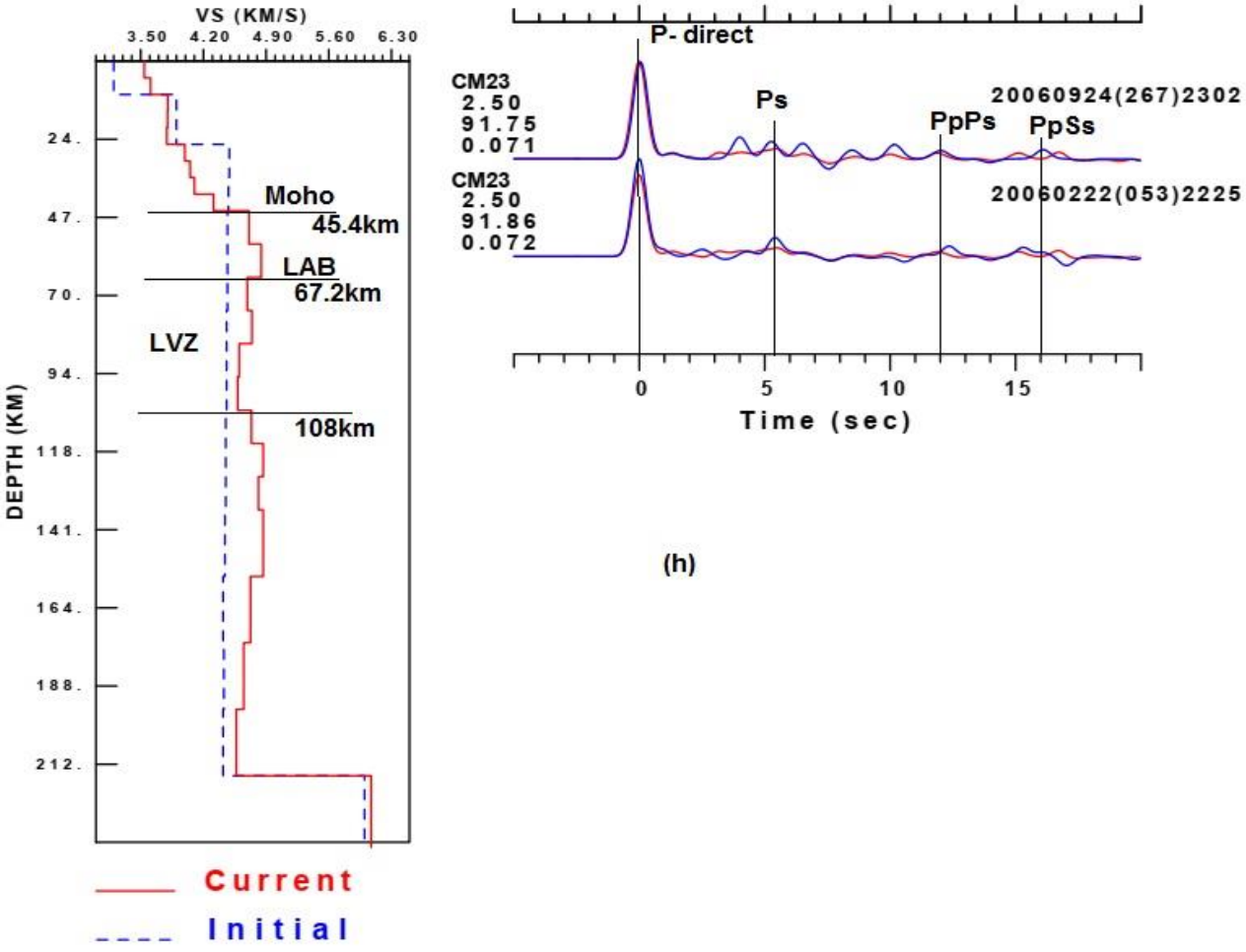

Figure III.2 (h) S-waves velocity model for CM23 station (Oku)

This station was situated in the locality of Oku in the North-West Cameroon. Two teleseismic events have answered the basic criteria, namely those on the 53rd and 267th days of year 2006 respectively at 12 Pm 25 min and 11 Am 02 min. For a Gaussian of 2.5 and the ray parameters of 0.073 and 0.072 respectively those events have permitted to get the respective misfits of 91.75% and 91.86%. These values show that the signal has been recorded without disruption in spite of the existing mount in this locality (Oku mount). These last values justify the good superposition of the P-Direct phase at the origin of times on the synthetic receiver functions. This last phase is followed by the Ps phase converted at 3.1 s and the multiple phases converted PpPs and PpSs at 12 s and16 s respectively. This proves the conversion of the wave in this locality.

The associated velocity model shows a succession of positive velocity anomalies until 45.4 km, of which the strongest would be located respectively at 10 km and 45 km of depth. This last depth would indicate the transition zone of the lithosphere between the crust and upper mantle. The succession of the positive velocity anomalies observed would translate the thick character of

the crust. Beyond this transition zone, another positive velocity anomaly is observed until 67.2 km followed by a sequence of velocity drops until 108 km of depth. This interval of drops would represent a low velocity zone of the upper mantle that permits to limit the lithosphere to 67.2 km of depth. The previous positive velocity anomaly observed before the Low velocity zone involves that, the lithospheric mantle is thick in the locality of Oku

The mean values obtained on the synthetics receiver functions in one hand and on the S-waves velocity models on the other hand are summarized on table III.1 and table III.2

a) Summary of the values coming from of synthetic receiver functions

Concerning the different synthetic receiver functions obtained in the Southern part regrouping the mounts, the different conversions and multiple conversions appearing and their corresponding time are summarized in the **Table III.1**

Table III.1: Interpretation of synthetic receiver functions of the southern part

Station	Localities	Percent of Signal Power Fit	t_{Ps} (s)	t_{PpPs}(s)	t_{PpSs}(s)
CM09	Ekona	44.86	3.1 ?	10.2?	15.2?
CM13	Kumba	83.28	3.5	10.5	13.8
CM15	Nkongsamba	68.34?	3.5?	10.5?	17?
CM16	Foumbot	84.83; 90.53	4.2	13.1	17.5
CM18	Mamfe	85.49; 79.67	3	9.8	17.2
CM19	Magba	89.91; 88.74	4	10.1	15.2
CM20	Wum	66.07; 81.98	4.5	10	19.5
CM23	Ndu	91.75; 91.86	5.1	12	16

Table III.1 shows that the synthetic receiver functions (observed in red colour and predicted in blue colour) have an important percentage of signal power fit (>80%) in the major stations, apart from that corresponding to CM09 and CM15 stations located respectively at Ekona and Nkongsamba where, there is no agreement between the two curves (44.86% and 68.34). This can be further explained by the development of the volcanic activity in the two areas and more precisely in the Ekona located at the corner of mount Cameroon. We observe again that the wave has really undergone conversion under the different stations and the time of the identical conversion and multiple conversions varies. This means that the medium crossed by the wave has a heterogeneous structure in the Southern part of volcanic province of Cameroon.

b) Summary of the values coming from the shear wave inversion curve

Using the different criteria initially enumerated, the mean values coming from the curves of shear wave velocity inversion are summarized in the **Table III.2**

Table III.2. Interpretation of the inversion curves of the southern part of the volcanic province of Cameroon.

Station	Localities	Average crustal Vs(m/s)	Moho depth (km)	Thickness interval of LVZ (km)	Average lithospheric Vs (km/s)	lithospheric thickness (km)	Lithospheric mantle thickness (Km)
CM09	Ekona	3.8?	26.4?	87.6<LVZ<120?	3.5?	87.6?	61.2?
CM13	Kumba	3.8	26.4	68.4<LVZ<96.4	4.1	68.4	42
CM15	Nkongsamba	3.6?	36?	67.2<LVZ<96.4?	4.2?	67.2?	31.2?
CM16	Foumbot	3.7	35	78<LVZ<108	4.1	78	43
CM18	Mamfe	3.8	26.4	67.2<LVZ<109.2	4	67.2	40.8
CM19	Magba	4	36	67.2<LVZ<116.8	4.1	67.2	31.2
CM20	Wum	3.8	26.4	57.6<LVZ<108	4	57.6	21.6
CM23	Ndu	3.9	45.4	67.2<LVZ<108	4.1	67.2	26.4

The question mark appears in the first and third lines of the table above because, at Ekona and Nkonsamgba areas, there is no agreement on the synthetic receiver functions. So the inversion curve cannot be interpreted with certitude. And furthermore, **Table III.2** shows that from the velocity models, the average velocity of the S waves in the crust and lithospheric mantle are 3.8 km/s and 4.1 km/s respectively. Transition zones are localized firstly, at the mean depth of 26.4 km around the mount Cameroon region and between 35 km and 45.4 km of depth beneath the other localities for the Moho and secondly they vary from 57.6 km to 68.4 km of depth at the boundary between the lithosphere and asthenosphere (LAB) with an average of 70 km, for low velocity zone thicknesses varying between depth of 57.6 km and 116.8 km. Observing the different shear wave velocity models obtained, it appears that, the crust in this part of the Volcanic Province of Cameroon presents a thin nature in majority beneath the stations. Whereas, the lithospheric mantle has a thick structure with the thickness varying between 26.4 km and 45.2 km of depth in this part. The deepest layers are situated in the localities Nkongsamba, Ndu, Magba, and Foumbot. Some similarities (or uniformities) concerning the S-wave velocity (thin structure) and crustal depth are observed at the stations CM09 (?), CM13 and CM18. These uniformities can

be justified by the fact that the area covered by these stations constitutes the transition zone between continental and oceanic part of the Volcanic Line.

III.1.2 Results and interpretations for the Northern part of the volcanic province of Cameroon

This second part of Volcanic Province of Cameroon is also subdivided into two regions which are: Adamawa plateau and the Garoua rift.

III.1.2.1 Results and interpretations for the Adamawa plateau region

The Adamawa plateau region has seven seismic stations (**Figure III.1 B**). The results of this region are given by **Figure III.3 (a, b, c, d, e, f)** and the interpretations follow the same criteria and method.

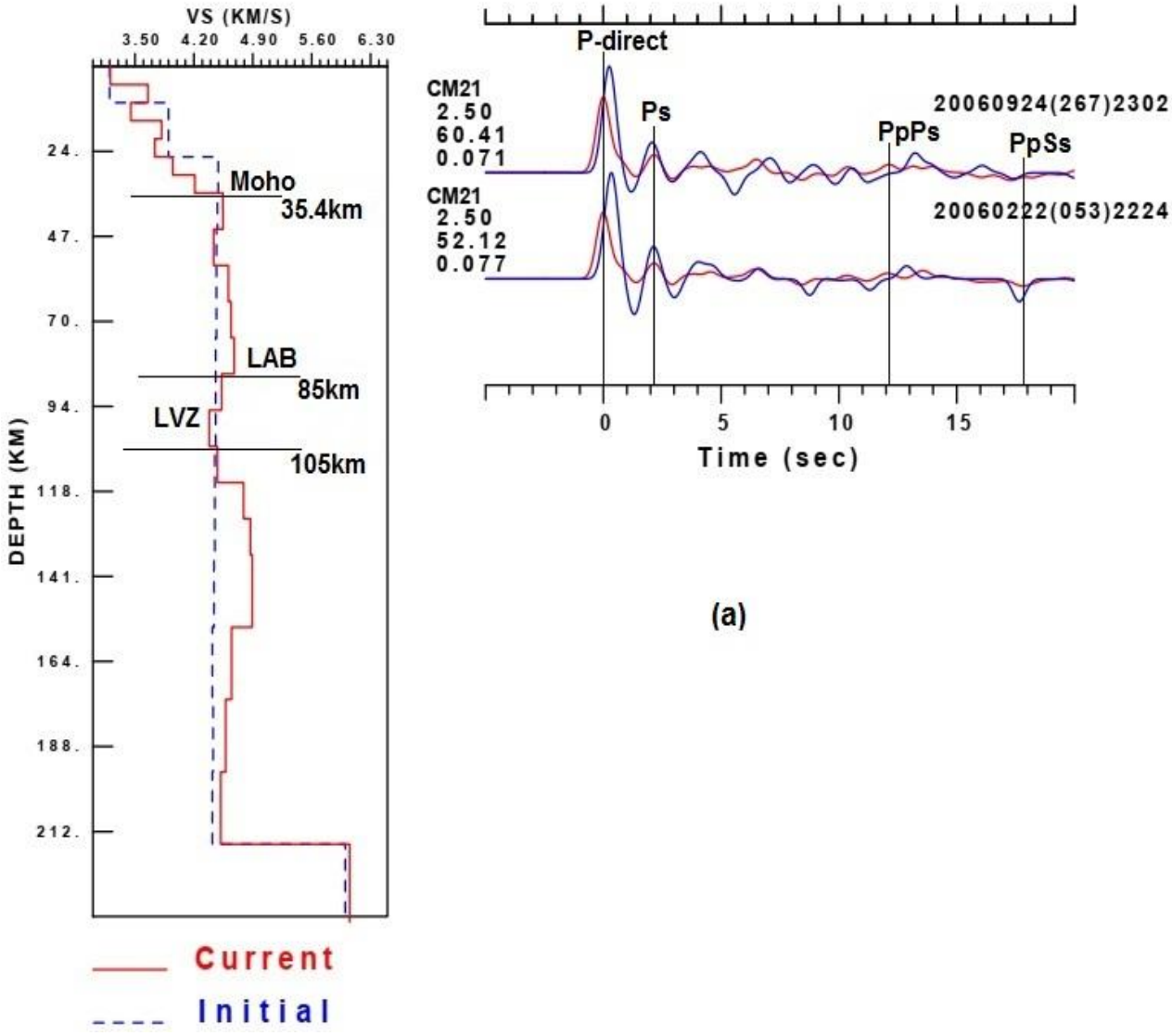

Figure III.3 (a) S-waves velocity model for CM21 station (Tibati)

This station was situated in the locality of Tibati in the Adamawa region. At the time of the treatment of the teleseismic events recorded, two of them, namely the one on the 53rd and 267th days of year 2006 respectively at 12 Am 25 min and 11 Pm 02 min have answered the basic criteria. For a Gaussian of 2.5 and the ray parameters of 0.077 and 0.071 respectively average misfits of 60.41% and 52.12% have been obtained. These average values indicate that the signal has undergone a disruption at the time of recording. This is equally observed on the synthetic receiver functions by non-superposition of the peaks of P-direct phase due to the time difference. This would be due to a major volcanic activity observed in this locality which is situated along the Foumban shear zone. Thus, an interpretation on the associated velocity model would be difficult.

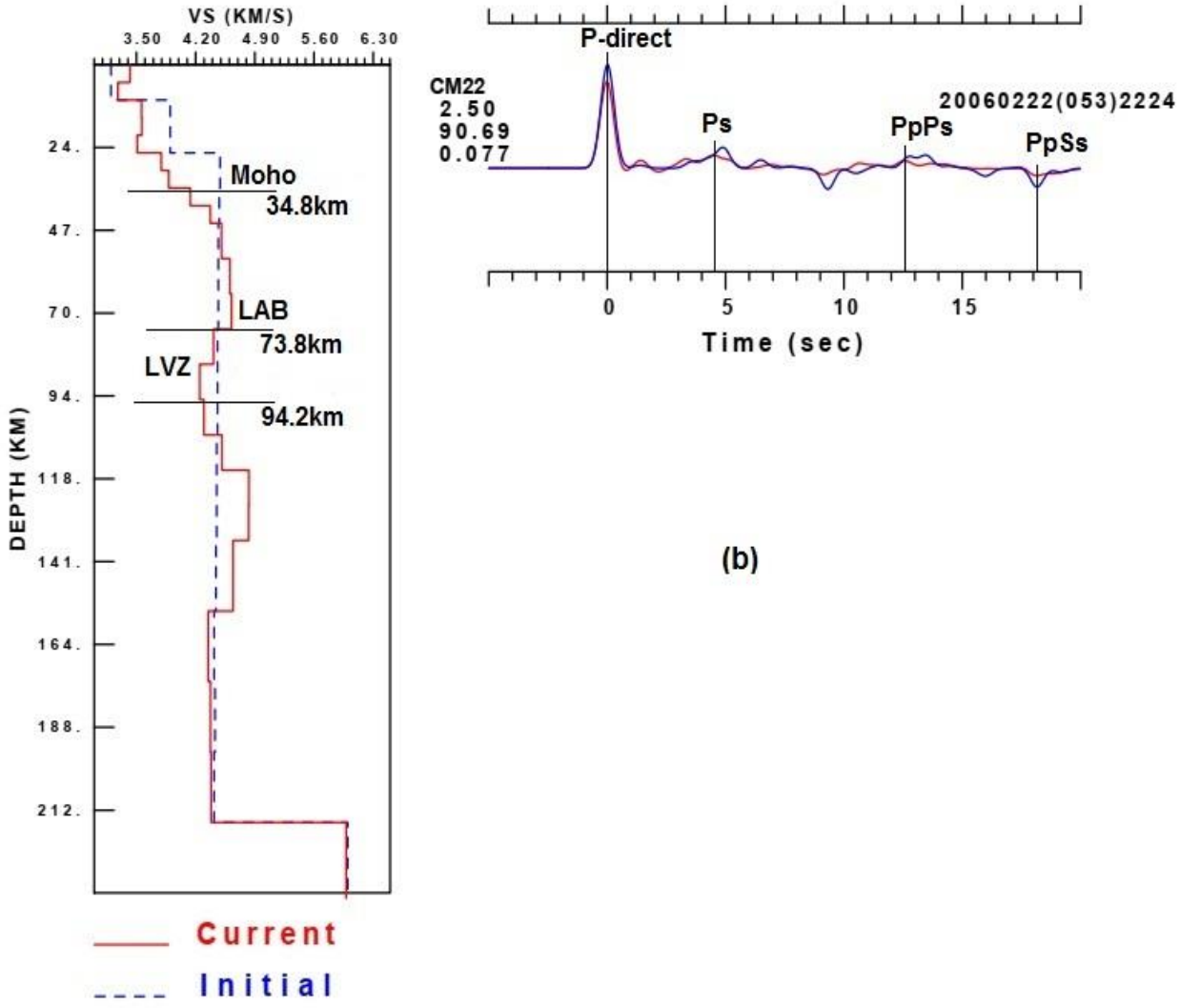

Figure III.3 (b) S-waves velocity model for CM22 station (Ngaoundal)

This station was situated in the locality of Ngaoundal. Only the teleseismic event corresponding to the 53rd day of the year 2006 at 10 Am 24 min has answered the basic criteria. For ray parameter of 0.077 and a Gaussian of 2.5, a satisfactory misfit of 90.69% has been

obtained at the time of the treatment of this event. This value shows that the wave doesn't practically have disruption at the time of its recording. This indicates a good correlation of the synthetic receiver functions. The P-direct phase corresponding ot the origin of times is followed by the Ps converted phase at 4.5 s and the multiple phases converted PpPs and PpSs at12.5 s and 18.4 s, respectively. This proves that the wave has really undergone a conversion at the level of Moho.

The S-wave velocity model associated to the synthetic receiver functions, presents a low drop of velocity at 5 km, followed by a strong velocity anomaly at 10 km. Beyond this depth, a very low drop of velocity is observed, followed by a sequence of positive velocity anomalies observed until 73.8 km. According to Christensens, 1996 and Christensens Money and, 1995, the transition zone between the crust and upper mantle would be located at about 34.8 km of depth. The alternation of the velocity anomalies would denote the thin character of the crust. Beyond 73.8 km, the negative velocity anomaly is observed until 94.2 km. This thickness would represent a low velocity zone of the upper mantle, which permits to limit the lithosphere at 73.8 km of depth. The sequence of positive velocity anomalies observed since a transition zone until the limit of lithosphere indicates the thick character of the lithospheric mantle.

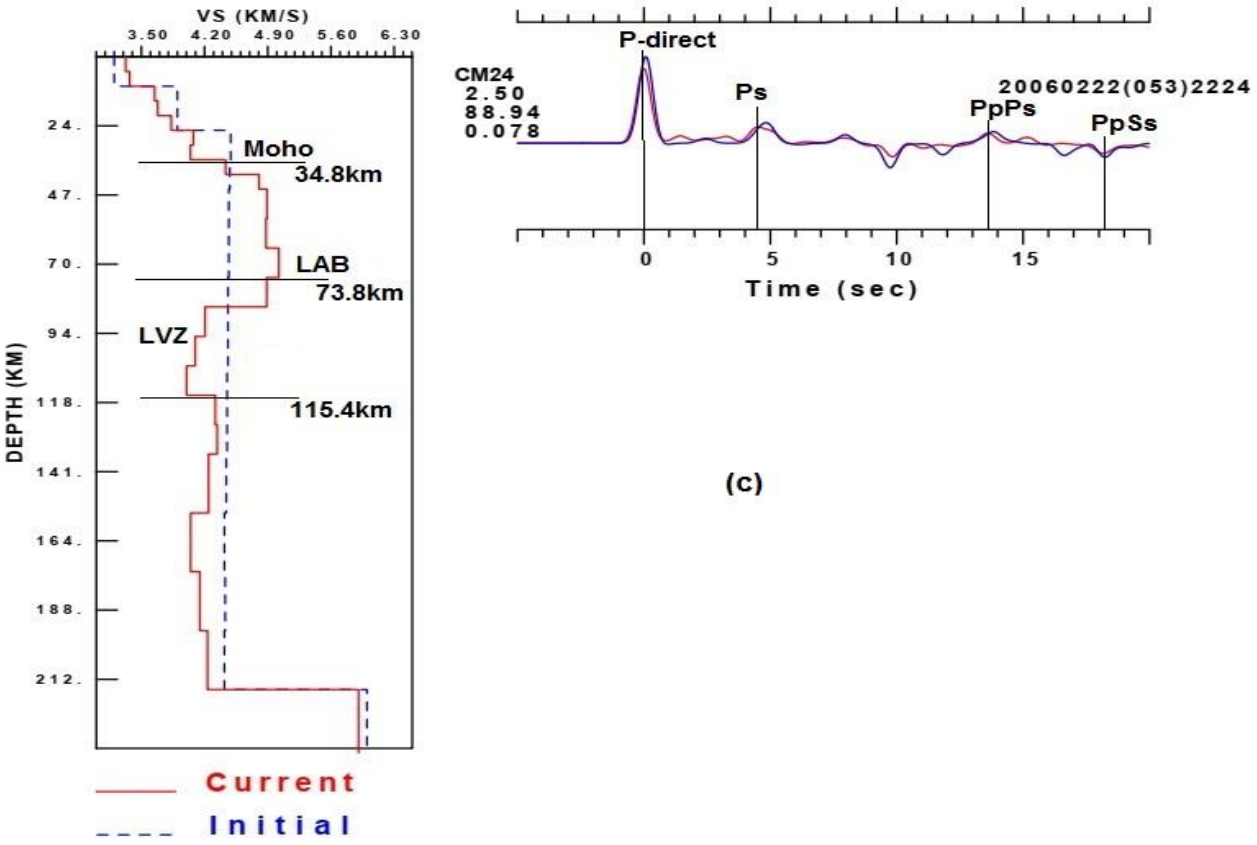

Figure III.3 (c) S-waves velocity model for CM24 station (Meinganga)

This station was situated in the locality of Meiganga. Only the corresponding teleseismic event on the 53rd day of the year 2006 at the time 10 Am 24 min has answered the initially fixed criteria at the time of the treatment. For a ray parameter of 0.078 and the gaussian of 2.5, a satisfactory misfit of 88.94% has been obtained. This value indicates a good correlation observed on the synthetic receiver functions. The P-direct phase corresponding to the origin of times is followed by the Ps converted phase at 4.5 s and multiple converted phases PpPs and PpSs at 13.8 s and 18.3 s respectively. This proves that the wave has really undergone a conversion at the level of the Moho. .

The velocity model obtained by inversion shows a sequence of positive velocity anomalies until 73.8 km. The strong ones are located respectively at 10 km and 34.8 km. The first one indicates the transition zone in the crust, whereas the second one would indicate the transition zone between the crust and upper mantle. Beyond this last transition zone, one observes a sequence of negative anomalies which would indicate a low velocity zone of the upper mantle. This zone allows to delimit the lithosphere at 73.8 km of depth. The sequence of the velocity anomalies observed since the surface until 73.8 km would be due to the thick character of the crust and the lithospheric mantle in Meinganga.

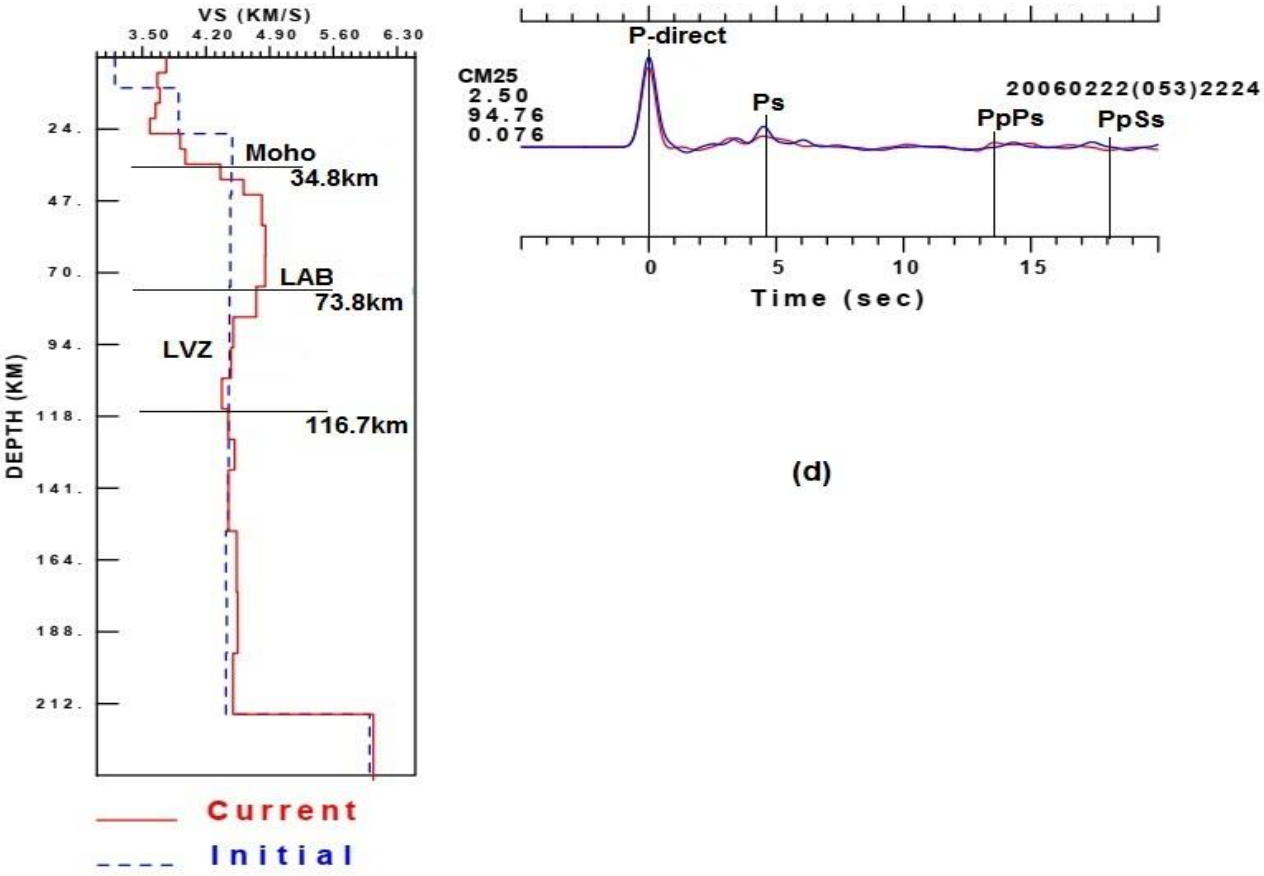

Figure III.3 (d) S-waves velocity model for CM25 station (Banyo)

This station was situated in the locality of Banyo in the Adamawa region. Only the corresponding teleseismic event on the 53rd day of the year 2006 and at the time 10 Am 24 min has answered the basic criteria. For a ray parameter of 0.076 and a Gaussian of 2.5, a satisfactory misfit of 94.76% has been obtained at the time of the inversion. This value shows that the wave doesn't practically have a disruption at the time of its recording. This indicates a good correlation on the synthetic receiver functions. The P-direct phase corresponding to the origin of times is followed by the Ps converted phase at 4.5 s and the multiple converted phases PpPsand PpSs at13.6 s and18 s, respectively. This proves that the wave has really undergone a conversion to the level of the Moho.

The associated velocity model presents firstly two positive velocity anomalies, of which the low one appears at 5 km and the other strong one at 10 km. Beyond this depth, two drops of velocity are observed until 20 km. These last anomalies are followed by a sequence of positive velocity anomalies until 85 km of depth. Based on Christensens, 1996 and Christensens Money and, 1995, the transition zone between the crust and upper mantle would be located at about 36.1 km of depth. Beyond 85 km of depth, a sequence of velocity drops is observed until 116.7 km of depth. This interval of drops would represent a low velocity zone of the upper mantle, which permits to limit the lithosphere at 85 km of depth. The alternation of positive and negative velocity anomalies observed before 36.1 km of depth would indicate the thin character of the crust, whereas the sequence of positive velocity anomalies observed at the level of lithospheric mantle would indicate the thick character of this part of the earth.

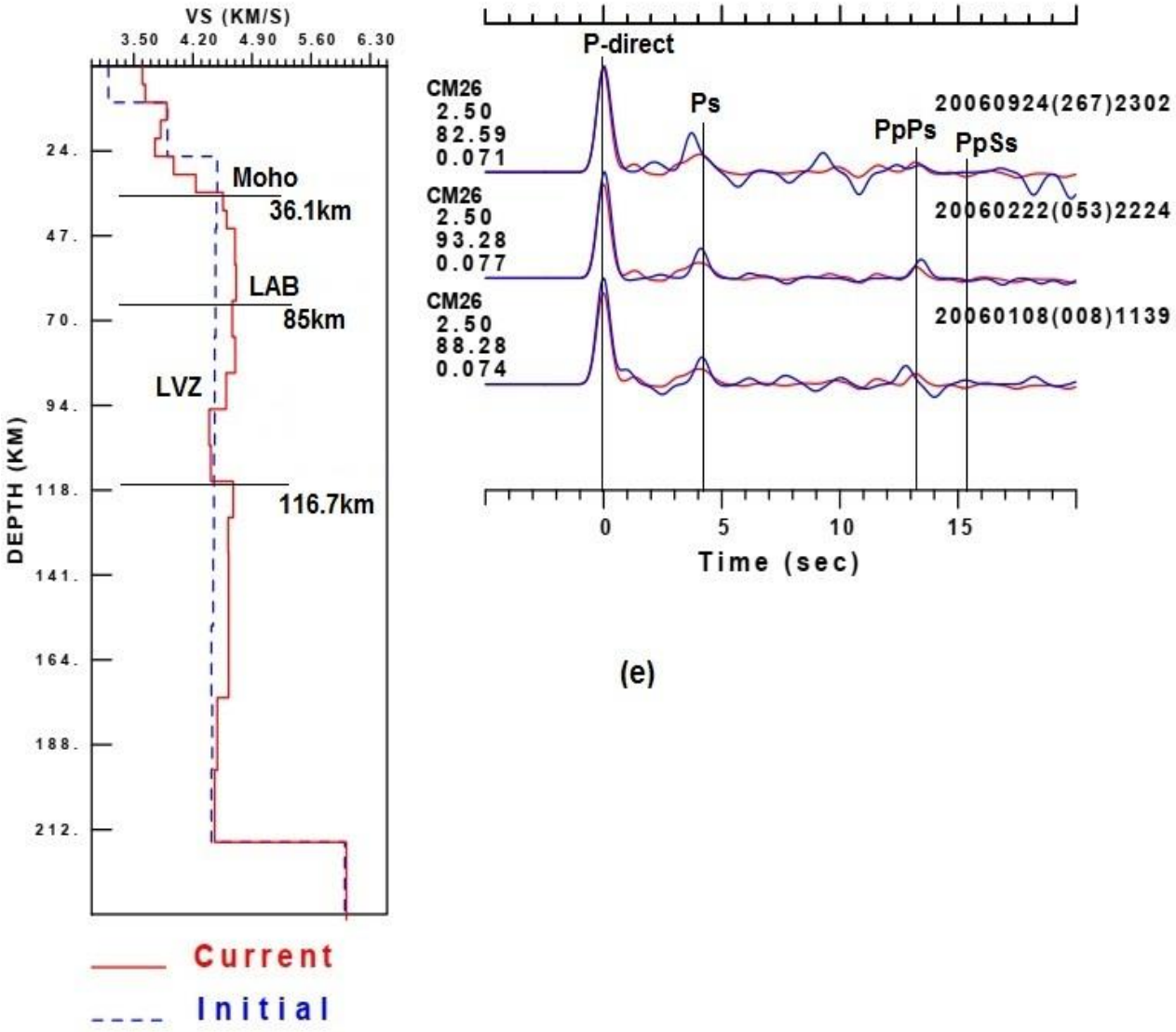

Figure III.3 (e) S-waves velocity model for CM26 station (Ngaoundere)

This station was situated in Ngaoundere. Unlike the previous, three teleseismic events satisfied the basic criteria. It is specifically those of the 8rd, 53rd and 267rd day of the year 2006 at the respective times: 11 Pm 39 min, 10 Am 24 min and 11 Am 02 min. For a Gaussian of 2.5 and the respective ray parameters of 0.074, 0.0.077 and 0.071, the satisfactory misfits of 88.28, 93.28 and 82.59 respectively have been obtained. These values show that, the wave has practically undergone no disruption. This is justified by the superposition of the P-direct phase observed at the origin of times on the synthetic receiver functions. This last phase is followed by the Ps conversion at4 s and the multiple converted phases PpPs and PpSs respectively at13.3 s and17.5 s. This proves that the wave has really undergone a conversion at the level of the Moho.

On the velocity model, two positive velocity anomalies are observed, of which one is very low situated at 5 km and the other less strong at 10 km depth. This last is followed by two others but, negative and very low on one hand and, of a sequence of positive velocity anomalies until 85 km of depth on other hand. Based on Christensens, 1996 and Christensens Money and, 1995, the transition zone between crust and upper mantle would be located at about 36.1 km of depth. Beyond 85 km of depth, a sequence of velocity drops is observed until 116.7 km. This interval of drops would represent a low velocity zone of the upper mantle, which permits to limit the lithosphere at 85 km of depth. The alternation of positive and negative velocity anomalies observed before 36.1 km of depth would indicate the thin character of the crust whereas the sequence of positive velocity anomalies observed in the lithospheric mantle would translate its thick character.

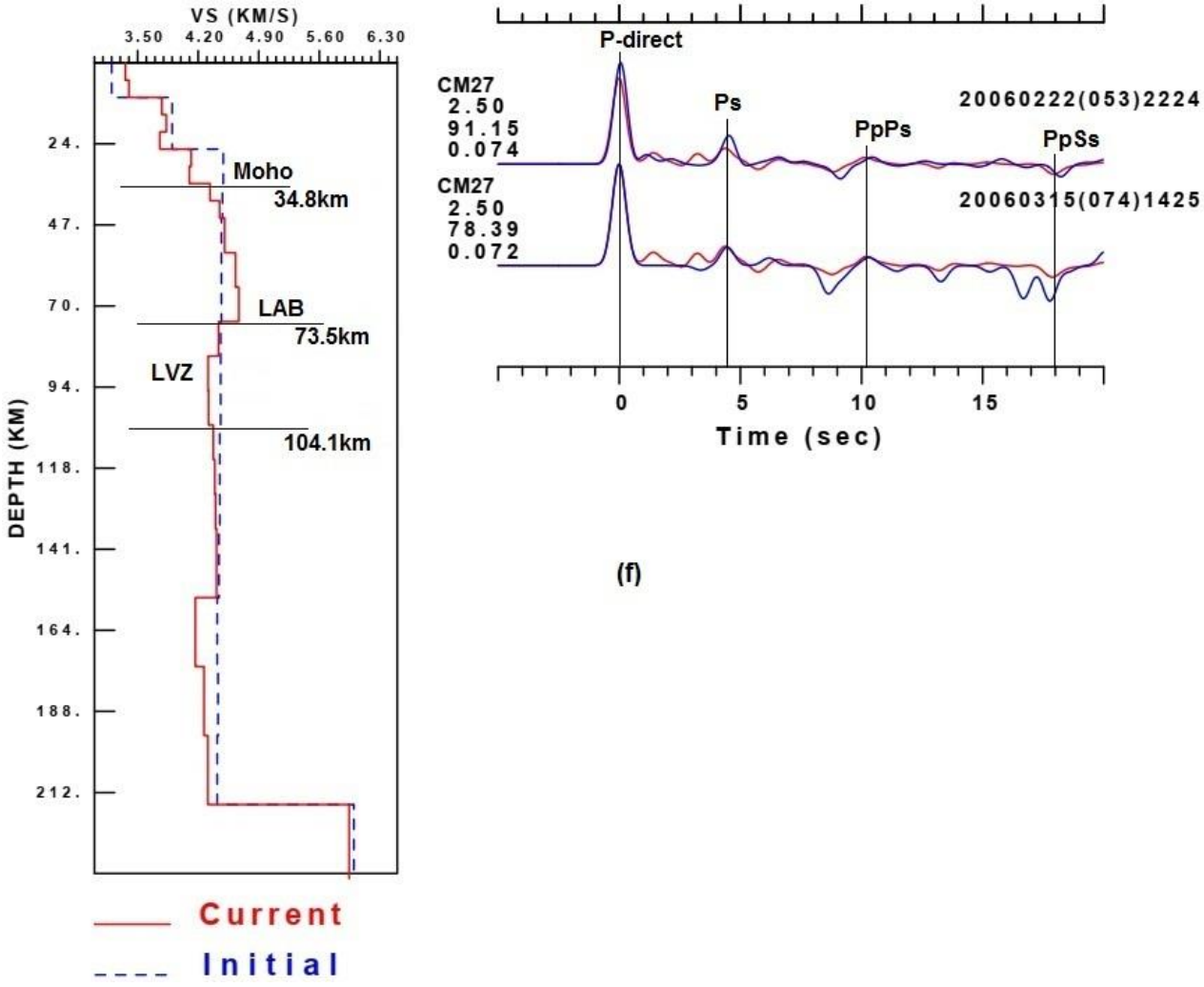

Figure III.3 (f): S-waves velocity model for CM27 station (Tignere)

This station was installed in the Tignere locality. Two teleseismic events, namely the one on the 53rd and 74th day of the year 2006 respectively at 10 Am 24 min and 2 Pm 25 min satisfied the basic criteria. For a Gaussian of 2.5 and the respective ray parameters of 0.074 and 0.072 the satisfactory misfits of 91.15% and 78.39% has been obtained respectively. These values show that the wave has practically undergone no disruption. This is justified by the superpositions of the P-direct phase observed at the origin of times on the synthetic receiver functions. This phase is followed by the Ps conversion at 4.6 s and the multiple converted phases PpPs and PpSs respectively at10.5 s and18 s. This proves that the wave has really undergone a conversion at the level of the Moho.

The S-wave velocity model obtained shows a sequence of positive velocity anomalies until 73.5 km depth with a very light drop appearing at 20 km. The strongest appear respectively at 10 km, 26 km and 34.8 km of depth. Based on Christensens, 1996 and Christensens Money and, 1995, the transition zone between the crust and upper mantle would be located at about 34.8 km of depth. Beyond 73.5 km, a sequence of negative velocity anomalies is observed until 104.1 km of depth. This interval of drops would represent a low velocity zone of the upper mantle that permits to limit the lithosphere to 73.5 km of depth. The sequence of positive velocity anomalies observed since the surface until 73.5 km would translate the thick behavior of the crust and lithospheric mantle.

The mean values obtained on the synthetics receiver functions in one hand and on the S-waves velocity models on the other hand are summarized on table III.3 and table III.4

a) Summary of the values coming from of synthetic receiver functions

Concerning the different synthetic receiver functions obtained in the Southern part regrouping the mounts, the different conversions and multiple conversions appearing and their corresponding time are summarized in the **Table III.3**

Table III.3: Interpretation of synthetic receiver functions

Station	Localities	Percent of Signal Power Fit	t_{Ps} (s)	t_{PpPs}(s)	t_{PpSs}(s)
CM21	Tibati	60.41; 52.12	2?	12?	17?
CM22	Ngaoundal	90.69	4.5	12.5	18.4
CM24	Meinganga	88.94	4.5	13.8	18.3
CM25	Banyo	94.76	4.5	13.6	18
CM26	Ngaoundere	82.59; 93.28; 88.28	4	13.3	17.5
CM27	Tignere	91.15; 78.39	4.6	10.5	18

Table III.3 shows that, the synthetic receiver functions have a very important percentage of Signal Power Fit (> 80%) except for that corresponding to CM21 located in the Tibati locality due to its location on the Foumban shear zone (FSZ). This justifies a stability of the curves of current and initial model and it causes the wave to undergo a rare conversion. The times of Ps and multiple conversions are practically uniform for some stations and different for others. It may express the heterogeneous character of the earth structure of the crust in this locality.

c) Summary of the values coming from the shear wave inversion curve

The principal values given by the S-wave velocity profile are summarized in the table III.4

Table III.4: Interpretation of the inversion curves

Stations	Localities	Average crustal Vs (km/s)	Moho depth (km)	thickness interval of LVZ (km)	Average lithospheric Vs (km/s)	Average lithospheric thickness (km)	Average lithospheric mantle (km)
CM21	Tibati	3.8?	35.4?	85 < LVZ< 105?	4.4?	85?	49.6
CM22	Ngaougal	3.7	34.8	73.8< LVZ< 94.2	4.4	73.8	39
CM24	Meinganga	3.8	34.8	73.8<LVZ<115	4.2	73.8	39
CM25	Banyo	3.9	34.8	73.8<LVZ<116.7	4.6	73.8	39
CM26	Ngaoundere	4	36.1	85<LVZ<116.7	4.6	85	48.9
CM27	Tignere	3.7	34.8	73.8<LVZ<104	4.4	73.8	39

Table III.4 shows from the velocity models that, the velocity of the S waves is 3.7 km/s in the crust and, more than 4 km/s in the lithosphere. The transition zones are firstly localized at an average depth of 35.1 km between the crust and the upper mantle (Moho) and secondly, at the depth varies between 73.8 km to 85 km at the boundary between the lithosphere and the asthenosphere (LAB). The low velocity zone (LVZ) thickness ranges between depth of 73.8 km and 116.7 km. In this zone of the Volcanic Province of Cameroon, according to the shear velocity profiles, the crust shows a thick behavior whereas the lithospheric mantle presents a thin behavior. The uniformities of the different results (concerning the different depths) presented in the different stations can be justified by the fact that, the different localities where the seismic stations have been installed (Ngaoundal, Meinganga, Banyo and Tignere) in this region describe the part of Central African Shear Zone (CASZ). But a question mark is observed in the table above. This is due by the fact that, the interpretation of the shear wave velocity profile at that station is uncertain because the percentage of the signal fit is less that 80%.

III.1.2.2 Results and interpretations for the Garoua rift region

The Garoua ritf region has five seismic stations (**Figure II.1 (B**)). The results of this region are presented in Figure III.3 and the interpretations follow the same criteria and method.

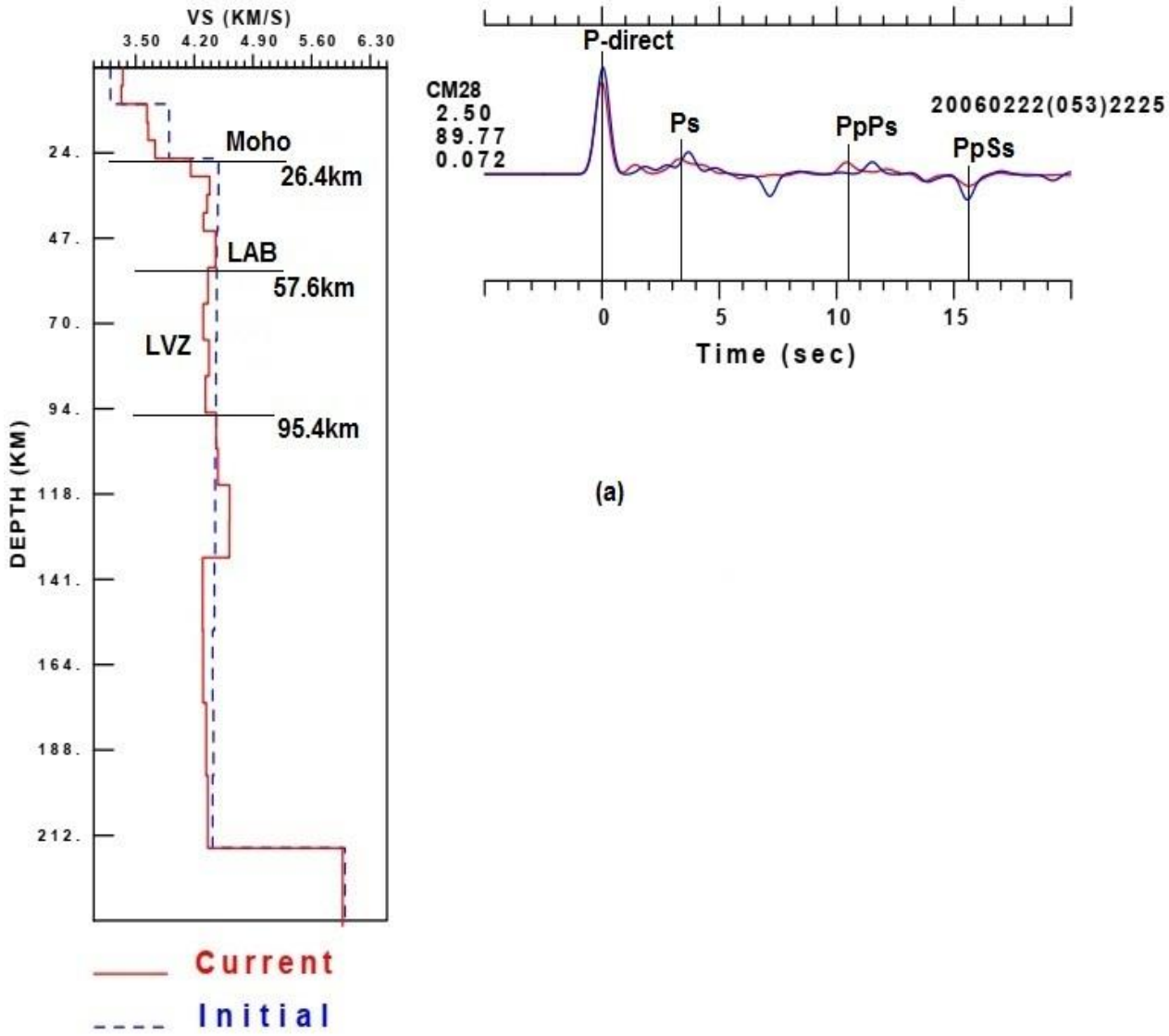

Figure III.4 (a) S-waves velocity model for CM28 station (Poli)

This station was installed in the locality of Poli in the North Cameroon. Only the corresponding teleseismic event on the 53rd day of the year 2006 at 10 Am 25 min has answered the basic criteria at the time of treatment. For a ray parameter of 0.072 and the Gaussian filter of 2.5, a satisfactory misfit of 89.77% has been obtained at the time. This value indicates a good correlation of the synthetic receiver functions. The P-direct phase corresponding to the origin of times is followed by the Ps converted phase at 3.2 s and multiple converted phases PpPse and PpSs at 10.5 s and 15.5 s respectively. This proves that the wave has really undergone a conversion at the level of the Moho.

Concerning the velocity model associated to the synthetic receiver functions, it appears a low negative velocity anomaly at 5 km of depth followed by a sequence of positive velocity anomalies until 28 km. Still based on Christensens, 1996 and Christensens Money and, 1995, the transition zone (Moho) between the crust and the upper mantle and more precisely the lithospheric mantle would be located around 26.4 km of depth. The sequence of positive velocity anomalies observed before this zone would translate the thick behavior of the crust. Beyond this transition zone, an alternation of positive and negative velocity anomalies is observed from 28 km until 57.6 km of depth. Beyond this one, a sequence of velocity drops is observed until 95.4 km. This last part would translate a low velocity zone, which allows us to limit the lithosphere to 57.6 km of depth in the locality of Poli. The alternation of velocity anomalies observed between the transition zone and the lower limit of the lithosphere would indicate the thin behavior of the lithospheric mantle.

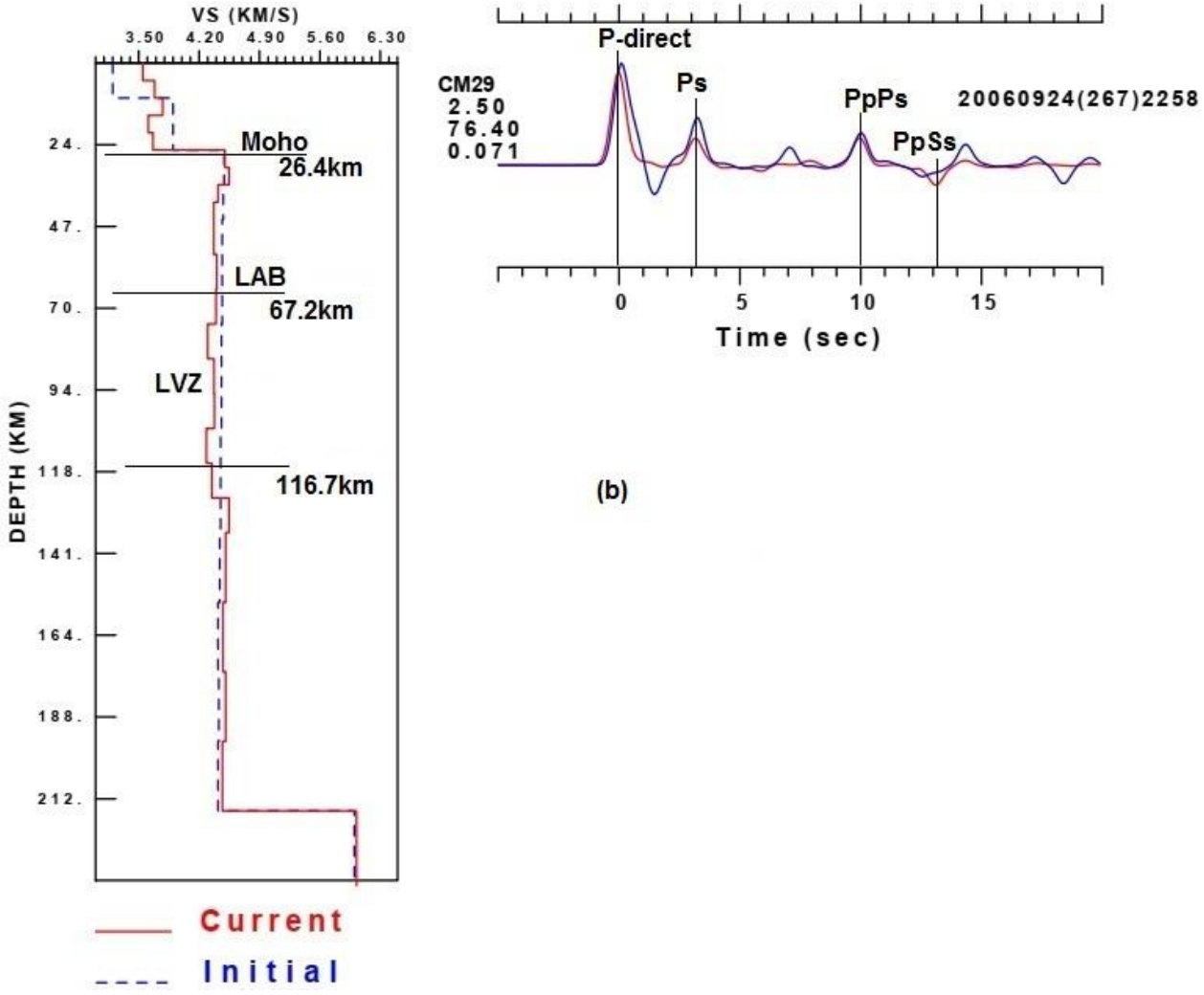

Figure III.4 (b) S-waves velocity model for CM29 station (Garoua)

This station was installed in the locality of Garoua in the North Cameroon. Only the corresponding teleseismic event on the 267rd day of the year 2006 taking place at 10 Am 58 min fulfilled the basic criteria at the time of the treatment. For a ray parameter of 0.071 and a Gaussian of 2.5, a satisfactory misfit of 76.40% has been gotten at the time of inversion. This value shows that the signal has been disrupted weakly. This disruption is justified by the time difference observed at the origin of times at the P-direct phase on the synthetic receiver functions. Nevertheless, the converted phase Ps appears at 3.1 s and the multiple converted phases PpPs and PpSs respectively at 9.9 s and 13 s exist. This proves that in spite of this disruption, the wave has undergone the conversions at the level of Moho.

The associated velocity model shows a sequence of two positive velocity anomalies until 10 km depth. This latter is followed by a velocity drop and two other positive velocity anomalies of which the strongest is located at 26.4 km. This last depth would translate the transition zone between the crust and upper mantle. The alternation of the velocity anomalies observed would translate the thin behavior of the crust in this locality. Beyond the zone, a positive and low velocity anomaly is perceptible followed by a sequence of two velocity drops that spreads on a large thickness before another positive and low velocity anomaly is also observed until 67.2 km of depth. Beyond this depth, a velocity drop is observed until 116.7 km. This last interval would translate a low velocity zone that allows us to limit the lithosphere at 67.2 km of depth. The alternation of the velocity anomalies observed would translate the thin behavior of the lithospheric mantle in this locality.

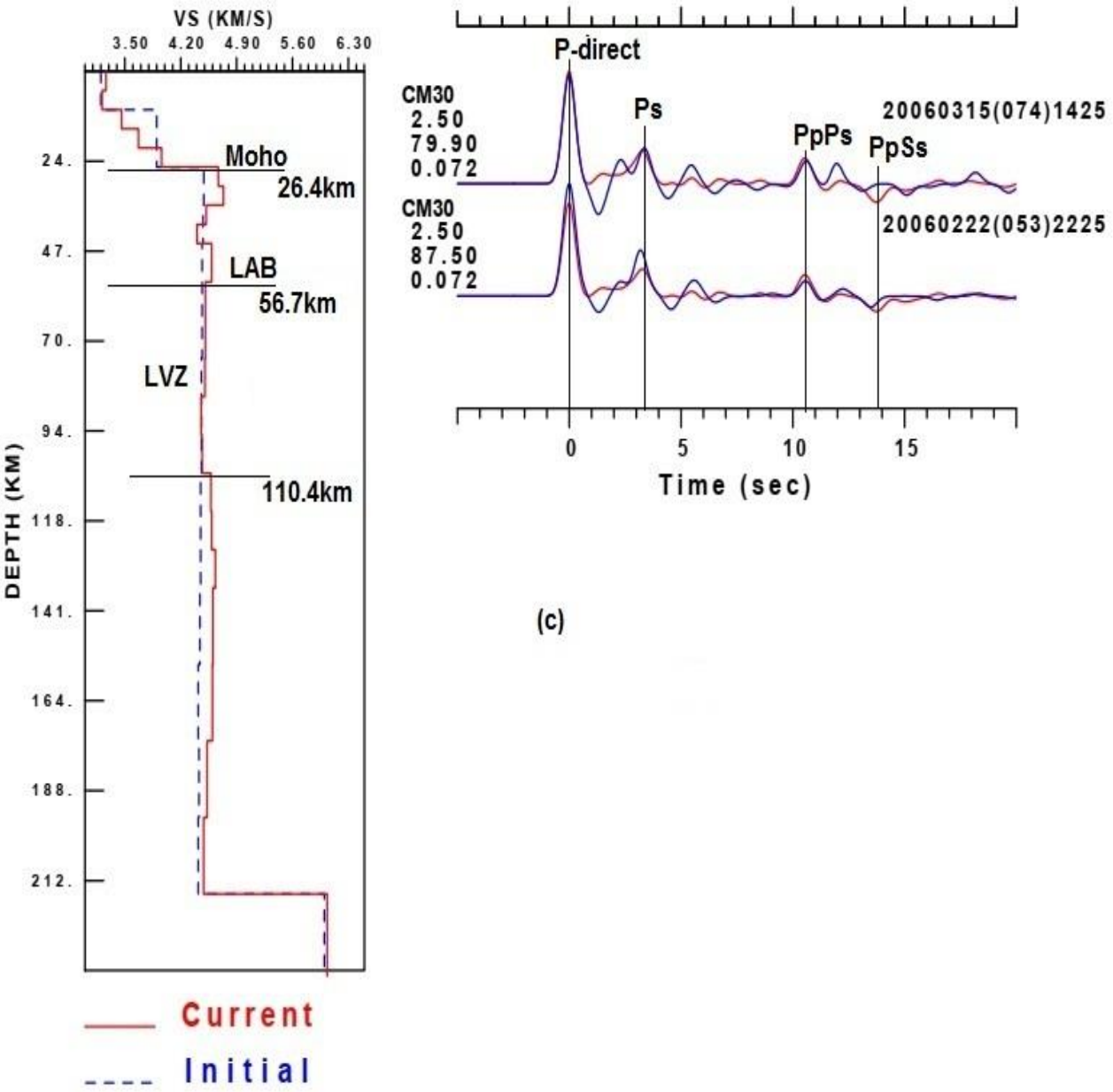

Figure III.4 (c) S-waves velocity model for CM30 station (Figuil)

This station was also situated in Figuil in the North region of Cameroon. Two teleseismic fulfilled the basic criteria, namely those on the 53rd and 74th day of the year 2006 respectively at 10 Am 25 min and 2 Pm 25 min. For a Gaussian filter of 2.5 and a double ray parameter of 0.072, respective misfits of 87.50% and 79.90% have been gotten. These values show that the wave has undergone very light disruptions. It is justified by the superposition of the P-direct phase observed at the origin of times on the synthetic receiver functions. This phase is followed by the Ps conversion at 3.2 s and the multiple converted phases PpPs and PpSs at10.5 s and13.5 s, proving that the wave has really undergone a conversion at the level of the Moho.

The velocity model obtained presents a succession of positive velocity anomalies until 28 km of depth. This succession is previously preceded by a negative velocity anomaly at 5 km of

depth. On this last sequence, the strongest are respectively at 10 km and 26.4 km. This last depth would indicate the transition zone between the crust and upper mantle. The succession of positive velocity anomalies observed would translate the thick character of the crust in Figuil. Beyond 28 km of depth, two velocity drops appear followed by a positive velocity anomaly that spreads until 56.7 km. Beyond this last depth, a low velocity drop is observed until 110.4 km of depth. This interval would translate a low velocity zone of the upper mantle that permits to limit the lithosphere at 56.7 km of depth. The alternation of velocity anomalies observed between the interval of 26.4 km to 56.7 km would translate the thin character of the lithospheric mantle. The alternation of the velocity anomalies observed would translate the thin behavior of the lithospheric mantle in this locality

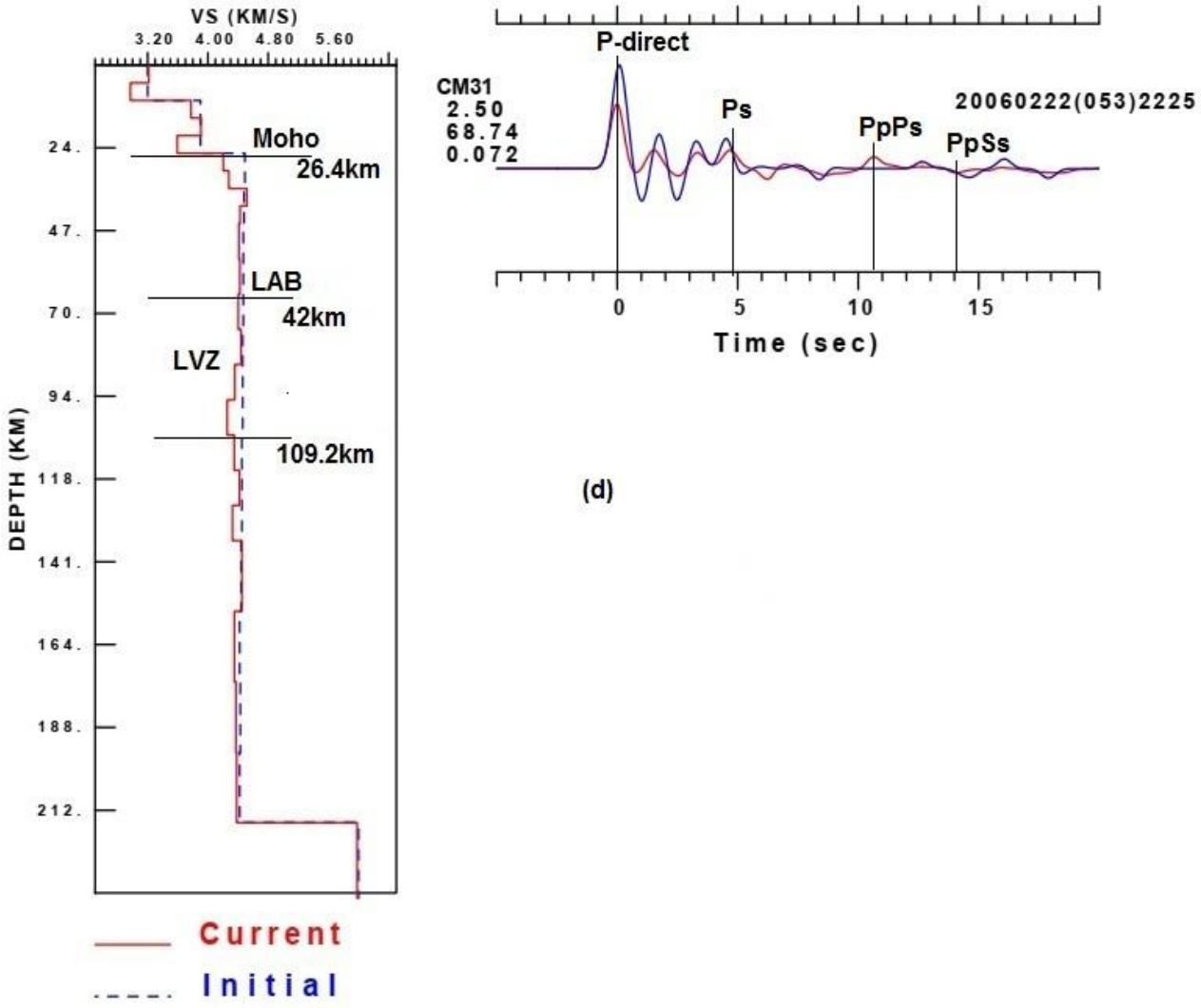

Figure III.4 (d) S-waves velocity model for CM31 station (Yagoua)

This station was also situated in the North Cameroon and more precisely in the locality of Yagoua. Only the teleseismic event corresponding to the 53rd day of the year 2006 occurred at 10 Am 25 min has answered the basic criteria at the time of treatment. For a ray parameter of 0.072 and a Gaussian filter of 2.5, a fairly low misfit of 68.74% has been gotten. This last value shows that, the wave has undergone a minor disruption, which is revealed by the slight time difference appearing at the level of P-direct phase on the synthetic receiver function this made that it is difficult to detect the converted phase and multiple phase to the level of the Moho. This disruption comes surely from a weakly active fault in this locality. It influences the velocity model that becomes difficult to interpret.

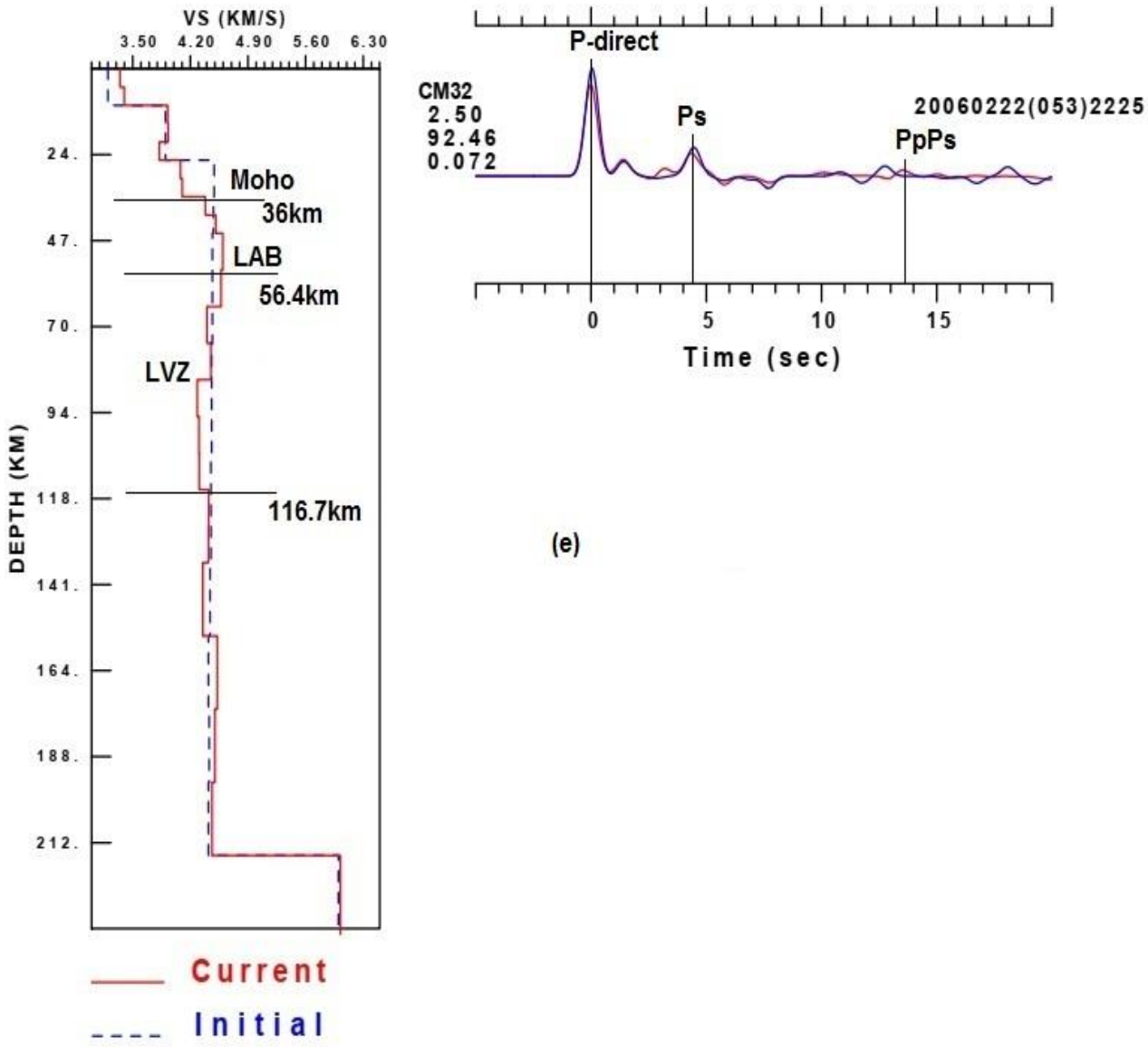

Figure III.4 (e) S-waves velocity model for CM32 station (Maroua)

This station was situated in the locality of Maroua at the Far North of Cameroon. As the previous station, the same teleseismic event has answered the initial criteria. An important misfit of 92.46% has been obtained for a Gaussian filter of 2.5 and ray parameter of 0.072. This value shows that the wave did not practically undergo a disruption. This is justified by the perfect superposition observed at the level of the P-direct phase at the origin of times on the synthetic receiver functions. This phase is followed by the Ps conversion at 4.6 s and the multiple converted phases PpPs and PpSs at 13.5 s.This proves that the wave has really undergone a conversion to the level of the Moho.

The corresponding velocity model presents two positive velocity anomalies of which, the strongest is located at 10 km of depth. The latter is followed by a velocity drop at 20 km and a sequence of positive velocity anomalies until 56.4 km of depth. Based on Christensens, 1996 and Christensens Money and, 1995, the transition zone (Moho) between the crust and the upper mantle would be located around 36 km. The alternation of anomalies observed before this last zone would translate the thin character of the crust. Beyond 56.4 km of depth, a sequence of velocity drops is observed until 116.7 km. This part of the upper mantle would translate a low velocity zone permitting to limit the lithosphere at 56.4 km of depth. The sequence of positive velocity anomaly observed after the transition zone would translate the thick character of the lithospheric mantle.

The mean values obtained on the synthetics receiver functions in one hand and on the S-waves velocity models on the other hand are summarized on table III.5 and table III.6

a) Summary of the values coming from of synthetic receiver functions

Concerning the different synthetic receiver functions obtained in the Garoua rift region, the different conversions and multiple conversions appearing and their corresponding time are summarized in the **Table III.5**

Table III.5: Interpretation of synthetic receiver functions of the Garoua rift region

Station	Localities	Percent of Signal Power Fit	t_{Ps} (s)	t_{PpPs}(s)	t_{PpSs}(s)
CM28	Poli	89.77	3.2	10.5	15.5
CM29	Garoua	76.40	3.1	9.9	13
CM30	Figuil	79.90; 87.50	3.2	10.5	13.5
CM31	Yagoua	68.74?	4.5?	10.7?	18.2?
CM32	Maroua	92.46	4.6	13.5	?

This table shows from the curves of the receiver functions obtained that, a better agreement is observed between the two curves, and the wave has really undergone the conversion as compared to the previous stations. The exception in this area exist at the station located in Garoua on one hand where, the attenuation of the wave begins to be observed at the station CM30 located at Figuil by increase of the conversion time and the weakness in the amplitude of the phases which, finally disappear in the station CM32 situated at Maroua. This can be due to inelastic material behavior or internal friction during wave propagation and expresses the heterogeneous character of the crust and anisotropy within the sub-crustal lithosphere of this zone. And the other hand at the station CM31 located at Yagoua locality where, the misfit is less than 80%. This means that, the wave has been disrupted in this locality. It can be surely due by a weakly active fault in this locality.

a) Summary of the interpretations of the shear wave inversion curve

The mean values given by the S-wave velocity profile are summarized in the table III.6.

Table III.6: Interpretation of the inversion curves

Station	Localities	Average crustal Vs (km/s)	Moho depth (km)	Thickness interval of LVZ (km)	Average lithospheric Vs (km/s)	Average lithospheric thickness (km)	Average lithospheric mantle thickness (km)
CM28	Poli	3.7	26.4	57.6<LVZ< 99.6	3.9	57.6	31
CM29	Garoua	4	26.4	67.2<LVZ<118.8	4	67.2	40.8
CM30	Figuil	4	26.4	56.4<LVZ<110.4	4.05	56.4	30
CM31	Yagoua	3.6 ?	26.4 ?	42<LVZ<109.2 ?	3.75 ?	42 ?	15.6 ?
CM32	Maroua	3.8	36	56.4<LVZ<98.4	3.9	56.4	20.4

The velocity models obtained by inversion of the receiver function followed by the different values coming from table III.6 at the Garoua rift sector allow us to say that the crust is thin with the mean S-waves velocity of the of 3.8 km/s and the mean thickness of 28 km. The lithospheric mantle is on the contrary thick with mean S-wave velocity of 3.9 km/s and its thickness varies between 15.6 km and 40.8 km. The Low Velocity Zone is located between 42 km and 62.2 km of depth. The discontinuities are situated firstly at 26.4 km of depth for the Moho except for the Maroua station where it is located at 36 km. It can be explained by the variation in topography of this region and the magmatic upwelling due by presence of the Mandara mountain

around the station. Secondly located between 42 km and 67.2 km in the upper mantle, in particularly at the boundary between the lithosphere and asthenosphere.

III.2 Discussions

In this section, we will start by comparing the different results obtained per by region and carry out comparison with other case studies in literature.

III.2.1 Comparison of the results per region

The interpretation of the results has followed two channels. So the comparison will be done follow the different types of curves obtained.

III.2.1.1 Comparison of the results of synthetic receiver functions

To bring out some similarities or differences appearing on the results of the synthetic receiver functions of our work, we shall firstly come out the different comparisons describe by the mean time of the Ps conversions and the subsequent reverberates PpPs and PpSs by region of the Volcanic Province Cameroon (Southern of Volcanic Province of Cameroon; Adamawa and Garoua rift regions) and secondly, followed by the comparison from literature (**Table III.7**)

Table III.7: Comparison of arrival times of the different Ps phases and the subsequent reverberants per region and with result of other studies.

Regions	This study			Other study (stacking of the receiver function)			Reference
	t_{Ps} (s)	t_{PpsP} (s)	t_{PpSs} (s)	t_{Ps} (s)	t_{PpsP} (s)	t_{PpSs} (s)	**Gallacher and Bastow (2012)**
Southern of CVL	4	12.1	16.6	4	13	18	
Adamawa plateau	4.4	12.7	18.8	3.5	11	15	
Garoua rift	3.7	11	17.6	3.2	10.5	14	

This table enables us to see that the time of the Ps conversions and the subsequent reverberates are highly different by localities. This difference shows that, the crustal structure along the Volcanic Province of Cameroon is heterogeneous. This heterogeneity has been confirmed recently by Tokam et *al.*, (2010) and Guidarelli and Aoudia (2016). Comparing our values with those obtained by Gallacher and Bastow (2012), there are slight differences concerning the multiple conversions. These differences can be explained by the method used in computing the same data.

III.2.1.2 Comparison of the results of the shear wave velocity models

The velocity models obtained at the different stations along the Volcanic Province of Cameroon show the similar velocity model structure where, the crust is thick in the Adamawa plateau and thin in the Garoua rift with the mean S-wave velocity of 3.8 km/s except at the southern part where at the stations CM09, CM13 and CM18 the crust is thick. This behavior is support respectively by the authors Nnange et al. (2000) for the Adamawa plateau region and Stuart et al. (1985), Poudjom et al. (1995), Kamguia et al. (2005) and Tokam et al. (2010) for the Garoua rift region. The difference observed in behavior with respect to the other mountains of the southern part could be justified by their localization at the transition zone between the continental and ocean part (the continent/ocean boundary) of the volcanic Line. Concerning the lithospheric mantle along the Volcanic Province of Cameroon, the behavior is thick beneath the plateau and mountains whereas it is thin in the rift. The comparison of the crust and lithosphere thickness along this line is showed by **Figure III.5 (a)** and **(b)**

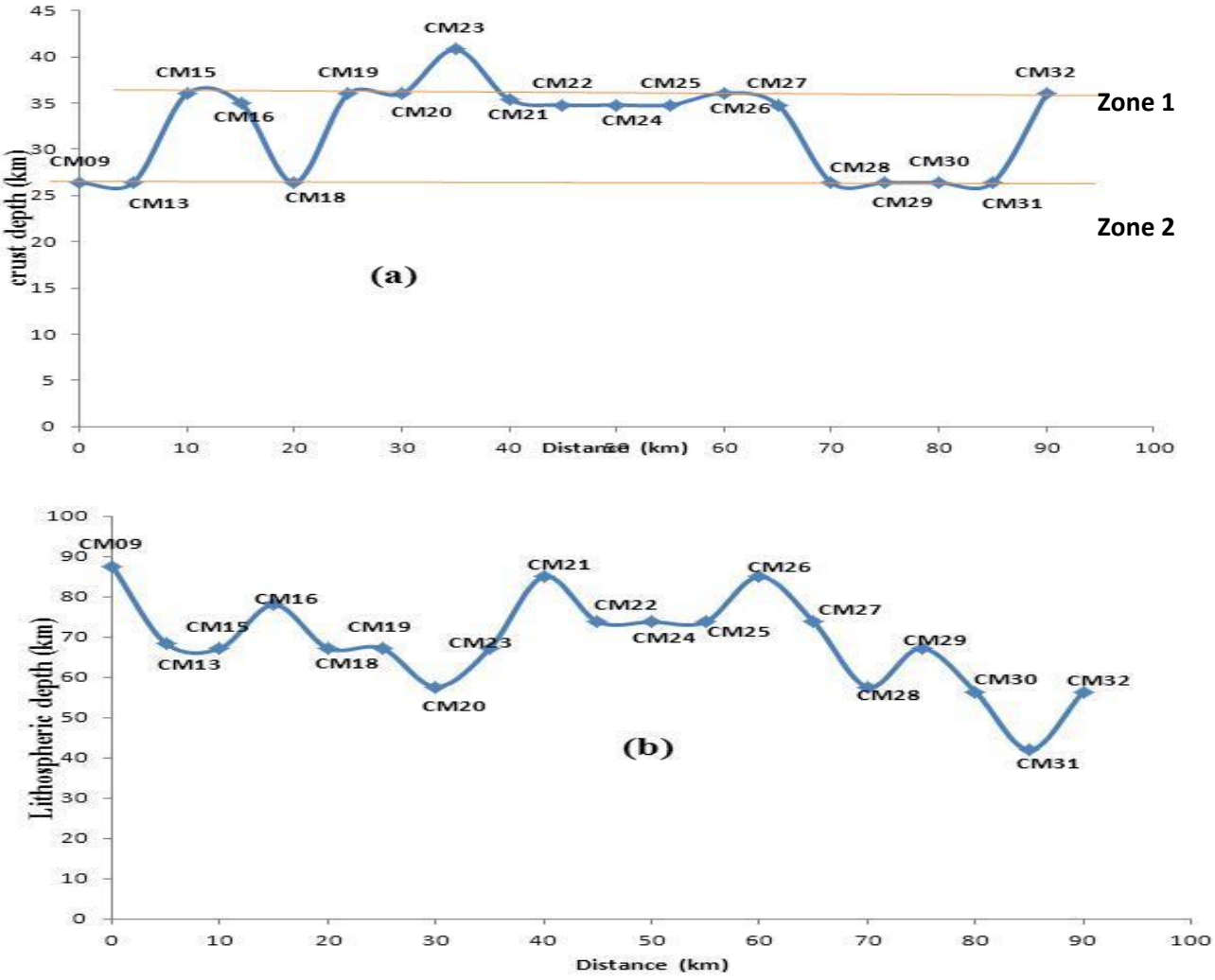

Figure III.5: Comparisons of the Moho depth (a) and lithospheric depth (b) by locality.

- Depth of the Moho representation in Figure III.4 (a) shows important variations in the thickness of the crust (between 26.4 km and 40.8 km) along the line of the Volcanic Province of Cameroon. We can also observe that, this curve shows two crustal iso-thickness zones. The first zone (Zone1) with mean thickness of 34.8 km is made up of the following stations CM15; CM16; CM19; CM20, CM21, CM22, CM24, CM25, CM26, CM27 and CM32 and the second zone (Zone 2) with the lowest thickness of 26.4 km is made up of stations CM09; CM13; CM18; CM28; CM29; CM30 and CM31. The thickest crustal is located in the Ndu locality (CM23) of the North West region. The low value of the thickness observed in zone 2 could be due to magmatic and asthenopheric upwelling **(**Milelli et al., 2012; Poudjom et al., 1995 and Marcel et al., 2010) and the consequence of the isostatic compensation. The lithosphere appears to be thin in nature with thickness varying between 57.6 km and 87.6 km which is less than 100 km as found by Guidarelli and Aoudia (2016). This can be attributed to the existence of the Low velocity zone that has already shown by Tabod et al. (1992) and Poudjom et al. (1997) which also has a varying thickness. The different S-velocity models obtained shown again that, the low velocity zone is continue in the mantle. This prolongation of the Low velocity Zone has been proved by Reusch et al. (2010) who found that a continuous low velocity zone (δV_S = -2 to -3%) underlies the entire CVL to a depth of at least 300 km and attributed this to a thermal anomaly of at least 280 K.

In order to confirm the previous results above, it is be important to compare them with already existing results. This is done with the help of **Tables III.8, III.9, III.10** and **Table III.11** below.

Table III.8: Comparing with previous estimates in the Southern part of CVL

Type of result	This study	Others studies	Types of data used	References
Average Vs of crustal (Km/s)	3.7	3.7	Seismic earthquakes	**Tokam et al. (2010)**
Average Vs of lithospheric mantle (Km/s)	4.4	4.4	Seismic earthquakes	**Tokam et al. (2010)**
Average depth moho (Km)	32.8	Between 19 km and 34 km	Gravity	**Marcel et al. (2010)**
		35.5	Seismic earthquakes	**Tokam et al. (2010)**
Average depth Lithospheric (Km)	between 57.6 and 87.6	?	?	**?**

Table III.9: Comparing with previous estimates in the Adamawa plateau region

Type of result	This study	Others studies	Types of data used	References
Average Vs of crustal (Km/s)	3.7	3.7	Seismic earthquakes	**Tokam et al. (2010)**
Average depth moho (Km)	35.1	33	Active Seismic sources	**Stuart et al. (1985)**
		33	Gravity	**Nnange et al. (2000)**
		35.5	Seismic earthquakes	**Tokam et al. (2010)**
Average depth Lithospheric (Km)	between 73.8 and 85	≅70	Gravity and active seismic	**Plomerova et al. (1993)**
		80	Gravity	**Poudjom et al. (1997)**

Table III.10: Comparing with previous estimates in the Garoua rift region

Type of result	This study	Others studies	Types of data used	References
Average Vs of crustal (Km/s)	3.7	3.7	Seismic earthquakes	**Tokam et al. (2010)**
Average depth moho (Km)	28	23	Seismic explosion	**Stuart et al. (1985)**
		24	Gravity	**Kamguia et al. (2005)**
		25.5	Seismic earthquakes	**Tokam et al. (2010)**
Average depth Lithospheric (Km)	between 42 and 67.2	?	?	**?**

Table III.11: Comparing with previous estimates in the CVL

Type of result	This study	Others studies	Types of data used	References
Average Vs of crustal (Km/s)	3.7	3.7	Seismic earthquakes	**Tokam et al. (2010)**
Average depth moho (Km)	between 28 and 35.1	33	Seismic explosion	**Stuart et al. (1985)**
		33	Gravity	**Nnange et al. (2000)**
		35 - 39	Seismic earthquakes	**Tokam et al. (2010)**
Average depth Lithospheric (Km)	between 42 and 87.6	< 100 km (~60 km)	Seismic earthquakes	**Firhwick (2010)**
		< 100 km	Seismic earthquakes	**Guidarelli and Aoudia (2016)**

These four tables show a slight difference between the results obtained in the scope of our study per locality and some obtained in previous studies. This could be justified by the method (inversion of the Rayleigh waves coming from the same data used by Tokam et al., 2010) or the type of data used (gravity data used by Poudjom et al., 1997; Kamguia et al., 2005 and Nnange et al., 2000). A great difference is observed when the results of this study are compared with the those obtained by Stuart et al. (1985) and Fairhead (1987). This could be due to the fact that the seismic data used by these authors were coming from artificial sources. And finally, only few studies to estimate the depth of lithosphere along the Volcanic Province of Cameroon have been done so far. Our study has situated this depth to be between 42 km and 87.2 km which justifies that, it is less than 100 km as suggest by Firhwick (2010) and Guidarelli and Aoudia (2016).

One dimension model of shear wave velocity obtained from the inversion of the receiver functions has been employed to study the structure of the lithospheric structure beneath the different localities constituting the Volcanic Province of Cameroon. The results obtained have been compared between them and those from previous study.

GENERAL CONCLUSION AND PERSPECTIVES

This work had as objective to study the structure of the lithosphere along the Volcanic Province of Cameroon using geophysical data. Thus, with respect to the available data base, the choice was made on earthquake data and more especially on the teleseismic data recorded from Cameroon during a seismic campaign carried out during the period of January 2005 to February 2007. After applying the inversion method on receiver functions obtained from P-waves extracted on seismograms, it was found that: **(1)** In its southern part, the volcanic province of Cameroon presents a thin and heterogeneous crust beneath the stations and it's depth varies between 26.4 km and 45.4 km. There is a crust thinker of 26.4 km beneath the mount Cameroun region and mean crust thickness of 35.8 km beneath the other localities. **(2)** The lithosphere on its mantle part is thick in nature with an equally variable depth between 57.6 km and 78 km. These limits have been obtained as a result of the existence of a Low velocity zone (LVZ) whose thickness also varies between 57.6 km and 116.8 km. The variations of the depth and the thickness of Low Velocity Zone in the Southern part would be due to the existence of the transition zone between the continental and oceanic parts of the volcanic line covered by the Mount Cameroon region. **(3)** The S wave velocity obtained by inversion of the P waves in this part has a mean velocities of 3.8 km/s and 4.1 km/s respectively in the crust and the lithospheric mantle. **(4)** In its Northern part, the Volcanic Province of Cameroon possesses two types of structures due to its geologic variation as Plateaus (Adamawa plateau) on one hand and a Rift (Garoua rift) on the other. With regard to the plateau and more precisely the Adamawa plateau region, the crust presents a thick and heterogeneous structure with a depth located at about 35.1 km and an S wave velocity of 3.7 km/s. The lithospheric mantle also presents a thick structure with a mean S-wave velocity of 4 km/s. The lithosphere in this region has a depth (LAB) that would vary between 73.8 km and 85 km for a Low velocity zone thickness which also varies between 73.8 km and 116.7 km. As for the Garoua Rift, the velocity models obtained present a crust having a thin and heterogeneous structure with a depth that would be located at around 28 km for a mean S-wave velocity of 3.8 km/s. In its mantle part, the lithosphere has on the contrary a thick structure with a mean S-wave velocity of 3.9 km/s. The lithosphere in this region has a variable depth between 42 km and 67.2 km for a Low velocity zone thickness that also varies between 42 km and 116.7 km. From all results of thickness, we observe that in the volcanic province of Cameroon, the lithosphere is shallower beneath the rift than under region (plateau and mounts). **(5)** The synthetic receiver functions associated to the different velocity models obtained, have led to the understanding that, the seismic waves have truly undergone the Ps conversions and the PpPs and PpSs multiple conversions at the level of the Moho in all localities beneath the Volcanic Province of Cameroon. However the time intervals of phase and multiple phases differ according to the locality traveled by the wave. These variations

are indicative of the heterogeneous character of the crust in this study area. The results obtained in this work have been compared to others existing in the study area. Some similarities have been noticed in some cases like in the depth and behavior of the crust, the mean velocity of the S waves in the crust and in the lithospheric mantle, and the existence of a Low Velocity Zone. The slight differences with other cases have to do with the depth of the lithosphere. These differences can be justified by the type of method or data used. Nevertheless the stations CM09 , CM15, CM21 and CM31 situated at Ekona, Nkongsamba, Tibati and Yagoua localities respectively do not product the good results especially with particularly the synthetic receiver function due to current volcanic activity of the mount Cameroon and the development of the volcanic activity around Nkongsamba where the station CM09 and CM15 were installed on one hand and, the Foumban shear fault (FSZ) that cross the station CM21 and CM31 containing respectively the localities of Tibati and Yagoua on the other hand.

Suggestion for further work

The important and most interesting results of this study resides in the fact that, the Low velocity zone (LVZ) led to the determination of the boundary between the lithosphere and the asthenosphere as well as the variation of this boundary. These results are consistent with a varying attitude and thus are consistent with result of previous studies. The advantage of the 1-D inversion of the receiver functions techniques is that, they provide good indication of the depth to seismic discontinuities though they give less information on the absolute velocities. Not understanding, a number of questions remain: What is the origin of this variation of the lithospheric depth? Is this the same at the Panafrican and Congo craton portion of Cameroon? What is the real thickness of the Low velocity Zone in the mantle that permitted to determinate the Lithosphere-asthenosphere boundary by the observation of 1-D model? What are the values of the temperature at the different transition zone obtained? The answer to these questions can be obtained through the combination of passive and active data seismic sources. This would lead to the study of the new seismicity in order to describe, the shallow and deep structures of the earth associated to the velocity of the waves involved by, applying focal mechanism to infer the parameters of existing fault sources and also describe the temperature profile of each layer on one hand and, the extension of the model of parameters on other hand. This could also be done by applying the S-receiver function method to obtain P-wave velocity models (because S-waves provide a useful complementary tool to the P-waves receiver functions method) and the stack of the receiver function, in other to compare the different results obtained.

REFERENCES

Ambeh, W.B., Fairhead, J.D. and Francis, D.J., 1989. Seismicity of the Mount Cameroon Region, West Africa. Journal of Afr. Earth Sci., 9:1-7.

Ammon, C.J., (1991). The isolation of receiver effects from teleseismics P waveforms, Bulletin of the Seismological Society of America, Vol. 81, No. 6, pp. 2504-2510.

Ammon, C.J., (1997). An overview of receiver-function analysis. Department of Geosciences Pennsylvania State University. *Unpublished notes.*

Aretouyap, Z., Njandjock N, P., Ekoro, N.H., Meli'i, J.L. and Lematio T, S.A., 2014. Investigation of Groundwater Quality Control in Adamawa-Cameroon Region. Journal of Applied Sciences 14 (19) 2309 – 2319.

Aretouyap, Z., Bisso, D., Njandjock N, P., Amougou M, J.E. and Asfahani, J., 2018. Hydrogeophysical Characteristics of Pan-African Aquifer Specified Through an Alternative Approach Based on the Interpretation of Vertical Electrical Sounding Data in the Adamawa Region, Central Africa, Natural Resources Research. https://doi.org/10.1007/s11053-018-9373-8

Ateba B., Dorbath, C., Ntepe N., Frogneux, M., Aka, F.T., Hell, J.V., Delmond, J.C. and Manguelle D, E., 2009. Eruptive and earthquake activities related to the 2000 eruption of Mount Cameroon volcano (West Africa). Journal of Volcanology and Geothermal Research, 179, 206-216.

Båth, M. and Stefánnson, R., 1966. S-P conversion at base of the crust, Ann. Geofis. , 19, 119-130.

Bock, G. and Kind, R., 1991. A global study of *S*-to-*P* and P-to-S conversions from the upper mantle transition zone, Geophys. J. Int., 107, 117–129.

Bormann, Peter., 2000. International Training Courses on Seismology and Seismic Risk Assessment. Seism. Res. Lett., 71, 5, 499-509.

Boukeke, D.B., 1994. Structures crustales d'Afrique Centrale déduites des anomalies gravimétriques et magnétiques: le domaine précambrien de la République Centrafricaine et du Sud Cameroun. Thèse de Doctorat, Univ. Paris XI, Orsay, 263 pp.

Browne, J.D. and Fairhead, J.D., 1983. Gravity study of the Central African Rift System: a model of continental disruption, 1, The Ngaoundere and Abu Gabra Rifts. Tectonophysics, 94, 187-203.

Burdick, L.J. and Langston, C.A., 1977. Modelling Crustal Structure through the use of converted phases in teleseismic body-waves forms, Bull. Seismol. Soc. Am , 67, 677-691.

Burke, K.C., Dessauvagie T, F.J. and Whiteman, A. J., 1971. Opening of the Gulf of Guinea and Geological history of the Benue Depression and Niger Delta. Nature, 233, 51 – 55.

Cassidy, J., 1992. Numerical experiments in broadband receiver function analysis, Bull. Seismol. Soc. Am., 82, 1453– 1474.

Chapellier, D. and Marie., J.L., 1998. Principe de base, Cours online de géophysique, Université de Lausanne. Institut français du pétrole.

Christensen, N.I., 1996. Poisson's ratio and crustal seismology. J. Geophys. Res., 101, 3139– 3156.

Christensen, N.I. and Mooney, W.D., 1995. Seismic velocity structure and composition of the continental crust: A global view. Journal of Geophysical Research, 100, B7, 9761-9788.

Clayton, R.W. and Wiggings R.A., 1976. Source shape estimation and deconvolution of teleseismic body waves. Geophys J Royal Astronom Soc 47 : 157-177

Coulon, C., Vidal, P., Dupuy, C., Baudin, P., Popoff, M., Maluski, H. and Hermitte, D., 1996. The Mesozoic to early Cenozoic magmatism of the Benue Trough (Nigeria); geochemical evidence for the involvement of the St. Helena plume. Journal of Petrology 37, 1341–1358.

Déruelle, B., Ngounouno, I. and Demaiffe, D., 2007. The 'Cameroon Hot Line' (CHL): A unique example of active alkaline intraplate structure in both oceanic and continental lithospheres. C. R. Geoscience 339 (2007) 589–600.

Déruelle, B., Moreau, C., Nkoumbou, C., Kambou, R., Lissom, J., Njongfang, E., Ghogomu, R.T. and Nono, A., 1991. The Cameroon Line: a review, In: Magmatism in Extensional Structural Settings. The Phanerozoic African Plate. Springer-Verlag, Berlin, Germany, pp. 274–327.

Dorbath, C., Fairhead, J.D. and Stuart, G.W., 1986. A teleseismic delay time study across the Central African Shear Zone in the Adamawa region of Cameroon. Geophys. J. R. Astr. Soc., 86, 751–766.

Dumont, J. F., 1987. Etude structurale des bordures Nord et Sud du plateau de l'Adamaoua: influence du contexte atlantique. *Géodynamique* 2(1), 55-68

Dziewonski, A.M. and Anderson, D.L., 1981. Preliminary reference earth model. Phys. Earth planet. Int., 25, 297–356.

Elf-Serepca., 1981. Service d'Exploration Carte Geologique du Bassin de Garoua (unpublished)

Fairhead, J.D. and Reeves, C.V., 1977. Teleseismics delay times, Bouguer anomalies and inferred thickness of the African lithosphere. Earth Planet. Sci. Lett., 36:63-76.

Farber S. and Müller G., 1980. Sp phases from the transition zone between the upper and lower mantle, Bull. seism. Soc. Am, 70, 487–508.

Farra V. and Vinnik L., 2000. Upper mantle stratification by P and S receiver functions, Geophys. J. Int., 141, 699–712.

Fitton, J.G., 1987. The Cameroon Line, West Africa: a comparison between oceanic and continental alkaline volcanism. Alkali igneous rocks. Geol. Soc. Spec. Publ., 30: 273-291.

Fitton, J.G. and Dunlop, H.M., 1985. The Cameroon Line, West Africa, and its bearing on the origin of oceanic and continental alkali basalt. Earth Planet. Sci. Lett., 72, 23–38.

Fitton, J.G., 1983 Active versus passive continental rifting: evidence from the West African rift system. Tectonophysics 94:473–481. https://doi. org/10.1016/0040-1951 (83)90030-6.

Fishwick, S., 2010. Surface wave tomography: imaging of the lithosphere-asthenosphere boundary beneath central and southern Africa. Lithos 120, 63-73.

Fitton, J.G., 1980. The Benue Trough and Cameroon Line–A migrating rift system in West Africa, Earth Planet. Sci. Lett., 51(1), 132–138.

Gallacher, R.J. and Bastow, I., 2012. The development ofmagmatism along the Cameroon Volcanic Line: evidence from teleseismic receiver functions, *Tectonics*, 31, TC3018, doi:10.1029/2011TC003028.

Guidarelli, M. and Aoudia, A., 2016. Ambient noise tomography of the Cameroon Volcanic Line and Northern Congo craton: new constraints on the structure of the lithosphere. *Geophys. J. Int.* 204, 1756–1765

Guiraud, R. and Maurin, C.J., 1992. Early Cretaceous rifts of Western and Central Africa. Tectonophysics, 213: 153-168.

Halliday, A., Davidson, J., Holden, P., DeWolf, C., Lee, D. and Fitton, J. G., 1990. Trace-element fractionation in plumes and the origin of HIMU mantle beneath the Cameroon line, Nature, 347(6293), 523–528.

Hedberg, J.D., 1968. A geological Ananlysis of the Cameroon Trend. Ph. D. thesis, University of Princeton.

Herrmann, R.B. and Ammon, J.C., 2002. Surface waves, receiver functions and crustal structure. Department of Geosciences Pennsylvania State University. *Unpublished notes.*

Jansson T, R.N., 2008. Receiver function modeling - Modeling local subsurface velocity structures using multiple diverse algorithms. Master thesis in Geophysics, Niels Bohr Institute, University of Copenhagen, 87 P.

Jeffreys, H. and Bullen, K.E., 1940. Seismological tables. British Association for the Advancement of Science, Burlington House, London.

Julià, J., Ammon, C.J. and Herrmann, R.B., 2003. Lithospheric structure of the Arabian Shield from the joint inversion of receiver functions and surface wave group velocities. Tectonophysics, 371, 1 –21.

Julià, J., Ammon, C.J. and Nyblade, A.A., 2005. Evidence for mafic lower crust in Tanzania, East Africa, from joint inversion of receiver functions and Rayleigh wave dispersion velocities. Geophys. J. Int., 162, 555–562.

Julià, J., Ammon, C.J. and Herrmann, R.B. and Correig, A.M., 2000. Joint inversion of receiver function and surface wave dispersion observations. Geophys. J. Int., 143, 99–112.

Kamguia, J., Manguelle D, E., Tabod, C.T. and Tadjou, J.M., 2005. Geological models deduced from gravity data in the Garoua basin, Cameroon. . Journal of Geophys. Eng., 2, 147-152.

Kampunzu, A.B., Caron, J.H. and Lubala, R.T., 1986. The East African rift, magma genesis and astheno-lithospheric dynamism. *Episodes* 9, 211-216.

Kennett B, L.N., 1991. IASPEI 1991 Seismological Tables. Australian National University, Research School of Earth Sciences, 167 pp.

Kennett B, L.N. and Engdahl, E.R., 1991. Travel times for global earthquake location and phase identification. Geophysical Journal International, 105, 429–465.

Kennett B, L.N., Engdahl, E.R. and Buland, R., 1995. Constraints on seismic velocities in the Earth from traveltimes. Geophys. J. Int. 122, 108-124.

Kikuchi, M. and Kanamori, H., 1982. Inversion of complex body waves, Bull. Seism. Soe. Am. 72, 491-506.

King, R. and Vinnik, L.P., 1988. The upper mantle discontinuities underneath the GRF arry from P-to-S converted phases. J Geophys 62: 138-147

King, S.D. and Anderson, D.L., 1995. An alternative mechanism of flood basalt formation, *Earth planet. Sci. Lett.,* **136,** 269–279.

Kosarev, G., Kind, R., Sobolev, S.V., Yuan, X., Hanka, W. and Oreshin, S., 1999. Seismic evidence for a detached Indian Lithospheric mantle beneath Tibet. Science, 283, 1306–1309.

Langston, C.A., 1979. Structure under Mount Rainier,Washington, inferred from teleseismic body waves, J. geophys. Res., 84, 4749–4762.

Langston, C.A., 1977. Corvallis, Oregon, crustal and upper mantle structure from teleseismic P and S waves, Bull. seism. Soc. Am, 67, 713–724.

Langston, C.A., 1981. Source inversion of seismic waveforms: The Koyna, India, earthquakes of 13 September 1967. Bulletin of the Seismological Society of America, 71 (1): 1-24.

Lasserre, M., 1961. Étude géologique de la partie orientale de l'Adamaoua (Cameroun Central) et les principales sources minéralisées de l'Adamaoua. *Bull. Dir. Mines et Géologie du Cameroun*, n° 4, 130 p., 14 fig., 6 table.

Le Maréchal, A. and Vincent, P.R., 1971. Le fossé crétacé du Sud Adamaoua (Cameroun). *Cahier O.R.S.T.O.M., sér. Géol.* 3(1), 67-83.

Lee, D.C., Halliday, A., Fitton, J.G. and Poli, G., 1994. Isotopic Variations With Distance And Time In The Volcanic Islands Of The Cameroon Line – Evidence For A Mantle Plume Origin. Earth And Planetary Science Letters, 123(1- 4), 119–138.

Li, X., Kind, R., Yuan, X., Wölbern, I., Hanka, W., 2004. Rejuvenation of the lithosphere by the Hawaiian plume, Nature, 427, 827–829.

Ligorría, J.P and Ammon, C.J., (1999). Iterative deconvolution and receiver function estimation. Bull. seism. Soc. Am., 89, 1395–1400.

Marcel, J., Njandjock N, P., Tabob, C.T, Manguelle D, E., 2010. Moho depth estimates for the Cameroon Volcanic Line from gravity data. Int J Econ Environ Geol 1:17–20

Marcel. J, Abate E, J.M., Njandjock N, P., Oumarou S. and Manguelle D, E., 2018. Validation of gravity data from the geopotential feld model for subsurface investigation of the Cameroon Volcanic Line (Western Africa). *Earth, Planets and Space* 70:42. https://doi.org/10.1186/s40623-018-0812-x

Meyers, J.B., Rosendahl, B.R., Harrison C, G.A. and Ding, Z.D., 1998. Deep-imaging seismic and gravity results from the offshore Cameroon Volcanic Line, and speculation of African hotlines. Tectonophysics, 284:31-63.

Milelli, L., Fourel, L. and Jaupart, C., 2012. A lithospheric instability origin for the Cameroon Volcanic Line, *Earth planet. Sci. Lett.*, 335–336, 80–87. Mooney, W.D.,

Laske, G. and Masters, T.G., 1998. CRUST 5.1: a global crustal model at 5◦x5◦, *J. Geophys. Res.*, 103, 727–747

Morgan, W.J., 1983. Hotspot tracks and the early rifting of the Atlantic. Tectonophysics, 94: 123-139

Ndjeng, E., 1994. Pole des caractères exoscopiques des grains de ` quartz des grès de Garoua sur l'interprétation du ´ paloéoenvironnement du bassin de la Bénoué du Crétacé superieur *Ann. Fac. Sci HS Chim. Sci. Nat.* 73–82.

Ndjeng, E. and Brunet, M., 1998. Modèle d'évolution géodynamique de deux bassins de l'Hauterivien–Barrémien du Nord-Cameroun: ´ les bassins de Babouri-Figuil et du Mayo Oulo-Leré (Fossé de la Benoué) *Géoscience au Cameroun ´* pp 163–5.

Ndougssa M, T., 2004. Etude géophysique, par la méthode gravimétrique, des structures profondes et superficielles de la région de Mamfé, Thèse de Doctorat/ PhD Université de Yaoundé I, (255p)

Ngako, V., Njonfang, E., Tongwa, A.F., Affaton, P. and Nnange, J.M., 2006. The North-South Paleozoic to Quaternary trend of alkaline magmatism from Niger-Nigeria to Cameroon: Complex interaction between hotspots and Precambrian faults. Journal of African Earth Sciences, 45, 241–256.

Nnange, J.M., Djallo, S., Fairhead, J.D. and Stuart, G.W., 1985. Earthquake activity in Cameroon during 1983. Rev. Sci. et Tech. Ser. Sci Terre, 1:1-2.

Nnange, J.M., Ngako, V., Fairhead, J.D. and Ebinger, C.J., 2000. Depths to density discontinuities beneath the Adamawa Plateau region, Central Africa, from spectral analysis of new and existing gravity data, *J. Afr. Earth Sci.*, **30**(4), 887–901

Nouayou, R., 2005. Contribution à l'étude géophysique du bassin sédimentaire de Mamfé par prospections audio et héliomagnétotellurique. Thèse de Doctorat d'état, University of Yaoundé 1.

Nsifa, N.E., 2006. Magmatisme et Evolution géodynamique de l'Archéen au Protérozoïque de la bordure nord-ouest du Craton du Congo (Complexe du Ntem) au Sud-Ouest Cameroun. Thèse de Doctorat d'etat, Faculté des Sciences, Université de Yaounde 1.

Owens, T.J., Zandt, G. and Taylor, S.R., 1984. Seismic evidence for an ancient rift beneath the Cumberland Plateau, a detailed analysis of broadband teleseismic P waveforms, J. geophys. Res., 89, 7783–7795.

Pasyanos, M.E., 2005. A variable resolution surface wave dispersion study of Eurasia, North Africa, and surrounding regions. J. of Geophys. Res., 110(B12), 22.

Pasyanos, M.E., and Nyblade, A.A., 2007. A Top to Bottom Lithospheric Study of Africa and Arabia. Tectonophysics, 444(1-4), 27–44.

Phinney, R.A., 1964. Structure of the Earth's crust from spectral behavior of long-period waves, *J. Geophys. Res.*, *69*, 2997-3017.

Plomovera, J., Babuska, V., Dorbath, C., Dorbath, L. and Lillie, R.J., 1993. Deep lithospheric structure across the Central African Shear Zone in Cameroon. Geophys. J. Int., 115:381-390.

Pokam. K, S. H., Tabod, C.T., Ndikum, E.N., Tokam K, A.P. and Gounou P, B.P., 2018. Thickness Variations in the Lithospheric Mantle and the Low Velocity Zone of the Adamawa Plateau (Cameroon) from Teleseismic Receiver Functions. Open Journal of Geology, 2018, 8, 529-542. https://doi.org/10.4236/ojg.2018.86032.

Poudjom Djomani, Y.H, Diament M. and Albouy Y., (1992). Mechanical behaviour of the lithosphere beneath the Adamawa Uplift (Cameroon, West Africa) based on gravity data *J. Afr. Earth Sci.* 15 81–90

Poudjom D, Y.H., Nnange, J.M., Diament, M., Ebinger, C.J. and Fairhead, J.D., 1995. Effective elastic thickness and crustal thickness variation in West Central Africa inferred from gravity data. Journal of Geophysical Research, 100(B11), 22,047–22,070.

Poudjom D, Y.H., Diament, M. and Wilson M., 1997. Lithospheric structure across the Adamawa plateau (Cameroon) from gravity studies Tectonophysics, 273, 317–27

Regnoult, J M., 1986. Synthèse Géologique du Cameroun (Yaounde: Direction des Mines et de la Géologie du Cameroun) 119 pp

Reusch, A.M., 2009. Investigating the upper mantle structure beneath Cameroon and Antartica. PhD Thesis, Pennsylvania State University.

Reusch, A.M., Nyblade, A.A., Wiens, D.A., Shore, P.J., Ateba B., Tabod, C.T and Nnange, J.M., 2010. Upper mantle structure beneath Camerron from body wave tomography and the origin of the Cameroon Volcanic Line, *Geochem. Geophys. Geosyst.*, **11,** Q10W07, doi:10.1029/2010GC003200.

Reusch, A.M., Nyblade, A.A., Tibi, R., Wiens, D.A., Shore, P.J., Ateba B., Tabod, C.T. and Nnange, J.M., 2011. Mantle transition zone thickness beneath Cameroon: evidence for an upper mantle origin for the Cameroon Volcanic Line, *Geophys. J. Int.*, **187,** 1146–1150.

Roch, E, Jeremine, E and Faure M, A., 1953. Itineraires géologiques dans le Nord Cameroun et le SW du territoire du Tchad *Bull. Service Mines* no 1

Sacks, I.S., Okada, H. and Snoke, J.A., 1977. Determination of the subducting lithosphere boundary by use of converted phases, Bull. seism. Soc. Am., 67, 1051–1060.

Schwoerer, P., (1965). Carte Géologique de Reconnaissance à L'Echelle 1 ′ /500000 Notice Explicative sur la Carte Garoua-Est (Yaoundé: Direction des Mines et de la Géologie du Cameroun)

Stuart, G.W., Fairhead, J.D., Dorbath, L. and Dorbath, C., 1985. A seismic refraction study of the crustal structure associated with the Adamawa plateau and Garoua rift, Cameroon, West Africa. Geophys. J.R. Astron. Soc., 81, 1-12.

Suh, C., Ayonghe, S., Sparks, R., Annen, C., Fitton, J.G., Nana, R. and Luckman, A., 2003. The 1999 and 2000 Eruptions of Mount Cameroon: Eruption Behaviour and Petrochemistry of Lava, Bull. Volcanol., 65(4), 267–281

Tabod, C.T. 1991. Seismological studies of the Cameroon Volcanic line in West Africa. PhD Thesis, University of Leeds.

Tabod, C.T., Fairhead, J.D., Stuart, G.W., Ateba B. and Ntepe N., 1992. Seismicity of the Cameroon Volcanic Line, 1982–1990, 1992**.** Tectonophysics 212, 303–320.

Tchameni, R., 1997. Géochimie et géochronologie des formations de l'archéen du Paléoprotérozoïque du Sud Cameroun (groupe du Ntem, Craton du Congo). Thèse de Doctorat, Université d'Orléans. France. 320p.

Tchameni, R., Mezger, K., Nsifa, N.E. and Pouclet, A., 2001. Crustal origin of Early Proterozoic syenites in the Congo Craton (Ntem Complex), south Cameroon. Lithos, 57, 23-42.

Tokam, A., Tabod, C.T., Nyblade, A.A. and Julià, J., 2010. Structure of the crust beneath Cameroon, West Africa, from the joint inversion of Rayleigh wave group velocities and receiver functions. Geophys. J. Int. 183, 1061-1076.

Tokam K, A.P., 2010. Crustal structure beneath Cameroon deduced from the joint inversion of Rayleigh wave group velocities and receiver functions. PhD Thesis, University of Yaounde I.

Toteu, S.F., Van S, R.W., Penaye, J. and Michard, A., 2001. New U–Pb and Sm–Nd data from north-central Cameroon and its bearing on the pre-Pan-African history of central Africa. Precambrian Res 108:45–73

Vicat J.P., Leger, J.M., Nsifa, E., Piguet, P., Nzenti, J.P., Tchameni, R. and Pouclet, A., 1996. Distinction au sein du craton congolais du Sud-Ouest du Cameroun, de deux épisodes doléritiques initiant les cycles orogéniques éburnéen (Paléoprotérozoïque) et

Pan-Africain (Néoprotérozoïque). Compte Rendu de l'Académie des Sciences, série IIa 323, 575-582.

Victor, C.T., 1999. Origine des Tremblements de Terre. Science Pp 1756-1758.

Vinnik, L.P. and Farra, V., 2002 Subcratonic low-velocity layer and flood basalts, Geophys. Res. Lett., 29, 1049, doi: DOI: arXiv:10.1029/2001GL014064.

Vinnik, L.P., Farra, V. and Kind, R., 2004. Deep structure of the Afro-Arabian hotspot by S receiver functions, Geophys. Res. Lett, 31, L11608, doi: DOI: arXiv:10.1029/2004GL019574.

Vinnik, L.P., Kumar, M.R., Kind, R. and Farra, V., 2003. Super-deep low-velocity layer beneath the Arabian plate, Geophys. Res. Lett, 30, 1415, doi: DOI: arXiv:10.1029/2002GL016590.

Vinnik, L.P., 1977. Detection of waves converted from P to SVin the mantle. Physics of the Earth and Planetary Interiors, 15, 39–45. Yuan, X., Kind, R., Li, X., and Wang, R., 2006. S receiver functions: synthetics and data example. Geophysical Journal International, 175(2), 555–564.

Wandji, P., Tsafack J, P.F., Bardintzeff, J.M., Nkouathio, D.G., Dongmo, A.K., Bellon, H., Guillou, H., 2009. Xenoliths of dunites, wehrlites and clinopyroxenites in the basanites from Batoke volcanic cone (Mount Cameroon, Central Africa): petrogenetic implications. Mineral. Petrol. 98, 81- 98

Wilson, M. and Guiraud, R., 1992. Magmatism and rifting in West and Central Africa, from Late Jurassic to Recent times. Tectonophysics 213, 203–225.

Wittlinger, G., Verge, J. and Tapponnier, P., 2004. Teleseismic imaging of subducting lithosphere and Moho offsets beneath western Tibet, Earth Planet. Sci. Lett, 221,117–130.

Yuan, X., Ni, J., Kind, R., Mechie, J. and Sandvol, E., 1997. Lithospheric and upper mantle structure of southern Tibet from a seismological passive source experiment, J. geophys. Res, 102, 27491–27 500.

Yuan, X., Kind, R., Li, X. and Wang, R., 2006. The S receiver functions: Synthetics and data examples, Geophys. J. Int., 165, 555–564, doi:10.1111/j.1365-246X.2006.02885.x.

Zandt, G. and Owens, T.J., 1986. Comparaison of crustal velocity profiles determined by seismic refraction and teleseismic method, Tectonophysics, 128, 155-161.

ANNEXES

ANNEX 1 : List of the different events used for this study

Event date	Event Time	Latitude (°)	Longitude (°)	Depth (km)	Magnitude			
01/11/05	04:36:00.97	36.917	27.867	34	MB 5.1	Ms 4.4	MW 5.1	
01/15/05	05:13:10.67	-5.991	39.221	10	MB 5.1	Ms 4.6	MW 5	
01/23/05	22:36:06.00	35.796	29.641	10	MB 5.4	Ms 5.4	MW 5.8	MW 5.8
01/29/05	21:01:09.04	-1.626	-15.52	10	MB 4.9	MW 5.5		
01/30/05	16:23:48.43	35.806	29.63	10	MB 5	Ms 4.7	MW 5.3	ML 4.9
01/31/05	01:05:33.56	37.535	20.155	31	MB 5.1	Ms 5.4	MW 5.7	MW 5.7
02/07/05	20:46:26.44	36.225	10.874	10	MB 4.9	Ms 5.1		
03/09/05	10:15:31.83	-26.91	26.789	5	MB 5	Ms 4.3		
03/21/05	16:14:38.53	-1.056	-24.59	21	MB 5.1	Ms 4.9	MW 5.4	
03/28/05	00:01:30.51	-0.299	-20.78	10	MB 5.1	Ms 4.8	MW 5.2	
04/12/05	13:55:52.78	-10.51	-13.09	10	MB 4.9	Ms 4.7	MW 5.1	
04/22/05	03:46:06.05	-10.23	-13.19	10	MB 5.1	Ms 4.8	MW 5.1	
05/14/05	23:46:50.53	35.687	31.582	69	MB 4.9	MW 5.1		
05/29/05	08:55:35.80	38.26	22.73	104	MB 4.7	MW 4.8	MD 5	
06/24/05	13:54:36.07	-1.07	-13.42	10	MB 4.9	Ms 4.8	MW 5.2	
07/10/05	13:10:12.16	42.389	19.812	4	MB 5.4	Ms 4.9	MW 5.2	ML 5.5
07/21/05	19:17:49.59	-8.13	-13.49	10	MB 5.3	Ms 4.8	MW 5.2	
07/30/05	21:45:00.00	39.437	33.089	5	MB 4.8	Ms 4.8	MW 5.2	ML 5.3
08/04/05	10:45:30.42	34.887	26.497	9	MB 4.8	Ms 4.8	MW 5	ML 4.7
08/15/05	07:53:42.59	-1.684	-13.05	10	MB 5.3	Ms 4.9	MW 5.3	
09/20/05	21:23:37.57	12.707	40.526	10	MB 5.2	Ms 5	MW 5.5	MW 5.4
09/22/05	03:12:34.07	12.697	40.461	10	MB 5	Ms 4.5		
09/24/05	05:15:33.94	12.674	40.519	10	MB 5	Ms 4.2	ML 4.7	
09/24/05	06:58:28.02	12.572	40.569	10	MB 5.2	Ms 4.4	ML 4.9	
09/24/05	07:36:08.51	12.625	40.536	10	MB 5	Ms 4.1		
09/24/05	19:24:02.66	12.471	40.634	11	MB 5.1	Ms 5	MW 5.6	MW 5.5
09/24/05	23:05:20.39	12.386	40.662	10	MB 4.8	Ms 4.2	ML 5.1	

09/25/05	00:37:28.56	12.447	40.603	10	MB	5	Ms	4.6			
09/25/05	10:02:12.73	12.366	40.505	10	MB	5.2	Ms	4.2			
09/25/05	11:20:03.76	12.421	40.578	10	MB	5.1	Ms	4.3			
09/26/05	09:33:51.40	12.5	40.5	8	MB	5.2	ML	5			
09/26/05	20:30:01.44	12.472	40.543	10	MB	5	Ms	4.2			
09/27/05	00:25:35.62	43.155	18.203	19	MB	4.8	ML	5.1	ML	5	
09/28/05	16:31:35.70	12.443	40.634	10	MB	5.1	ML	5			
10/02/05	23:24:41.94	12.02	40.537	10	MB	5	Ms	4.1	ML	4.8	
10/04/05	04:19:40.43	12.461	40.646	10	MB	4.5	ML	5			
10/17/05	05:45:16.00	38.131	26.505	8	MB	5.1	Ms	5.2	MW	5.5	ML 5.7
10/17/05	09:46:53.90	38.2	26.5	10	MB	5.4	Ms	5.7	MW	5.8	MW 5.8
10/18/05	15:26:00.26	37.622	20.918	14	MB	5.2	Ms	5.3	MW	5.6	MW 5.5
10/20/05	21:40:04.09	38.152	26.751	10	MB	5.5	Ms	5.7	MW	5.9	MW 5.9
11/06/05	12:11:18.30	11.696	43.625	10	MB	4.5	ML	5			
11/25/05	09:30:56.90	35.02	23.32	32	MB	5.2	Ms	4.6	ML	5.2	ML 5
12/05/05	12:19:56.62	-6.224	29.83	22	MB	6.4	Ms	7.2	MW	6.8	MW 6.7
12/06/05	05:53:08.98	-6.081	29.642	10	MB	5.3	Ms	5.2			
12/08/05	03:16:34.03	-6.279	29.512	10	MB	5	Ms	5.1			
12/09/05	23:30:23.93	-6.176	29.709	10	MB	5.5	Ms	5.3			
01/08/06	11:34:55.64	36.311	23.212	66	MB	6.5	MW	6.7	MW	6.7	
01/09/06	16:40:44.26	37.05	-14.12	10	MB	5.3	Ms	4.9	MW	5.3	
01/09/06	20:59:38.34	-6.099	29.743	25	MB	5.3	Ms	4.6			
01/10/06	01:09:34.19	37.057	-14.13	10	MB	5.4	Ms	5.2	MW	5.5	ML 5
02/02/06	09:49:49.90	27.884	34.411	2	MB	4.5	ML	5	ML	4.5	
02/17/06	13:24:02.03	-1.48	-15.1	10	MB	5	Ms	5.1	MW	5.8	MW 5.6
02/22/06	22:19:07.80	-21.32	33.583	11	MB	6.5	Ms	7.5	MW	7	MW 7
02/23/06	01:23:42.20	-21.37	33.525	10	MB	5.3	Ms	5.5	MW	5.8	
02/23/06	02:22:07.71	-21.42	33.488	10	MB	5.3					
02/23/06	21:32:05.62	-21.31	33.536	10	MB	5	Ms	4.4			
03/04/06	00:53:31.78	1.133	-27.88	10	MB	5.1	Ms	5	MW	5.6	
03/09/06	17:55:55.35	0.791	-26.13	10	MB	5.4	Ms	5.6	MW	6	MW 5.9

03/15/06	11:52:54.07	-21.19	33.527	10	MB	5.3	Ms	4.9				
03/15/06	14:19:48.69	-21.14	33.719	10	MB	5.5	Ms	5.5	MW	5.6	MW	5.6
03/20/06	19:44:25.19	36.623	5.328	10	MB	5	Ms	4.9				
03/22/06	11:35:13.05	-21.34	33.258	10	MB	5	Ms	5.1				
03/23/06	06:14:41.51	-21.24	33.456	10	MB	5						
03/30/06	03:14:40.74	-1.311	-15.92	10	MB	5						
04/02/06	06:44:31.82	34.893	3.807	10	MB	4.7	MW	5.1				
04/03/06	00:49:42.80	37.59	20.95	20	MB	4.8	MW	5	ML	4.8		
04/04/06	22:05:05.08	37.64	20.962	16	MB	4.8	Ms	5.1	MW	5.5	MW	5.3
04/08/06	22:03:03.92	-0.253	-18.14	10	MB	5	Ms	4.7	MW	5.3		
04/09/06	23:27:19.81	35.168	27.244	32	MB	5.1	Ms	4.4	MW	5.3	ML	4.9
04/11/06	00:02:41.50	37.64	20.92	18	MB	5.1	Ms	5.1	MW	5.5	MW	5.4
04/11/06	17:29:28.40	37.68	20.91	18	MB	5.1	Ms	5.3	MW	5.5	ML	5.4
04/12/06	16:52:01.20	37.61	20.95	19	MB	5.2	Ms	5.4	MW	5.7	MW	5.6
04/14/06	18:41:39.49	-21.41	33.651	26	MB	5.3	Ms	4.8	MW	5.2		
04/19/06	15:16:24.60	37.66	20.93	19	MB	4.9	Ms	4.6	MW	5.4	MD	5.2
04/27/06	04:18:28.14	0.338	30.078	10	MB	5.3	Ms	4.5	MW	5.2		
04/30/06	03:08:49.47	12.822	49.1	10	MB	4.9	MW	5	ML	4.9		
05/29/06	02:20:06.20	41.801	15.903	31	MB	5	Ms	4.7	MW	4.6	ML	4.9
06/21/06	15:54:44.60	39.007	20.595	10	MB	4.5	Ms	4.2	ML	5.2	ML	4.6
06/24/06	02:49:26.40	38.36	20.5	14	MB	4.5	ML	5	ML	4.6		
06/24/06	10:22:09.06	-17.72	41.826	1	MB	5						
06/25/06	04:51:56.89	-17.7	41.814	10	MB	5.1						
06/30/06	01:07:28.06	-21.11	33.258	10	MB	5.1						
07/10/06	07:21:37.88	-11.63	-13.43	10	MB	5.3	Ms	5.3	MW	5.5	MW	5.5
07/11/06	18:48:14.91	-21.1	33.307	10	MB	5	Ms	4.1				
07/29/06	02:03:16.98	13.07	51.015	10	MB	5						
08/01/06	12:01:43.44	-7.07	-12.83	10	MB	5	Ms	4.6				

08/06/06	07:49:46.76	40.163	19.735	8	MB	4.9	ML	5.1	ML	5		
08/08/06	21:20:09.00	40.185	19.751	11	MB	4.9	Ms	3.9	ML	5	ML	5
08/13/06	10:35:12.70	34.42	26.566	32	MB	5.2	Ms	4.5	ML	5	MD	4.7
08/23/06	00:53:34.08	-21.27	33.402	20	MB	5.1	Ms	4.3				
08/28/06	22:48:59.80	38.06	20.34	18	MB	4.2	ML	5	ML	4.6		
09/17/06	07:30:11.10	-17.69	41.827	10	MB	5.5	Ms	5	MW	5.1		
09/17/06	13:24:54.48	-17.71	41.811	10	MB	5						
09/24/06	22:56:21.74	-17.74	41.814	10	MB	5.6	Ms	5.4	MW	5.7	MW	5.5
10/19/06	09:34:51.00	42.3	19.8	6	MB	5	ML	4.3				
11/13/06	08:53:57.75	-12.51	-14.77	10	MB	5.3						
11/17/06	23:42:40.81	-12.72	-14.7	10	MB	5.1						
11/20/06	20:16:06.24	-21.13	33.112	10	MB	5.1						
12/03/06	08:19:51.31	-0.538	-19.74	10	MB	4.9	Ms	5	MW	5.6	MW	5.5
12/21/06	09:07:46.26	12.039	43.55	10	MB	5						
12/21/06	18:30:52.90	39.32	23.6	23	MB	4.6	Ms	4.6	ML	5.4	ML	5

<u>ANNEX 2:</u> Representation of the different seismograms used in this study

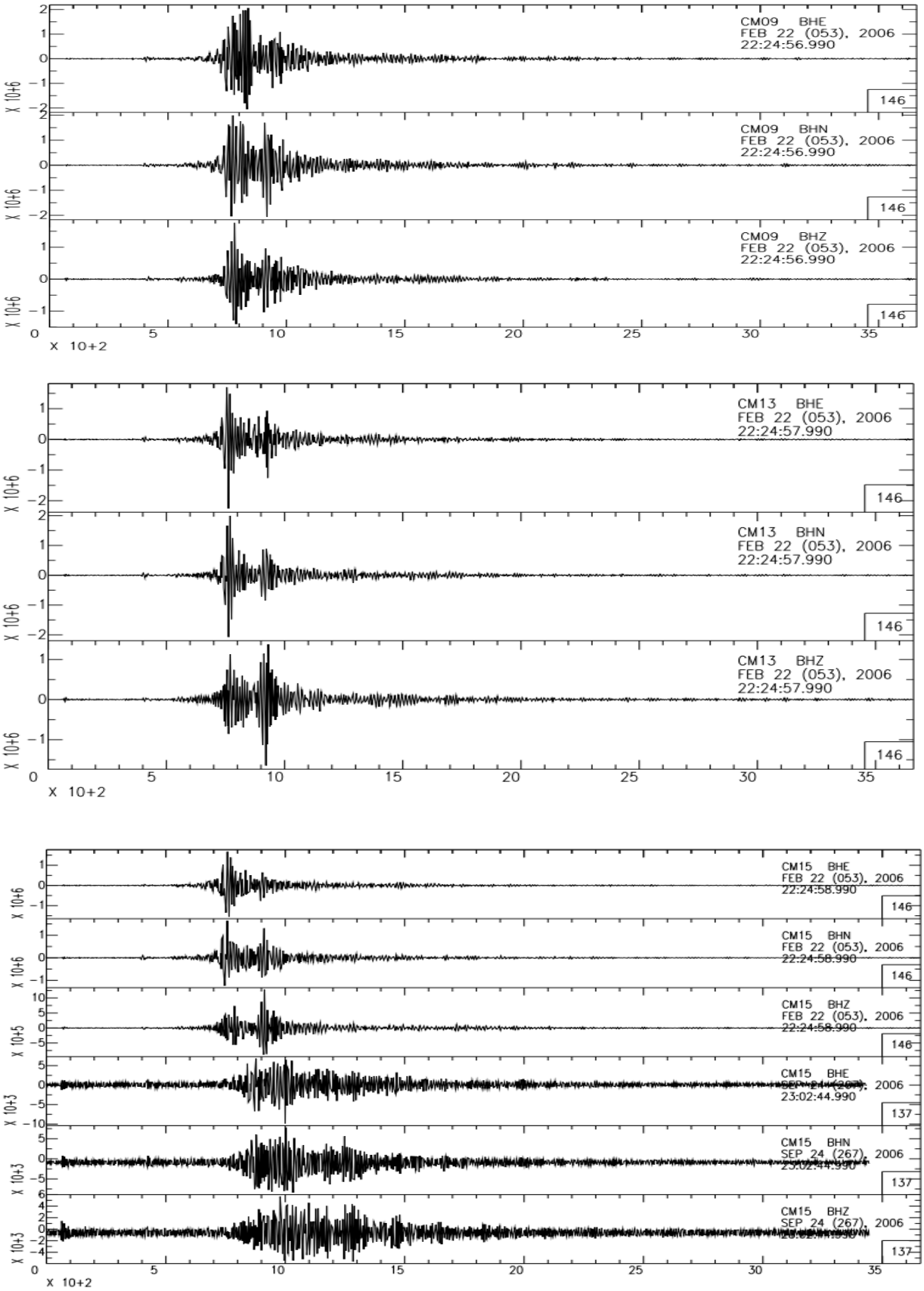

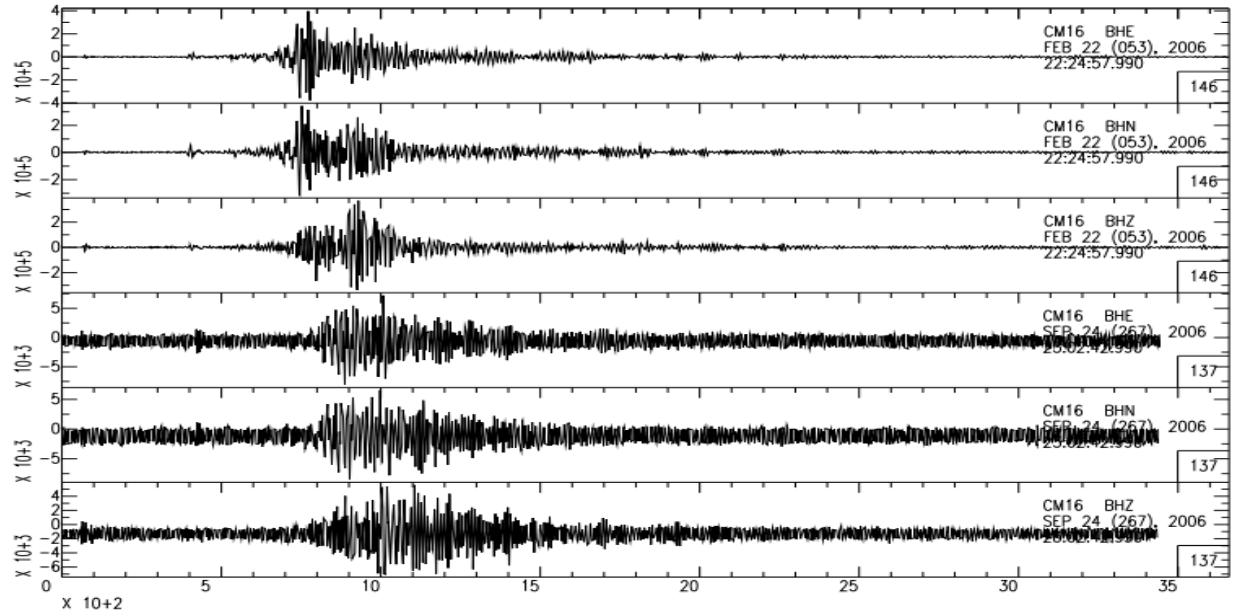
CM16 BHE
FEB 22 (053), 2006
22:24:57.990
146
CM16 BHN
FEB 22 (053), 2006
22:24:57.990
146
CM16 BHZ
FEB 22 (053), 2006
22:24:57.990
146
CM16 BHE
SEP 24 (267), 2006
23:02:42.990
137
CM16 BHN
SEP 24 (267), 2006
23:02:42.990
137
CM16 BHZ
SEP 24 (267), 2006
23:02:42.990
137
X 10+5
X 10+3
X 10+2

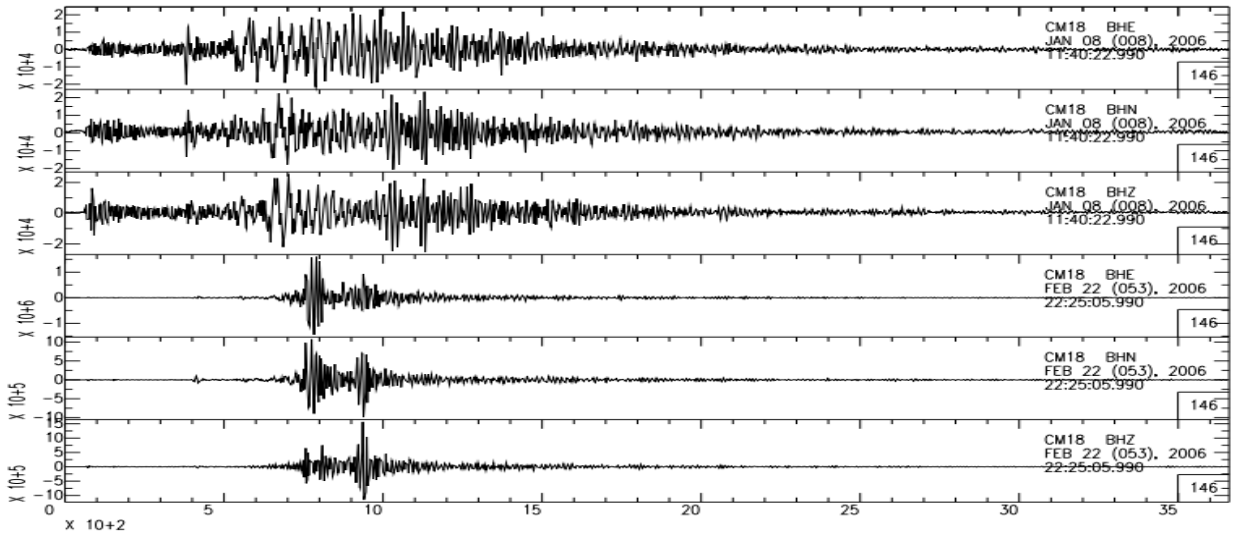
CM18 BHE
JAN 08 (008), 2006
11:40:22.990
146
CM18 BHN
JAN 08 (008), 2006
11:40:22.990
146
CM18 BHZ
JAN 08 (008), 2006
11:40:22.990
146
CM18 BHE
FEB 22 (053), 2006
22:25:05.990
146
CM18 BHN
FEB 22 (053), 2006
22:25:05.990
146
CM18 BHZ
FEB 22 (053), 2006
22:25:05.990
146
X 10+4
X 10+6
X 10+5
X 10+2

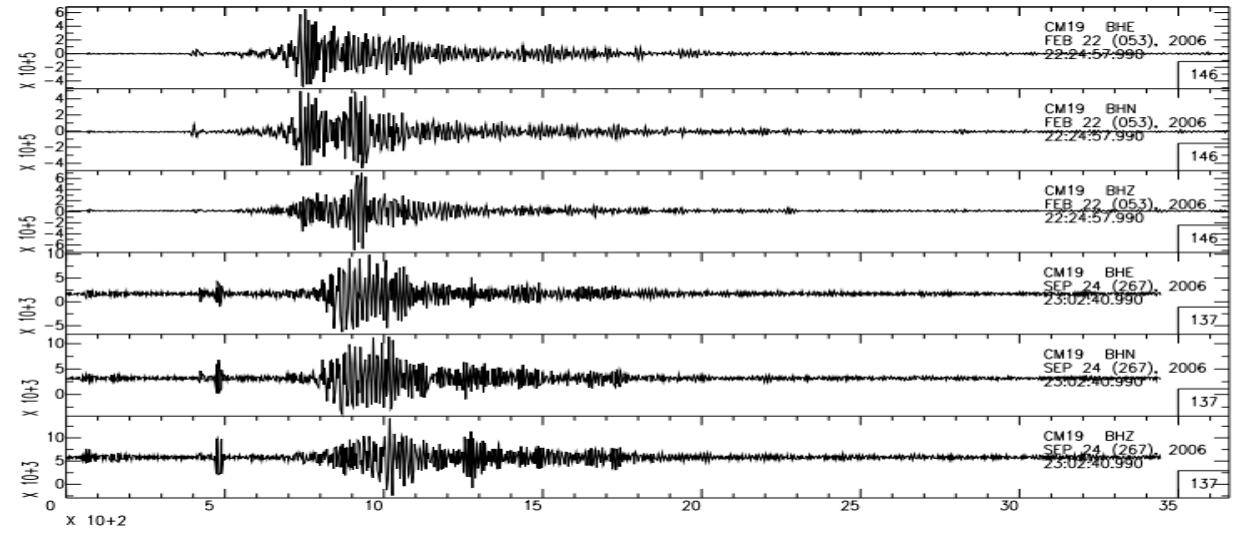
CM19 BHE
FEB 22 (053), 2006
22:24:57.990
146
CM19 BHN
FEB 22 (053), 2006
22:24:57.990
146
CM19 BHZ
FEB 22 (053), 2006
22:24:57.990
146
CM19 BHE
SEP 24 (267), 2006
23:02:40.990
137
CM19 BHN
SEP 24 (267), 2006
23:02:40.990
137
CM19 BHZ
SEP 24 (267), 2006
23:02:40.990
137
X 10+5
X 10+3
X 10+2

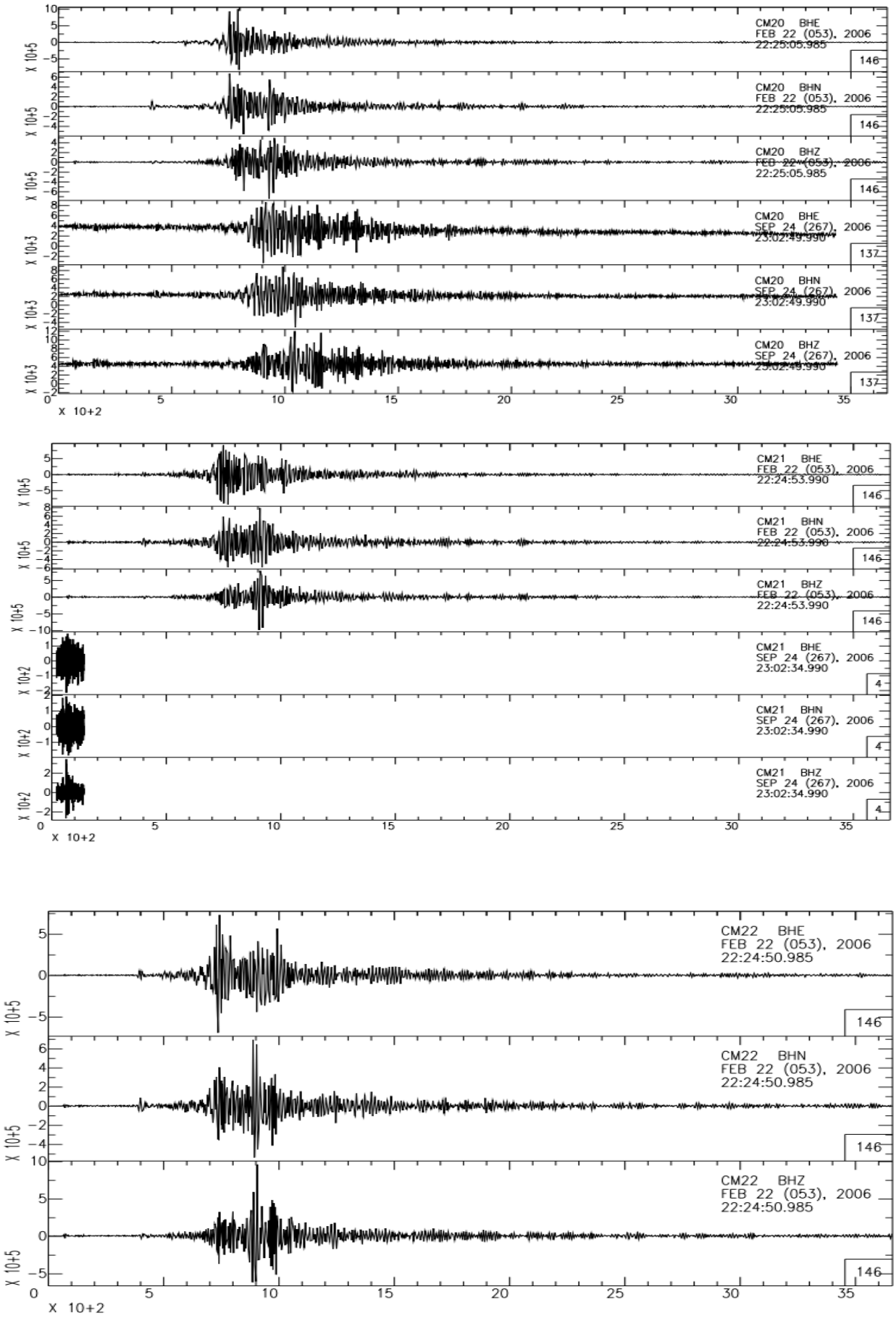
CM20 BHE
FEB 22 (053), 2006
22:25:05.985
146
CM20 BHN
FEB 22 (053), 2006
22:25:05.985
146
CM20 BHZ
FEB 22 (053), 2006
22:25:05.985
146
CM20 BHE
SEP 24 (267), 2006
23:02:49.990
137
CM20 BHN
SEP 24 (267), 2006
23:02:49.990
137
CM20 BHZ
SEP 24 (267), 2006
23:02:49.990
137
CM21 BHE
FEB 22 (053), 2006
22:24:53.990
146
CM21 BHN
FEB 22 (053), 2006
22:24:53.990
146
CM21 BHZ
FEB 22 (053), 2006
22:24:53.990
146
CM21 BHE
SEP 24 (267), 2006
23:02:34.990
4
CM21 BHN
SEP 24 (267), 2006
23:02:34.990
4
CM21 BHZ
SEP 24 (267), 2006
23:02:34.990
4
CM22 BHE
FEB 22 (053), 2006
22:24:50.985
146
CM22 BHN
FEB 22 (053), 2006
22:24:50.985
146
CM22 BHZ
FEB 22 (053), 2006
22:24:50.985
146
X 10+5
X 10+3
X 10+2
X 10+2

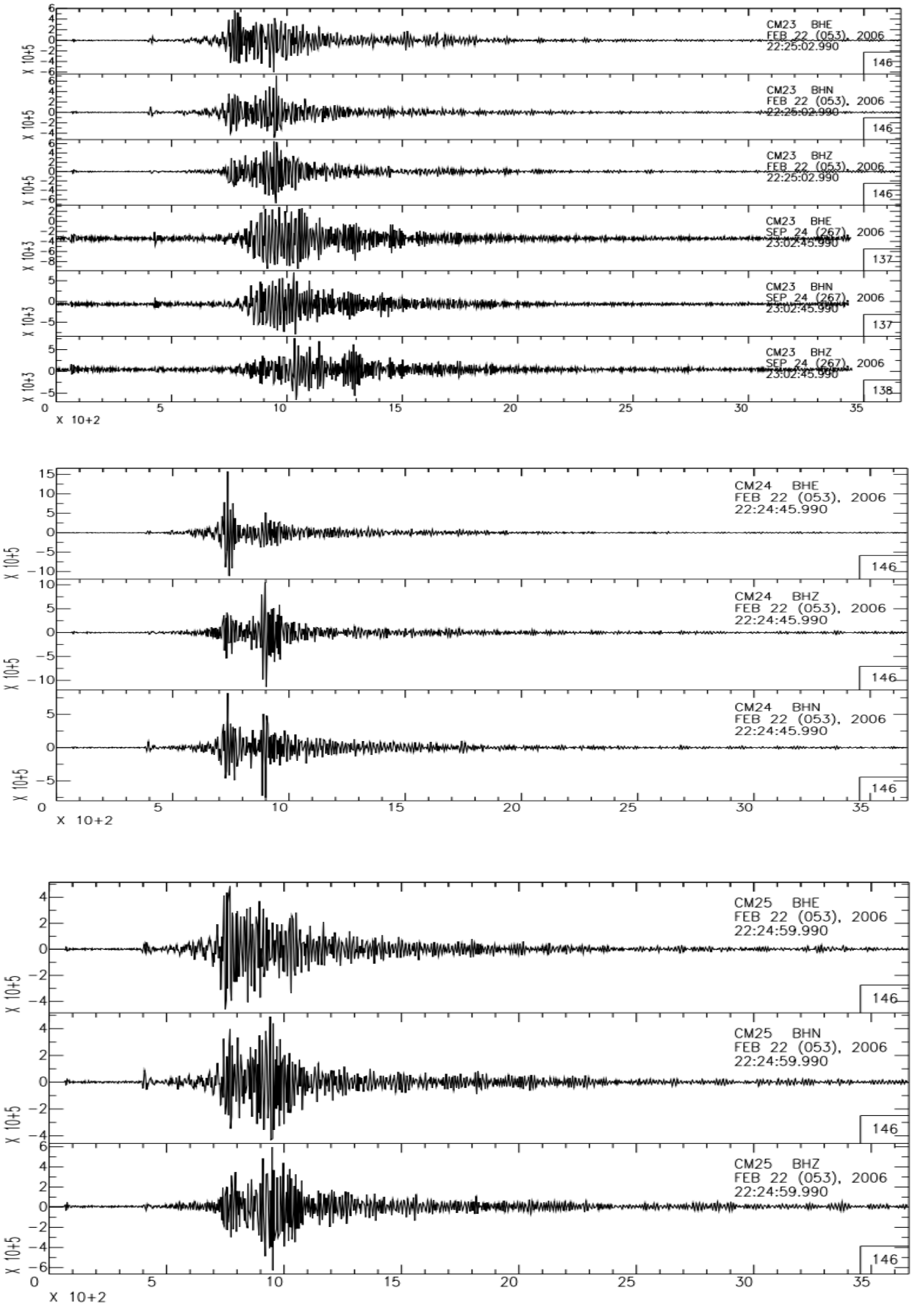
CM23 BHE
FEB 22 (053), 2006
22:25:02.990
146
CM23 BHN
FEB 22 (053), 2006
22:25:02.990
146
CM23 BHZ
FEB 22 (053), 2006
22:25:02.990
146
CM23 BHE
SEP 24 (267), 2006
23:02:45.990
137
CM23 BHN
SEP 24 (267), 2006
23:02:45.990
137
CM23 BHZ
SEP 24 (267), 2006
23:02:45.990
138
X 10+5
X 10+3
X 10+2
CM24 BHE
FEB 22 (053), 2006
22:24:45.990
146
CM24 BHZ
FEB 22 (053), 2006
22:24:45.990
146
CM24 BHN
FEB 22 (053), 2006
22:24:45.990
146
X 10+5
X 10+2
CM25 BHE
FEB 22 (053), 2006
22:24:59.990
146
CM25 BHN
FEB 22 (053), 2006
22:24:59.990
146
CM25 BHZ
FEB 22 (053), 2006
22:24:59.990
146
X 10+5
X 10+2

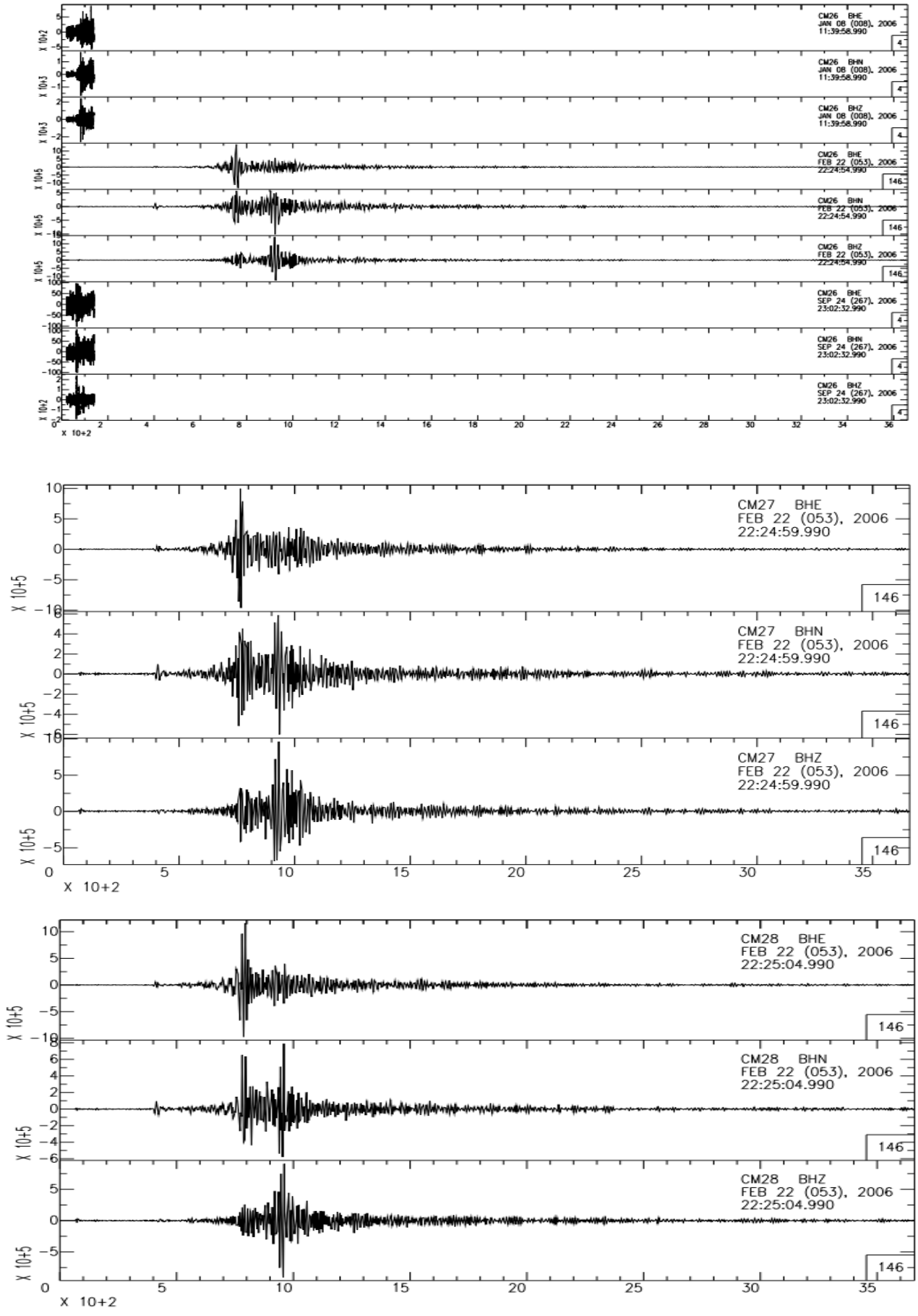
CM26 BHE
JAN 08 (008), 2006
11:39:58.990
CM26 BHN
JAN 08 (008), 2006
11:39:58.990
CM26 BHZ
JAN 08 (008), 2006
11:39:58.990
CM26 BHE
FEB 22 (053), 2006
22:24:54.990
CM26 BHN
FEB 22 (053), 2006
22:24:54.990
CM26 BHZ
FEB 22 (053), 2006
22:24:54.990
CM26 BHE
SEP 24 (267), 2006
23:02:32.990
CM26 BHN
SEP 24 (267), 2006
23:02:32.990
CM26 BHZ
SEP 24 (267), 2006
23:02:32.990
X 10+2
CM27 BHE
FEB 22 (053), 2006
22:24:59.990
CM27 BHN
FEB 22 (053), 2006
22:24:59.990
CM27 BHZ
FEB 22 (053), 2006
22:24:59.990
X 10+5
X 10+2
CM28 BHE
FEB 22 (053), 2006
22:25:04.990
CM28 BHN
FEB 22 (053), 2006
22:25:04.990
CM28 BHZ
FEB 22 (053), 2006
22:25:04.990
146

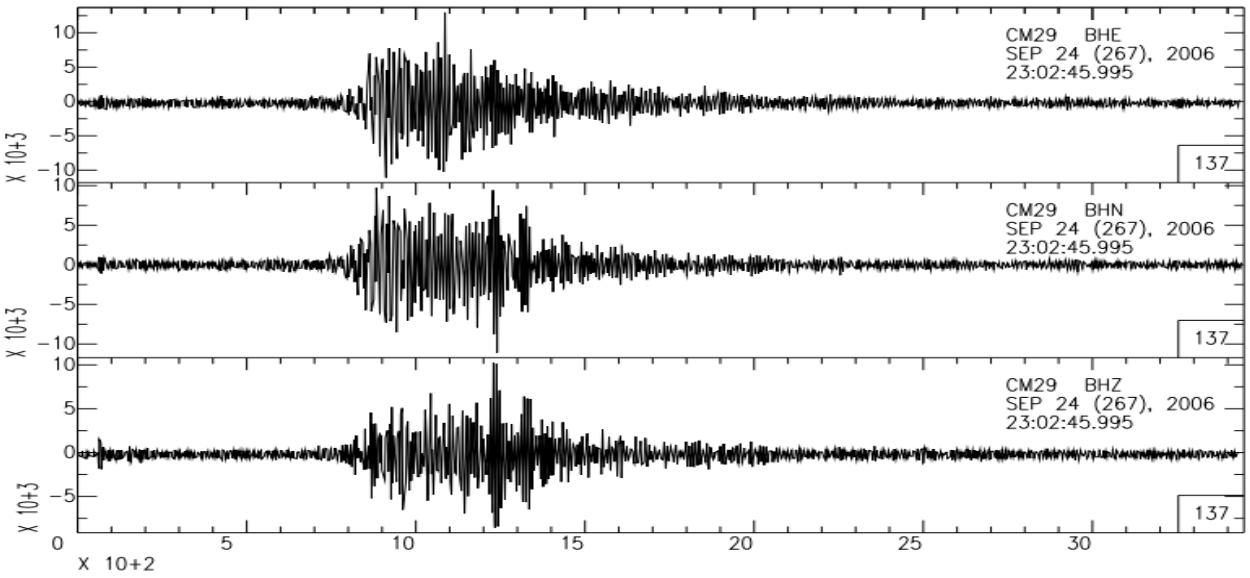
CM29 BHE
SEP 24 (267), 2006
23:02:45.995
137
CM29 BHN
SEP 24 (267), 2006
23:02:45.995
137
CM29 BHZ
SEP 24 (267), 2006
23:02:45.995
137
X 10+3
X 10+2

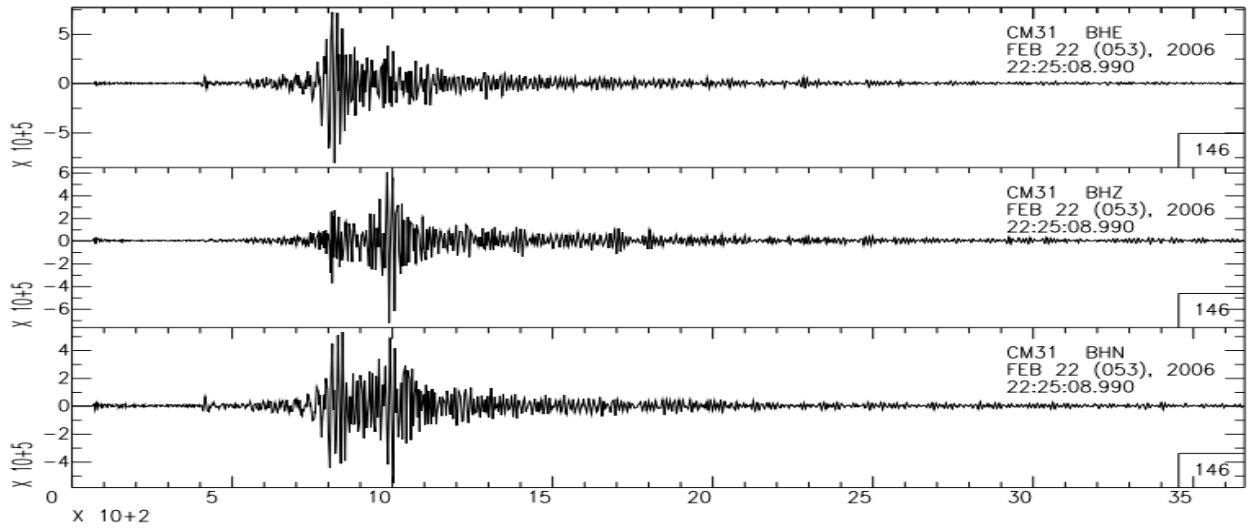
CM31 BHE
FEB 22 (053), 2006
22:25:08.990
146
CM31 BHZ
FEB 22 (053), 2006
22:25:08.990
146
CM31 BHN
FEB 22 (053), 2006
22:25:08.990
146
X 10+5
X 10+2

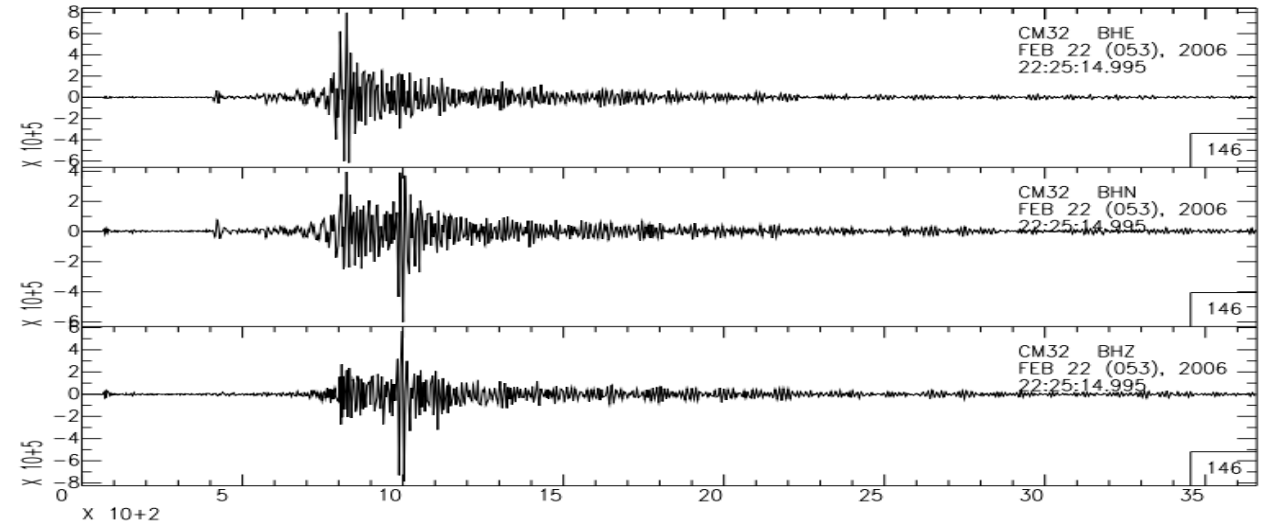
CM32 BHE
FEB 22 (053), 2006
22:25:14.995
146
CM32 BHN
FEB 22 (053), 2006
22:25:14.995
146
CM32 BHZ
FEB 22 (053), 2006
22:25:14.995
146
X 10+5
X 10+2

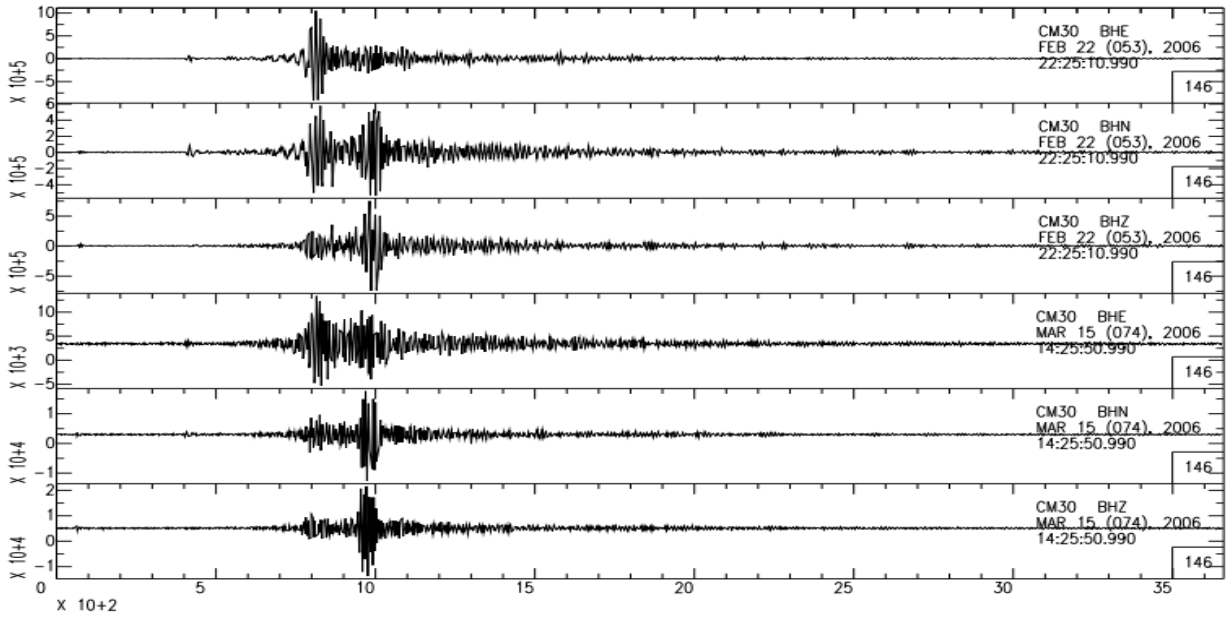
CM30 BHE
FEB 22 (053), 2006
22:25:10.990
146
CM30 BHN
FEB 22 (053), 2006
22:25:10.990
146
CM30 BHZ
FEB 22 (053), 2006
22:25:10.990
146
CM30 BHE
MAR 15 (074), 2006
14:25:50.990
146
CM30 BHN
MAR 15 (074), 2006
14:25:50.990
146
CM30 BHZ
MAR 15 (074), 2006
14:25:50.990
146
X 10+5
X 10+5
X 10+5
X 10+3
X 10+4
X 10+4
X 10+2

ANNEX 3: Receiver functions used for this study

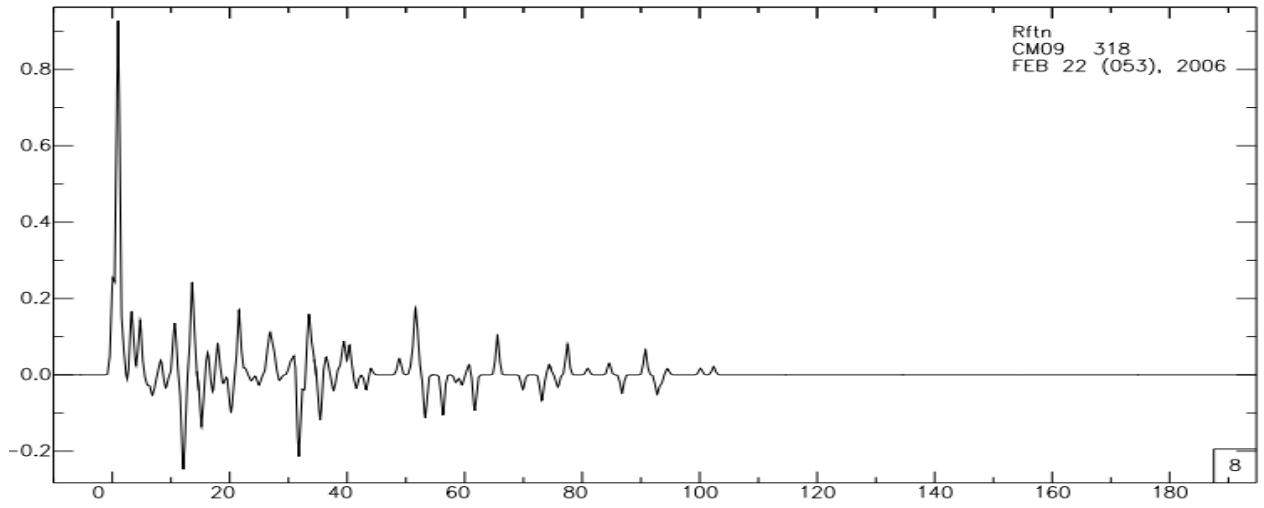

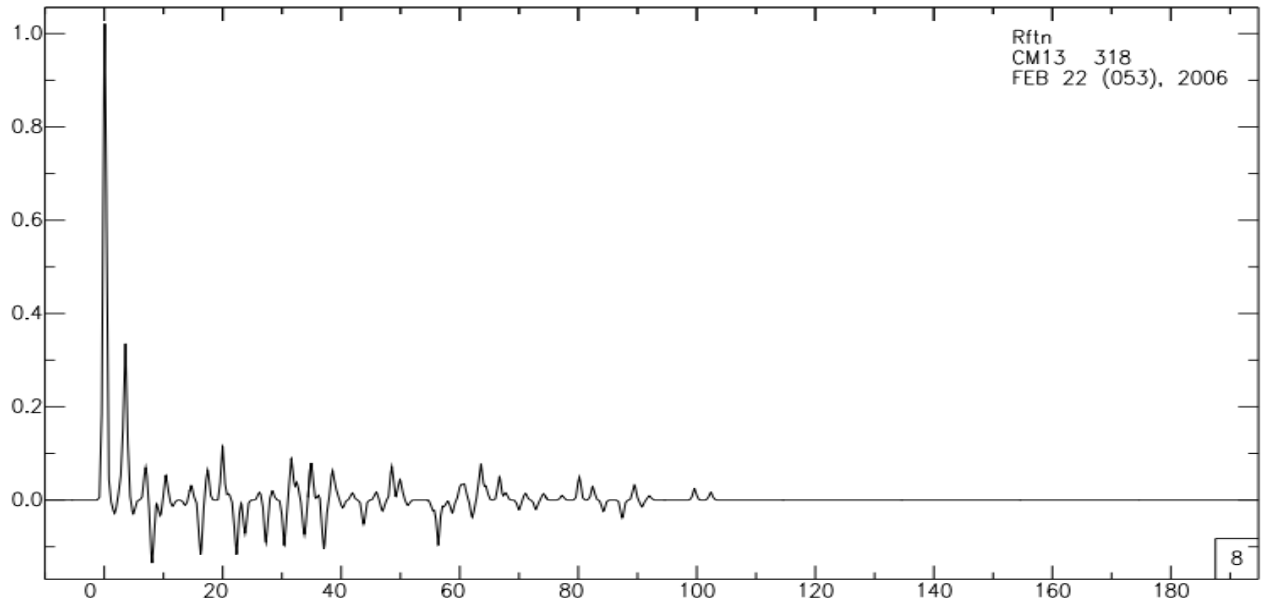

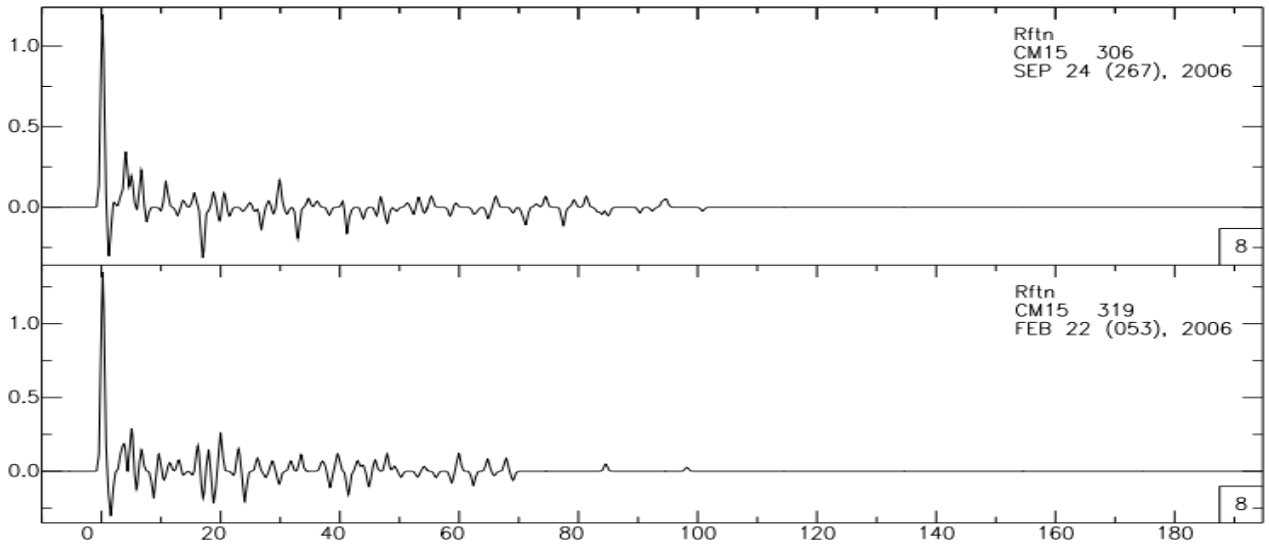

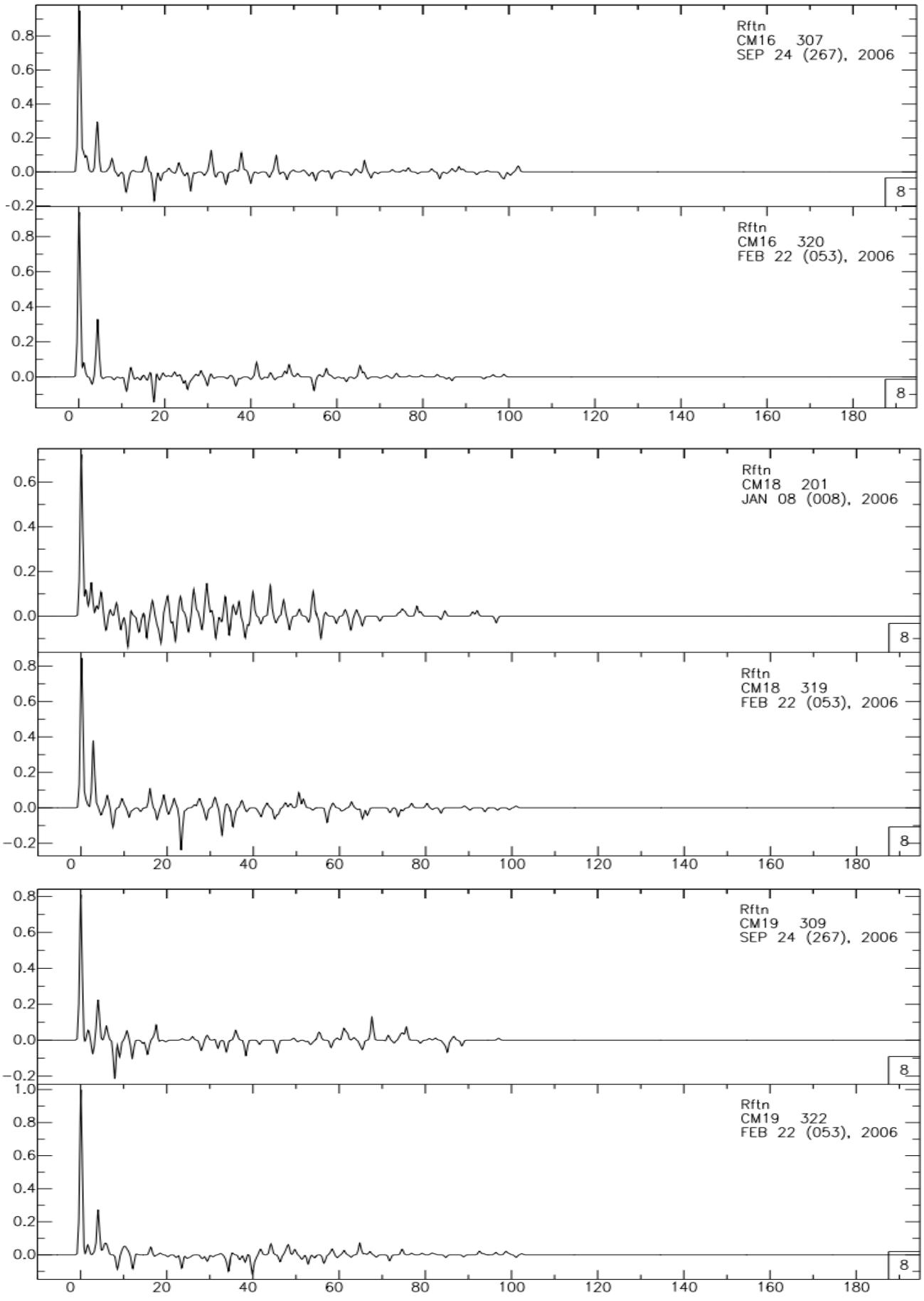
Rftn
CM16 307
SEP 24 (267), 2006
Rftn
CM16 320
FEB 22 (053), 2006
Rftn
CM18 201
JAN 08 (008), 2006
Rftn
CM18 319
FEB 22 (053), 2006
Rftn
CM19 309
SEP 24 (267), 2006
Rftn
CM19 322
FEB 22 (053), 2006

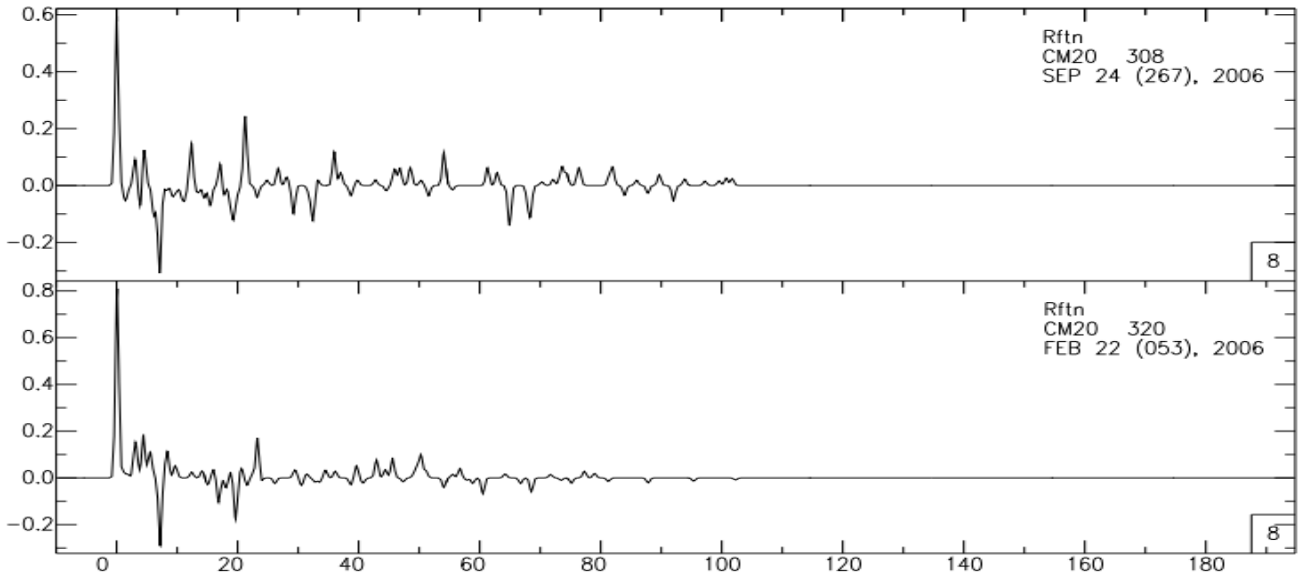
Rftn
CM20 308
SEP 24 (267), 2006
8

Rftn
CM20 320
FEB 22 (053), 2006
8
0
20
40
60
80
100
120
140
160
180

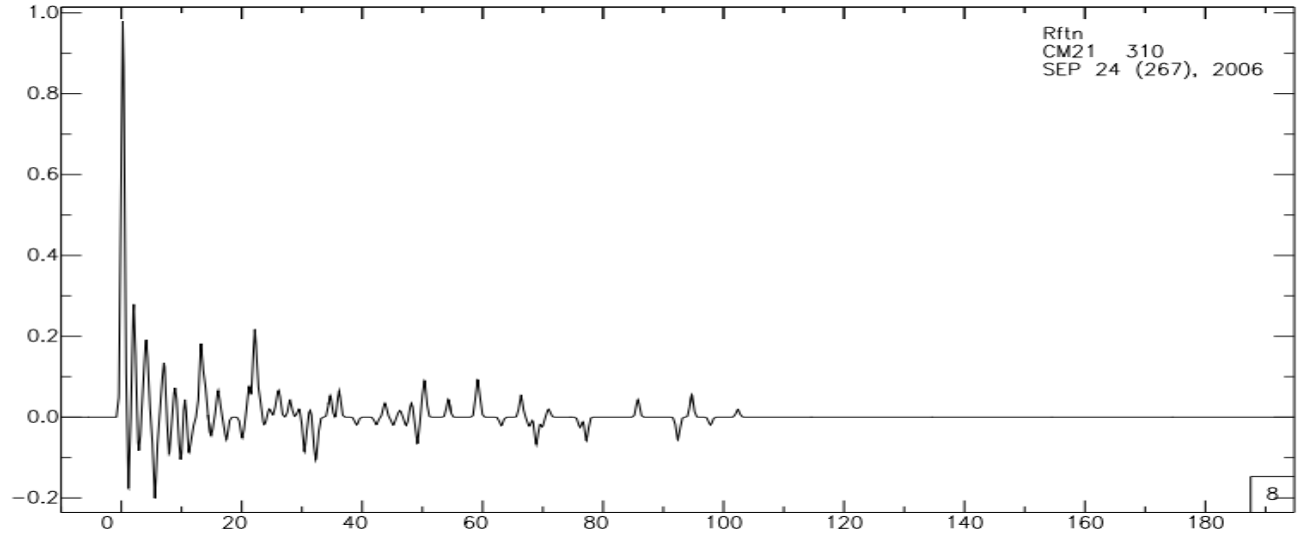
Rftn
CM21 310
SEP 24 (267), 2006
8
0
20
40
60
80
100
120
140
160
180

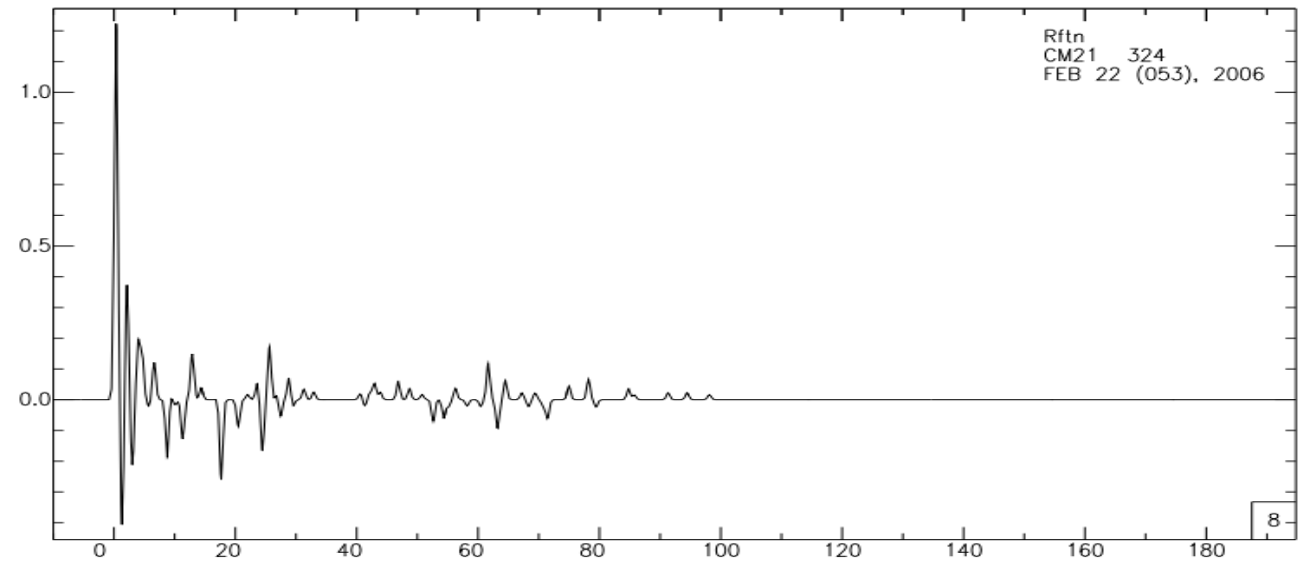
Rftn
CM21 324
FEB 22 (053), 2006
8
0
20
40
60
80
100
120
140
160
180

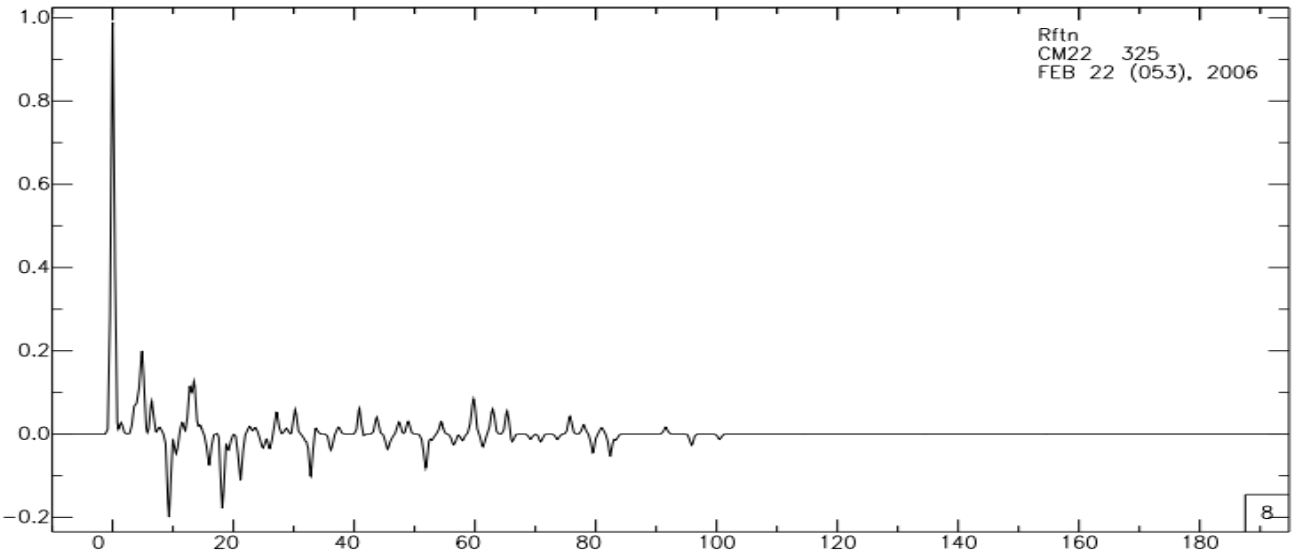
Rftn
CM22 325
FEB 22 (053), 2006
8

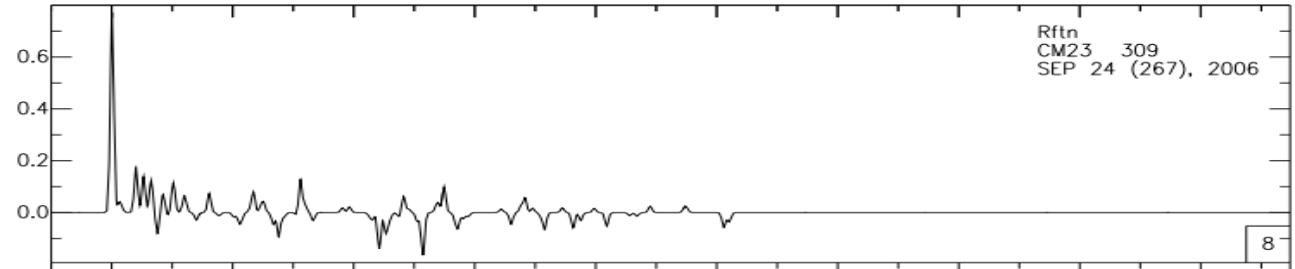
Rftn
CM23 309
SEP 24 (267), 2006
8

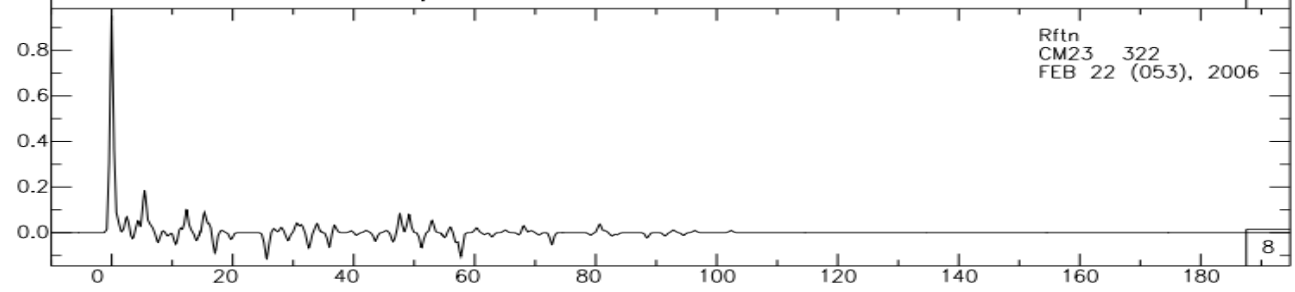
Rftn
CM23 322
FEB 22 (053), 2006
8

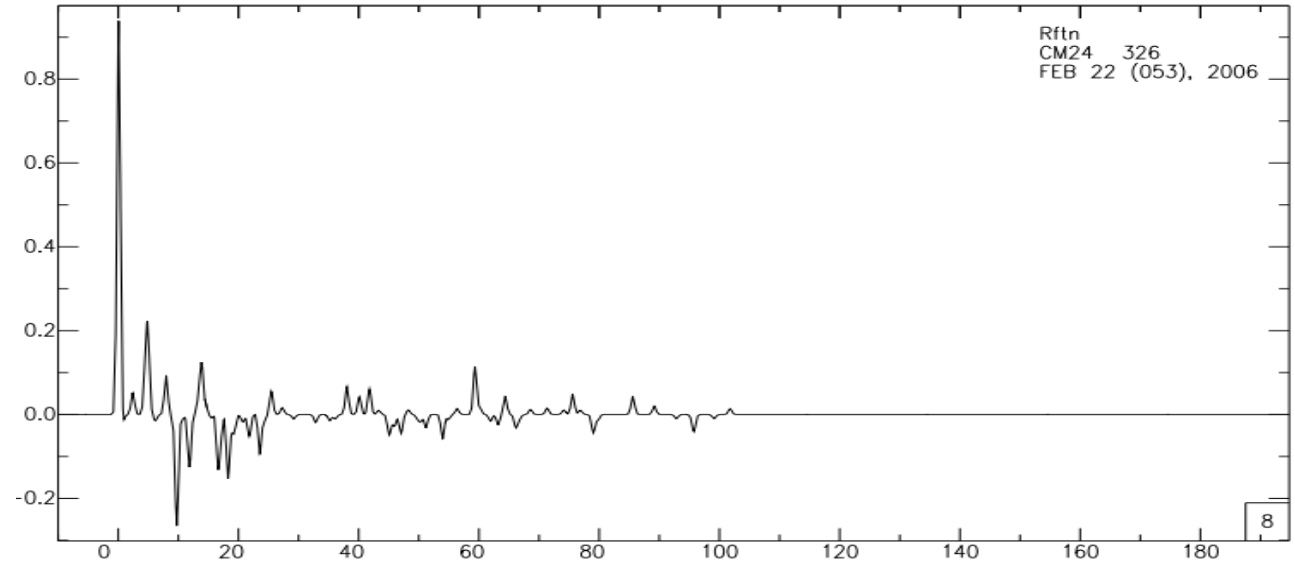
Rftn
CM24 326
FEB 22 (053), 2006
8

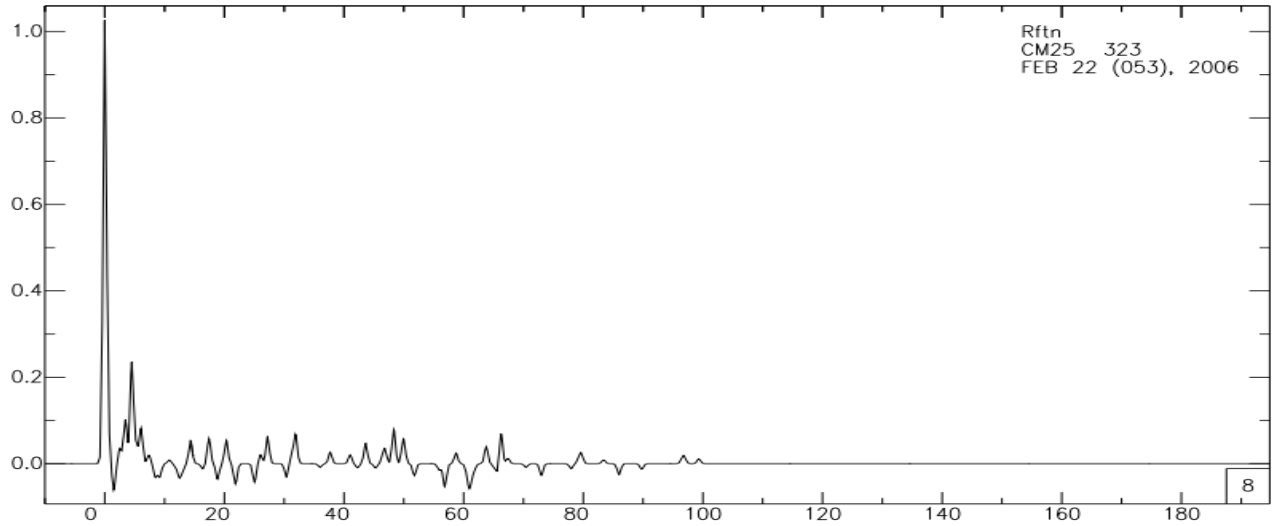
Rftn
CM25 323
FEB 22 (053), 2006
8

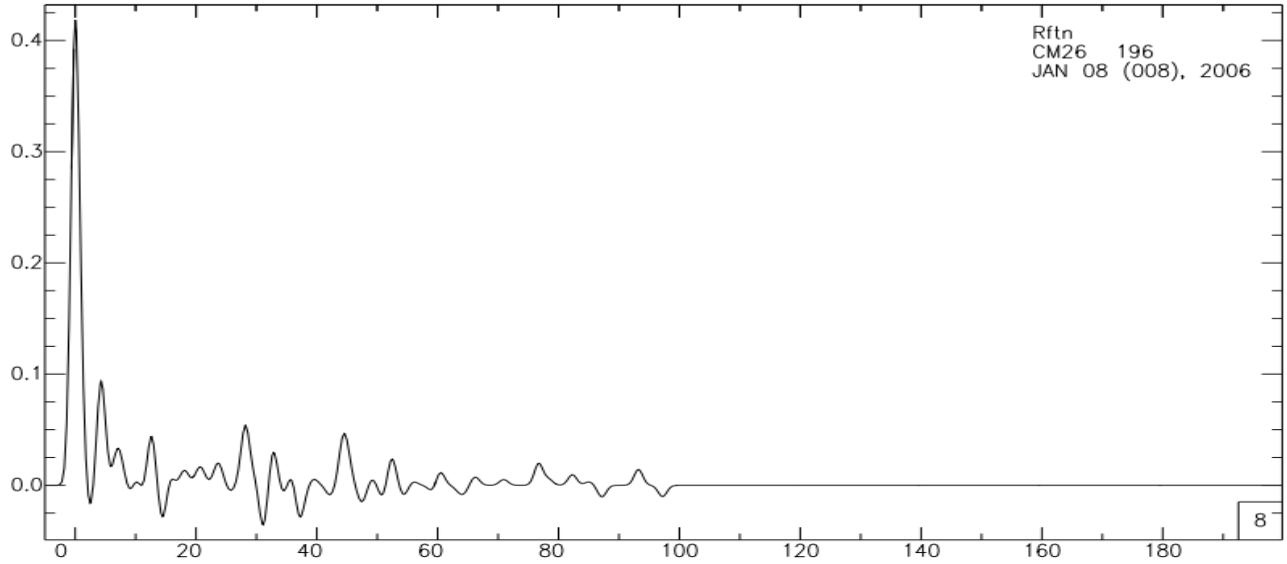
Rftn
CM26 196
JAN 08 (008), 2006
8

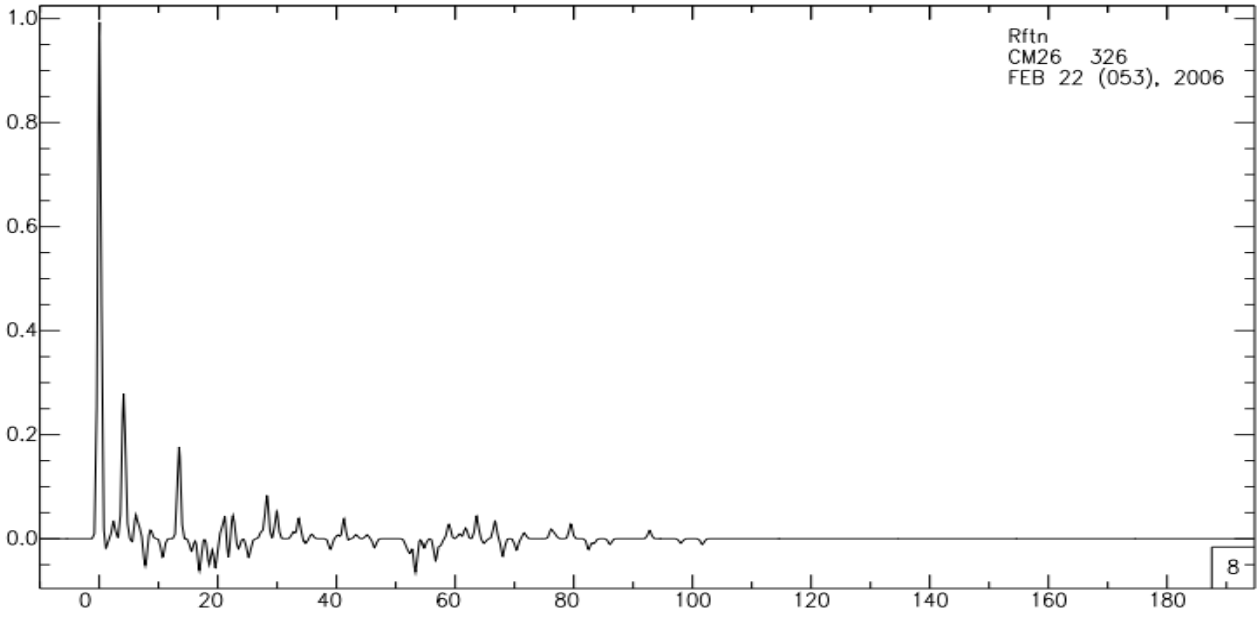
Rftn
CM26 326
FEB 22 (053), 2006
8

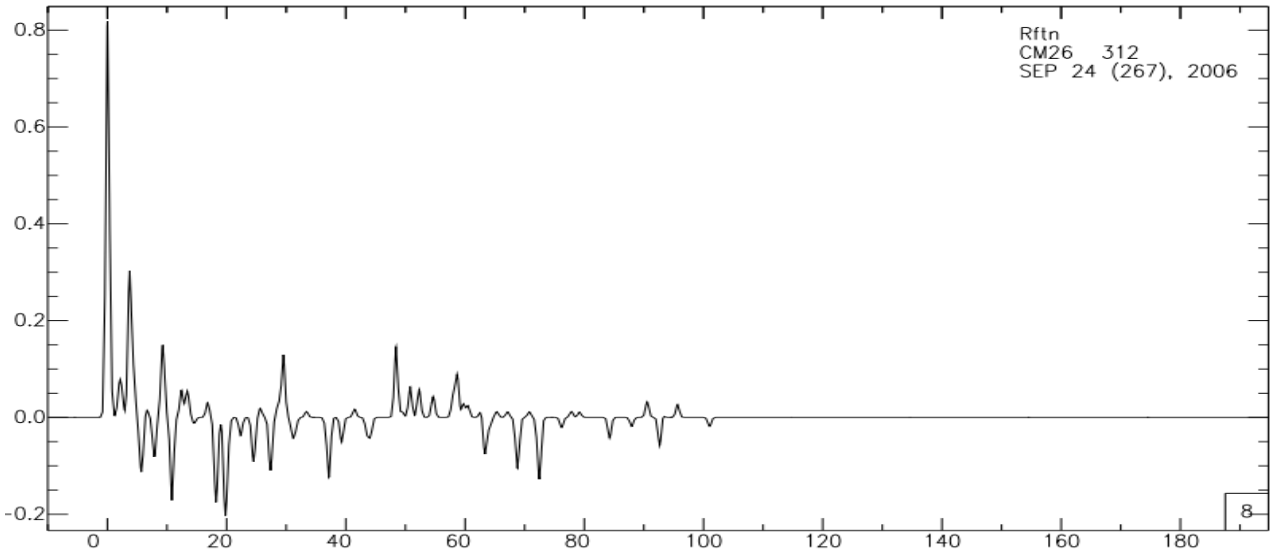
Rftn
CM26 312
SEP 24 (267), 2006
0.8
0.6
0.4
0.2
0.0
-0.2
0
20
40
60
80
100
120
140
160
180
8

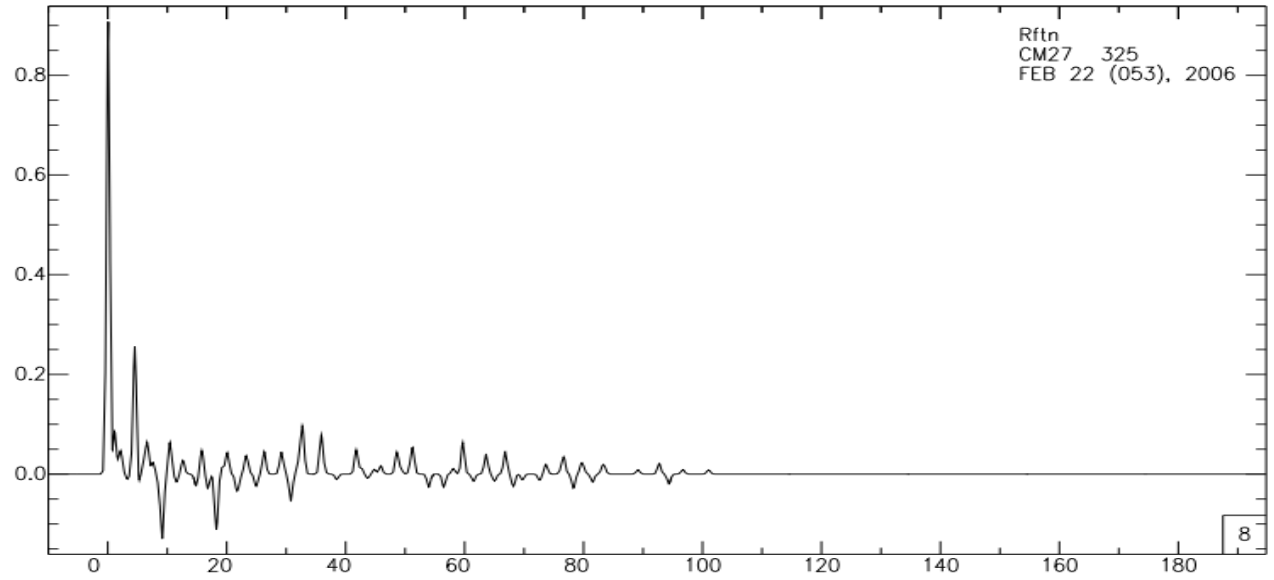
Rftn
CM27 325
FEB 22 (053), 2006
0.8
0.6
0.4
0.2
0.0
0
20
40
60
80
100
120
140
160
180
8

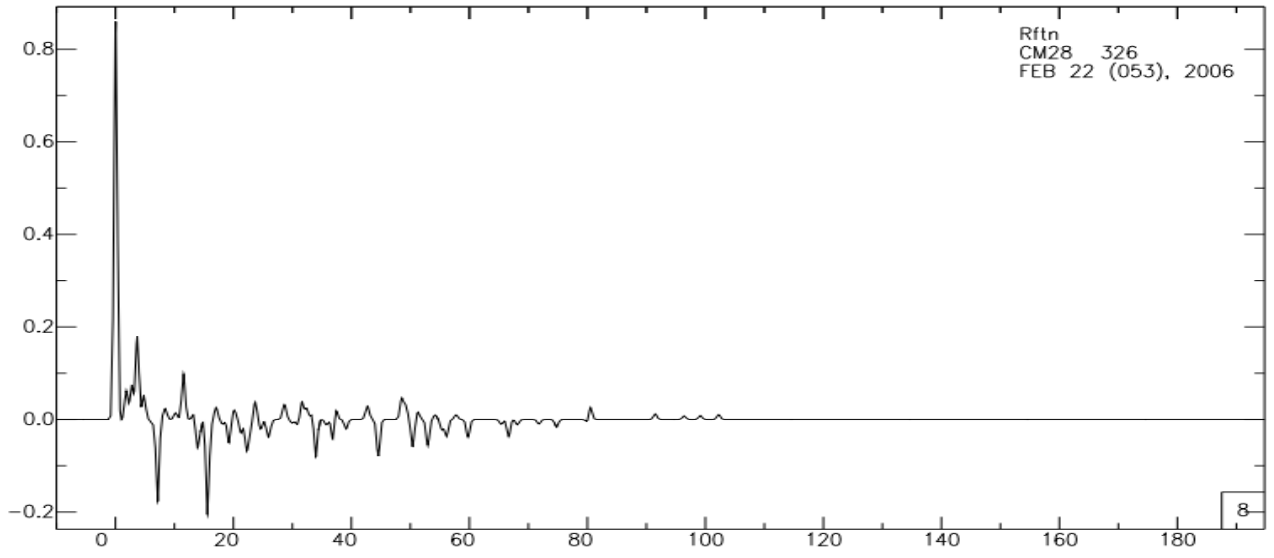
Rftn
CM28 326
FEB 22 (053), 2006
0.8
0.6
0.4
0.2
0.0
-0.2
0
20
40
60
80
100
120
140
160
180
8

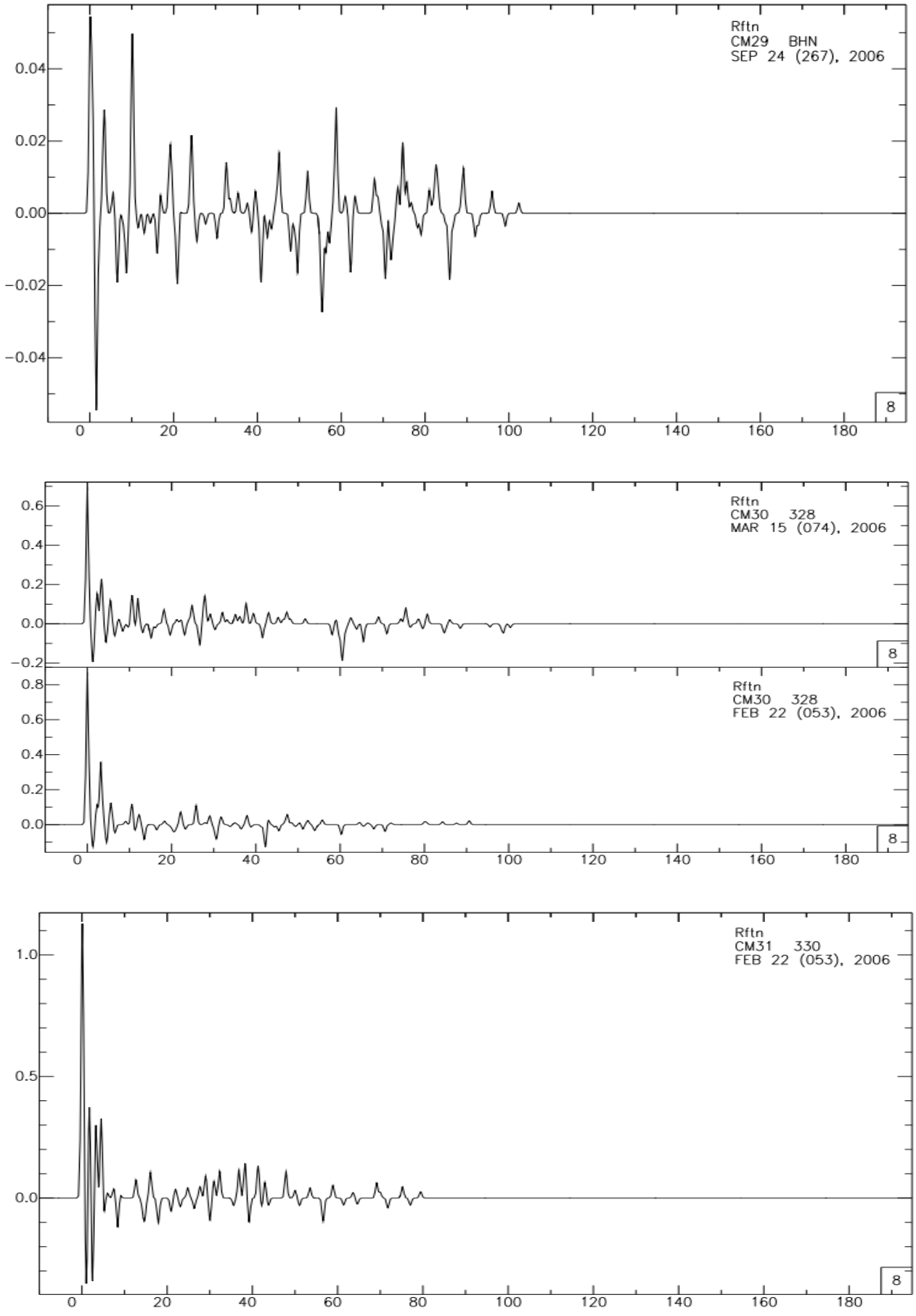
Rftn
CM29 BHN
SEP 24 (267), 2006
Rftn
CM30 328
MAR 15 (074), 2006
Rftn
CM30 328
FEB 22 (053), 2006
Rftn
CM31 330
FEB 22 (053), 2006

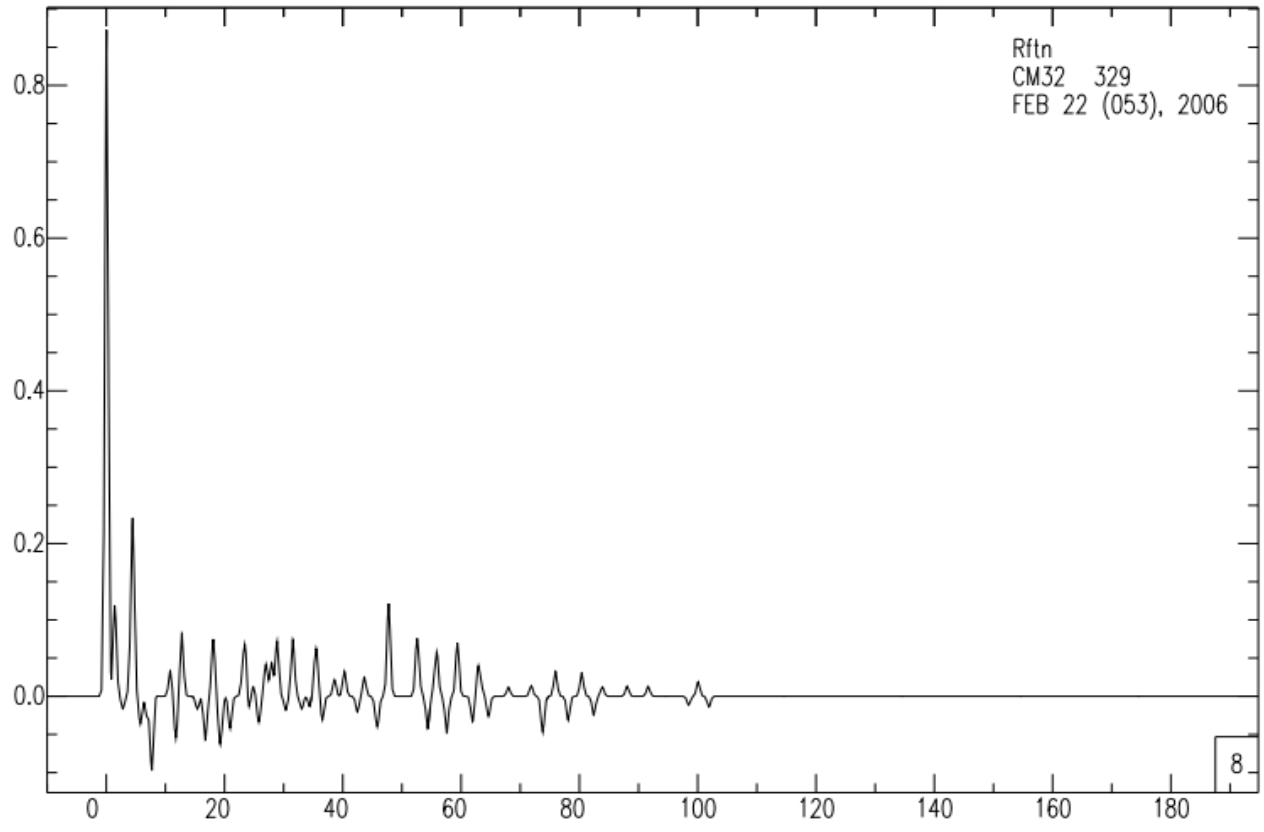
Rftn
CM32 329
FEB 22 (053), 2006
0.8
0.6
0.4
0.2
0.0
0
20
40
60
80
100
120
140
160
180
8

PUBLICATIONS

1. **Thickness Variations in the Lithospheric Mantle and the Low Velocity Zone of the Adamawa Plateau (Cameroon) from Teleseismic Receiver Functions**

Authors: Pokam Kengni Serge. H, Charles T. Tabod, Ndikum N Eric, Tokam Kamga Alain. P, Gounou Pokam Blaise. P

Journal: ***Open Journal of Geology*** **Vol. 8 No. 2 of May issue 2019**

2. **Depth variation of the Lithosphere beneath Garoua Rift Region (Cameroon Volcanic Line) studied from Teleseismic P-waves**

Authors: Pokam Kengni Serge. H, Charles T. Tabod, Ndikum N Eric, Tokam Kamga Alain. P, Gounou Pokam Blaise. P

Journal: ***Open Journal of Earthquake Research*** **Vol. 8 No. 2 of May issue 2019**

3. **Voxel Solution and 3D Sub-Surface Imaging in the Douala Sedimentary Sub-Basin (Cameroon)**

Authors: Eric N. Ndikum, J. Victor Kenfack, F. Koumetio, Serge H. Pokam Kengni, Charles T. Tabod

Journal: ***Physics of the Earth and Planetary Interiors*****. Volume 294 of September issue 2019**

4. **Characterization of Pan-African Aquifer Layers by the Least Squares Inversion Method Applied on Geoelectric Data**

Authors: Kana T. Idriss, Serge. H. Pokam Kengni, Eric N. Ndikum, Blaise P. Gounou Pokam, Charles T. Tabod

Journal : ***International journal of Geosciences.*** **Vol. 10 No. 2 of October issue 2019**

Scientific Research Publishing

Open Journal of Geology, 2018, 8, 529-542
http://www.scirp.org/journal/ojg
ISSN Online: 2161-7589
ISSN Print: 2161-7570

Thickness Variations in the Lithospheric Mantle and the Low Velocity Zone of the Adamawa Plateau (Cameroon) from Teleseismic Receiver Functions

Serge H. Pokam Kengni[1,2*], Charles T. Tabod[1,2], Eric N. Ndikum[1,3], Alain-Pierre Kamga Tokam[1], Pascal Gounou Pokam[1]

[1]Department of Physics, Faculty of Science, University of Yaounde I, Yaounde, Cameroon
[2]Department of Physics, Faculty of Science, The University of Bamenda, Bamenda, Cameroon
[3]Department of Physics, HTTC Bambili, The University of Bamenda, Bamenda, Cameroon
Email: *pokamhugue@yahoo.fr

How to cite this paper: Kengni, S.H.P., Tabod, C.T., Ndikum, E.N., Kamga Tokam, A.-P. and Pokam, P.G. (2018) Thickness Variations in the Lithospheric Mantle and the Low Velocity Zone of the Adamawa Plateau (Cameroon) from Teleseismic Receiver Functions. *Open Journal of Geology*, **8**, 529-542.
https://doi.org/10.4236/ojg.2018.86032

Received: May 7, 2018
Accepted: June 11, 2018
Published: June 14, 2018

Abstract

Teleseismic events recorded by stations located in the Adamawa Plateau have been treated using the inversion method of receiver functions. These six stations are part of a network of 32 large strip seismic stations installed in Cameroon between 2005 and 2007. This method allowed us to investigate the lithospheric mantle in that region. The results obtained from the velocity model have been compared to some existing results in this region. These results show the existence of a thick crust having an average thickness of about 35.2 km and a corresponding S wave velocity of 3.7 km/s. For an average S wave velocity of 4.4 km/s the lithospheric mantle appears to be thin in nature and has a thickness that varies from 39 km and 49.6 km. Beyond the lower lithospheric mantle, there exists a low velocity zone, whose thickness varies between 20 km and 43.9 km. The variation of the low velocity zone leads to variation of the lower boundary of the lithospheric mantle boundary at the depths ranging from 73.8 km and 85 km.

Keywords

Low Velocity Zone, Receiver Function, Teleseismic, Lithospheric Mantle, Adamawa Plateau

1. Introduction

Situated between latitudes 6˚ and 8˚ North and longitudes 11˚ and 16˚ East, the

Adamawa plateau in Cameroon (**Figure 1**) presents itself like a volcanic axis characterized by region of the fissured basaltic volcanism. The fault leaving Foumban joins this region and cuts across it nearly diagonal. It can also be noted that, this region is one of the zones in Cameroon where one can meet several geological accidents.

The basement of this region consists of a Precambrian magmatic gneiss complex (**Figure 1**) that recorded Pan-African granitization [2]. That basement is overlain by a sequence of basaltic to andesitic lavas that are largely of Tertiary age [3]. These lavas are essentially alkaline indicating an affinity to continental rifts [4]. The sedimentary formations here are mainly composed of conglomerates and marl of the Cretaceous Mbere and Djerem Troughs, [3] [5]. These formations have undergone intense tectonic activities resulting in the displacement of basin structures which were frequently filled by volcanic material upwelling through deep fractures in the Adamawa region. Three major tectonic structures are associated with the Adamawa plateau: the Cameroon Volcanic Line (CVL), the Foumban Shear Zone (FSZ) and the South Adamawa Trough (**Figure 1**). The FSZ is part of the Central African Shear Zone (CASZ), which is a succession of major Pan-African faults, trending ENE-WSW and extending over about 2000 km from Cameroon to Sudan [6] [7]. This shear zone in Central Cameroon is characterized by a wide band of mylonites that display a dextral sense of displacement [2] [7]. In a pre-opening of the South Atlantic, these faults extend towards western Brazil through the Pernambuco fault [8]. The South Adamawa Trough corresponds to the Cretaceous Mbere and Djerem sedimentary basins, limited to the North by the CASZ and characterized by conglomerates and mylonites localized along the fault zone [3] [9]. Two areas of seismicity exit, one of which is linked to Foumban fault and crosses the Adamawa Plateau while the other is associated with the north border of the Congo Craton. A majority of the earthquakes recorded in the Adamawa plateau region are generally in relation with the activity of the Volcanic Line of Cameroon [10]. The gravity analysis in the area by [11] highlighted a N70˚ trending anomaly coinciding with the strike of the fractures affecting the basement [12] used joint inversion of Rayleigh wave group velocities and receiver functions to study the structure of

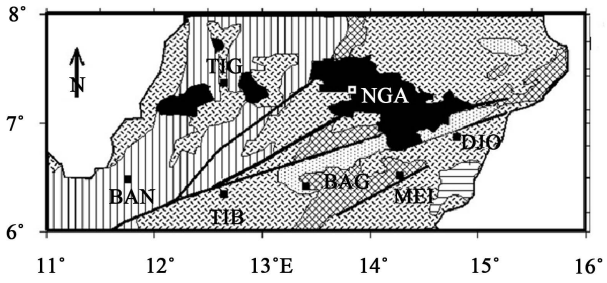

Figure 1. Geologic map of study area (modified from [1]). 1: High grade metamorphosed paleoproterozoic gneiss; 2: Syn-tectonic panafrican granite; 3: Principal undifferentiated panafrican Gneiss; 4: Panafrican Metasediments; 5: Envelope of cretaceous sediments; 6: Cenozoic volcanism; 7: Central cameroon fault line.

the crust beneath Cameroon. The lithosphere beneath Cameroon is characterised by a heterogeneous crust with a relatively constant thickness and a low velocity uppermost mantle at the edge of the Congo Craton [13].

Previous geophysical research works studied the lithosphere without establishing its boundary and depth. This study will strive at examining the boundary of the lithosphere.

2. Data and Methodology

The data used for this study were recorded between January 2005 and February 2007 by the Cameroon Broadband Seismic Experiment, which consisted of 32 portable broad-band seismometers installed across the country (**Figure 2**). Each station (**Table 1**) was equipped with a broad-band seismometer (Guralp CMG-3T or Streckeisen STS-2), a 24-bit Reftek digitizer and a GPS (Global Positioning System) clock.

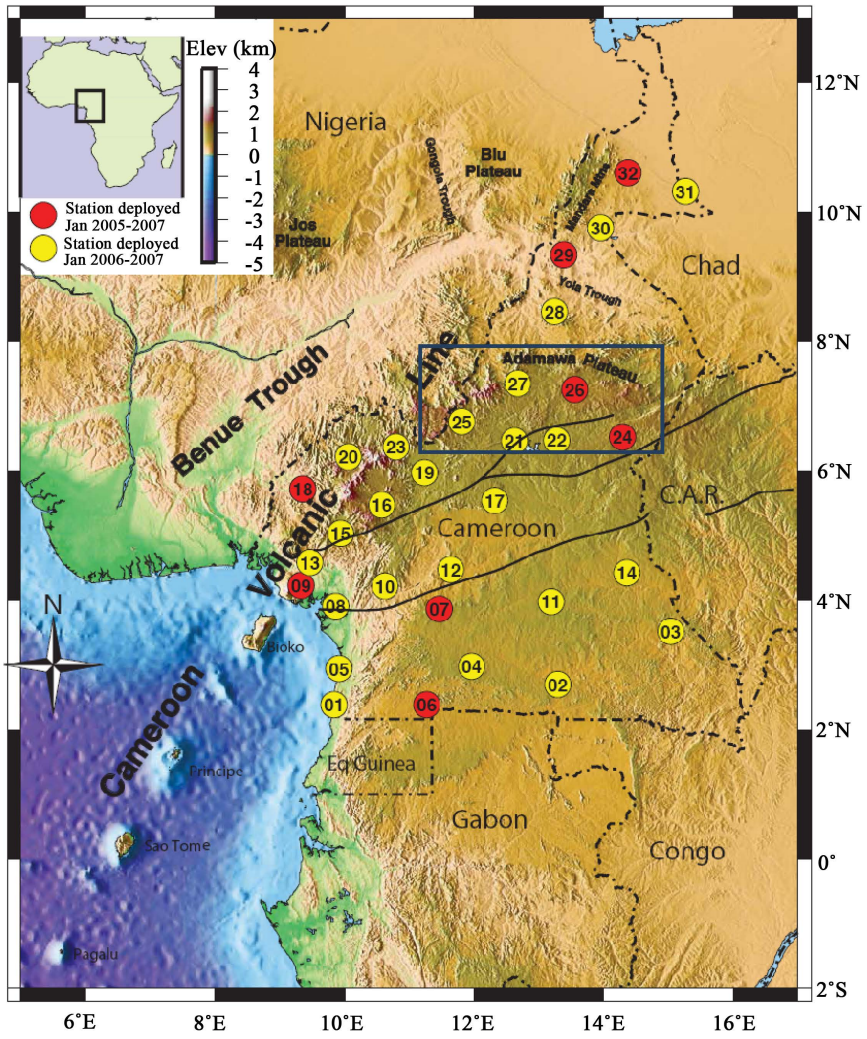

Figure 2. Colour elevation map showing seismic station locations and shear zones. The circled numbers refer to station codes, for example, 22 refers to station CM22 and the rectangle represents the study area.

Table 1. Characteristics of the different stations used to record the teleseismic events.

Station code	Town	Installation year	Latitude (˚)	Longitude (˚)	Elevation (km)
CM21	Tibati	2006	6.46	12.62	0.87
CM22	Ngaoundal	2006	6.47	13.26	0.97
CM24	Meinganga	2005	6.52	14.28	1.05
CM25	Banyo	2006	6.75	11.81	1.12
CM26	Ngaoundere	2005	7.26	13.54	1.23
CM27	Tignere	2006	7.35	12.66	1.12

Data were recorded continuously at a rate of 40 samples per second. In the study area, two stations (red color) were installed in 2005 January and operated during 2 years; the remaining four stations (yellow color) operated only during the second year of the experiment. The station spacing during the second year (2006) of operation was about 50 to 150 km.

Data from the Cameroon Broadband Seismic Experiment have been used to perform inversion of P-wave receiver functions. Receiver functions are chronological temporal series computed using the seismic components recorded at the large band station. They are generated by the time domain iterative deconvolution method of [14], applied to seismograms rotated into vertical, radial and transverse components and can be used to image velocity contrasts across discontinuities.

2.1. Estimation of the Receiver Functions

Receiver functions were computed using data from teleseismic events (**Table 2**) that occurred at epicentral distances between 30˚ and 95˚ with magnitudes ≥5.5.

To compute the receiver functions, visual inspection is first applied in order to confirm the presence of the signal and if the different types of waves which appear on the three components of the seismogram can be identified (**Figure 3**).

Then the selected waveforms were decimated to 10 samples per second, windowed between 20 s and 140 s after the leading P arrival, de-trended, tapered and high pass filtered above 50 s to remove low-frequency, instrumental noise. Radial and transverse receiver functions were then obtained from the filtered traces by rotating the original horizontal components around the corresponding vertical component into the great circle path, and deconvolving the vertical component from the radial component through the iterative time domain deconvolution procedure of [14], with 200 iterations using the Gaussian a = 2.5 corresponding at to the frequency 1.2 Hz because it helps to discriminate gradational transitions from sharp discontinuities in the receiver structure under the station [15]. The recovery percentage of the original radial waveform was evaluated from the rms misfit between the original radial waveform and the convolution of the radial receiver function with the original vertical component. Events that were recovered to less than 85 per cent were rejected. The remaining waveforms were visually inspected for coherence and stability (**Figure 4**).

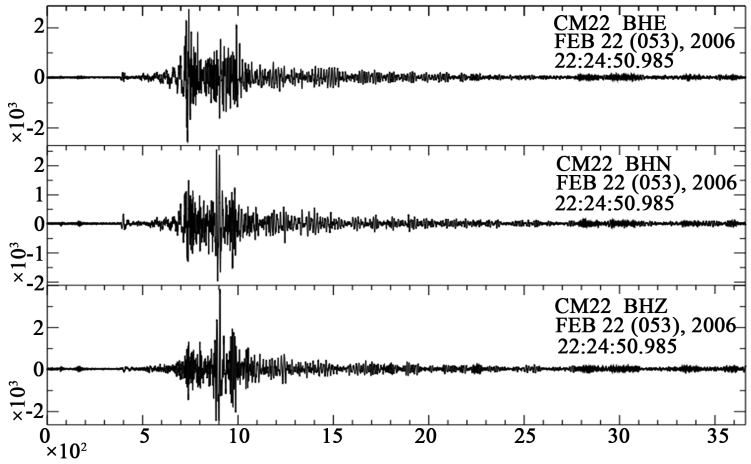

Figure 3. Three components of seismogram recorded at station CM22 for event of 22/02/2016.

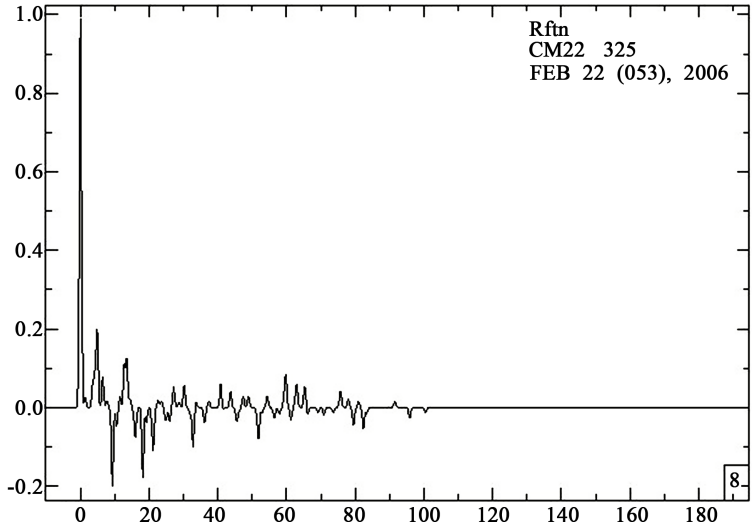

Figure 4. Example of the receiver function computed from station CM22 using teleseismes events. The horizontal axis represents the time in second (s) while the vertical axis represents the amplitude of P-wave in meter (m).

Table 2. Events with magnitude *M*b ≥ 5.5 used for the study.

Event date mm/dd/yy	Event time h:min:s	Latitude (˚)	Longitude (˚)	Depth (km)	Magnitude	Epicentral distance (˚)
10/20/05	21:40:04:01	38.152	26.751	10	5.5	33.1
12/05/05	12:19:56:06	−6.224	29.83	22	6.4	21
12/09/05	23:30:23:09	−6.176	29.709	10	5.5	20.9
01/08/06	11:34:55:06	36.311	23.212	66	6.5	30.2
02/22/06	22:19:07:01	−21.324	33.583	11	6.5	34.5
03/15/06	14:19:48:07	−21.136	33.719	10	6.5	33.9
09/17/06	07:30:11:00	−17.694	41.827	10	5.5	37
09/24/06	22:56:21:07	−17.737	41.814	10	5.6	37.5

2.2. Inversion of the Receiver Functions

Receiver functions are traditionally inverted to obtain an S-wave velocity model that produces an estimation of shear velocity structure under a given seismic station. There is no guarantee that a unique inversion result will be obtained, as the method seeks to minimize the differences between observed and synthetic receiver functions. The inversion was performed using the method developed by [16] [17]. The method is based on a linearized inversion procedure that minimizes a weighted combination of least squares norms for each data set, a model roughness norm and a vector-difference norm between inverted and pre-set model parameters. The velocity models obtained are consequently a compromise between fitting the observations, model simplicity and a priori constraints. The starting model used in this inversion consisted of an isotropic medium of constant velocity layers that increase in thickness with depth. The thicknesses of the first, second and third layers are, respectively, 45 km, 90 km and 80 km, while the thickness increases at each instant to 5 km between 0 and 45 km depth, to 10 km between 45 and 135 km and 20 km below a depth of 135 km and a linear shear wave velocity increase in the crust from 3.2 to 4.0 km/s and 4.0 to 4.7 km/s in the lithospheric mantle overlying a flattened PREM (Preliminary Reference Earth Model) model [18] for the mantle.

3. Results and Discussion

3.1. Results

Results from the inversion of the receiver functions computed for the six stations studied are shown in **Figure 5**. The interpretations are summarized in **Table 3** and **Table 4** presented a head.

Table 3 summarizes the main information given by the curves of the synthetic receiver functions above and **Table 4** regroups the main information that the velocity model curves convey.

Table 3 shows that the synthetic receiver functions have very important percent of Signal Power Fit (>80%) apart of that corresponding to CM21 located at Tibati. This justifies a stability of the curves of current and initial model and it causes the wave to undergo a rare conversion. The times of Ps conversion (t_{Ps}) are practically uniform at close to 0.2 s.

Table 3. Interpretation of synthetic receiver functions.

Stations	Localities	Percent of Signal Power Fit	t_{Ps}(s)
CM21	Tibati	60.41; 52.12	2?
CM22	Ngaoundal	90.69	4.7
CM24	Meinganga	88.84	4.7
CM25	Banyo	94.76	4.6
CM26	Ngaoundere	82.59; 93.28 and 88.28	4.6
CM27	Tignere	91.15 and 78.39	4.7

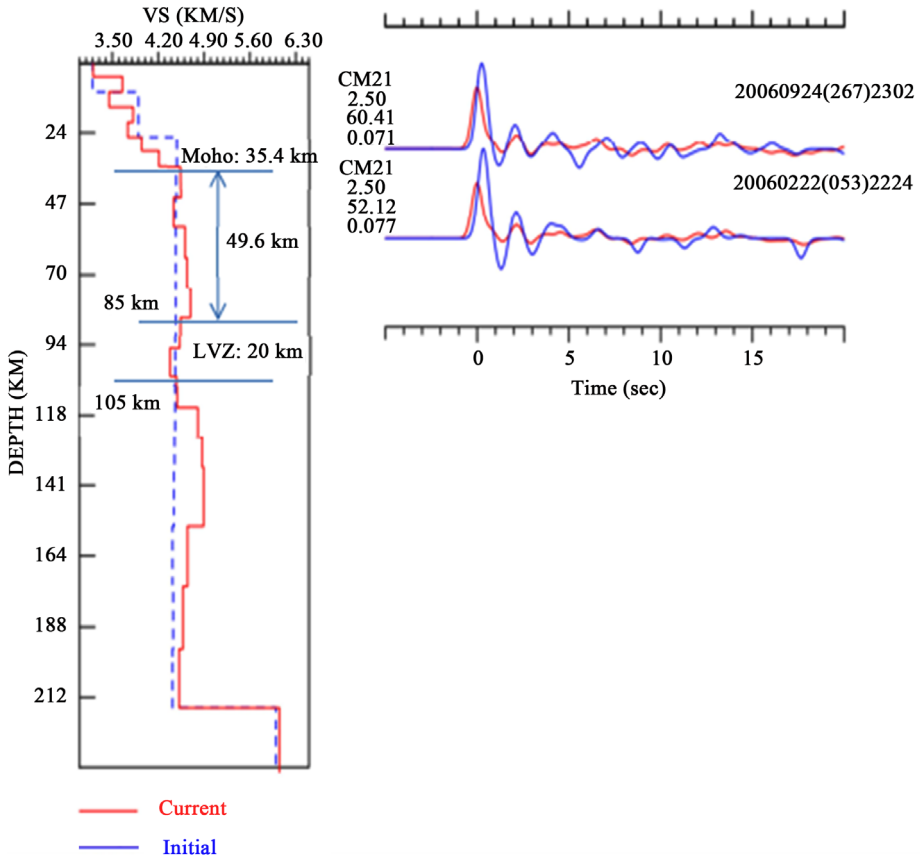
VS (KM/S)
3.50 4.20 4.90 5.60 6.30
DEPTH (KM)
24
47
70
94
118
141
164
188
212
Moho: 35.4 km
49.6 km
85 km
LVZ: 20 km
105 km
Current
Initial
CM21
2.50
60.41
0.071
20060924(267)2302
CM21
2.50
52.12
0.077
20060222(053)2224
0
5
10
15
Time (sec)

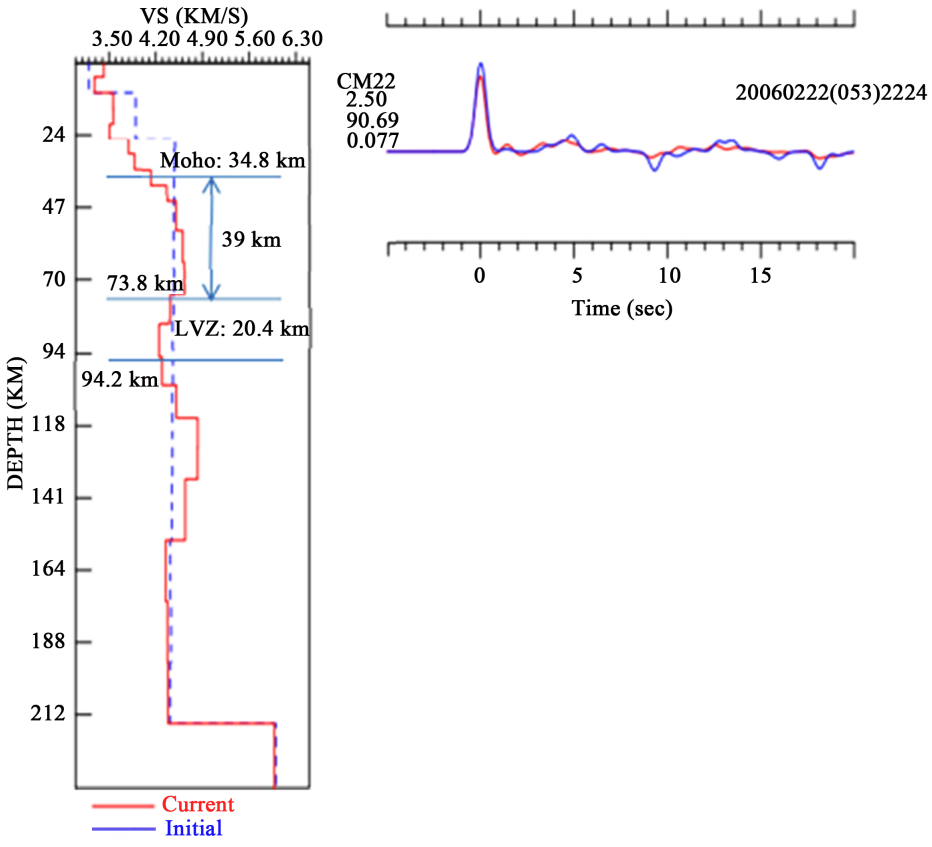
VS (KM/S)
3.50 4.20 4.90 5.60 6.30
DEPTH (KM)
24
47
70
94
118
141
164
188
212
Moho: 34.8 km
39 km
73.8 km
LVZ: 20.4 km
94.2 km
Current
Initial
CM22
2.50
90.69
0.077
20060222(053)2224
0
5
10
15
Time (sec)

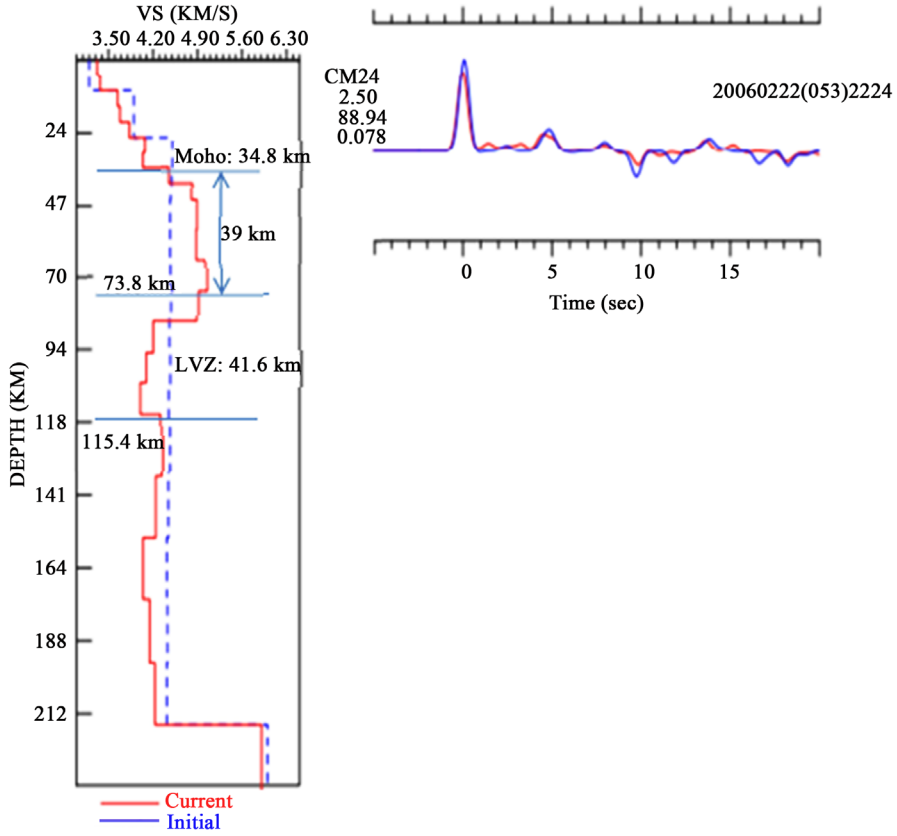
VS (KM/S)
3.50 4.20 4.90 5.60 6.30
DEPTH (KM)
24
47
70
94
118
141
164
188
212
Moho: 34.8 km
39 km
73.8 km
LVZ: 41.6 km
115.4 km
Current
Initial
CM24
2.50
88.94
0.078
20060222(053)2224
0
5
10
15
Time (sec)

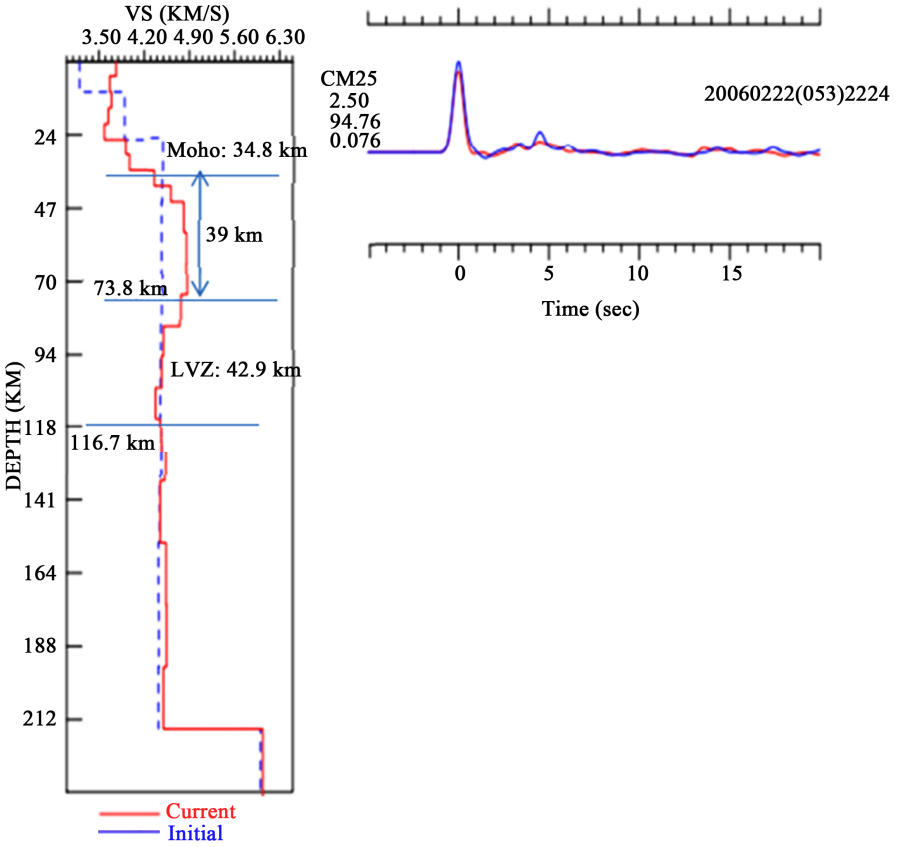
VS (KM/S)
3.50 4.20 4.90 5.60 6.30
DEPTH (KM)
24
47
70
94
118
141
164
188
212
Moho: 34.8 km
39 km
73.8 km
LVZ: 42.9 km
116.7 km
Current
Initial
CM25
2.50
94.76
0.076
20060222(053)2224
0
5
10
15
Time (sec)

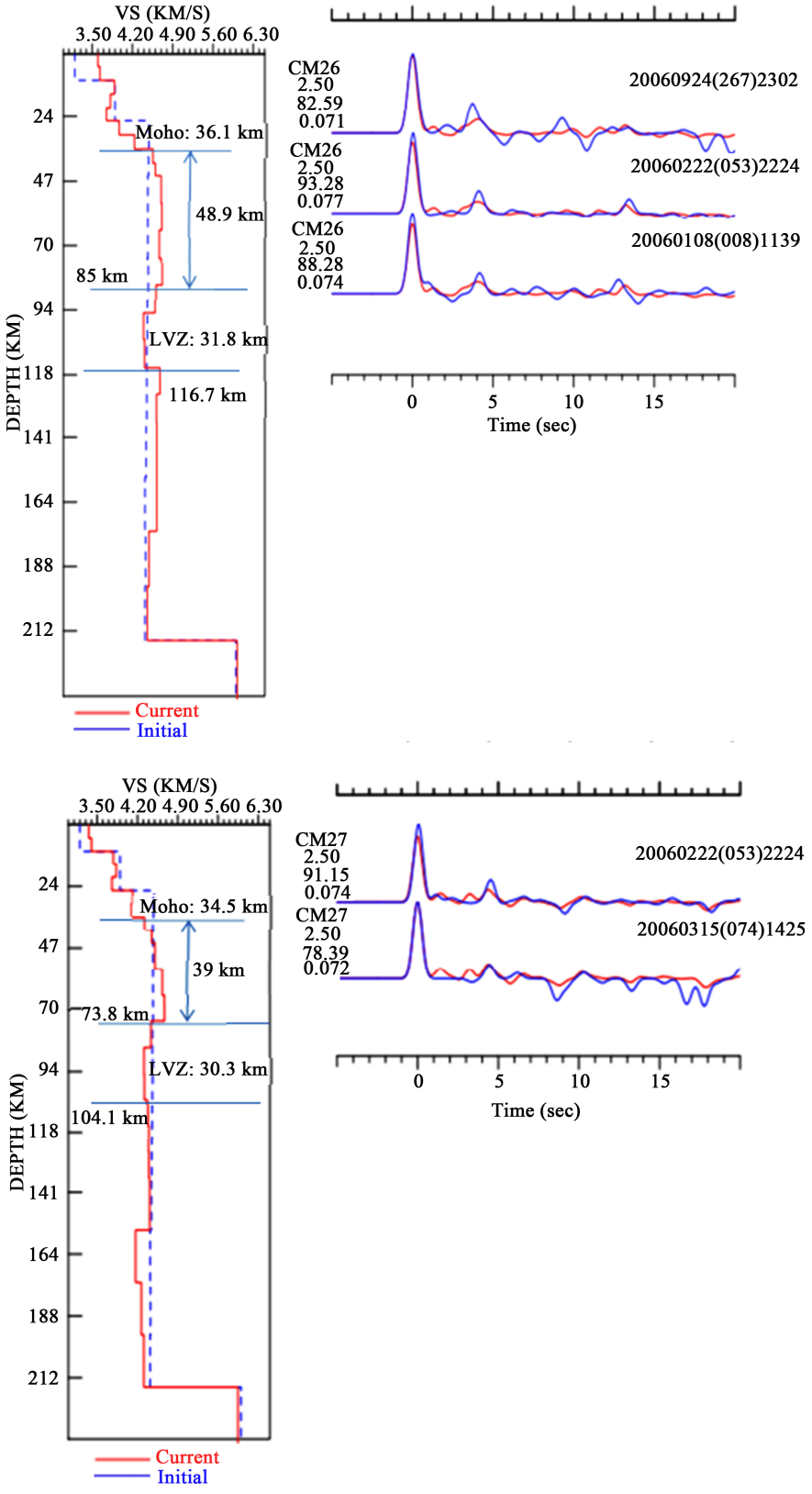

Figure 5. Shear velocity profiles for each of six stations. The solid line shows the depth delimitation. (2.5 is the Gaussian filter; 91.15 is Percent of Signal Power Fit; 0.074 is the ray parameter 053 is the day of year).

Table 4. Interpretation of the inversion curves.

Stations	Localities	Average crustal Vs (km/s)	Moho depth (km)	Average lithospheric mantle Vs (km/s)	Average lithospheric mantle thickness (km)	thickness interval of LVZ (km)
CM21	Tibati	3.8?	35.4?	4.4?	49.6?	85 < LVZ < 105?
CM22	Ngaougal	3.7	34.8	4.4	39	73.8 < LVZ < 94.2
CM24	Meinganga	3.8	34.8	4.2	39	73.8 < LVZ < 115
CM25	Banyo	3.9	34.8	4.6	39	73.8 < LVZ < 116.7
CM26	Ngaoundere	4	36.1	4.6	48.9	85 < LVZ < 116.7
CM27	Tignere	3.7	34.8	4.4	39	73.8 < LVZ < 104

Table 4 shows from the velocity models that the mean velocity of the S waves is 3.7 km/s in the crust and more than 4 km/s in the lithospheric mantle. Discontinuities are localized; firstly at an average depth 35.1 km between for the crust and upper mantle (Moho) and secondly with variation from 73.8 km to 85 km at the boundary between the lithospheric and asthenosphere. The lithospheric mantle and the low velocity zone thicknesses varies between 39 km and 49.6 km and between and 73.8 km and 116.7 km respectively.

3.2. Discussions

3.2.1. Comparison of the Synthetic Receiver Function by Localities

Comparing the different synthetics receivers functions, it is observed that the current (red colour) and initial (blue color) synthetic receiver functions are stable (Percent of Signal Power Fit is more than 80%) and the time of Ps conversion phase practically homogeneous at 0.2 s except for CM21 located at Tibati where they are not stable. This non stability would be due to the Foumban shear fault that crosses the Tibati locality.

3.2.2. Comparison with Previous Estimates

The uniformity of the time of Ps conversion at the level of the moho (Table 3) and the low amplitudes as seen on the synthetic receiver functions suggest a homogenous nature of the crust in the Adamawa plateau region Tokam *et al.* (2010). The small length interval of the secondary wave velocity Vs at the crust and lithospheric mantle expresses the fact that the lithospheric mantle is thin in the Adamawa plateau region.

Comparison with the previous estimations are showed in Table 5.

Table 5 shows that, estimates of average S-wave velocity Vs in the crust and upper mantle on one hand and the moho depth on the other hand are in very good agreement to previous estimates based on both gravity and seismic data in the region. A slight difference is noticed at the level of the depth of the moho and the lithospheric mantle boundary. This can be justified by the type of method or data used.

Table 5. Comparing with previous estimates.

Type of result	This study	Others studies	Types of data used	References
Average Vs of crustal (Km/s)	3.7	3.7	seismic	[12]
Average Vs of lithospheric mantle (Km/s)	4.4	4.4	seismic	[12]
Average depth moho (Km)	35.1	33	seismic	[19]
		33	gravity	[20]
		35.5	seismic	[12]
Average depth Lithospheric (Km)	between 73.8 and 85	≅70	Gravity and seismics	[21]

3.2.3. Comparison the Lithospheric Mantle and the Thickness Low Velocity Zone (LVZ) of Different Localities

A comparison of the lithospheric mantle and low velocity zone thickness (LVZ) for localities in the Adamawa plateau region is shown in **Figure 6**.

These figures show that the lithospheric mantle and low velocity zone thicknesses are not uniform in this region but that they are variable which also entails a variation of the depth of the lithospheric mantle in this region.

4. Conclusions

The teleseismic events recorded between 2005 and 2007 from the six seismic stations installed in the Adamawa Plateau have been treated with the receiver function method to investigate the lithospheric mantle and the crust. It was found from this survey that: 1) the synthetic receiver functions obtained show the existence of Ps conversion at 4.7s at the moho; 2) the crust in this region is thick with an S wave velocity of 3.7km/s and an average depth of 35.1 km; 3) the lithospheric mantle has a thickness that varies between 39 km and 49.6 km for an average S wave velocity greater than 4 km/s; 4) In this region, there exist a low velocity zone which has a variable thickness ranging between 20 km and 43.9 km and the lithosphere-asthenosphere boundary also varies between 73.8 km and 85 km according the low velocity zone position. The results obtained in this work have been compared to others existing in this region. Some similarities have been noticed in some cases like in the depth of the crust, the velocity of the S waves in the crust and in the lithospheric mantle, and the existence of a Low Velocity Zone. The slight differences with other cases have to do with the depth of the lithospheric mantle. These differences can be justified by the type of method or data used. Nevertheless an alone station (CM21) situeted at Tibati locality does not product the good results especially with particularly the synthetic receiver function due to the Foumban shear fault that across that station. In this work, though the boundary of the lithosphere has been studied, it will never the less be important to carry out geodynamic studies to investigate the causes of the observed variations as well as the level of stability of this lithospheric boundary.

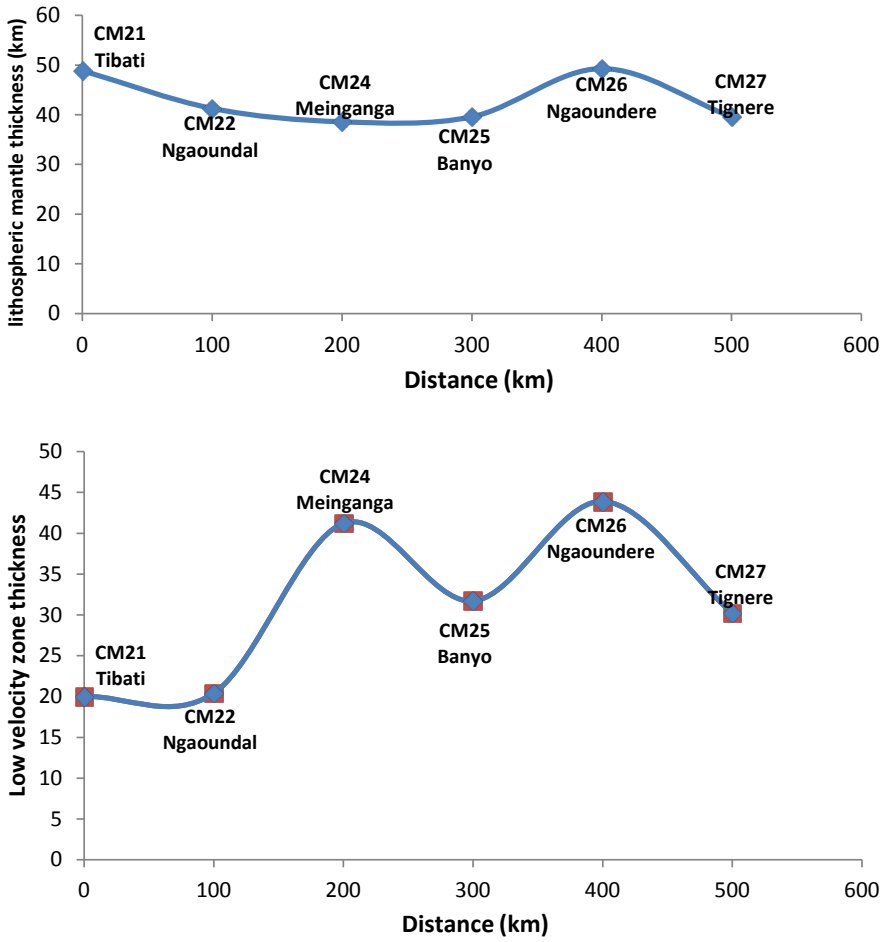

Figure 6. Comparison the lithospheric mantle thickness and the thickness Low velocity zone (LVZ) of different localities.

Acknowledgements

We wish to express our gratitude to the team and sponsor of the Cameroon broadband seismic experiment for the data that was colled and has been used in this work.

References

[1] Ngnotué, T., Nzenti, J.P., Barbey, P. and Tchoua, F.M. (2000) The Ntui-Betamba High Grade Gneisses in Cameroon. *Journal of African Earth Sciences*, **31**, 369-381. https://doi.org/10.1016/S0899-5362(00)00094-4

[2] Dumont, J.F. (1987) Etude structurale des bordures Nord et Sud du plateau de l'Adamaoua: Influence du contexte atlantique. *Géodynamique*, **2**, 55-68.

[3] Le Maréchal, A. and Vincent, P.R. (1971) Le fossé crétacé du Sud Adamaoua (Cameroun). *Office de la Recherche Scientifique et Technique outre-mer*: *Série Géologie* (*Cahiers O.R.S.T.O.M.*: *Série Géologie*), **3**, 67-83.

[4] Kampunzu, A.B., Caron, J.H. and Lubala, R.T. (1986) The East African Rift, Magma Genesis and Astheno-Lithospheric Dynamism. *Episodes*, **9**, 211-216.

[5] Lasserre, M. (1961) Étude géologique de la partie orientale de l'Adamaoua (Cameroun Central) et les principales sources minéralisées de l'Adamaoua. *Bulletin*

de la Direction Mines et Geologie du Cameroun, No. 4, 130 p.

[6] Cornacchia, M. and Dars, R. (1983) Un trait structural majeur du continent africain. Les linéaments centrafricains du Cameroun au Golfe d'Aden. *Bulletin de la Société Géologique de France*, **25**, 101-109. https://doi.org/10.2113/gssgfbull.S7-XXV.1.101

[7] Ngako, V., Jegouzo, P. and Nzenti, J.P. (1991) Le Cisaillement Centre Camerounais. Rôle structural et géodynamique dans l'orogenèse panafricaine. *Compte Rendus de l'Academie des sciences de Paris*, t. 313, sér. II, 457-463.

[8] De Almeida, F.F.M., Hasui, Y., Brito Neves, B.B. and Fuck, R. (1991) Brasiliano Structural Provinces: An Introduction. *Earth Science Reviews*, **17**, 1-29. https://doi.org/10.1016/0012-8252(81)90003-9

[9] Ngangom, E. (1983) Etude tectonique du fossé de la Mbéré et du Djerem, Sud Adamaoua. In: Popoff, M. and Tiercelin, J.J., Eds., *Rifts et fossés anciens*, *Centres de Recherches e Exploration-Production Elf-Aquitaine Pau*, Vol. 7, 339-347.

[10] Tabod, C.T., Fairhead, J.D., Stuart, G.W., Ateba, B. and Ntepe, N. (1992) Seismicity of the Cameroon Volcanic Line, 1982-1990. *Tectonophysics*, **212**, 303-320. https://doi.org/10.1016/0040-1951(92)90297-J

[11] Noutchogwe, T.C., Tabod, C.T. and Manguelle-Dicoum, E. (2006) A Gravity Study of the Crust Beneath the Adamawa Fault Zone, West Central Africa. *Journal of Geophysics and Engineering*, **3**, 82-89. https://doi.org/10.1088/1742-2132/3/1/009

[12] Tokam, A., Tabod, C.T., Nyblade, A.A. and Julià, J. (2010) Structure of the Crust beneath Cameroon, West Africa, from the Joint Inversion of Rayleigh Wave Group Velocities and Receiver Functions. *Geophysical Journal International*, **183**, 1061-1076. https://doi.org/10.1111/j.1365-246X.2010.04776.x

[13] Guidarelli, M. and Aoudia, A. (2016) Ambient Noise Tomography of the Cameroon Volcanic Line and Northern Congo Craton: New Constraints on the Structure of the Lithosphere. *Geophysical Journal International*, **204**, 1756-1765. https://doi.org/10.1093/gji/ggv561

[14] Ligorría, J.P. and Ammon, C.J. (1999) Iterative Deconvolution and Receiver Function Estimation. *Bulletin of the Seismological Society of America*, **89**, 1395-1400.

[15] Julià, J. (2007) Constraining Velocity and Density Contrasts across the Crust: Mantle Boundary with Receiver Function Amplitudes. *Geophysical Journal International*, **171**, 286-301. https://doi.org/10.1111/j.1365-2966.2007.03502.x

[16] Julià, J., Ammon, C.J., Herrmann, R.B. and Correig, A.M. (2000) Joint Inversion of Receiver Function and Surface Wave Dispersion Observations. *Geophysical Journal International*, **143**, 99-112. https://doi.org/10.1046/j.1365-246x.2000.00217.x

[17] Julià, J., Ammon, C.J. and Herrmann, R.B. (2003) Lithospheric Structure of the Arabian Shield from the Joint Inversion of Receiver Functions and Surface Wave Group Velocities. *Tectonophysics*, **371**, 1-21. https://doi.org/10.1016/S0040-1951(03)00196-3

[18] Dziewonski, A.M. and Anderson, D.L. (1981) Preliminary Reference Earth Model. *Physics of the Earth and Planetary Interiors*, **25**, 297-356.

[19] Stuart, G.W., Fairhead, J.D., Dorbath, L. and Dorbath, C. (1985) A Seismic Refraction Study of the Crustal Structure Associated with the Adamawa Plateau and Garoua Rift, Cameroon, West Africa. *Geophysics Journal Royal Astronomical Society*, **81**, 1-12. https://doi.org/10.1111/j.1365-246X.1985.tb01346.x

[20] Nnange, J.M., Ngako, V., Fairhead, J.D. and Ebinger, C.J. (2000) Depths to Density Discontinuities beneath the Adamawa Plateau Region, Central Africa, from Spectral Analysis of New and Existing Gravity Data. *Journal of African Earth Sciences*, **30**,

887-901. https://doi.org/10.1016/S0899-5362(00)00058-0

[21] Plomerova, J., Babuska, V., Dorbath, L., Dorbath, R. and Lillie, R.J. (1993) Deep Lithospheric Structure across the Central African Shear Zone in Cameroon. *Geophysical Journal International*, **115**, 381-390. https://doi.org/10.1111/j.1365-246X.1993.tb01193.x

Scientific Research Publishing

Open Journal of Earthquake Research, 2019, 8, 116-131
http://www.scirp.org/journal/ojer
ISSN Online: 2169-9631
ISSN Print: 2169-9623

Depth Variation of the Lithosphere beneath Garoua Rift Region (Cameroon Volcanic Line) Studied from Teleseismic P-Waves

Serge H. Kengni Pokam[1,2*], Charles T. Tabod[1,2], Eric N. Ndikum[1,3], Alain P. Tokam Kamga[1], Blaise P. Pokam Gounou[1]

[1]Department of Physics, Faculty of Science, University of Yaounde I, Yaounde, Cameroon
[2]Department of Physics, Faculty of Science, The University of Bamenda, Bamenda, Cameroon
[3]Department of Physics, HTTC Bambili, The University of Bamenda, Bamenda, Cameroon
Email: *pokamhugue@yahoo.fr

How to cite this paper: Pokam, S.H.K., Tabod, C.T., Ndikum, E.N., Kamga, A.P.T. and Gounou, B.P.P. (2019) Depth Variation of the Lithosphere beneath Garoua Rift Region (Cameroon Volcanic Line) Studied from Teleseismic P-Waves. *Open Journal of Earthquake Research*, **8**, 116-131.
https://doi.org/10.4236/ojer.2019.82008

Received: October 17, 2018
Accepted: May 27, 2019
Published: May 30, 2019

Abstract

Teleseismic events have been selected from a database of earthquakes with three components which were recorded between February 2005 and January 2007 by five seismic stations across the Garoua rift region which constitutes a part of the Cameroon Volcanic Line (CVL). The iterative time deconvolution performed by [1] applied on these teleseismic events, permitted us to obtain P-receiver functions. The latter were subsequently inverted in order to obtain S-wave velocity models with respect to depth which were then associated to the synthetic receiver functions. This made it possible to explain the behavior of the wave and the medium through which they traveled. The main results obtained indicate that: (1) The lithosphere appears to be thin in its crustal part with a mean Moho depth of 28 km and S wave velocity of 3.7 km/s. (2) In its mantle part, the lithosphere is thick in nature having a thickness that varies between 42 km and 67.2 km. The greatest depth is noticed towards the center located around Garoua while the least depth corresponds to a location around Yagoua in the North. The Low velocity zone which makes it possible to determine the depth of the lithosphere was seen to have a thickness which varies between 42 km and 118.8 km. (3) The synthetic receiver functions associated to shear velocity models reveal that, on one hand the wave has really undergone a conversion and multiple conversions such that the existing Ps phase and subsequent reverberations PpPs and PpSs have mean times of 3.7 s, 11 s and 17.6 s respectively. On the other hand, they reveal an attenuation shown by the decrease in the amplitude of the aforementioned phases along a South-North direction in the Garoua rift.

Keywords

Teleseismic, Receiver Functions, Depth of Lithosphere, Low Velocity Zone, Garoua Rift Region

1. Introduction

The Garoua rift region is the continuation of the Northern section of Cameroon Volcanic Line and the part of the large Benue trough which, is situated between the latitude 8˚ and 11˚ North and longitudes 13˚ and 16˚ East. It is bounded to the west by the Federal Republic of Nigeria, to the North by the Mandara Mounts and to the south by the Adamawa plateau (**Figure 1**).

Structural and geological studies by [2] and [3] show that the Garoua basin is an E-W to N120 trending trough infilled by Middle to Upper Cretaceous marine sandstones. These sediments have also been described by [4] and [5]. The Garoua sandstone series overlap an approximately E-W trending trough called the Tcheboa trough, similar to the Figuil, Hama-koussou and Mayo-Oulo basins [6] [7]. The whole region of the Garoua basin presents outcrops of sandstone and intrusive granites, which form the basement complex below the sediments, and intrusive diorites along the Poli-Lere axis [8]. Some hypovolcanic dykes are also found within the Garoua sandstones. The basaltic lavas (**Figure 1**) found here are similar to those of the Cameroon Volcanic Line [9]. The basin is limited by normal faults which outcrop on its northern and southern borders [3] [8] [10].

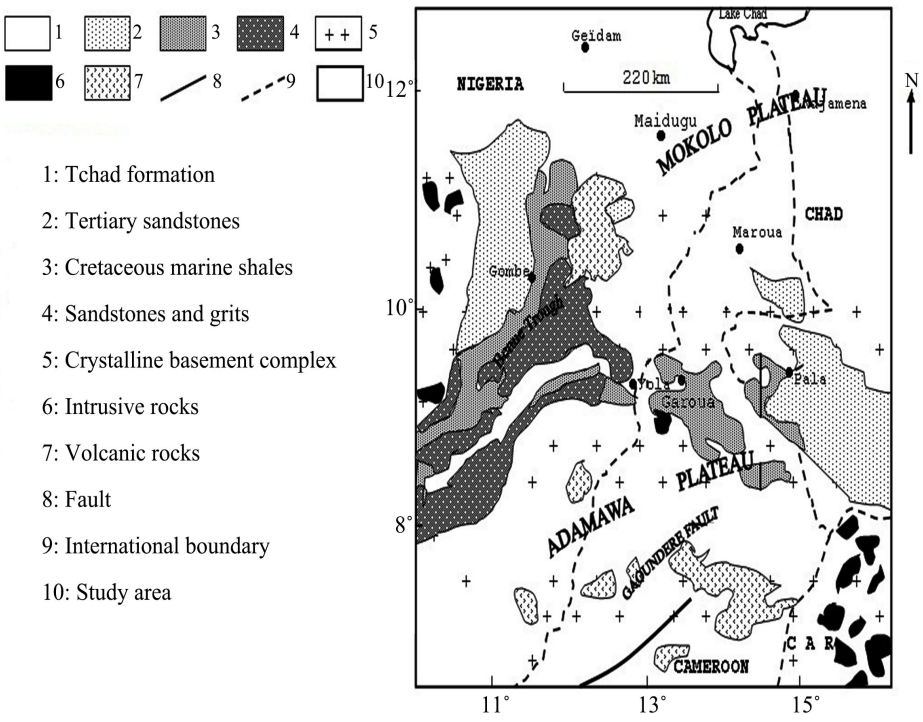

Figure 1. Simplify geological map of Garoua rift region (modified after [11]).

Some geophysical works have been carried out in the Garoua rift region and particularly in the Garoua basin area. The regional structural setting of the Garoua Basin is characterized by three major normal faults striking mainly in the NW-SE to NNE-SSW direction [12]. The continental crust underneath the basin (about 24 km) is thinner than the normal crust, but may be a little thicker to the east. This thinning of the crust is due to extensional regional stress and the uplift of the Asthenosphere is as a consequence and this result from an isostatic compensation. This leads to an average sedimentary pile thickness of about 6 km from results obtained by [11] and [12]. This thinning is probably due to the extensional process of basin formation in the Cretaceous. The Moho is found to be uplifted in the basin, and would be the result of this extension and the associated thermal and isostatic compensation. [13] reveal a crustal thinning in some parts of the Central African Shear Zone (CASZ) including the Garoua basin. Other gravity studies by [14] [15] and [16] suppose an uplifting of the upper mantle resulting in an abnormally thin continental crust. The continental crust is thinner below the trough and its associated basins (15 km to 24 km thick) than the normal 33 km [13] [17] and [18]. [19] used records of quarry blasts (active source seismic data) on a North-South profile across the Adamawa plateau performed a study of the crustal structure associated with the Adamawa plateau and the Garoua Rift. This study revealed a considerable thinning of the Crust when moving south of the Adamawa Plateau towards the Garoua Rift region. The Crust thins from 33 km south of the Adamawa Plateau to about 23 km at the Garoua rift region. The crustal thickness of 22 km obtained by [18] varies as a function of the density contrast between the lower crust and the upper mantle. Recently gravity data acquired from Earth Gravitational Model (EGM-2008) were analyzed by [20] to estimate the sedimentary thickness, extension and shape of the Garoua Basin, North Cameroon. Two dimensional (2-D) forward modeling of the gravity data using Grav2dc v2.06, which uses the Talwini's algorithm was conducted along three profiles oriented NE-SW, NNE-SSW and WNW-ESE to verify the lateral variations of the sediment pile beneath these profiles. Accordingly, Garoua is made up of alternating succession of horsts and grabens bounded to the north and south by normal faults infilled with sedimentary rocks underlain by a rifted basement. The gravity models suggest an average thickness of sediments of 9 km with a graben-shaped and extents over 80 km. [21] used the surface waves tomography to indicate that the mantle beneath the CVL is characterized by slow seismic wave velocity and the lithosphere-asthenosphere boundary is shallower than 100 km (~60 km). [22] from the receiver functions technic applied on the Raleigh waves have shown that, the crust is thin with the mean thickness of 25.5 km for an average crustal S-wave velocity of 3.4 km/s. [23] used body wave tomography to image the mantle seismic structure beneath Cameroon using data from the 2005-2007 CBSE network. They found that a continuous low velocity zone (δVs = −2% to −3%) underlies the entire CVL to a depth of at least 300 km and attributed this to a thermal anomaly of at least 280

K. [24] stacked the receiver functions using a 3-D velocity model, revealing Ps conversions from the mantle transition zone discontinuities at depths of ~410 and 660 km. Results yield a nearly uniform transition zone thickness (251 ± 10 km) that is similar to the global average, implying that any thermal anomalies in the upper mantle beneath the CVL do not extend as deep as the transition zone. [25] stacked receiver functions to study crustal structure using earthquakes recorded by the Cameroon Broadband Seismic Experiment. In regions of the CVL unaffected by the Cretaceous extension associated with the breakup of Gondwana (e.g. the Garoua rift), Vp/Vs ratios are markedly low (network average 1.74) compared to hot spots elsewhere, providing no evidence for either melt or cooled mafic crustal intrusions due to CVL magmatism. The character of P-to-S conversions from beneath the CVL also indicates that lower-crustal intrusions (often termed underplate) are not present beneath the region. Although the previous investigations of the lithosphere where done with artificial seismic sources which led to interpretations leaning on inappropriate velocity models [13] [17] [18] [19] or with potential methods [11] [14] [15] [16] [20] that present a low resolution power or studied the crust using active sources [19] on one hand. The other investigations provided important measurements and high-resolution image of the lithospheric structure in Cameroon using the stack method of the receiver functions resulting from the surface waves [25] or focused mainly on the mantle [23] and [24] in other hand**.** In this present work, we will come out a 1-D velocity model of S-waves of the lithosphere from the inversion of the P-waves receiver functions having the properties to propagate beyond the crust. This shear wave velocity models could also provide information regarding its structure.

2. Data and Methodology

2.1. Data

The data used in this study consist of the earthquakes recorded by 32 portable broad-band seismometers installed across the country between January 2005 and February 2007 by the Cameroon Broadband Seismic Experiment. The data were collected by a team of geoscientist from the University of Yaounde I and the Institute of Geological and Mining Research-Cameroon in partnership with researchers from Pen State University in the United State of America. The seismic network comprised 5 broadband stations (**Table 1**) equipped with a broad-band seismometer (Guralp CMG-3T or Streckeisen STS-2), a 24-bit Reftek digitizer and a GPS (Global Positioning System) clock (**Figure 2**).

Data were recorded continuously at a rate of 40 samples per second. In the study area, two stations (red color) were installed in 2005 January and operated during 2 years; the remaining four stations (yellow color) operated only during the second year of the experiment. The station spacing during the second year (2006) of operation was about 50 to 150 km [26]. From the earthquake data recorded, the teleseismic events that occurred at epicentral distances between 30˚

and 95˚ with magnitudes $M_B \geq 5.5$. have been selected (Table 2) to construct the S-wave velocity models beneath the different stations of the Garoua rift by application of the P-wave receiver functions technique.

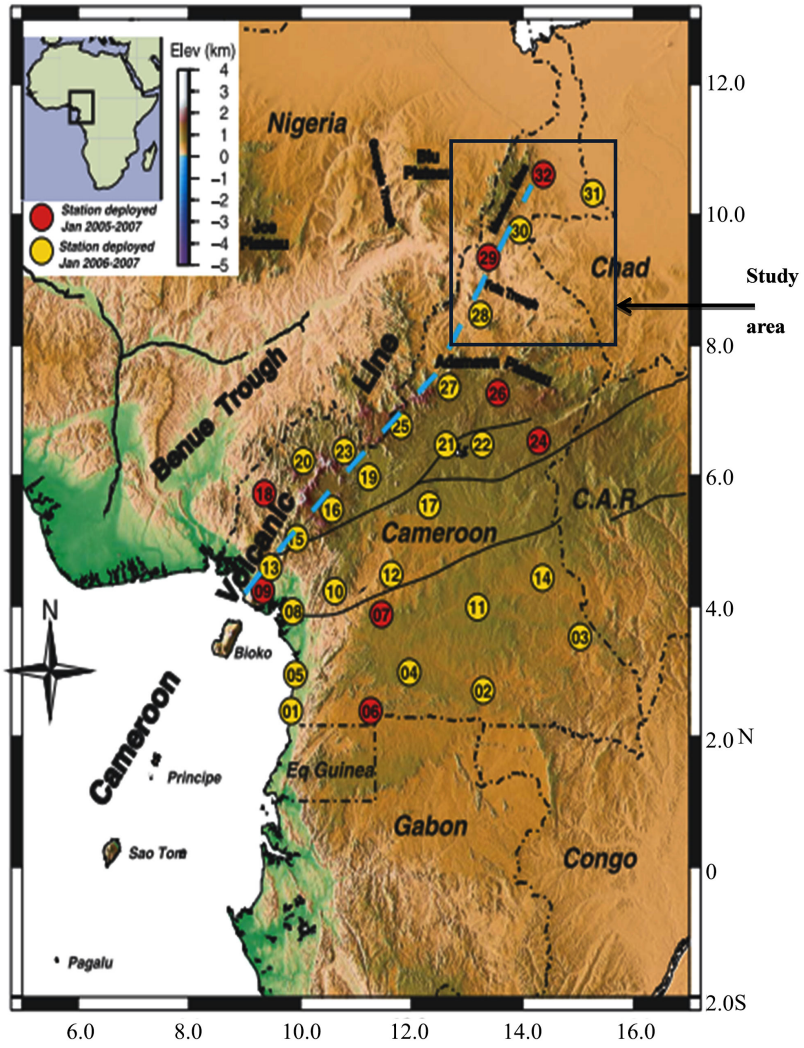

Figure 2. Colour elevation map showing seismic station locations and shear zones. The circled numbers refer to station codes, for example, 28 refers to station CM28 and the blue rectangle represents the study area (Modified after [22]).

Table 1. Characteristics of the different stations which recorded the teleseismic events.

Station code	Town	Installation year	Latitude (˚)	Longitude (˚)	Elevation (km)
CM28	Poli	2006	9:07	8.45	0.48
CM29	Garoua	2005	10:42	9.35	0.26
CM30	Figuil	2006	10:42	9.35	0.26
CM31	Yagoua	2006	9:24	9.75	0.29
CM32	Maroua	2005	10:05	10.33	0.33

Table 2. Events with magnitude $M_B \geq 5.5$ used for the study.

Event date mm/dd/yy	Event time h:min:s	Latitude (˚)	Longitude (˚)	Depth (km)	Magnitude	Epicentral distance (˚)
10/20/05	21:40:04:01	38.152	26.751	10	5.5	33.1
12/05/05	12:19:56:06	−6.224	29.83	22	6.4	21
12/09/05	23:30:23:09	−6.176	29.709	10	5.5	20.9
01/08/06	11:34:55:06	36.311	23.212	66	6.5	30.2
02/22/06	22:19:07:01	−21.324	33.583	11	6.5	34.5
03/15/06	14:19:48:07	−21.136	33.719	10	6.5	33.9
09/17/06	07:30:11:00	−17.694	41.827	10	5.5	37
09/24/06	22:56:21:07	−17.737	41.814	10	5.6	37.5

2.2. Methodology

2.2.1. Computation of the Receiver Functions

The treatment of the teleseismic is based on the receiver function method. The receiver functions are time series, computed from three component seismograms, which show the relative response of earth structure near the receiver. They are generated by the time domain iterative deconvolution method of [1], applied to seismograms constituted to the North, East and Vertical components which are then rotated into radial, transverse and vertical components respectively which can be used to image velocity contrasts across discontinuities.

The computation of the receiver functions began with a visual inspection in order to confirm the presence of the signal. Then after, if the wave forms which appear on the three components of the seismogram can be identified (**Figure 3**), then the selected waveforms were decimated to 10 samples per second, windowed between 20 s and 140 s after the leading P arrival, de-trended, tapered and high pass filtered above 50 s to remove low-frequency, instrumental noise.

Radial and transverse receiver functions were then obtained from the filtered traces by rotating the original horizontal components around the corresponding vertical component into the great circle path (**Figure 4**), and deconvolving the vertical component from the radial component through the iterative time domain déconvolution procedure of [1], with 200 iterations using the Gaussian a = 2.5 corresponding at to the frequency 1.2 Hz because, it helps to discriminate gradational transitions from sharp discontinuities in the receiver structure under the station [27].

To complete the estimation of the receiver functions, the recovery percentage of the original radial waveform was evaluated from the rms misfit between the original radial waveform and the convolution of the radial receiver function with the original vertical component [26]. Events that were recovered to less than 85 percent were rejected. The remaining waveforms were visually inspected for coherence and stability (**Figure 5**).

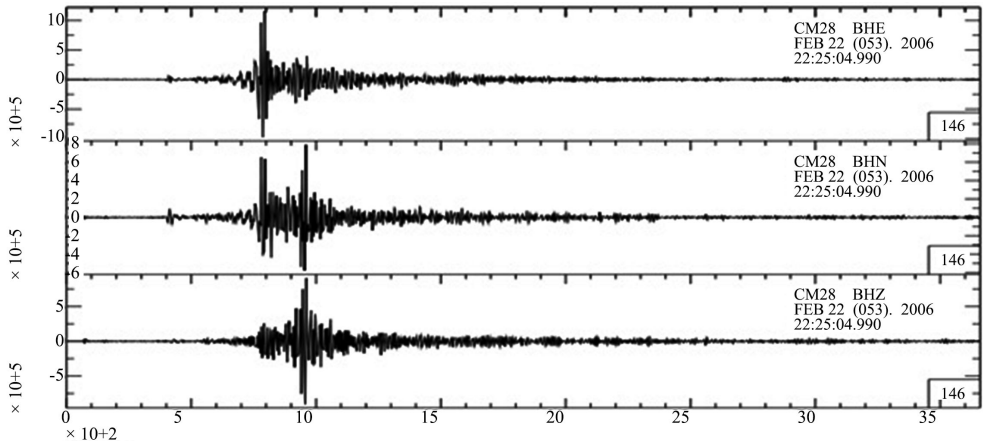

Figure 3. Example of the good seismogram at the station CM28.

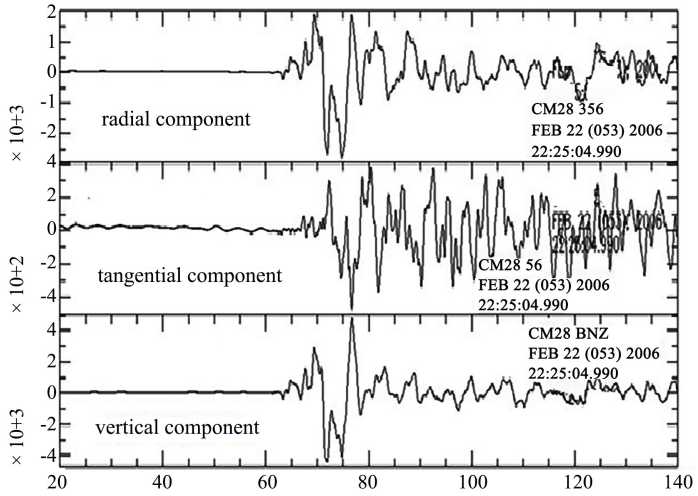

Figure 4. Example of seismogram windowed, filtredand rotated at station CM28.

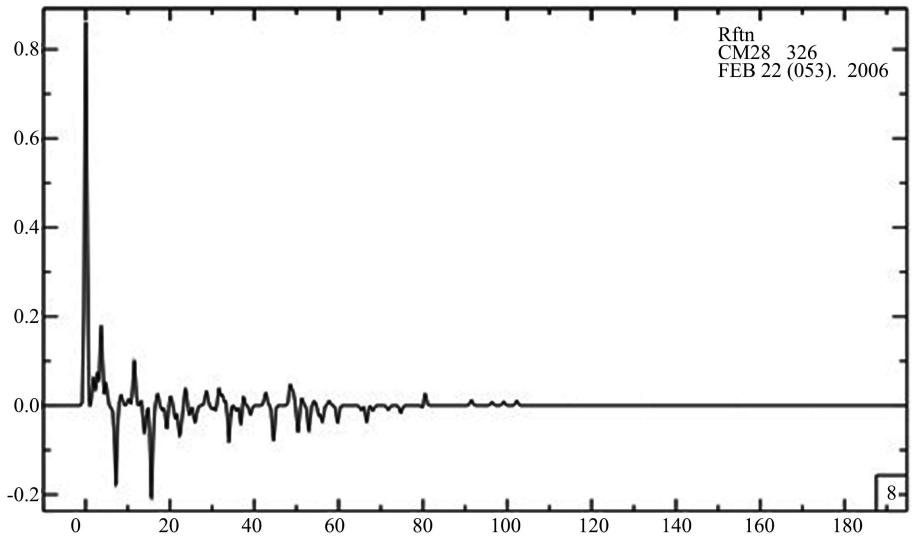

Figure 5. Example of the good receiver function computed at station CM28. The horizontal axis represents the time in second (s) while the vertical axis represents the amplitude of P-wave in millimeter (mm).

2.2.2. Inversion of the Receiver Functions

In this work, the P-waves were inverted to obtain an S-wave velocity model that produces an estimation of shear velocity structure beneath a given seismic station. There is no guarantee that a unique inversion result will be obtained, as the method seeks to minimize the differences between observed and synthetic (or predicted) receiver functions. The inversion was performed using the Rftn96 program developed by [28] and [29]. The method is based on a linearized inversion procedure that minimizes a weighted combination of least squares norms for each data set, a model roughness norm and a vector-difference norm between inverted and pre-set model parameters. The velocity models obtained are consequently a compromise between fitting the observations, model simplicity and a priori constraints. The velocity models are associated at the synthetic receiver functions. Synthetic seismograms are generated using a fast three dimension ray tracing scheme based on [30]. The earth model is parameterized in terms of constant velocity, planar, dipping layers over half-space. The P and S wave velocities, density, strike and dip angles, and thickness are specified for each layer in the model. Synthetic vertical radial and transverse seismograms are generated by specifying a back azimuth and ray parameter for the plan of P-wave incident at the base of the model. The starting model used in this inversion consisted of an isotropic medium of constant velocity layers that increase in thickness with depth. The thicknesses of the first, second and third layers are, respectively, 45 km, 90 km and 80 km, while the thickness increases by steeps of 5 km between 0 and 45 km depth, by 10 km between 45 and 135 km and by 20 km below the depth of 135 km. Also the linear shear wave velocity increase in the crust from 3.2 to 4.0 km/s and from 4 to 4.7 km/s in the lithospheric mantle overlying a flattened PREM (Preliminary Reference Earth Model) model [31] for the mantle. Having determined path lengths for each layer, the arrival time for each phase can be calculated. In addition, to the P-arrival and Ps conversions, the synthetic seismogram may include the free-surface multiples associated with each interface.

3. Results and Discussions

3.1. Results

The different results coming from the inversion of the receiver function computed for the five seismic stations studied are shown in **Figure 6** (a, b, c, d and e).

The different interpretations are presented in **Table 3** and **Table 4**.

Regrouping the types and times of different conversions and multiple conversions coming from the curves of synthetic receiver functions from the Garoua rift stations, **Table 3** shows that, a good agreement exists between the curves, and the wave has really undergone conversion. The particularity in this area come from the station located in Garoua where, attenuation of the wave starts being observed by the variation of the conversion and the subsequent reverbera-

tion time and the weakness in the amplitude of the phases which, finally disappear at the station CM32 situated at Maroua. This can be due to inelastic material behavior or internal friction during wave propagation and expresses the heterogeneous character of the crust and anisotropy within the sub-crustal lithosphere of this zone.

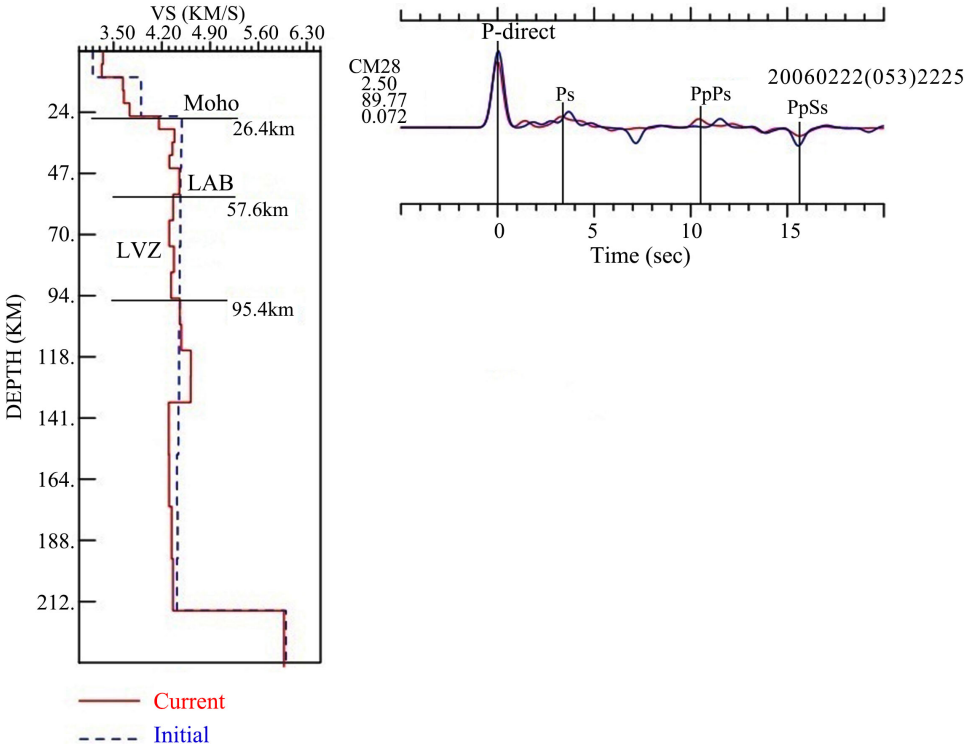

(a)

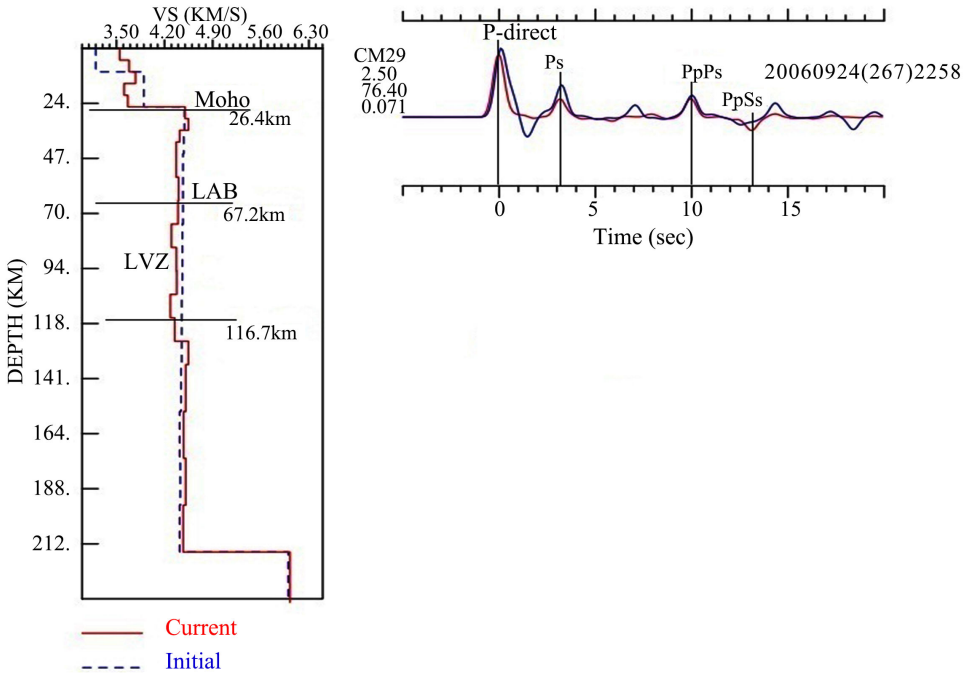

(b)

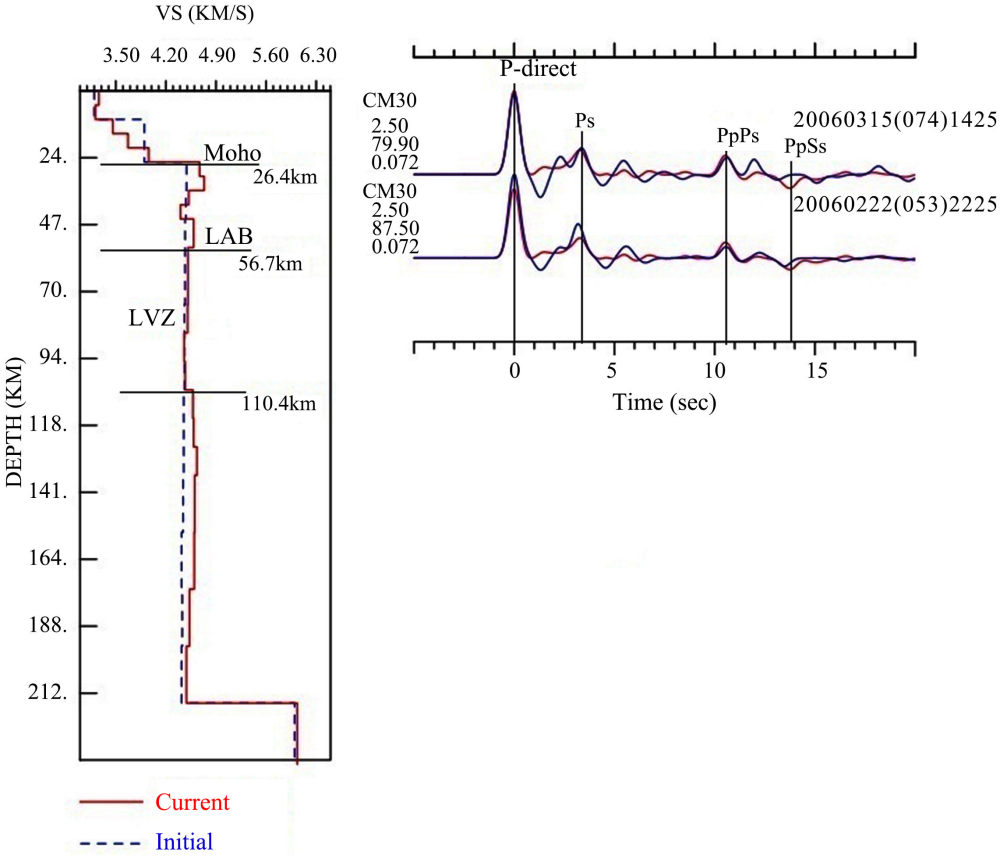
VS (KM/S)
3.50 4.20 4.90 5.60 6.30
DEPTH (KM)
24.
47.
70.
94.
118.
141.
164.
188.
212.
Moho
26.4km
LAB
56.7km
LVZ
110.4km
Current
Initial
P-direct
CM30
2.50
79.90
0.072
Ps
PpPs
PpSs
20060315(074)1425
CM30
2.50
87.50
0.072
20060222(053)2225
0
5
10
15
Time (sec)

(c)

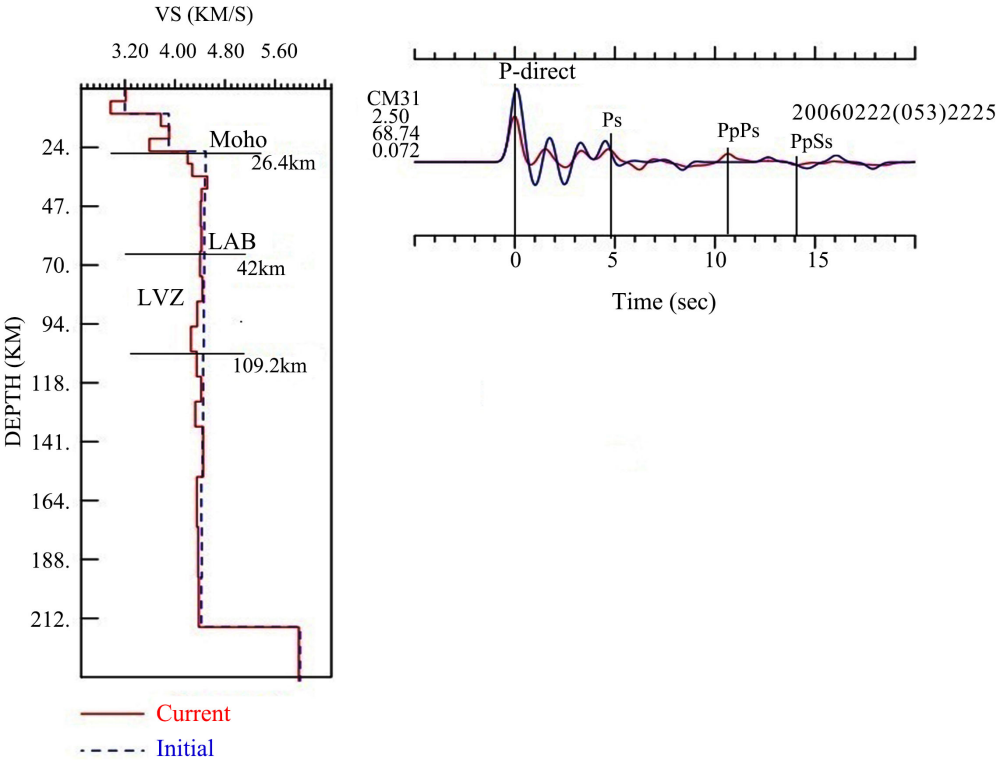
VS (KM/S)
3.20 4.00 4.80 5.60
DEPTH (KM)
24.
47.
70.
94.
118.
141.
164.
188.
212.
Moho
26.4km
LAB
42km
LVZ
109.2km
Current
Initial
P-direct
CM31
2.50
68.74
0.072
Ps
PpPs
PpSs
20060222(053)2225
0
5
10
15
Time (sec)

(d)

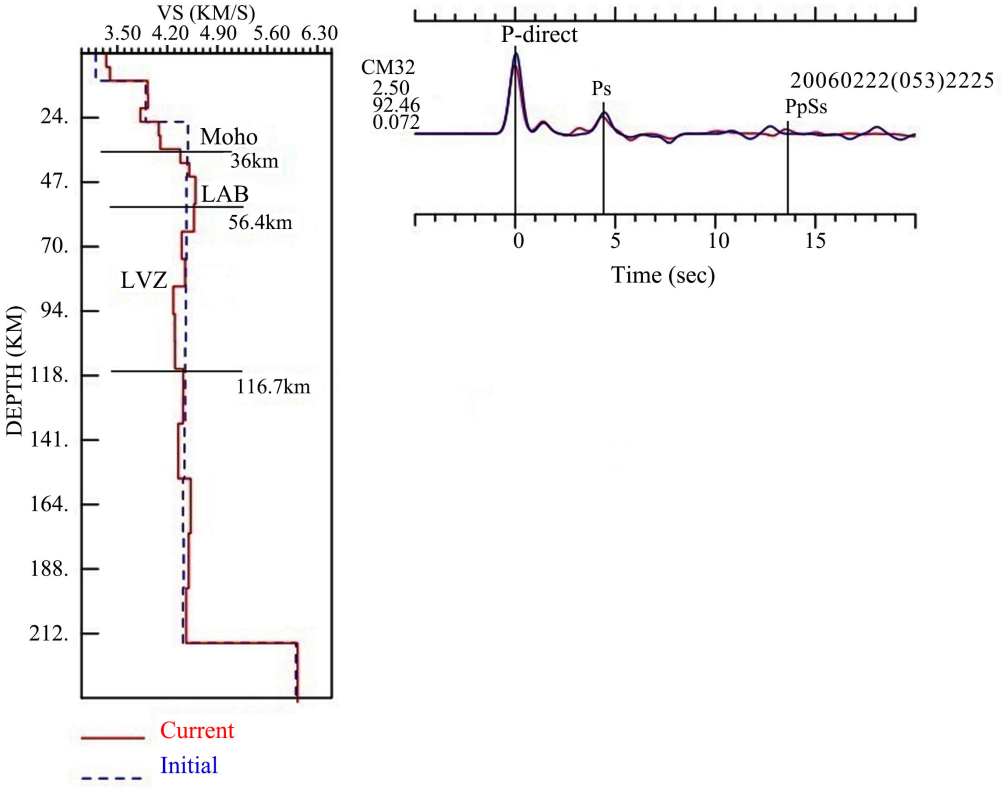

(e)

Figure 6. (a), (b), (c), (d), (e): Shear velocity profiles for Garoua rift region (Cameroon Volcanic Line). Moho: Mohovicic discontinuity; LAB: Lithosphere-Asthenosphere Boundary; LVZ: Low Velocity Zone.

Table 3. Interpretation of the synthetic receiver functions.

Station	Localities	Percent of Signal Power Fit	t_{Ps} (s)	t_{PpPs} (s)	t_{PpSs} (s)
CM28	Poli	89.77	3.2	10.5	15.5
CM29	Garoua	76.40	3.1	9.9	13
CM30	Figuil	79.90; 87.50	3.2	10.5	13.5
CM31	Yagoua	68.74	4.5	10.7	18.2
CM32	Maroua	92.46	4.6	13.5	

Table 4. Interpretation of the S-wave velocity profile.

Station	Localities	Average crustal Vs (km/s)	Moho depth (km)	Thickness interval of LVZ (km)	Average lithospheric Vs (km/s)	Average depth of lithosphere (km)	Average lithospheric mantle thickness
CM28	Poli	3.7	26.4	57.6 < LVZ < 95.4	3.9	57.6	31.2
CM29	Garoua	4	26.4	67.2 < LVZ < 116.7	4	67.2	40.8
CM30	Figuil	4	26.4	56.4 < LVZ < 110.4	4	56.4	30
CM31	Yagoua	3.6	26.4	42 < LVZ < 109.2	3.7	42	15.6
CM32	Maroua	3.8	36	56.4 < LVZ < 116.7	3.9	56.4	20.4

The velocity models obtained by inversion of the receiver function followed by the different values coming from Table 4 for the Garoua rift sector allow us to say that the crust is thin with a mean S-waves velocity of the of 3.8 km/s and the mean thickness of 28 km except at Maroua where it is 36 km. While the lithospheric mantle has a mean S-wave velocity of 3.9 km/s and its thickness varies between 15.6 km and 40.8 km. The low velocity zone is located between 42 km and 116.7 km of depth and the discontinuities are situated at 26.4 km of depth for the Moho except for the Maroua station where it is located at 36 km and between 42 km and 67.2 km for the Lithosphere-Asthenosphere Boundary (LAB).

3.2. Discussions

3.2.1. Comparison of the Synthetic Receiver Functions Results by Station and with Previous Estimates

Observing the different times of Ps phase and subsequent reverberations (PpPs and PpSs) obtained at each station (Table 4), in addition to their different amplitudes, one notes respectively an increase and a decrease from the station CM28 to station CM32. This leads to the deduction that the wave is converted and attenuates according along the South-North direction of the Garoua rift. Previous estimates of the conversion time in the Garoua rift region have been carried out by [25] and the comparison with the new estimates is shown in Table 5.

Comparing the values of this study with those obtained by [25], one observes that, there is slight difference with respect to the different conversions. This difference can be explained by the method used in computing the same data.

3.2.2. Comparison of the Shear Wave Velocity Model Results by Locality and with Previous Estimates

a) Comparison of the shear wave velocity model by locality

The shear velocity models obtained in each locality present a thin behavior in the crustal part of lithosphere. This behavior is supported by [11] [19] and [22]. The mantle part of the lithosphere is thick, with the depth of the lithosphere that varies beneath the Garoua rift region between 42 km and 67.2 km (Figure 7). It comes out again that, the deepest part of the lithosphere is located in the center of the rift (Garoua) and the section having the least depth is located at the North, more precisely in the Yagoua locality (Figure 7).

b) Comparison of the shear velocity model results with previous estimates

Many studies have already been carried out on this behavior and the depth in this area by some geoscientist like [11] [22]. Comparisons with previous estimates of the shear wave velocities as well as with the thickness of the crust and lithosphere are done in Table 6.

Table 6 shows that, estimates of average S-wave velocity (Vs) in the crust are in very good agreement with the previous estimates [22] based on the same seismic data in the Garoua rift region. The main difference between this study and

previous studies is at the level of the depth of the Moho. This difference comes from the type of data and method used (active data, surface data and geopotential method). On the depth of the lithosphere, no evaluation has been done till date but for one study on the Cameroon volcanic line (covering the Garoua rift region) which situated the depth of the lithosphere to approximately to 60 km [21]. The lithospheric depth has been determined by the existing of the low velocity zone started at the same depth. This low velocity zone has been confirmed by [23] that found a low-velocity anomaly beneath the CVL extending to at least 300 km plausibly related to a thermal perturbation.

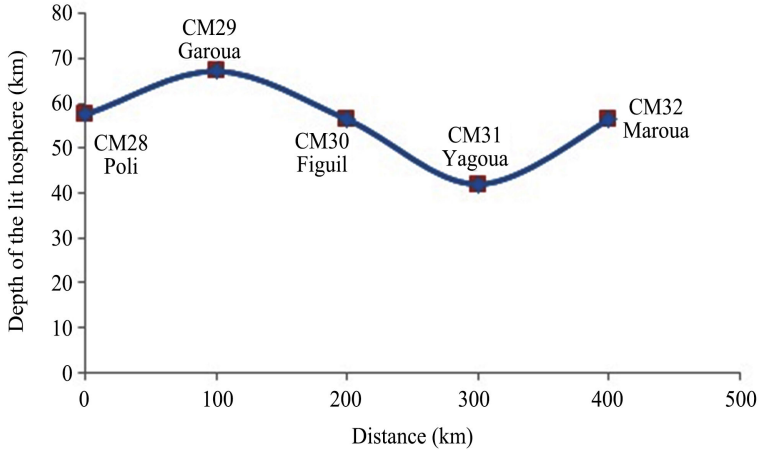

Figure 7. Variation of the depth of lithosphere beneath the Garoua rift region.

Table 5. Comparison of arrival times of the different Ps phases and the subsequent reverberants with those of previous results.

Region	This study by inversion of the receiver functions			Other study by stacking of the receiver function)			Reference
Garoua rift	t_{Ps} (s)	t_{PpsP} (s)	t_{PpSs} (s)	t_{Ps} (s)	t_{PpsP} (s)	t_{PpSs} (s)	[25]
	3.7	11	17.6	3.2	10.5	14	

Table 6. Comparing shear velocity model with previous estimates in the Garoua rift.

Type of result	This study	Others studies	Types of data used	References
Average Vs of crustal (km/s)	3.7	3.7	Seismic earthquakes	[22]
Average depth moho (km)	28	23	Seismic explosion	[19]
		24	Gravity	[11]
		25.5	Seismic earthquakes	[22]
Average depth of Lithosphere (km)	between 42 and 67.2			

4. Conclusion

Iterative deconvolution has been applied on teleseismic events recorded between 2005 and 2007 to obtain the receiver functions. These receiver functions have been inverted to study the lithosphere-Asthenosphere Boundary beneath the Garoua rift region. It was found from this study that: 1) The synthetic receiver functions associated to the shear velocity model obtained show the existence of a Ps phase and subsequence reverberations PpPs and PpSs at 3.7 s, 11 s and 17.6 s respectively. The amplitude of the subsequent reverberations decrease and finally disappears at station CM32 passing through stations CM29, CM30 and CM31. The existence of the different phases and the low amplitude of the different phases lead to the deduction that, the wave has really undergone conversion and attenuation along the South-North direction of the Garoua rift region. 2) The lithosphere has a thin nature in its crustal part with the Moho located at a mean depth of 28 km according to the S-wave velocity of 3.7 km/s. The lithosphere is thick in its mantle part with its limit depth that varies between 42 km and 67.2 km of depth. The deepest part of the lithosphere in the Garoua rift region is situated towards the center that is located around Garoua while the least depth is situated around Yagoua to the North due to the existence of the first low velocity zone (LVZ) in the upper mantle whose thickness also varies between 42 km and 116.7 km. The different results obtained in this study have been compared to previous results existing in this region. Some similarities have been noticed in some cases like in the velocity of the S waves in the crust and the time of PpPs phase. The main differences with other results were noticed in the times of Ps and PpSs phases and Moho depth. These differences can be justified by the type of method or data used. In this study, though studies have been carried out on the boundary and the behavior of the lithosphere, it will never the less be important to carry out a study on the origin of the variation noticed in the depth of the lithosphere.

Acknowledgements

We wish to express our gratitude to the team and sponsor of the Cameroon broadband seismic experiment and particularly to Dr Tokam Kamga Alain who provide the database and the software.

Conflicts of Interest

The authors declare no conflicts of interest regarding the publication of this paper.

References

[1] Ligorría, J.P. and Ammon, C.J. (1999) Iterative Deconvolution and Receiver Function Estimation. *Bulletin of the Seismological Society of America*, **89**, 1395-1400.

[2] Elf-Serepca (1981) Service d'Exploration Carte Geologique du Bassin de Garoua.

[3] Regnoult, J.M. (1986) Synthese Géologique du Cameroun. Direction des Mines et

de la G éologie du Cameroun, Yaounde, 119 p.

[4] Roch, E., Jeremine, E. and Faure Muret, A. (1953) Itineraires géologiques dans le Nord Cameroun et le SW du territoire du Tchad Bull. Service Mines no 1.

[5] Schwoerer, P. (1965) Carte Géologique de Reconnaissance à L'Echelle 1/500000 Notice Explicative sur la Carte Garoua-Est. Direction des Mines et de la Géologie du Cameroun, Yaoundé.

[6] Ndjeng E. (1994) Pole des caractères exoscopiques des grains de quartz des grès de Garoua sur l'interprétation du paloéoenvironnement du bassin de la Bénoué du Crétacé superieur. *Ann. Fac. Sci HS Chim. Sci. Nat.*, 73-82.

[7] Ndjeng, E. and Brunet, M. (1998) Modèle d'évolution géodynamique de deux bassins de l'Hauterivien-Barrémien du Nord-Cameroun: Les bassins de Babouri-Figuil et du Mayo Oulo-Leré (Fossé de la Benoué). Géoscience au Cameroun, 163-165.

[8] Poudjom Djomani, Y.H., Diament, M. and Albouy, Y. (1992) Mechanical Behaviour of the Lithosphere beneath the Adamawa Uplift (Cameroon, West Africa) Based on Gravity Data. *Journal of African Earth Sciences*, **15**, 81-90. https://doi.org/10.1016/0899-5362(92)90009-2

[9] Ngounouno, I., Nkoumbou, C. and Loule, J.P. (1997) Relation entre l'évolution tectono-sédimentaire et le magmatisme du fossé de Garoua (Nord Cameroun). *Africa Geoscience Review*, **4**, 451-460.

[10] Poudjom Djomani, Y.H. and Diament, M. (1992) Modélisation 2-D d'un profil gravimétrique au Cameroun. Stage de fin de première année de Magistère IPGP.

[11] Kamguia, J., Manguelle-Dicoum, E., Tabod, C.T. and Tadjou, J.M. (2005) Geological Models Deduced from Gravity Data in the Garoua Basin, Cameroon. *Journal of Geophysics and Engineering*, **2**, 147-152. https://doi.org/10.1088/1742-2132/2/2/009

[12] Mouzong, M.P., Kamguia, J., Nguiya, S., Shandini, Y. and Manguelle-Dicoum, E. (2014) Geometrical and Structural Characterization of Garoua Sedimentary Basin, Benue Trough, North Cameroon, Using Gravity Data. *Journal of Biology and Earth Sciences*, **4**, E25-E33.

[13] Dorbath, C., Fairhead, J.D. and Stuart, G.W. (1986) A Teleseismic Delay Time Study across the Central African Shear Zone in the Adamawa Region of Cameroon. *Geophysical Journal of the Royal Astronomical Society*, **86**, 751-766. https://doi.org/10.1111/j.1365-246X.1986.tb00658.x

[14] Poudjom Djomani, Y.H. (1993) Apport de la gravimétrie à l'étude de la lithosphère continentale et implications géodynamiques. Etude d'un bombement intraplaque: Le massif de l'Adamaoua (Cameroun). Thèse de Doctorat, Université de Paris-Sud, Orsay.

[15] Poudjom Djomani, Y.H., Diament, M. and Wilson, M. (1997) Lithospheric Structure across the Adamawa Plateau (Cameroon) from Gravity Studies. *Tectonophysics*, **273**, 317-327. https://doi.org/10.1016/S0040-1951(96)00280-6

[16] Noutchogwe, T.C.B. (2004) Apport de la gravimétrie à l'étude de la bordure méridionale du plateau de l'Adamaoua (Cameroun). Thèse de Doctorat 3è cycle Université de Yaoundé I, Cameroon.

[17] Cratchley, C.R., Louis, P. and Ajakaiye, D.E. (1984) Geophysical and Geological Evidence for the Benue-Chad Basin Cretaceous Rift Valley System and Its Tectonic Implications. *Journal of African Earth Sciences*, **2**, 141-150. https://doi.org/10.1016/S0731-7247(84)80008-7

[18] Benkelil, J. (1988) The Origin and Evolution of the Cretaceous Benue Trough (Nigeria). *Journal of African Earth Sciences*, **8**, 251-282.

https://doi.org/10.1016/S0899-5362(89)80028-4

[19] Stuart, G.W., Fairhead, J.D., Dorbath, L. and Dorbath, C. (1985) A Seismic Refraction Study of the Crustal Structure Associated with the Adamawa Plateau and Garoua Rift, Cameroon, West Africa. *Geophysical Journal of the Royal Astronomical Society*, **81**, 1-12. https://doi.org/10.1111/j.1365-246X.1985.tb01346.x

[20] Kuisseu, T.S., Djieto, L.A.E., Agyingi, C.M., Shandini, Y., Mbohlieu, T.Y. and Ndifor, B.D. (2018) Geometrical Configuration of the Garoua Basin, North Cameroon as Deduced from Earth Gravitational Model (EGM-2008). *Anuario do Instituto de Geociencias*, **41**, 167-176. https://doi.org/10.11137/2018_2_167_176

[21] Fishwick, S. (2010) Surface Wave Tomography: Imaging of the Lithosphere-Asthenosphere Boundary beneath Central and Southern Africa. *Lithos*, **120**, 63-73. https://doi.org/10.1016/j.lithos.2010.05.011

[22] Tokam, A., Tabod, C.T., Nyblade, A.A. and Julià, J. (2010) Structure of the Crust beneath Cameroon, West Africa, from the Joint Inversion of Rayleigh Wave Group Velocities and Receiver Functions. *Geophysical Journal International*, **183**, 1061-1076. https://doi.org/10.1111/j.1365-246X.2010.04776.x

[23] Reusch, A.M., Nyblade, A.A., Wiens, D.A., Shore, P.J., Ateba, B., Tabod, C. and Nnange, J.M. (2010) Upper Mantle Structure beneath Cameron from Body Wave Tomography and the Origin of the Cameroon Volcanic Line. *Geochemistry, Geophysics, Geosystems*, **11**, Q10W07. https://doi.org/10.1029/2010GC003200

[24] Reusch, A.M., Nyblade, A.A., Tibi, R., Wiens, D.A., Shore, P.J., Bekoa, A., Tabod, C.T. and Nnange, J.M. (2011) Mantle Transition Zone Thickness beneath Cameroon: Evidence for an Upper Mantle Origin for the Cameroon Volcanic Line. *Geophysical Journal International*, **187**, 1146-1150. https://doi.org/10.1111/j.1365-246X.2011.05239.x

[25] Gallacher, R.J. and Bastow, I. (2012) The Development of Magmatism along the Cameroon Volcanic Line: Evidence from Teleseismic Receiver Functions. *Tectonics*, **31**, TC3018. https://doi.org/10.1029/2011TC003028

[26] Pokam, K.S.H., Tabod, C.T., Ndikum, E.N., Tokam, K.A.P. and Gounou, P.B.P. (2018) Thickness Variations in the Lithospheric Mantle and the Low Velocity Zone of the Adamawa Plateau (Cameroon) from Teleseismic Receiver Functions. *Open Journal of Geology*, **8**, 529-542. https://doi.org/10.4236/ojg.2018.86032

[27] Julià, J. (2007) Constraining Velocity and Density Contrasts across the Crust: Mantle Boundary with Receiver Function Amplitudes. *Geophysical Journal International*, **171**, 286-301. https://doi.org/10.1111/j.1365-2966.2007.03502.x

[28] Julià, J., Ammon, C.J., Herrmann, R.B. and Correig, A.M. (2000) Joint Inversion of Receiver Function and Surface Wave Dispersion Observations. *Geophysical Journal International*, **143**, 99-112. https://doi.org/10.1046/j.1365-246x.2000.00217.x

[29] Julià, J., Ammon, C.J. and Herrmann, R.B. (2003) Lithospheric Structure of the Arabian Shield from the Joint Inversion of Receiver Functions and Surface Wave Group Velocities. *Tectonophysics*, **371**, 1-21. https://doi.org/10.1016/S0040-1951(03)00196-3

[30] Langston, C.A. (1977) Corvallis, Oregon, Crustal and Upper Mantle Structure from Teleseismic P and S Waves. *Bulletin of the Seismological Society of America*, **67**, 713-724.

[31] Dziewonski, A.M. and Anderson, D.L. (1981) Preliminary Reference Earth Model. *Physics of the Earth and Planetary Interiors*, **25**, 297-356. https://doi.org/10.1016/0031-9201(81)90046-7

Physics of the Earth and Planetary Interiors 294 (2019) 106293

Contents lists available at ScienceDirect

Physics of the Earth and Planetary Interiors

journal homepage: www.elsevier.com/locate/pepi

Voxel solution and 3D sub-surface imaging in the Douala sedimentary sub-basin (Cameroon)

Eric N. Ndikum[a,b,d,*], J. Victor Kenfack[f], F. Koumetio[c], Serge H. Pokam Kengni[a,e], Charles T. Tabod[a,e]

[a] Department of Physics, University of Yaoundé 1, Yaoundé, Cameroon
[b] Department of Fundamental Sciences, Higher Technical Teacher Training College (HTTTC) Bambili, The University of Bamenda, Cameroon
[c] Department of Physics, Faculty of Science, University of Dschang, PO Box 67, Cameroon
[d] Department of Physics, HTTC Bambili, The University of Bamenda, Cameroon
[e] Department of Physics, Faculty of Science, The University of Bamenda, Cameroon
[f] Department of Earth Science, Faculty of Science, University of Dschang, PO Box 67, Cameroon

ARTICLE INFO

Keywords:
Douala sub-basin
Bouguer anomaly
Residual anomaly
Intrusive body
3D surface-oriented model
3D voxel solution

ABSTRACT

Gravity data consisting of a total of 128 data points located between latitudes 3° 21′N and 4° 9′ N and longitudes 8° 27′ E and 9° 16′ E have been computed for Bouguer and residual anomaly maps in this study. From the plots of these maps which are characterized by very high positive ring shaped contours towards the centre, which are suggestive of a subsurface intrusive body, three anomaly zones as well as two minor peaks were identified. The maps were also characterized by W-E alignment of contours to the N and S as well as approximately NNW-SSE alignments to the E and to some extent, the W of the study area. A layered earth model which constitutes a depth model built using the geosoft montaj extension, GM-SYS 3D, was used to provide a surface-oriented model for this intrusive body. Using constant layers added to a 3D model at depths of 5 km, 10 km, 15 km, 20 km, 25 km, 30 km, 33 km, 35 km and 39 km; each in the absence of the others, forward calculations were employed to calculate the density contrast of each layer while their densities were recalculated using constant density inversion. Structural inversion of each of these layers then generated their surface-oriented models. The optimum inverse model for the intrusive body was obtained at a depth of about 33 km. The model has a surface and surroundings with a density of about 2.5 g/cm^3 which corresponds to that of sedimentary basins. It also presents an intrusive body with density of about 2.77 g/cm^3 located at a depth of about 6.1 km with its bottom located at about 33 km giving an average vertical height of about 26.9 km. This 3D relief sub-surface model was used to define the geometry of the starting model for 3D data voxels to generate the block structure of the intrusive body. Applying the basic statistical kriging algorithm, the 3D voxel solution of the intrusive body underneath this study area as well as its corresponding calculated maps were generated. This solution is similar in features to that of the surface-oriented solution and presents a block structure of the intrusive body with a major peak at a depth of about 6.2 km and having a relatively sharp sloping boundary towards its NE edge and gradual sloping edges towards its NW, W and E limits. Its density of 2.77 g/cm^3 is further confirmation to the fact that this body is of igneous origin. This model however shows evidence that this block extends further south beyond this study area and consequently requires more data in this direction to image it fully. These results from the 3D surface-oriented solution and the 3D voxel solution are in good agreement with previous results from 2.5D studies in this very area of study.

1. Introduction

The Douala sedimentary sub-basin being one of the basins located in the gulf of Guinea constitutes a region of interest due to both its oil production activities and its rich geologic potentials. Very few published results from geophysical research in this basin are available for public consultation. Of these research works, a handful of them have made use of gravity data. Koumetio et al. (Koumetio et al., 2009) carried out 2.5D gravity modeling along Bouguer gravity profiles to highlight two major structures in the southern part of the Douala

* Corresponding author at: Department of Physics, University of Yaoundé 1, Yaoundé, Cameroon.
E-mail address: ndikumeric@yahoo.com (E.N. Ndikum).

https://doi.org/10.1016/j.pepi.2019.106293
Received 6 February 2019; Received in revised form 18 July 2019; Accepted 19 July 2019
Available online 22 July 2019
0031-9201/

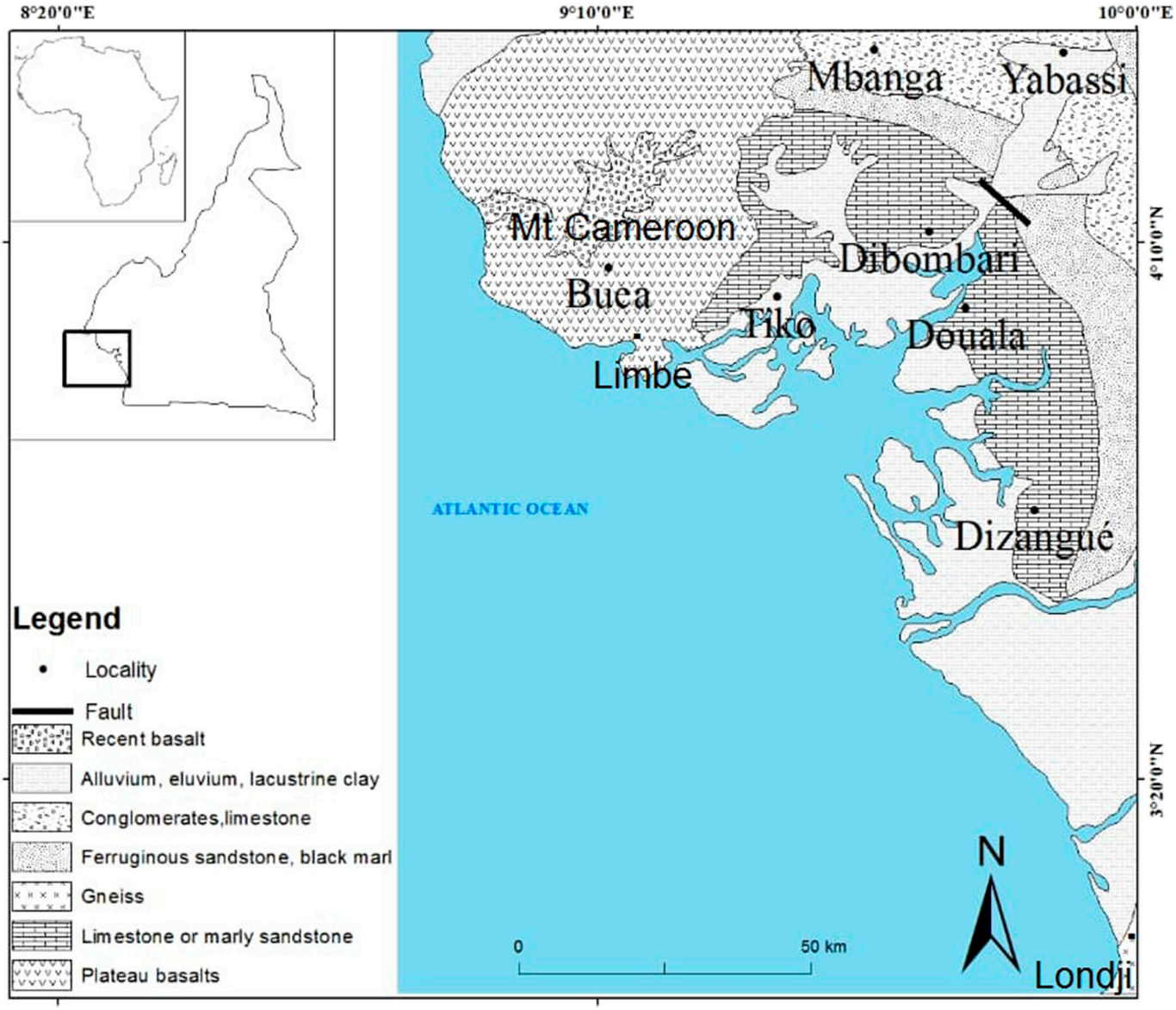

Fig. 1. Geologic map of study area (modified from (Dumort, 1968))

sedimentary sub-basin; a half-dome of mantle material explained by isostatic compensation and a pillar of high density rocks probably representing an upper mantle intrusion down to a depth of about 14 km. Ndikum et al. (Ndikum et al., 2014) employed upward continuation and polynomial separation methods, spectral analysis, the ideal body theory, the multi-scale horizontal derivative of the vertical derivative (MSHDVD) method and 2.5D modeling along a NW-SE profile to indicate the presence of an intrusive igneous block with a density of 2.77 g/cm^3 at a depth of about 5.9 km in the NW portion of the Douala basin. By carrying out 2.5D gravity modeling along a second profile oriented WWS-EEN, Ndikum et al. (Ndikum et al., 2017) went further to highlight the presence of two major blocks; an intrusive body at a depth of about 4.25 km and a pillar of igneous material at a depth of about10.8 km, both having a density of about 2.77 g/cm^3. In the Kribi/Campo sub-basin, which is the southern portion of the Douala/Kribi-Campo sedimentary basin and is located to the south of the Douala sub-basin, geophysical studies have also suggested the presence of intrusive bodies of igneous origin. Through 2.5D modeling, Koumetio et al. (Koumetio et al., 2012) suggested the presence of two dense intrusive igneous blocks in the upper crust in the Kribi-Edea zone whose surfaces lie locally at depths between 0.9 and 1 km, but generally between depths of 3.5 and 4 km. Further south of the Kribi-Campo sub-basin, to the SE edge around Bipindi, Koumetio et al. (Koumetio et al., 2014) used 3D modeling techniques to characterize two dissymmetrical blocks of the same type of rock with a density contrast of – 0.095 g/cm^3 in comparison to its metamorphic surroundings. Malquaire et al. (Malquaire et al., 2017) carried out 3D gravity modeling in the northern part of the Kribi-Campo sub-basin to indicate the presence of a dense intrusive igneous body of density 2.74 g/cm^3 in the upper crust of the Kribi zone located at a depth range of 0.5 to 1.5 km.

Information on the intrusive body located in the NW portion of the Douala basin, as highlighted by 2.5D models along different profiles, indicate variation in depth to the surface of blocks as well as in the number of blocks present. This information is nevertheless very insufficient to fully characterize these variations. This is as a result of the limitations of the 2.5D modeling technique used in the studies which furnished this information. It is consequently not possible to determine the manner in which the intrusive body varies in depth across this region, the level to which it extends as well as the relationship between this body and those highlighted by studies to the south of the Douala sub-basin and further south in the Kribi-Campo sub-basin.

It is therefore important to employ modeling techniques on gravity

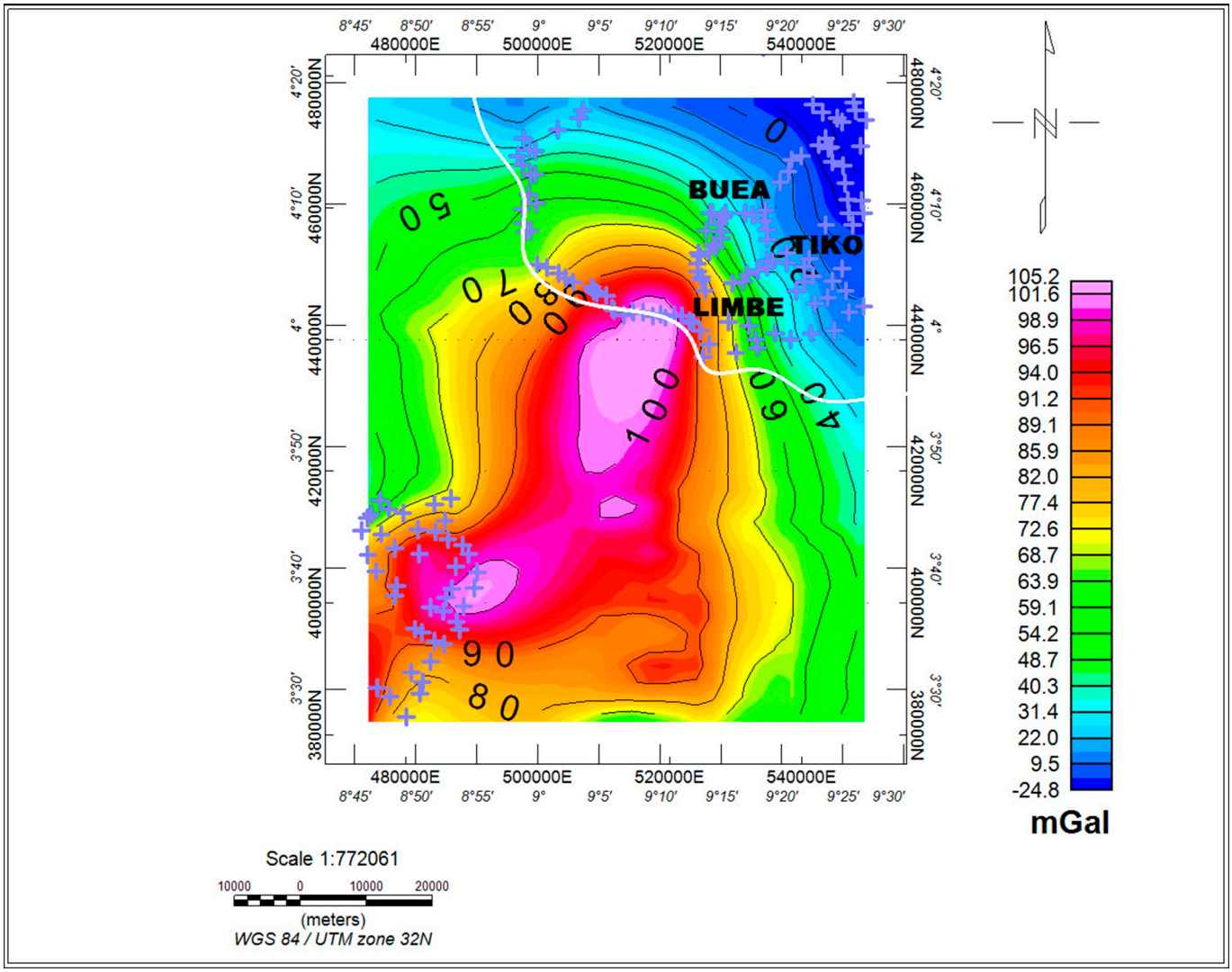

Fig. 2. Bouguer anomaly map of the NW portion of the Douala sedimentary sub-basin with location of data points as blue crosses. The white curve represents the approximate boundary between the continent and the Atlantic Ocean. (For interpretation of the references to colour in this figure legend, the reader is referred to the web version of this article.)

data which can generate a model of the intrusive body in this portion of the Douala sub-basin which presents a continuous relief surface view as well as its underlying block structure. This study will make use of two Oasis Montaj packages, GM-SYS 3D and 3D Voxel, to implement such techniques in order to attain the aforementioned.

The gravity data for this study is an extract of gravity data that was first acquired during a detailed gravity survey of Cameroon and Central Africa undertaken by the Office de la Recherche Scientifique et Technique d'Outre-Mer (ORSTOM) from 1963 to 1968 (Collignon, 1968; Louis, 1970). Other geophysical (gravity) campaigns were conducted after these initial ones from 1970 to 1990 (Albouy and Godivier, 1981; Okereke, 1984; Poudjom et al., 1995; Tadjou et al., 2008). These measurements were corrected for the effect of the luni-solar tidal and instrumental drift (assumed to be linear in time); and then after when free-air reduction referenced to the ellipsoid and an infinite plate reduction with a constant reduction density of 2.67 g/cm^3 (Collignon, 1968; Crenn, 1957) were applied, the simple Bouguer anomaly values obtained. The accuracy of the data is about ± 0.5 mGal. This study made use of a total of 128 data points located between latitudes 3° 21′N and 4° 9′ N as well as longitudes 8° 27′ E and 9° 16′ E.

2. Geologic and tectonic settings

The Douala sedimentary sub-basin which lies between latitudes 3°03′N and 4°06′N and longitudes 9°00′ and 10°00′E (Fig. 1) and has a total surface area of 12,805 km^2; is located on the South coast of Cameroon with the surface areas of its onshore and offshore portions being about 6955 km^2 and 5850 km^2 respectively (Kenfack et al., 2012a). Stretching from the south-eastern border of Mount Cameroon right up to Londji, the Douala sedimentary sub-basin is bounded to the north by the Cameroon volcanic line, to the south by the Kribi-Campo sub-basin and to the east by the late Proterozoic Pan-African belt. The pre-rift, rift, transition and drift megasequences related to the tectonic evolution over the African cratonic basement and associated Atlantic margin constitute the basic stratigraphy of this sub-basin. Four main phases of evolution related to the pre, syn and post-rift separation of Africa from South America summarize the regional stratigraphy and tectonics of the Douala sub-basin (Kenfack et al., 2012b). Seven major Formations related to the geodynamic and sedimentary evolution of this basin constitute its lithostratigraphy (Nguene et al., 1992; Regnoult, 1986; SNH/UD, 2005). They include the Mundeck Formation (Aptian-Cenomanian), the Logbadjeck Formation (Cenomanian-Campanian), the Logbaba Formation (Maastrichtian), the N'kapa Formation

(Paleocene-Eocene), the Souellaba Formation (Oligocene), the Matanda Formation (Miocene) and the Wouri Formation (Plio-Pleistocene) (Ngon et al., 2012). Since many of the *syn*-rift features that would normally be expected in the Douala basin are not apparent at depth in this area, although they are abundant in the corresponding South American segment, rifting in the Douala basin would appear to have been asymmetrical. During the passive "drift" phase of the continental margin evolution at 84 Ma (Santonian), 65 Ma (Cretaceous/Tertiary boundary) and 37 Ma (late Eocene), several additional tectonic events occurred. Generally, changes in plate motion and intraplate stress fields due to convergent and collision events between Africa and Europe are considered to be responsible for these events; and they resulted in uplift, deformation and erosion at the basin margins. Gravity sliding led to significant mass wasting of the continental margin, which contributed towards reservoir formation, seems to have come about as a result of the Santonian uplift and possibly the late Eocene events. The final uplift event relates to the growth of the Cameroon Volcanic Line (CVL) and effectively lasts from 37 Ma through to present day on the northwest margin of the basin (Kenfack et al., 2012b).

3. Methodology

3.1. Inversion of gravity data

The interpretation of gravity data can be carried out either through the direct (forward) methods or the indirect (inverse) methods of geophysics. Both methods shall be employed in this study to process the Bouguer and anomaly fields (Figs. 2 to 4) obtained from the gravity data.

In order to interpret the gravity data in this study area, the Oasis montaj software (version 8.3.3) extension GM-SYS 3D shall be employed. GM-SYS 3D is a 3D gravity and magnetic modeling package for surface-oriented models defined by a number of stacked surface grids with density, susceptibility and remanent magnetization distributions specified by the layer below each surface. It uses calculations performed in the wave number domain and are based on Dr. Bill Pearson's implementation of R.L. Parker's algorithm (Parker (1972) in Geosoft Online Help (2014)).

GM-SYS 3D has therefore been used to build depth models in order to provide surface-oriented models of the possible surface disposition of the indicative intrusive body noticed on the plots of the Bouguer and residual anomaly fields. Plots of these models are relief plots which indicate the variation in depth of surfaces with particular densities, where each surface is a constant layer at a specific density. GM-SYS 3D was thus used to build layered earth models with the gravity data in this zone. A new model was therefore generated with a constant surface layer at 0 km and its bottom at a depth of 40 km. The geometry of the model was adopted from the residual field. For each layer added at a chosen depth of the model, a constant density value could be assigned or the default value of 2.67 retained. For the purposes of this study, a constant density value of 2.77 g/cm^3 suggested as the density of the intrusive body from previous 2.5D studies in this region (Ndikum et al., 2014; Ndikum et al., 2017; Koumetio et al., 2012) was used. Then after the survey data, which in this case is the Bouguer data, was loaded into the model with the background density of the study area chosen to be that of the average density of the surrounding sedimentary basin equal to 2.5 g/cm^3 (Telford et al., 1990). Forward calculations were carried out to determine the calculated density contrast of the layer after which constant density inversion for this layer was undertaken to recalculate the density of the layer with respect to the forward calculations. Finally, structural inversion was carried out on the layer to generate the surface-oriented model of the layer.

The aforementioned steps in the processing of a layer were applied at constant layers positioned at depths of 5 km, 10 km, 15 km, 20 km, 25 km, 30 km and 35 km; in order to study the behavior of the intrusive body at these depths and also to determine its upper and lower depth limits. The plot of the model for the layer at a depth of 33 km is shown in Fig. 5. The surface colour variations depict relief with depth.

3.2. Voxel model

The relief plots obtained using GM-SYS 3D show variation in depth of a surface with particular density and describes a volume of the earth which extends from the top surface to a specified bottom elevation. The relief surface plot generated by GM-SYS 3D does not indicate the thickness of the structure underlying this surface. This surface can therefore be simply some few kilometers thick, as in the case of sills which are located between earth layers, giving the possibility of non-uniformity in body structure beneath this surface. This raises the need to generate a model for the block structure underlying this surface using 3D data voxels. The 3D relief sub-surface results obtained through the forward and inverse modeling techniques associated to GM-SYS 3D served as the starting model for the 3D voxel solution to define its geometry (x, y and z coordinates).

The word Voxel is the short form of the term "volume pixel" used in three dimensional modeling and the discussion of data cubes. It actually signifies the smallest distinguishable box-shaped part of a three-dimensional image. This implies it is the 3D conceptual counterpart of the 2D pixel [22]. Being a quantum unit of a volume, each voxel has a numeric value(s) associated with it that represents some measurable properties or independent variables of the real objects/phenomena. The x, y and z coordinates of one of the eight corners (or perhaps the centre) of a voxel are used to identify it. This smallest distinguishable box-shaped element of three dimensional space in geosoft can either be the 3D data voxel or the Lithology voxel.

The basic statistical kriging algorithm has been used to create a 3D data voxel solution of the intrusive body underneath this study area (Fig. 6) and the corresponding calculated anomaly map of this solution (Fig. 7).

4. Results

4.1. Bouguer and residual anomaly maps

The Bouguer anomaly map (Fig. 2) for this study area was generated by gridding the gravity data using the minimum curvature grid and then plotting with contour intervals of 10 mGal.

Very high positive anomalies which are expressed as ring like contours and located to the North West portion of the Douala sedimentary basin appear on the Bouguer anomaly map. The portion of the study area covering the anomalous zone used in this study has a surface area which stretches over about 79 km to the east and 73 km to the north.

This Bouguer anomaly map indicates a peak value of about 104.7 mGal around longitude 9° 12′ E and latitude 3° 54′ N which corresponds to a culmination of ring like contours. The presence of the ring like contours is the signature of the presence of a sub-surface intrusive body whose topmost surface corresponds to the position of peak value.

The residual anomaly map was obtained from the Bouguer anomaly map by eliminating the regional component (Fig. 3) generated through upward continuation at an optimum height of 30 km, a value which was estimated in previous studies by (Tadjou et al., 2008; Ndikum, 2015). The residual anomaly map was then used to generate a voxel plot (Fig. 4). This voxel plot was built with a geometry consisting of 33 and 31 number of cells to the east (longitude) and north (latitude) respectively, a cell size of 2425.9 m, east and north origins of 475,475.5 m and 400,272.7 m respectively and the azimuth to the north of 0° (the units of distance are with respect to WGS 84 / UTM Zone 32° N). The residual anomaly map also possesses a peak value at approximately the same position as the Bouguer anomaly map.

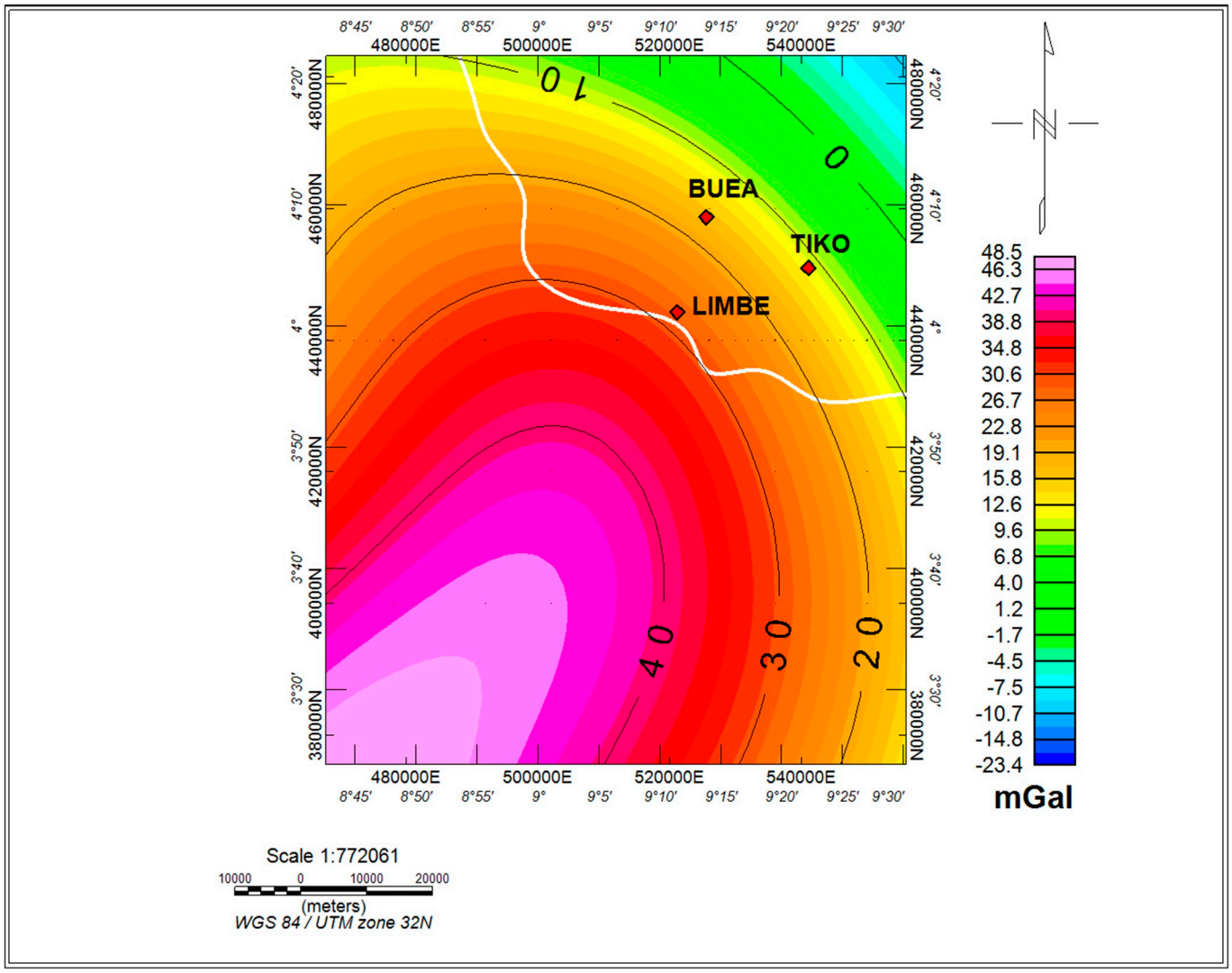

Fig. 3. Plot of regional anomaly map of the study area.

4.2. 3D relief of sub-surface

A summary of the characteristics of the surface oriented plots for layers at different depths beneath the study area generated using GM-SYS 3D is presented in Table 1.

The surface-oriented models retained bodies with a calculated density of approximately 2.77 g/cm^3 (Table 1) for a constant layer at a depth of 33 km beneath a surface layer with calculated density is about 2.5 g/cm^3 corresponding to the density of the sedimentary milieu in the basin (Fig. 5).

The surface-oriented plot emphasizes a body which begins with a major peak located at a depth of about 6.1 km and having a sharp edge towards its NE limit as suggested by the sharp changes in the contour lines to the NE limit of the principal anomaly zone on the Bouguer and residual anomaly maps. The image of the surface of the intrusive body towards the south clearly indicates that the body stretches beyond this study area.

4.3. Voxel solution

Based on the relief plots obtained using GM-SYS 3D, a 3D voxel solution of the underlying intrusive body was built (Fig. 6) as well as the corresponding calculated Bouguer anomaly map (Fig. 7).

5. Discussions

The Bouguer anomaly plot (Fig. 2) presents three principal zones of anomaly which move from a very high positive anomaly zone located towards the centre, through an average positive zone to an average negative zone. These peaks are characteristic of the manner in which density varies on the Bouguer anomaly map. Generally, density varies from a peak value around the centre of the high positive zone and attenuates in all directions. For most portions of the map, the variation is gradual with the exception of a sharp change to the NE which suggests a rapid change in structure. To the other sides of the high positive zone where the variation is gradual, the intrusive body is expected to be extending or to have limits with gentle slopes. Generally, contour lines have a W-E alignment to the north and south of the study area while they have approximately NNW-SSE alignments to the east and to some extent, to the west. Further south to the principal peak, are two minor peaks whose positions in the neighborhood of the principal peak zone are indicative of other peak portions of the same subsurface intrusive body which stretches forth in this direction. The voxel plot of the residual anomaly also shows three principal anomaly zones, the one major and two minor peaks in the principal zone and the extension of the sub-surface intrusive body southwards. The variation of density around the peaks are similar in orientation to those of the Bouguer anomaly field.

The body model from the surface-oriented plot has a density of 2.77 g/cm^3 and is located at a depth of about 6.1 km with its bottom located at about 33 km giving an average vertical height of about 26.9 km. The surface-oriented inversion results are therefore

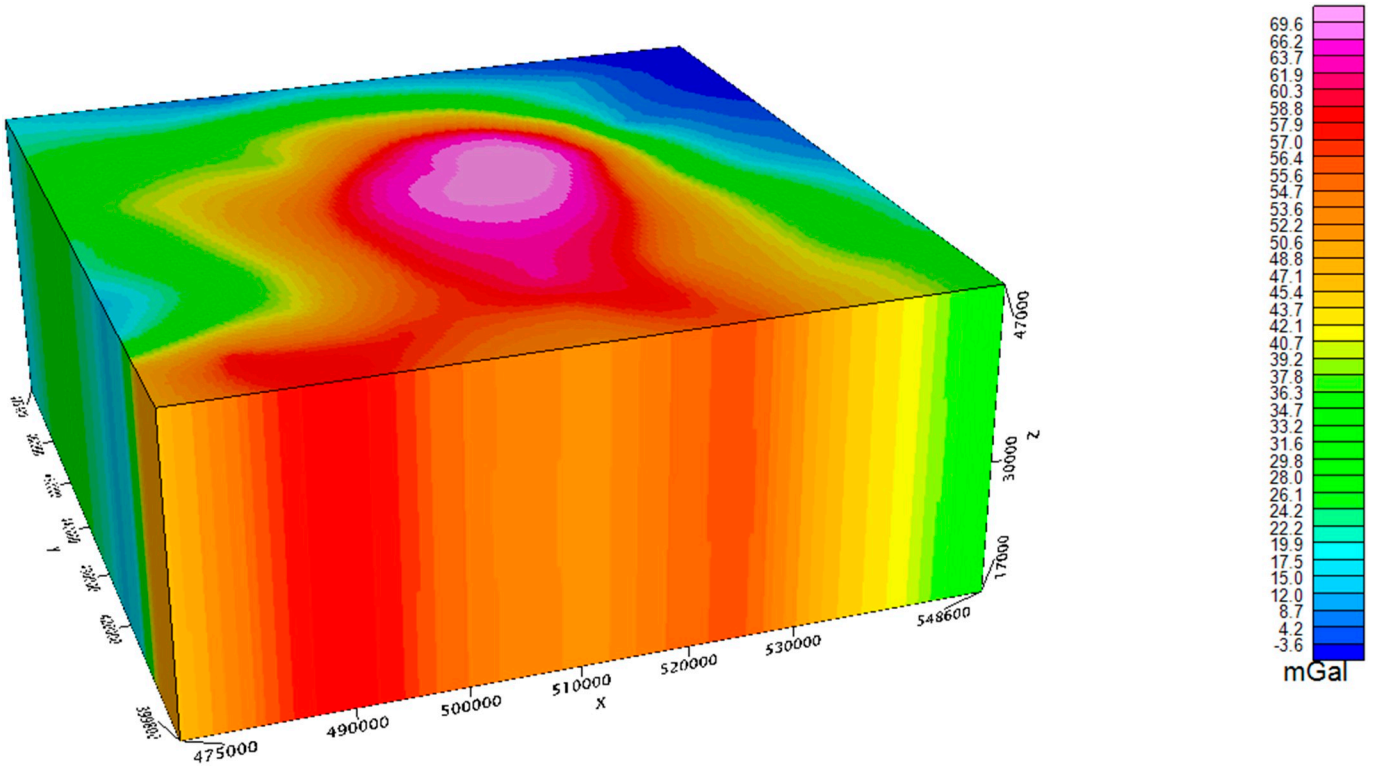

Fig. 4. Voxel plot of the residual anomaly map of the study area.

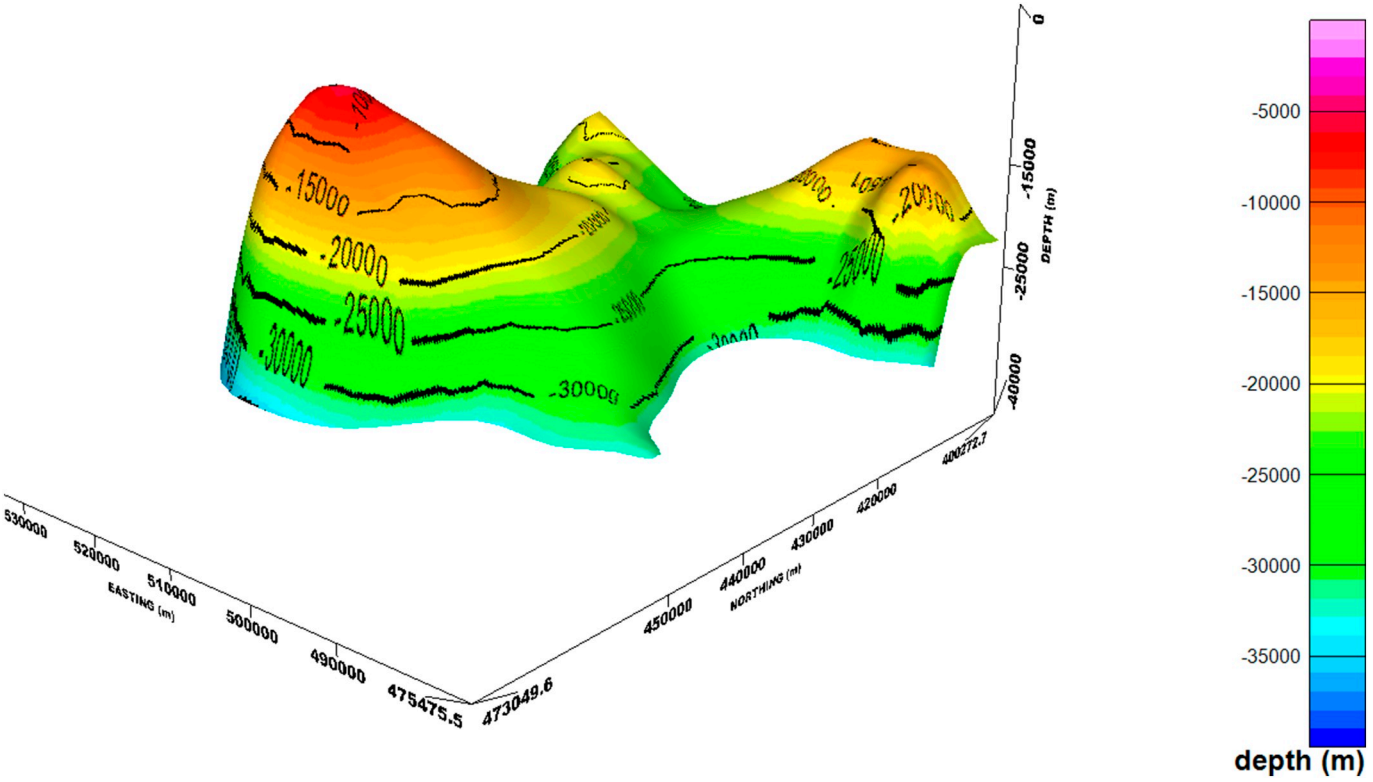

Fig. 5. Surface-oriented plot of intrusive body beneath the Douala sub-basin (SW view with inclination of 21.4° and azimuth of 139.8°).

comparable to previous 2.5D studies carried out in this study area that obtained density values in the range 2.77 to 3.5 (Ndikum et al., 2014; Ndikum et al., 2017; Koumetio et al., 2012).

The plot emphasizes a body which begins with a major peak located at a depth of about 6.1 km and having a sharp edge towards its NE limit as suggested by the sharp changes in the contour lines to the NE limit of the principal anomaly zone on the Bouguer and residual anomaly maps.

From the SW view of the inversion model, it can be noticed that if a WWS-EEN profile is drawn to begin from the western edge of the minor peak at the SW corner of the plot (which is at a depth of about 14.8 km)

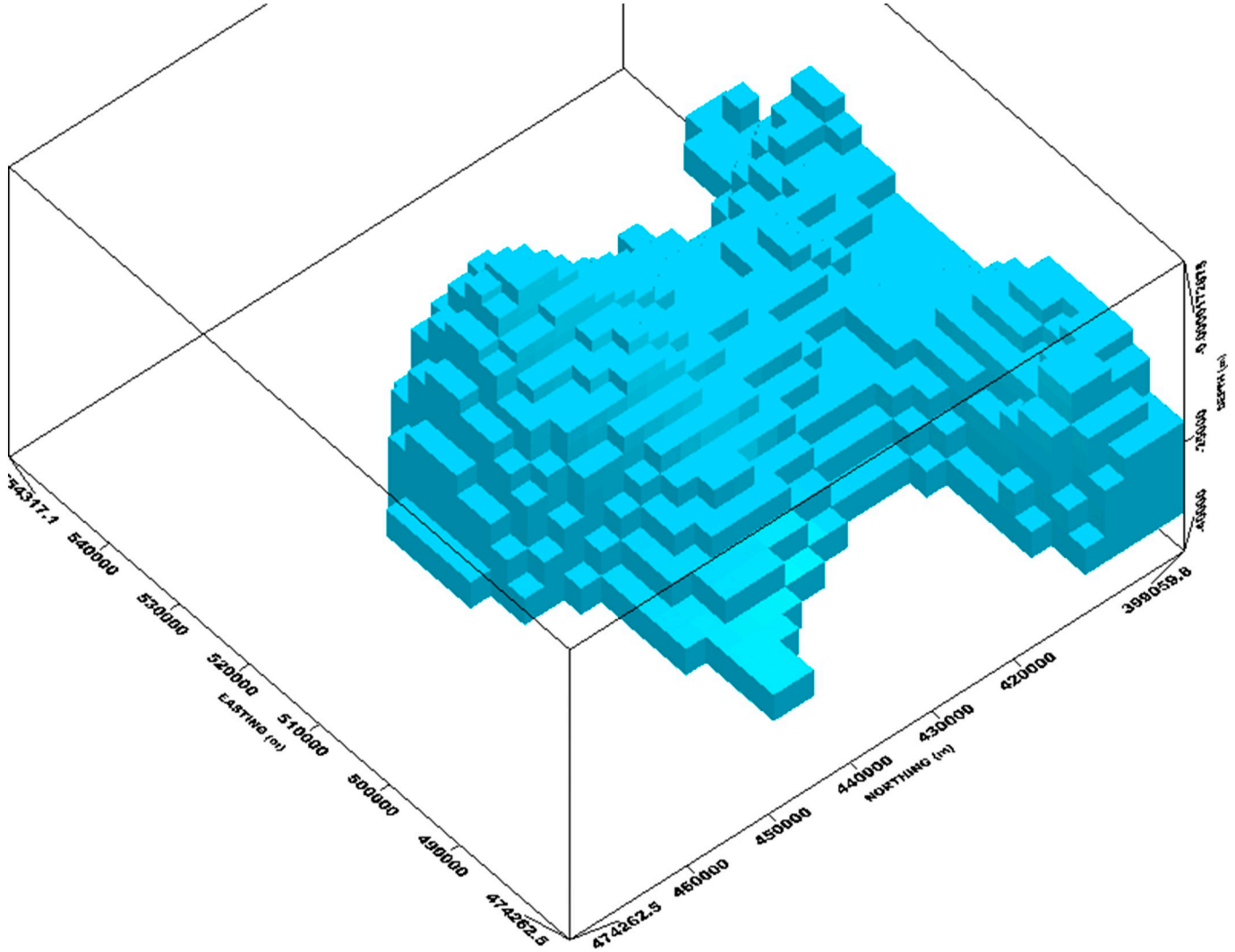

Fig. 6. 3D voxel solution for block model of intrusive body beneath Douala sub-basin with density of 2.77 g/cm^3 (viewed from the SW with inclination of 47.6° and azimuth of 130.6°).

going across the hollow portion to touch the major peak; a 2.5D inversion will probably indicate the presence of two blocks as a result of the hollow separation. This is the case of the 2.5D studies of (Ndikum et al., 2017; Koumetio et al., 2012) which located two major blocks beneath this study area. By the help of surface-oriented plots from this study, these two structures have been shown to be portions of the same intrusive body.

The image of the surface of the intrusive body towards its southern limit clearly indicates that the body stretches beyond this study area. This suggests that the intrusive body observed in this portion of the Douala sub-basin could be a part of the different intrusive bodies highlighted by results of geophysical studies to the south of the Douala sub-basin and even further south in the Kribi-Campo sub-basin (Koumetio et al., 2012; Koumetio et al., 2014; Malquaire et al., 2017). Processing gravity data for surface-oriented plots over the area extending southwards from this present study area across to the Kribi-Campo sub-basin will make it possible to verify this observation.

The block structure of the intrusive body obtained by 3D voxel solutions with respect to depth shows very striking similarities with the surface-oriented solutions from GM-SYS 3D. It dismisses the possibility of the body with the surface-oriented plot being simply a rock layer spreading laterally between sedimentary layers. It presents a block that extends from the surface-oriented plot vertically downwards through the crust. The block presents a body with major peak at a depth of about 6.2 km having a relatively sharp sloping boundary towards its NE edge and gradual sloping edges towards its NW, W and E limits. The presence of a minor peak close to and almost merging with the principal peak can also be observed; as well as two minor peaks further south. The southern end of this body, as depicted by the block, shows evidence of the continuation of this body further south beyond this study area. This confirms the need to process more gravity data beyond the southern limit in order to obtain the full view of this intrusive body. From the value of the density of this block (2.77 g/cm^3), further confirmation is obtained to the fact that this intrusive body is of igneous origin as suggested by the results of previous studies (Koumetio et al., 2009; Ndikum et al., 2014; Ndikum et al., 2017).

6. Conclusion

Gravity data from the North West portion of the Douala sedimentary basin; has been gridded and plotted on a Bouguer anomaly map that indicated three principal zones of anomaly which varied from a very high positive anomaly zone located towards the centre, through an average positive zone to an average negative zone. Similar density characteristics have been emphasized by the voxel plot of the residual anomaly field.

A surface-oriented model has been built using the geosoft montaj

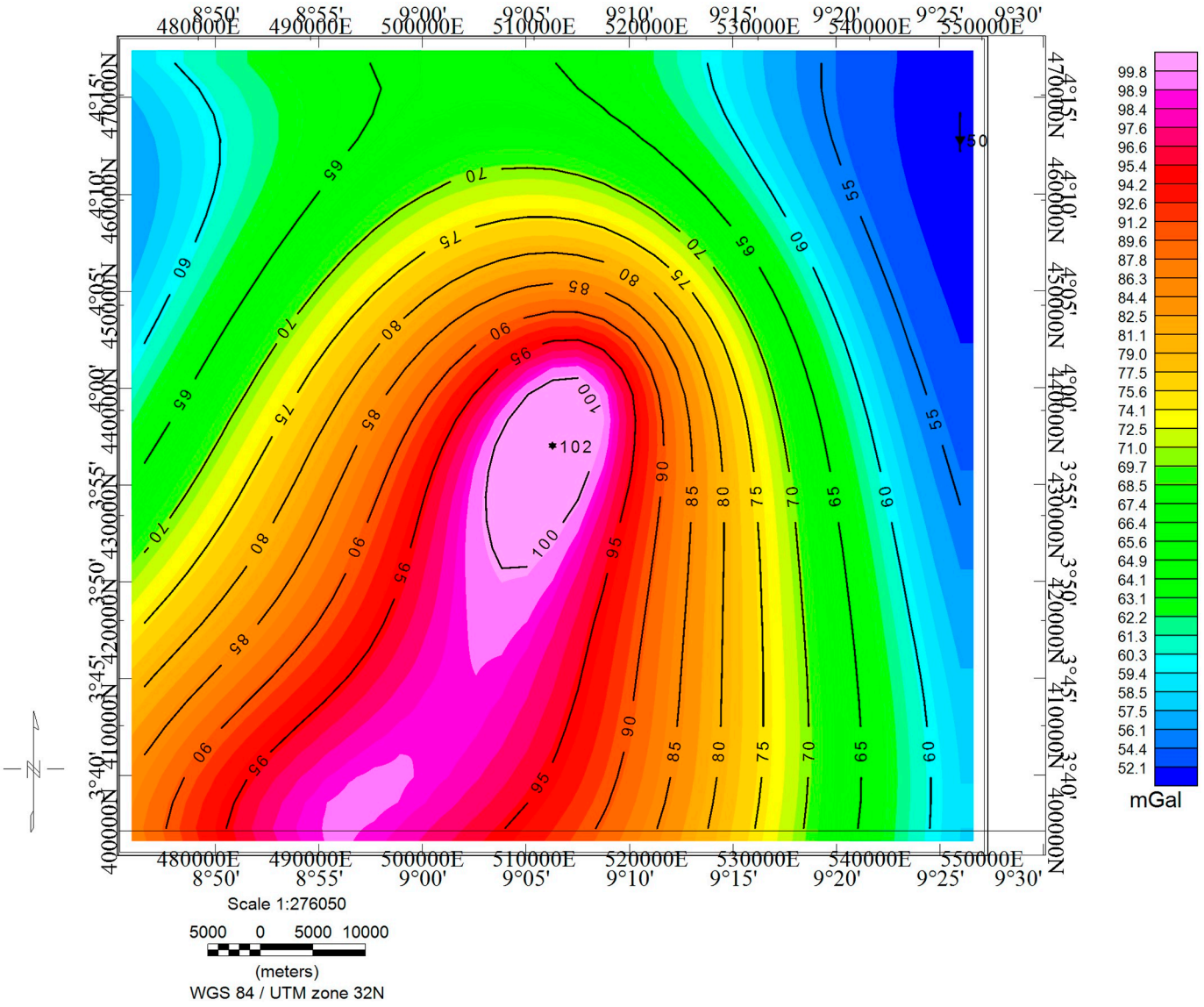

Fig. 7. Gravity effect generated by the 3D voxel solution of block model for intrusive body beneath Douala sub-basin computed using constant density of 2.77 g/cm^3.

Table 1
Results of surface-oriented inversion plots at different depths.

Serial number	Depth of constant layer (km)	Initial constant density of layers (g/cm^3)	Calculated density of constant layers (g/cm^3)		Depth to peak portion of inverted oriented sub-surface (m)	Depth to bottom portion of inverted oriented sub-surface (m)
			Surface layer	Body layer		
1	05	2.77	1.105	2.77	4222	5000
2	10	2.77	1.892	2.77	6839	10,000
3	15	2.77	2.185	2.77	7202	15,000
4	20	2.77	2.331	2.771	6114	20,000
5	25	2.77	2.419	2.77	5208	25,000
6	30	2.77	2.477	2.772	5488	30,000
7	33	2.77	2.504	2.771	6081	33,000
08	35	2.77	2.519	2.773	7976	35,000
09	39	2.77	2.545	2.775	17,366	39,000

extension, GM-SYS 3D. This model has a surface and surrounding with a density of about 2.5 g/cm^3 which corresponds to that of the sedimentary milieu of the basin. It presents an intrusive body having density of about 2.77 g/cm^3 located at a depth of about 6.1 km with its bottom located at about 33 km giving an average vertical height of about 26.9 km. These results greatly agree with previous results from 2.5D studies in this very zone of study.

A 3D voxel solution was then generated for the intrusive body portrayed by the surface-oriented solution. The block structure of the intrusive body possesses a major peak at a depth of about 6.2 km having a relatively sharp sloping boundary towards its NE edge and gradual sloping edges towards its NW, W and E limits. It also has one minor peak very close to the major peak and almost merged to it, as well as two other minor peaks located further south. The density of the block in this 3D solution is approximately equal to 2.77 g/cm^3. This further confirmed the fact that this body is of igneous origin. These results suggest that the intrusive body beneath this study area extends further south and could be the same body highlighted to the south of the Douala sub-basin and even in the Kribi-Campo sub-basin.

Acknowledgment

We wish to sincerely appreciate the two anonymous reviewers who forwarded very insightful and constructive contributions towards the amelioration of this paper.

References

Albouy, Y., Godivier, R., 1981. Cartes Gravimétriques de le République Centrafricaine. ORSTOM, Paris.

Collignon, F., 1968. Gravimetrie et Reconnaissance de la Republique Federale du Cameroun. [Gravimetry and Recognition of the Federal Republic of Cameroon]. vol. 35 ORSTOM, Paris.

Crenn, Y., 1957. Measure Gravimétriques et magnétiques dans la partie central de l'A.O.F. Interpretation géologique. Publi. série géophys. ORSTOM. Fr, Paris, pp. 43.

Dumort, J.C., 1968. République Fédérale du Cameroun, Direction Des Mineset de la Géologie du Cameroun, 69 p. (Reconnaissance Geologic Map and Explanatory Note on the Douala-West Sheet (1: 500000)). Federal Republic of Cameroon, Directorate of Mines and Geology of Cameroon, (69 p). Carte géologique de reconnaissance et note explicative sur la feuille Douala-Ouest (1:500000).

Geosoft Online Help @ 2014 Geosoft Inc. www.geosoft.com.

Kenfack, P.L., Ngaha, P.R.N., Ekodeck, G.E., Ngueutchoua, G., 2012a. Mineralogic characterization and petroleum potential of clays (shales) of the N'Kapa formation (Paleocene-Eocene) in the Douala sedimentary sub-basin (South-West Cameroon). Int. J. Geosci. 3, 696–709. https://doi.org/10.4236/ijg.2012.34070.

Kenfack, P.L., Njike, P.R.N., Ekodeck, G.E., Ngueutchoua, G., 2012b. Fossils dinoflagellates from the northern border of the Douala sedimentary Sub-Basin (south-West Cameroon): age assessment and Paleoecological interpretations. Geosciences 2, 117–124. https://doi.org/10.5923/j.geo.20120205.03.

Koumetio, F., Tabod, C.T., Manguelle-Dicoum, E., 2009. Evidence for upper mantle intrusion in the West African coastal sedimentary basins from gravity data: the case of the southern part of the Douala Basin, Cameroon. Glob. J. Geol. Sci. 7, 181–187.

Koumetio, F., Njomo, D., Tabod, C.T., Noutchogwe, T.C., Manguelle-Dicoum, E., 2012. Structural interpretation of gravity anomalies from the Kribi-Edea zone, South Cameroon: a case study. J. Geophys. Eng. 9, 664–673. https://doi.org/10.1088/1742-2132/9/6/664.

Koumetio, F., Njomo, D., Tatchum, C.N., Tokam, K.A.P., Tabod, C.T., Manguelle- Dicoum, E., 2014. Interpretation of gravity anomalies by multi-scale evalution of maxima of gradients and 3D modelling in Bipindi region (South-West Cameroon). Int. J. Geosci. 5, 1415–1425. https://doi.org/10.4236/ijg.2014.512115.

Louis, P., 1970. Contribution Géophysique à la Connaissance Géologique du Bassin du lac Chad. ORSTOM, Paris.

Malquaire, K.P.R., Louise, O.A.M., Nfor, N., Eliezer, M.-D., 2017. 3D modelling from new and existing gravity data of an intrusive body in the northern part of Kribi-Campo Sub-Basin in Cameroon. Int. J. Geosci. 8, 984–1003. https://doi.org/10.4236/ijg.2017.88056.

Ndikum, E.N. (2015) Gravity Study of the Douala Sedimentary Basin. PhD Thesis University of Yaounde I, Yaounde, (91 p).

Ndikum, E.N., Tabod, C.T., Essimbi, B.Z., Koumetio, F., Noutchogwe, C.T., 2014. Gravity model for an anomalous body located in the NW Protion of the Douala sedimentary Sub-Basin, Cameroon (Central Africa). Open Journal of Geology 4, 524–541. https://doi.org/10.4236/ojg.2014.410039.

Ndikum, E.N., Tabod, C.T., Koumetio, F., Tatchum, N.C., Victor, K.J., 2017. Evidence of some major structures underlying the Douala sedimentary Sub-Basin: West African Coastal Basin. J. Geosci. Environ. Protect. 5, 161–172. https://doi.org/10.4236/gep.2017.57013.

Ngon, G.F.N., Etame, J., Ntamak-Nida, M.J., Mbog, M.B., Mpondo, A.M.M., Martine, G., Yongue-Fouateu, R., Bilong, P., 2012. Geological study of sedimentary clayey materials of the Bomkoul area in the Douala region (Douala sub-basin, Cameroon) for the ceramic industry. C. R. Geoscience 344, 366–376. https://doi.org/10.1016/j.crte.2012.05.004.

Nguene, F.R., Tamfu, S., Loule, J.P., and Ngassa, C. (1992) Paleoenvironnements of the Douala and Kribi/Campo subbasins in Cameroon, West African. Géologie Africaine: colloque de Géologie Africaine, Libreville, recueil des communications, 6–8 May 1991, pp. 129–139.

Okereke, C. (1984) A Gravity Study of the Lithospheric Structure beneath West Africa Rift System in Nigeria and Cameroon. Ph.D Thesis, University of Leeds, Leeds.

Parker, R.L., 1972. The rapid calculation of potential anomalies. J. R. Astron. Soc. 31, 447–455.

Poudjom, D.Y.H., Nnange, J.M., Diament, M., Ebinger, C.J., Fairhead, J.D., 1995. Effective elastic thickness and crustal thickness variation in West Central Africa inferred from gravity data. J. Geophys. Res. 100 (B11), 22047–22070. https://doi.org/10.1029/95JB01149.

Regnoult, J.M., 1986. Synthèse gélogique du Cameroun. D.M.G, Yaoundé, Cameroun (118 p).

SNH/UD, 2005. Stratigraphie séquentielle et tectonique des dépôts mésozoïques syn-rifts du bassin de Kribi/Campo. Rapport non publié (134 p).

Tadjou, J. M., Manguelle-Dicoum, E., Nguiya, S. and Kamguia, J. (2008) Caractéristiques des Anomalies Gravimétriques du Sous-Bassin Sédimentaire de Kribi-Campo (Sud-Cameroun). Africa Geosci. Rev., 1–2, 39–50.

Telford, W.M., Geldart, L.P., Sheriff, R.E., 1990. Applied Geophysics, 2nd edition. Cambridge University Press, Cambridge, pp. 6–61.

Scientific Research Publishing

International Journal of Geosciences, 2019, 10, 845-859
https://www.scirp.org/journal/ijg
ISSN Online: 2156-8367
ISSN Print: 2156-8359

Characterization of Pan-African Aquifer Layers by the Least Squares Inversion Method Applied on Geoelectric Data

Kana T. Idriss[1], Serge H. Pokam Kengni[1,2], Ndikum Eric Ndoh[1,3*], Blaise P. Gounou Pokam[1], Charles T. Tabod[1,2]

[1]Department of Physics, Faculty of Science, University of Yaounde I, Yaounde, Cameroon
[2]Department of Physics, Faculty of Science, University of Bamenda, Bamenda, Cameroon
[3]Department of Physics, HTTC Bambili, University of Bamenda, Bamenda, Cameroon
Email: *ndikumeric@yahoo.com

How to cite this paper: Idriss, K.T., Kengni, S.H.P., Ndoh, N.E., Pokam, B.P.G. and Tabod, C.T. (2019) Characterization of Pan-African Aquifer Layers by the Least Squares Inversion Method Applied on Geoelectric Data. *International Journal of Geosciences*, **10**, 845-859.
https://doi.org/10.4236/ijg.2019.1010048

Received: June 3, 2019
Accepted: October 8, 2019
Published: October 11, 2019

Abstract

Geoelectric data obtained from forty (40) vertical electrical soundings collected with a Schlumberger device in the Adamawa plateau region, also known as the Cameroon water tower, have been treated by the least-squares inversion method. In order to study the nature and thickness of the aquifer and the necessary geoelectric parameters, quantitative and qualitative interpretations of the data were made. The results obtained showed that: about four to five geoelectric layers have been delimited in the study area with a dominance of the KH curve, which can be used as a reference for future studies. The first two layers constitute an association of clay and laterite with resistivity values ranging from 58 to 9122 Ω·m and whose thickness is between 0.6 and 13.4 m. The third layer is a potentially aquiferous laterite composed of clay, laterite and especially clay sand and cracked/good granite, with a dominance of sandy alteration whose resistivity values are between 81 and 960 Ω·m and its thickness between 12.2 and 26.8 m. The fourth and fifth layers are made up of cracked/good granite with a resistivity ranging from 12 - 10705 Ω·m with an average value of 1817 Ω·m. This study also shows that the North-East, South-West and South sectors could be the groundwater convergence zones and that the average depth of the basement aquifer roof is about 28.3 m. The geoelectric sections of certain demarcated vertical electrical sounding stations are consistent with the geologic description of the area.

Keywords

Adamawa Plateau Region, Vertical Electrical Sounding, Geoelectric Sections, Aquifer, Groundwater

1. Introduction

1.1. Study Context

The Adamawa Plateau, located in the Adamawa region which is one of the ten regions of Cameroon, is considered as the water tower of the country. Despite this appellation, many people lack drinking water especially in rural areas where the search for sources of reliable drinking water has become an important issue for villages in this region of Cameroon. In fact, the population growth has led to a serious shortage of drinking water, which is why the drinking water points must be exploited with the greatest care in order to avoid their exhaustion and their sustainable use. This poses a great challenge for citizens and the government [1], who has to deal with the inadequate supply of drinking water in the region, which has become a chronic problem. In addition to the high population growth, the shortage of drinking water due to insufficient knowledge of the potential of the underground aquifer especially with respect to the characteristics of the latter, and the aggressive use of water [2], it is also important to pay attention to the quality of the water used [3]. It is therefore very necessary to first highlight the existence of these aquifers and their hydrogeological characteristics. As a result, the integration of aquifer parameters calculated from existing drill locations and surface resistivity parameters extracted from surface electrical measurements shall be used effectively. This work, which is an application of the geoelectric prospecting method, attempts to provide a solution to the above-mentioned problem with the aim of producing a database that could be used for detailed groundwater exploration activities in the study area.

1.2. Hydrogeological and Geologic Settings

The Adamawa plateau which is the study area of this work is found in the Adamawa region of Cameroon, which is located in the heart of Central Africa between latitudes 6˚N and 8˚N and Longitudes 11˚E and 16˚E. The vegetation encountered is of shrub savanna type with the preponderance of cereal crops. Climate changes in this region where the average temperature (between 21˚C and 29˚C) increases; average annual rainfall (800 mm to 1600 mm) decreases and groundwater has increased up to 4 m in 15 years [4]. Geologically, the Adamawa plateau region of Cameroon (**Figure 1**) presents itself as a volcanic axis characterized by a fissured basaltic volcanism. The fault leaving Foumban, joins it and crosses away almost diagonal. It is one of the zones in Cameroon where one can meet several geological accidents.

The basement of the Adamawa plateau region consists of a Precambrian granito-gneiss complex (**Figure 1**) that recorded Pan-African granitization [6]**.** That basement is overlain by a sequence of basaltic to andesitic lavas that are largely of Tertiary age [7]. These lavas are essentially alkaline indicating an affinity to continental rifts [8]. The sedimentary formations here are mainly composed of conglomerates and marl of the Cretaceous Mbere and Djerem Troughs [7] [9]. These formations have undergone intense tectonic activity resulting in the emplacement

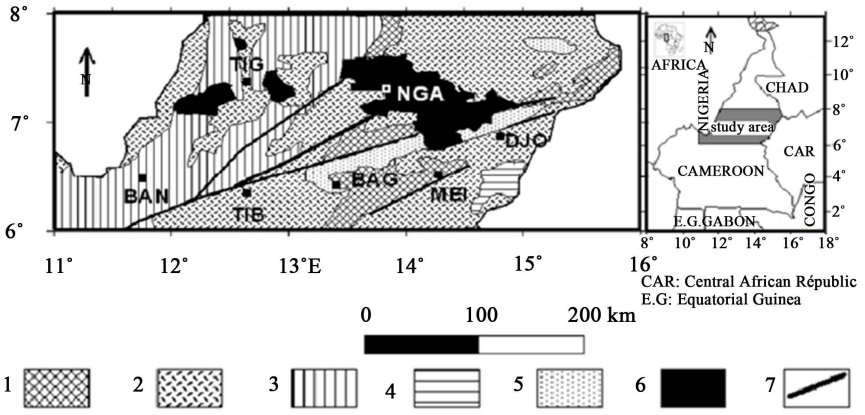

Figure 1. Geologic map of study area (modified from [5]). 1: High grade metamorphosed paleoproterozoic gneiss; 2: Syn-tectonic panafrican granite; 3: principal undifferentiated panafrican Gneiss; 4: panafrican Metasediments; 5: envelope of cretaceous sediments; 6: cenozoic Volcanism; 7: Central Cameroon fault line.

of basin structures which were frequently filled by volcanic material upwelling through deep fractures in the Adamawa region.

The Adamawa plateau is sometimes called the "water tower" of Cameroon, since a large number of rivers of the country have their sources in this region and experience floods from May to September during the rainy season. The rivers of the region flow into three different basins: the Niger River, Lake Chad, and the Atlantic Ocean. The hydrogeology of the region is marked by continuous alterite aquifers. In the granito-gneisses, this reservoir is generally from 1 to 20 m where it is characterized by clay dominance [10]. These aquifers overcome a cracked horizon of the granite-Gneissic basement fed by rainwater and stream beds. It constitutes the aquifer that is essentially prospecting because it concentrates most of the groundwater reserves and is supposed to be protected from seasonal fluctuations [11]. We can note the presence of wells and boreholes that are functional all year round, resulting from multiple development support programs.

1.3. Recent Geophysical Works and Problem Statement

The Adamawa plateau has also been the subject of a recent study that portrays the study of the hydrogeophysical characteristics of the Pan-African aquifer [12]. This study establishes unequal distribution of transmissivities by an alternative approach based on the interpretation of vertical electrical sounding data. Another study based on electrical resistivity tomography (ERT) and self-potential data was carried out at Meiganga in the Department of Mbere, in the Adamawa region [13]. This made it possible to delimit the groundwater producing areas in this locality and the resistivities of the geological formations encountered. However, these studies do not show a geophysical mapping of the aquifer and a station-by-station geoelectric study in various localities in the region. The types of data used in these studies do not make it possible to sufficiently assess the cha-

racteristics of aquifer zones throughout the region. All these aforementioned raise the need to carry out a geophysical study using a more direct method of all vertical electrical soundings conducted in the region.

2. Data Acquisition and Methodology

2.1. Data Acquisition

The Schlumberger configuration of a linear electrodes array (AMNB) was used to locate and characterize aquifers. With this technique, whereby electrical resistivity variations are expressed as a function of depth, forty (40) Vertical Electrical Sounding (VES) have been carried out in the study area using the terrameter model SAS-300B. The operational principle rests on the fact that ground injection of current through current electrodes A and B enables the measurement of the potential drop between potential probes M and N (**Figure 2**). Potential electrodes M and N are kept fixed at the center of the array while current electrodes A and B are moved outward symmetrically [14]. By increasing the distance between the current electrodes from 3 to 166 m, the layer resistance ΔV/I was directly measured, and its apparent resistivity ρ_a was calculated using Ohm's law (Equation (1)) while taking Equation (2) into consideration. Apparent resistivity depends on several factors such as true layer resistivities, their boundary, and the location of electrodes. However, lack of uniformity or split of layers can be observed.

$$\rho_a = K\frac{V_{MN}}{I_{AB}} \tag{1}$$

- K (in m) is the geometric factor depending on the array of electrodes;
- V_{MN}: potential drop between electrodes M and N, in mV;
- I_{AB}: electric current injected between electrodes A and B, in mA. Where:

$$K = \frac{2\pi}{\left(\frac{1}{AM} - \frac{1}{BM} - \frac{1}{AN} + \frac{1}{BN}\right)} \tag{2}$$

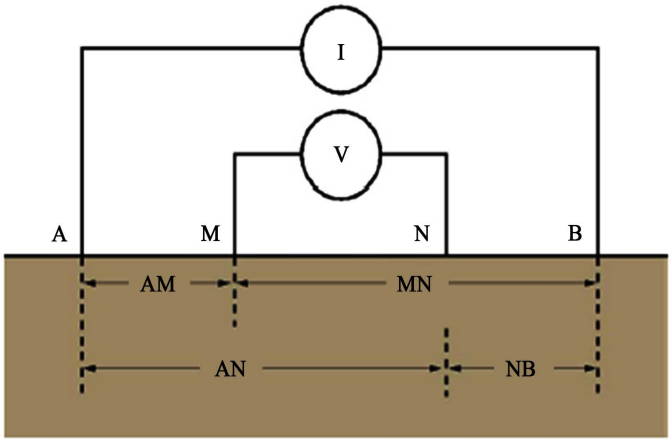

Figure 2. Principle of implementation of the geoelectrical method.

2.2. Methodology

The curve-matching technique was used in this study to calibrate and interprete the sounding curves [15]. Calibration was conducted with experimental boreholes drilled in the vicinity of several VES points. These experimental parameters were thereafter accurately interpreted using an inverse technique program [16] [17]. In this case, a weighted least squares inversion algorithm was used to propose geoelectrical models of the study area. The process here is done in several steps which include:

a) Importing survey data collected in the field

On the sample sheet used during the data collection, two variables were used for the modeling: the values of the spacings of AB/2 and that of apparent resistivity ρ_a. Thus using the modeling tool JOINTEM (joint interpretation of electromagnetic and geoelectrical soundings using 1-D layered earth model), more precisely in the box denoted "method by direct current", abilogarithmic paper is employed whose abscissa takes the values of AB/2 and its ordinate takes values of ρ_a.

b) Matching curves

The inversion process involves bringing the theoretical curve so that it superimposes itself the most possible on the points of soundings. This curve has well defined parameters which are the number of layers, the resistivity of layers and the thickness or depth of the layers (Figure 3). However the overlaying of the curves can be correct but the parameters obtained do not reflect the reality, and so there will be need to change these parameters from the information available at first sight. This is in order to obtain a quadratic error average (RMS) value as small as possible and the sum of damping factors equal to one. This process was carried out taking into account several precautions, such as the precision of various

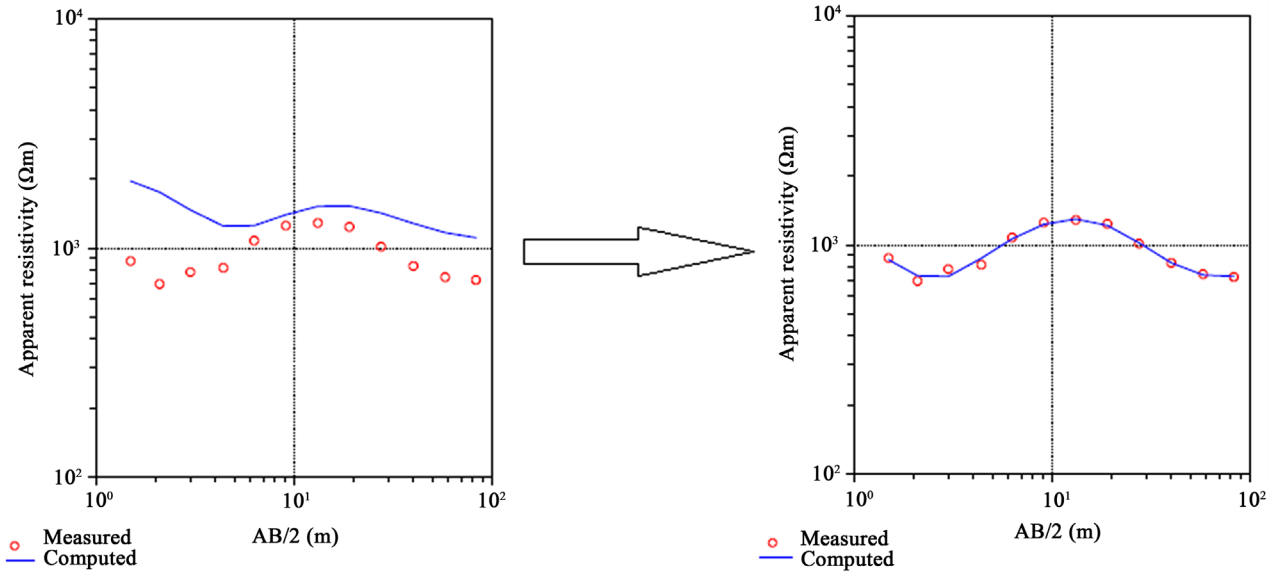

Figure 3. Principle of least squares inversion of vertical electrical sounding data (this figure illustrates the superposition of the computed curve in blue on the points of measurement in red).

calculations, a reasonable geologic concept and the hypothesis of a one-dimensional (1D) medium [18]. The geologic conditions of the region were favorable for assuming 1D model for vertical electrical soundings data interpretation [12].

3. Results and Discussion

3.1. Results

The results of this study are from a quantitative study done with vertical electrical sounding curves summarized in a table and from a qualitative study through cartography.

3.1.1. Geoelectrical Survey Curves

In the study area, forty (40) vertical electrical soundings were performed and interpreted. Their interpretation made it possible to propose a geoelectrical succession that is as close as possible to the geophysical measurements made in the field (**Figure 2**). Several types of curves have also been identified. In addition, the presence of some drilling logs in the area made it possible to draw a geoelectrical section of the subsoil of the area (**Figure 4**) which highlights the presence of topsoil, laterite, lateritic clay, clayey sand and granite described by **Figure 5**. The interpretations of these curves are regrouped in **Table 1**.

The curves obtained in this study, as presented on **Table 1**, are of AA, AK, HA, KH, KQ, QH and QQ types for the four (04) layer terrain models and HKH, KHA and KQH for the five (05) layer terrain models. The most representative curves are of type KH with a rate of 22.5%. The dominance of these curve types shows a homogenous subsurface succession, and, in most sounding curves the same layers were found.

Close to the surface, a dominance of the laterite and sometimes associated with the clay was obtained whose resistivity varies between 457 - 9122 Ω·m and the thickness between 0.6 - 6.5 m. There is also the presence of topsoil at stations S.1, S.2, S.9, S.10, S.17, S.18, S.21 and S.36 with a resistivity varying from 61 - 381 Ω·m and the thickness between 0.2 - 3.2 m.

The second layer, more or less weathered, is a clay-laterite complex dominated by clay. Its resistivity varies between 58 - 4828 Ω·m and the thickness between 1.3 - 13.4 m. At stations S.12, S.31 and S.32, the lithology makes it possible to deduce a very resistant granite upwelling with a resistivity range of 5822 - 15,000 Ω·m and thickness range of 3.3 - 5.3 m. This second layer contributes to the development of groundwater because it allows the infiltration of surface water to the cracked medium of the basement.

The third and fourth layers have been identified as potential aquifer zones. The third layer is dominated by clayey sand with a resistivity range of 81 - 960 Ω·m and thickness of 12.2 - 26.8 m. Using lithology, an alteration was highlighted which is clay at stations S.1, S.9 and S.36 with resistivity ranging from 42 - 69 Ω·m and thickness of 6.4 - 12.1 m. Laterite was also found at stations S.7, S.8, S.15, S.22 and S.26 with a resistivity of 1251 - 2669 Ω·m and thickness

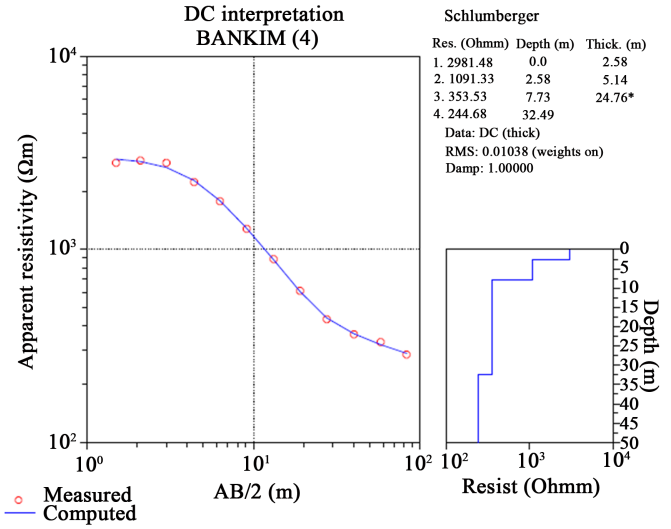
DC interpretation
BANKIM (4)
Schlumberger
Res. (Ohmm) Depth (m) Thick. (m)
1. 2981.48 0.0 2.58
2. 1091.33 2.58 5.14
3. 353.53 7.73 24.76*
4. 244.68 32.49
Data: DC (thick)
RMS: 0.01038 (weights on)
Damp: 1.00000
Apparent resistivity (Ωm)
AB/2 (m)
Resist (Ohmm)
Depth (m)
Measured
Computed

(a)

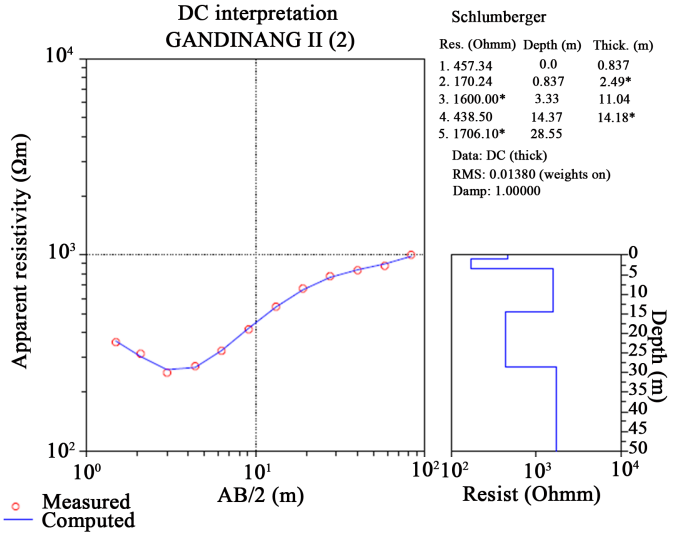
DC interpretation
GANDINANG II (2)
Schlumberger
Res. (Ohmm) Depth (m) Thick. (m)
1. 457.34 0.0 0.837
2. 170.24 0.837 2.49*
3. 1600.00* 3.33 11.04
4. 438.50 14.37 14.18*
5. 1706.10* 28.55
Data: DC (thick)
RMS: 0.01380 (weights on)
Damp: 1.00000
Apparent resistivity (Ωm)
AB/2 (m)
Resist (Ohmm)
Depth (m)
Measured
Computed

(b)

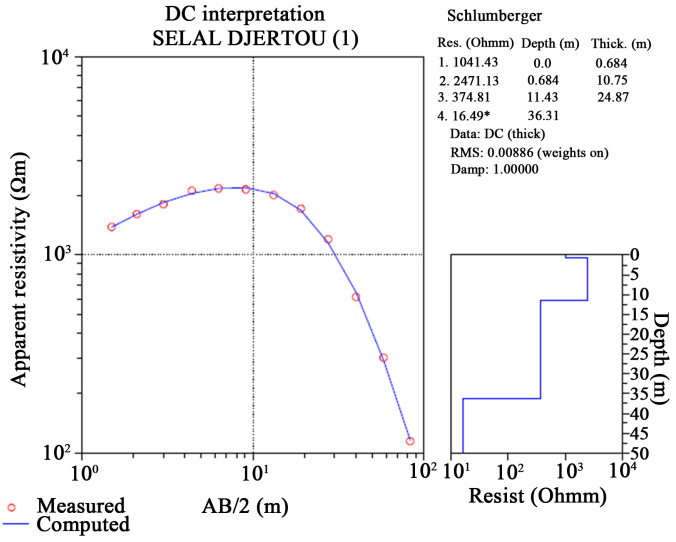
DC interpretation
SELAL DJERTOU (1)
Schlumberger
Res. (Ohmm) Depth (m) Thick. (m)
1. 1041.43 0.0 0.684
2. 2471.13 0.684 10.75
3. 374.81 11.43 24.87
4. 16.49* 36.31
Data: DC (thick)
RMS: 0.00886 (weights on)
Damp: 1.00000
Apparent resistivity (Ωm)
AB/2 (m)
Resist (Ohmm)
Depth (m)
Measured
Computed

(c)

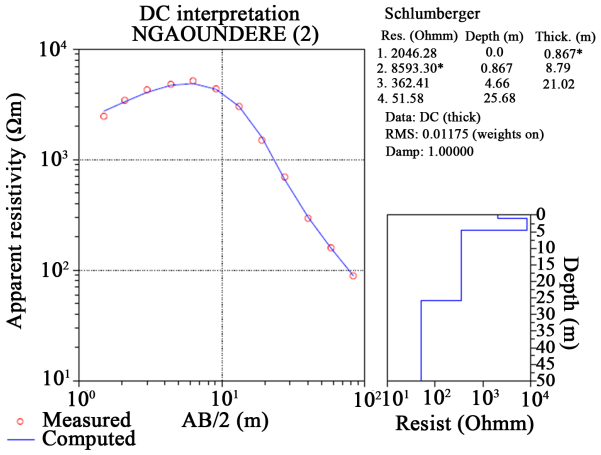

(d)

Figure 4. (a): The computer interpretation curve of S.4; (b): The computer interpretation curve of S.22; (c): The computer interpretation curve of S.19; (d): The computer interpretation curve of S.12.

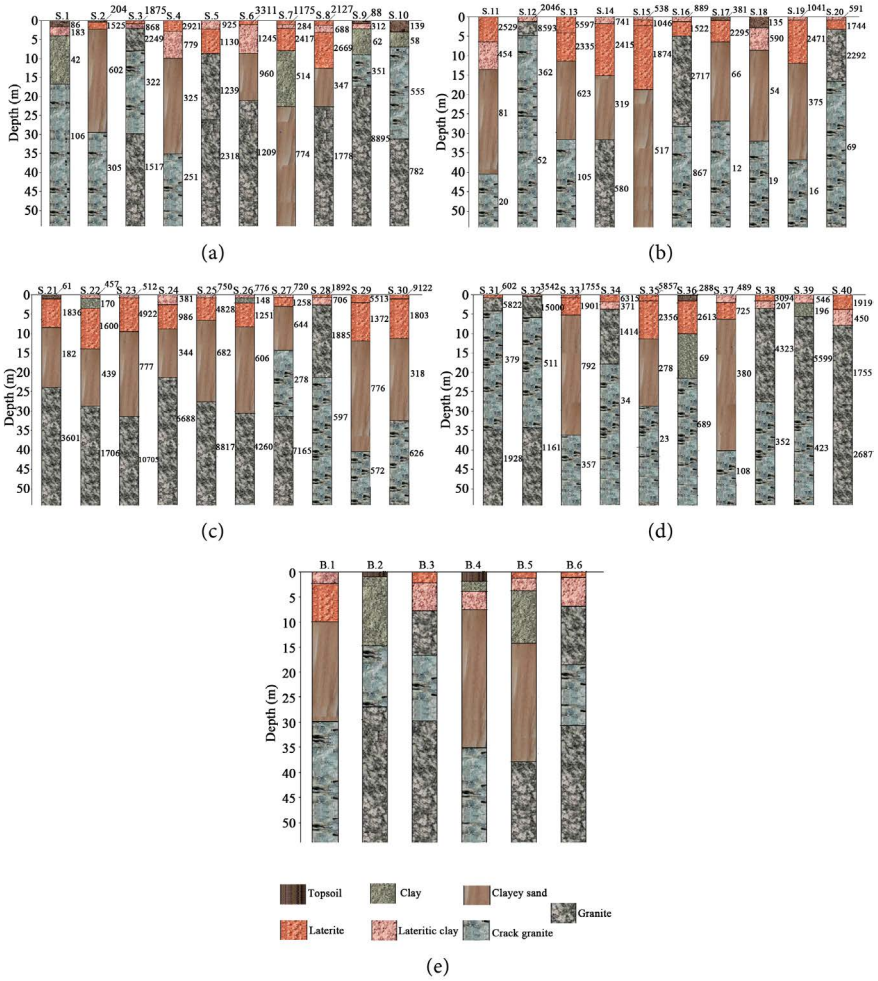

Figure 5. (a): Geoelectrical cuts from S1 to S10; (b): Geoelectrical cuts from S.11 to S.20; (c): Geoelectric cuts from S.21 to S.30; (d): Geoelectric cuts from S.31 to S.40; (e): Drill cuts in some localities in the study area.

Table 1. Resistivity sounding results.

Stations	Resistivity $\rho_1/\rho_2/\ldots/\rho_n$	Thickness $h_1/h_2/\ldots/h_{n-1}$	Total thickness	Lithology	Curve type
S.1: Bankim (1)	86/183/42/106	2/2.5/12.1	16.6	Topsoil/Lateritic Clay/Clay/Cracked Granite	KH
S.2: Bankim (2)	204/1525/602/305	0.2/2.5/26.8	29.5	Topsoil/laterite/Clay sand/Cracked Granite	KQ
S.3: Bankim (3)	1875/868/2249/322/1517	0.7/1.2/6/22	30	laterite/Lateritic Clay/Granite/Cracked Granite/Granite	HKH
S.4: Bankim (4)	2921/779/325/251	3.1/7/25.2	35.2	Laterite/Lateritic Clay/Clayey sand/Cracked Granite	QQ
S.5: Bankim (5)	925/1130/1239/2318	2.5/6.3/17.9	26.7	Lateritic clay/Laterite/Granite/Granite	AA
S.6: Bankim (6)	3311/1245/960/1209	1/7.7/12.3	21	Laterite/Lateritic Clay/Clayey sand/Granite	QH
S.7 Meidougou (1)	1175/284/2417/514/774	0.8/0.8/6/15	22.6	Laterite/Lateritic Clay/Laterite/Clay/Clayey Sand	HKH
S.8 Meidougou (2)	2127/688/2669/347/1778	1.4/2.1/9/10	22.5	Laterite/Lateritic Clay/Laterite/Clayey Sand/Granite	HKH
S.9: Banyo (1)	88/312/62/351/8895	0.6/1.7/6.4/8.4	17	Topsoil/Laterite Clay/Clay/Cracked Granite/Granite	KHA
S.10 Banyo (2)	139/58/555/7826	3.2/4/23.9	31.1	Topsoil/Clay/Cracked Granite/Granite	HA
S.11 Ngaoundéré (1)	2529/454/81/20	6.5/7.1/26.8	40.4	Laterite/Lateritic Clay/Clayey Sand/Cracked Granite	QQ
S.12 Ngaoundéré (2)	2046/8593/362/52	0.9/3.8/21	25.7	Laterite/Granite/Cracked Granite/Cracked Granite	KQ
S.13 Ngaoundéré (3)	5597/2335/623/105	4.2/6.9/20.3	31.4	Laterite/Laterite/Clayey Sand/Cracked Granite	QQ
S.14 Ngaoundéré (4)	741/2415/319/580	1.7/13.4/16.3	31.4	Lateritic clay/Laterite/Clayey Sand/Granite	KH
S.15 Ngaoundéré (5)	538/1046/1874/517	0.6/1.7/16.5	18.8	Lateritic Clay/Laterite/Laterite/Clayey Sand	AK
S.16 Kaka	889/1522/2717/867	1.2/3.8/23	28	Lateritic clay/Laterite/Granite/Cracked Granite	AK
S.17 Leswoka (1)	381/2295/66/12	0.9/5/21	26.9	Topsoil/laterite/Clayey sand/Cracked Granite	KQ
S.18 Leswoka (2)	135/590/54/19	2.5/6.4/22.8	31.7	Topsoil/Laterite Clay/Clayey Sand/Cracked Granite	KQ
S.19 Selal Djertou (1)	1041/2471/375/16	0.7/10.8/24.9	36.4	Lateritic clay/Laterite/Clayey Sand/Cracked Granite	KQ
S.20 Selal Djertou (2)	591/1744/2292/69	0.7/2.4/13.2	16.3	Lateritic clay/Laterite/Granite/Cracked Granite	AK

Continued

S.21 Gandinang (1)	61/1836/182/3601	1.1/7.5/15.4	24	Topsoil/laterite/Clayey sand/Granite	KH
S.22 Gandinang (2)	457/170/1600/439/1706	0.9/2.5/11/14.2	28.6	Lateritic Clay/Clay/Laterite/Clayey sand/granite	HKH
S.23 MbarangII (1)	512/4922/777/10705	0.7/8.7/21.3	30.7	Lateritic Clay/Laterite/Clayey Sand/Granite	KH
S.24 Mbarang II (2)	381/986/344/6688	2.3/6.6/12.2	21.1	Lateritic clay/Laterite/Clayey Sand/Granite	KH
S.25 Mbarang II (3)	750/4828/682/8817	0.6/6.2/20.8	27.6	Lateritic clay/Laterite/Clayey Sand/Granite	KH
S.26 Mbarang II (4)	776/148/1251/606/4260	0.7/1.3/6.1/22.7	30.8	Lateritic Clay/Clay/Laterite/Clayey Sand/Granite	HKH
S.27 Dabo-loy (1)	720/1258/644/278/7165	0.6/2.1/11.9/16.8	31.4	Lateritic clay/Laterite/Clayey Sand/Cracked Granite/Granite	KQH
S.28 Dabo-loy (2)	1892/706/1885/597	0.6/1.8/18.9	21.3	Laterite/Lateritic Clay/Granite/Cracked Granite	HK
S.29 Ngaoundal (1)	5513/1372/776/572	2/10.2/28	40.2	Laterite/laterite/Clayey sand/Cracked Granite	QQ
S.30 Ngaoundal (2)	9122/1803/318/626	0.9/9.8/21.8	32.5	Laterite/laterite/Clayey sand/Cracked Granite	QH
S.31 Ngaoundal (3)	602/5822/379/1928	0.8/3.3/30.7	34.8	Laterite/Granite/Cracked Granite/Granite	KH
S.32 Ngaoundal (4)	3542/15000/511/1161	0.4/5.3/28.6	34.3	Laterite/Granite/Cracked Granite/Granite	KH
S.33 Ngaoundal (5)	1755/1901/792/357	0.9/4.6/30.6	36.1	Laterite/Laterite/Clayey Sand/Cracked Granite	KQ
S.34 Tibati (1)	6315/371/1414/34	1.6/1.8/14.2	17.6	Laterite/Lateritic Clay/Granite/Cracked Granite	HK
S.35 Tibati (2)	5857/2356/278/23	1.3/11.2/16.4	28.9	Laterite/Laterite/Clayey Sand/Cracked Granite	QQ
S.36 Tibati(3)	288/2613/69/689	1.3/8.7/11.9	21.9	Topsoil/Laterite/Clay/Cracked Granite	KH
S.37 Tibati (4)	489/725/380/108	2.1/4.1/33.8	40	Lateritic clay/Laterite/Clayey Sand/Cracked Granite	KQ
S.38 Kontcha	3094/207/4323/352	1.5/2/23.8	27.3	Laterite/Lateritic clay/Granite/Cracked Granite	HK
S.39 Sabongari	546/196/5599/423	2/3/25.2	30.2	Lateritic clay/Clay/Granite/Cracked Granite	HK
S.40 Galim-Tignère	1919/450/1755/2687	3.5/3.9/25.2	32.6	Laterite/Lateritic clay/Granite/Granite	HK

between 6 - 16.5 Ω·m. Finally, the presence of the cracked/good granitic basement was noticed at stations S.3, S.5, S.10, S.12, S.16, S20, S.28, S.31, S.32, S.34, S.38, S.39 and S.40 whose resistivity varies between 362 - 5599 Ω·m and the thickness between 6 - 30.7 m. The fourth layer is relatively current-conducting and dominated by weathered granite whose resistivity varies between 278 - 351 Ω·m and the thickness between 8.4 - 22 m; and also by clayey sand with a resistivity range of 347 - 606 Ω·m and thickness between 10 - 22.7 m.

The fourth and fifth layers would be good/cracked granitic basement with a resistivity ranging from 12 - 10,705 Ω·m. Fracturing is intense at stations S.1, S.11, S.12, S.13, S.17, S18, S19, S20, S.34, S.35 and S.37; with a resistivity range of 16 - 108 Ω·m or an average of 47 Ω·m and an infinite thickness, because they form the last layer and could constitute a good confined aquifer. This strong resistivity contrast found in the basement zone is due to the fact that the resistivity of the rocks depends on several factors such as the content of interstitial fluids, weathering and fracturing [19].

Resistivity measurements separate the subsurface into different layers based on their resistivity values. Litho-log data was obtained from borehole data from the study area. These litho-logs were compared with the geoelectric sections for areas close to borehole points. The correlation was based on the fact that a litho-log differs from a geoelectric log when the boundaries of the litho-log do not coincide with the boundaries of different resistivity.

3.1.2. Iso-Resistivity and Iso-Depth Maps of the Aquifer Roof

The aim of the iso-resistivity map is to obtain a visual representation of the apparent resistivity of the zones where the vertical electrical soundings were carried out. A proposal is presented here as an example of a reconstruction corresponding to the map of apparent resistivities for the value AB/2 = 83 m as shown in Figure 6.

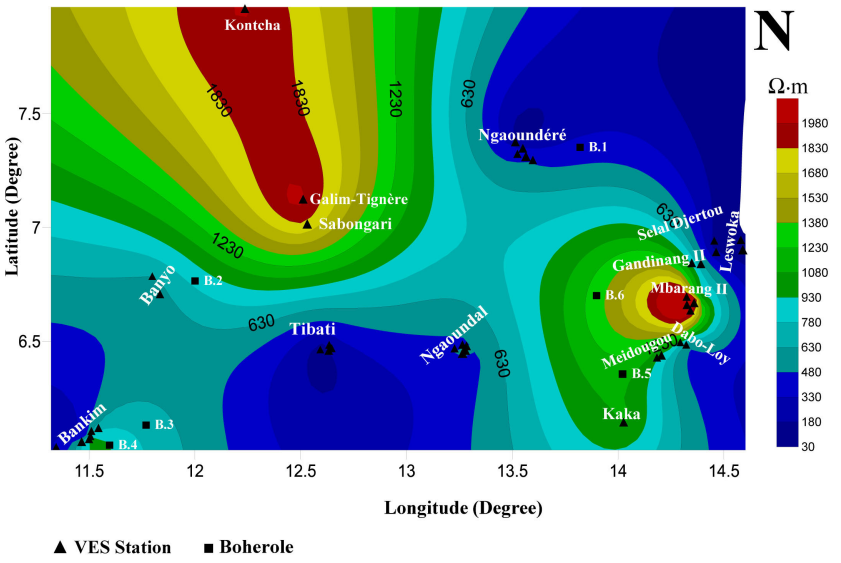

Figure 6. Iso-resistivity map of the aquifer in the study area.

The apparent resistivity ranges from less than 30 Ω·m to more than 1980 Ω·m with the North-East, South-West and South sectors particularly conducive (ρ_a < 330 Ω·m). These could be the areas of convergence of groundwater through cracked granite. On the other hand, the North-West and East sectors are very resistant (ρ_a > 1980 Ω·m) which would be healthy granite.

The iso-depth map of the aquifers (Figure 7) shows that, the depth varies between 16 m and more than 40 m, with an average of 28.3 m. This depth would actually be that of rock where we can have cracked zones, because the hydrogeological investigations is based on the search for the zones of cracking of the base which have in general a very good permeability [20]. From a hydraulic point of view, it is the depth from which the first arrivals of water are very likely. However, we note that zones with high aquifer potential have depths greater than 28 m.

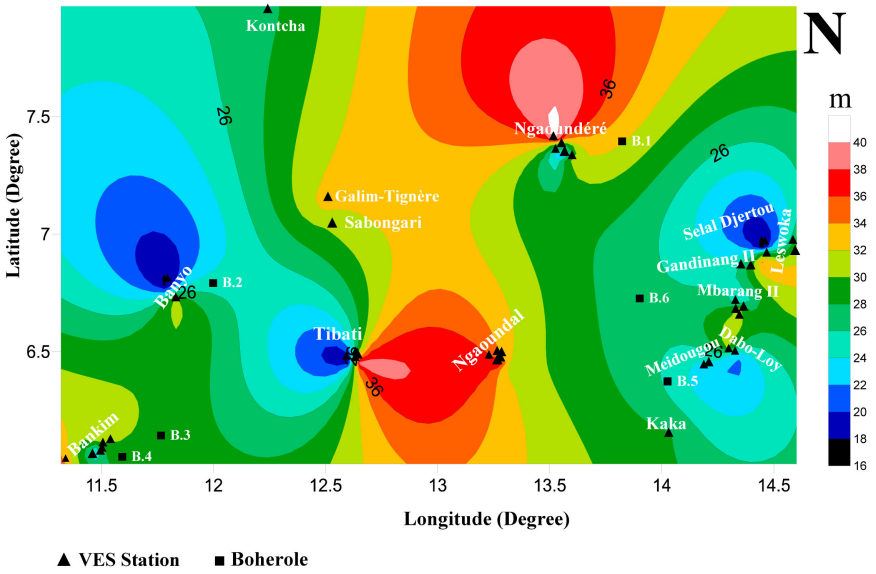

Figure 7. Depth to the top of aquifer in the area.

3.2. Discussions

The interpretation of the vertical electrical soundings made it possible to highlight the geoelectrical models of the basement of the study area. To this end, the subsoil of the study area has been subdivided into three major groups. The first is a shallow (<14 m) superficial infiltration zone dominated by laterite whose resistivity is quite high (>1000 Ω·m) and clay (<600 Ω·m). The second zone is a weathered zone which, in the majority of cases constitutes a superficial aquifer with a resistivity range between 81 Ω·m and 960 Ω·m and thickness range between 12.2 m and 26.8 m. This weathered zone overcomes a granitic horizon that presents a large variety of resistivity range (between 12 Ω·m and 10705 Ω·m) thus highlighting the strong heterogeneity of rock. The deep water producing areas would be around 16 m and 40 m of depth. However it could be noted that the results obtained by tomographic and Self-Potential data analysis in part of

the region of Meiganga (Meying *et al*., 2018) revealed the presence of lateritic formations (lateritic soils, laterites) with high resistivity values (>2000 Ohm·m), a gneissic weathered/fractured arena with low resistivity values (<850 Ohm·m) which represents the aquifer training and the gneissic basement. As a result, the inverted resistivity models have revealed productive groundwater zones at depths of 20 to 25 m and are considered to be deeper groundwater zones with depths of about 10 to 13 m, for shallow groundwater [13]. However, some differences are observed when the results are compared, this may be due to the greater investigation area which is more extensive in the case of our study but also the type of data exploited.

In addition, a comparative study between the geophysical parameters obtained in the most recent study by inverse slope method [12] and those obtained by the least-squares inversion has been carried out and shows by **Table 2**.

This table shows that the parameters of the aquifer are almost similar with both approaches. Therefore, the results obtained are in agreement with those of Arétouyap *et al.* (2018).

Table 2. Comparison of the results from studies using two approaches in the area of study.

Method	Geophysical parameters
Inverse slope method	For the first set, aquifer resistivity varies between 212 and 640 Ω·m and its thickness between 20 and 30 m. For the second trend, the aquifer resistivity ranges from 111 to 962 Ω·m and the thickness from 10 to 30 m.
Least-squares inversion	The weathering aquifer has a resistivity that varies between 81 and 960 Ω·m and the thickness between 12.2 and 28.6 m. The average resistivity of the deep aquifer is 1817 Ω·m.

Alteration is an important factor in the search for groundwater, because the weathered layers are very porous and weakly permeable due to the presence of clay. Weathered layers are known to have a very good water storage function [21]. The stations of great hydrogeological interest are S.2, S.4, S.11, S.13, S.17, S18, S19, S.23, S.25, S.26, S.29, S.30, S.33 and S.37 because they have weathered and fractured formations of great thicknesses On the other hand, the weathered layers are weak thicknesses and almost non-existent in some stations like S.3, S.12, S.16, S20, S.28, S.31, S.32, S.38, S.39 and S.40.

The interpretation carried out on vertical electrical sounding curves corroborate with lithological data from boreholes in the area.

4. Conclusion

Forty (40) vertical electrical soundings were exploited by the least-squares inversion method to characterize the aquifers in the Adamawa Plateau region of Cameroon. This study shows that: 1) the geological layers identified in this zone are made up of: top soil, laterite, clay, clay sand and granite whose resistivities have been determined; 2) Several types of curves have been identified: AA, AK, HA, KH, KQ, QH and QQ for the four (04) layer models and HKH, KHA and KQH

corresponding to five (05) layer terrain models; 3) The sectors that could well be groundwater convergence zones are located to the North-East, South-West and South of the Adamawa plateau; 4) The roof of the basement aquifer varies between 16 m and 40 m, an average of 28.3 m. Cracked aquifers are less sensitive to pollution, unlike aquifers of laterites. However, in most cases, the laterites more crack horizon constitutes a composite aquifer that functions as a whole, especially when it is exploited by deep drilling. Hence, there is the need to focus on the thickness of the weathered layer and the conductive character of the underlying layer which is the cracked horizon. However, the thickness of the granite layer may not be fully evaluated at very great depth through this work. It nonetheless provides an overview of shallow subsurface aquifer systems and delineates areas for the groundwater development programs in the region.

Acknowledgements

We wish to express our gratitude to the team and sponsor of this geoelectic campaign particularly to Mr. Gounou Pokam Blaise Pascal who provided the data for this work.

Conflicts of Interest

The authors declare no conflicts of interest regarding the publication of this paper.

References

[1] Teikeu, A.W., Njandjock, N.P., Ndougsa, M.T. and Tabod, T.C. (2012) Geoelectric Investigation for Groundwater Exploration in Yaounde Area, Cameroon. *International Journal of Geosciences*, **3**, 640-649. https://doi.org/10.4236/ijg.2012.33064

[2] Enyegue, A.N.F.M., Ndougsa, M.T., Njandjock, N.P., Assembe, S. and Manguelle, D.E. (2014) Groundwater Exploration Using Geoelectrical Investigation in Bafia Area, Cameroon *Journal of Earth Sciences and Geotechnical Engineering*, **4**, 61-75.

[3] Aretouyap, Z., Njandjock, N.P., Ekoro, H.N., Meli, L.J. and Lépatio, A.T. (2014) Investigation of Groundwater Quality Control in Adamaoua-Cameroon Region. *Journal of Applied Sciences*, **14**, 2309-2319.

[4] Aretouyap, Z., Njandjock, N.P., Bisso, D., Nouayou, R., Lengue, B. and Lépatio, A.T. (2014) Climate Variability and Its Possible with Water Resources in Central Africa. *Journal of Applied Sciences*, **14**, 2219-2233.

[5] Ngnotue, T., Nzenti, J.P., Barbey, P. and Tchoua, F.M. (2000) The Ntui-Betamba High Grade Gneisses in Cameroon. *Journal of African Earth Sciences*, **31**, 369-381. https://doi.org/10.1016/S0899-5362(00)00094-4

[6] Dumont, J.F. (1987) Etude structurale des bordures Nord et Sud du plateau de l'Adamaoua: Influence du contexte atlantique. *Géodynamique*, **2**, 55-68.

[7] Le Maréchal, A. and Vincent, R.P. (1971) Le fossé crétacé du Sud Adamaoua (Cameroun). *Cahier O.R.S.T.O.M., sér. Géol.*, **3**, 67-83.

[8] Kampunzu, B.A., Caron, H.J. and Lubala, T.R. (1986) The East African Rift, Magma Genesis and Astheno-Lithospheric Dynamism. *Episodes*, **9**, 211-216. https://doi.org/10.18814/epiiugs/1986/v9i4/002

[9] Lasserre, M. (1961) Étude géologique de la partie orientale de l'Adamaoua (Cameroun Central) et les principales sources minéralisées de l'Adamaoua. *Bull. Dir. Mines et Géologie du Cameroun*, No. 4, 130 p.

[10] Djeuda, T.B.H., Tanawa, E., Temgoua, E., Siakeu, J. and Ngo, M.B. (1999) Modèle de circulation, mécanisme de recharge et temps relatif de séjour des eaux des nappes souterraines des altérites en milieu cristallin: Cas du bassin versant de l'Anga'a, Yaoundé-Cameroun. Collect. Géocam, 2/1999, Ed. Press. Univ. de Yaoundé, Yaoundé, 117-126.

[11] Gnamba, M.F., Oga, Y.S.M., Gnagne, T., Lasm, T. and Beimi, J. (2014) Analyse de la productivité des aquifères de fissures du socle paléoprotérozoïque de la région de katiola (centre-nord de la Côte d'Ivoire). *European Scientific Journal*, **10**, 79-98.

[12] Aretouyap, Z., Bisso, D., Njandjock, N.P., Amougou, M.L.E. and Asfahani, J. (2018) Hydrogeophysical Characteristics of Pan-African Aquifer Specified through an Alternative Approach Based on the Interpretation of Vertical Electrical Sounding Data in the Adamawa Region, Central Africa. *Natural Resources Research*, **28**, 63-77. https://doi.org/10.1007/s11053-018-9373-8

[13] Meying, A., Bidichael, W.W.E., Gouet, D., Ndougsa, M.T., Kuiate, K. and Ngoh, J.D. (2018) Hydrogeophysical Investigation for Groundwater Resources from Electrical Resistivity Tomography and Self-Potential Data in the Méiganga Area, Adamawa, Cameroon. *Hindawi International Journal of Geophysics*, **2018**, Article ID: 2697585. https://doi.org/10.1155/2018/2697585

[14] Telford, W.M., Geldart, L.P. and Sheriff, R.E. (1990) Applied Geophysics. Cambridge University Press, Cambridge, 870 p. https://doi.org/10.1017/CBO9781139167932

[15] Orellana, E. and Mooney, H.M. (1966) Master Tables and Curves for Vertical Electrical Sounding over Layered Structures. Interciencia, Madrid.

[16] Zohdy, R.A.A. (1989) A New Method for the Automatic Interpretation of Schlumberger and Wenner Sounding Curves. *Geophysics*, **54**, 245-253. https://doi.org/10.1190/1.1442648

[17] Zohdy, R.A.A. and Bisdorf, R.J. (1989) Schlumberger Sounding Data Processing and Interpretation Program. US Geological Survey, Washington DC.

[18] Dey, H. and Morrison, H. (1979) Resistivity Modeling for Arbitrarily Shaped 3-D Structures. *Geophysics*, **44**, 753. https://doi.org/10.1190/1.1440975

[19] Chapellier, D. (2001) Prospection électrique de surface. Cours Online de Géophysique. Univ. Lausanne, 34 p.

[20] Engalenc, M., Grellot, U.C. and Lachaud, J.C. (1979) Inter-African Committee of Hydraulic Studies. Vol 2. 193 p.

[21] CIEH (1981) Méthodes d'étude et de recherché de l'eau souterraine des roches cristallines de l'Afrique de l'Ouest. *Géohydraulique*, **38**, 100 p.